Functional Connectivity and Machine Learning for Psychiatric Drug Development

Joules, Richard Bryan

Awarding institution:
King's College London

Functional Connectivity and Machine Learning for Psychiatric Drug Development

Richard Joules[1]

A thesis submitted for in part of the fulfilment of requirements for the degree of

Doctor of Philosophy

2015

First Supervisor: Dr. Mitul Mehta[1]
Second Supervisor: Dr. Orla Doyle[1]

[1]Department of Neuroimaging, Centre for Neuroimaging Sciences, Institute of Psychiatry, Kings College London

Acknowledgements

I would like to acknowledge the help and support of the many colleges, mentors and friends who have helped me over the course of this PhD. First and foremost, I would like to thank my supervisors, Dr. Mitul Mehta, Dr. Orla Doyle and Prof. Michael Brammer. Their guidance, advice and support have made this work possible, not only have they taught me a great deal but have demonstrated boundless patience with my occasionally less than conventional working style.

I am also very grateful to the various colleagues with whom I have shared an office over the course of this PhD, they have offered interesting diversions and constant support; specifically I would like to thank Luis Lacerda, Dr Mattia Veronese and Dr Judith Nottage.

I would also like to extend my gratitude to my friends and colleges at the CNS who have provided guidance, expertise and discussion; specifically I am very grateful to Dr. Vincent Giampietro, Dr. Cedric Ginestet, Prof. Federico Turkheimer, Dr. Paul Expert, Dr. Owen O'Daly, Leon Aksman and Anthony Gabay. I'm also very grateful to Chris Webb and Rodney Lewis for their amusing sarcasm and patience in the face of relentless IT requests.

Likewise, I am very grateful to the staff at the Centre for Neuroimaging Sciences who have fostered an encouraging and supportive working environment in which it has been a pleasure to undertake this PhD.

Last but certainly not least, I would like to thank my partner Elisabeth Monaghan, for enriching my life, her encouragement, endless generosity and countless cups of tea which have seen me through the both the bright and the more challenging parts of this PhD.

Abstract

The human brain is a complex biological network consisting of spatially separated but functionally integrated regions. Study of functional connectivity gained immense popularity in recent years providing new insight into the mechanisms underlying complex functions and the fundamental organisation of the brain. This has led to the emergence of new techniques for investigating connectivity, such as the application of pattern recognition techniques and the investigation of network dynamics. While highly promising, the application of these new techniques to pharmacological imaging data has not yet been fully explored.

In this thesis we apply pattern recognition techniques to functional connectivity measures obtained for pharmacological imaging data to discriminate patterns of whole brain connectivity. Furthermore, we demonstrate that consideration of functional connectivity dynamics provides additional insight into the effect of pharmacological interventions. Specifically, we explore the effects of the N-methyl-D-aspartate receptor antagonist, ketamine, on the connectivity within the human brain. We argue that the investigation of connectivity is a more appropriate tool for the investigation of this compound due to the highly distributed pattern of effects, as compared to traditional approaches investigating amplitude effects. We demonstrate the applicability of pattern recognition techniques for the discrimination pharmacological states using measures of regional connectivity over the whole brain, using network interactions and through the inspection of network dynamics. We expand upon traditional approaches in our investigation, introducing a new approach to investigate network effects and temporal dynamics of connectivity organisation.

Contents

Figures

Tables

Chapter 1: Introduction

The human brain is a highly complex, inter-connected organ. Traditional study of the brain has attempted to localise specialised regions responsible for specific tasks and behaviours. It is only relatively recently that the brain has been studied in the context of a network, rather than a collection of isolated regions. This interpretation of the brain as a collection of highly integrated specialised regions which interact to achieve high level functions provides a more biologically informed perspective of brain function.

Within the neuroimaging literature there are several prominent methods for the investigation of functional connectivity (FC) effects. The most prominent amongst these are graph theory analysis, independent component analysis (or similar blind source separation techniques) and dynamic causal modelling. The applicability of these methods depends on the modality of the data acquired. This thesis will exclusively focus on the use of graph theory analysis as applied to functional magnetic resonance imaging (fMRI) data.

The primary focus of this thesis is the use of FC approaches applied to pharmacological imaging data. Specifically, we investigate connectivity effects of the N-methyl-d-Aspartate receptor (NMDAR) antagonist, ketamine. This compound has been demonstrated to elicit distributed glutamatergic effects (Deakin et al. 2008). As such we propose FC will provide a more principled method of investigation for this compound than traditional amplitude based approaches. To this end, we explore emerging techniques and develop new frameworks for investigation of FC effects which we apply to the analysis of ketamine in order to explore this hypothesis.

This thesis emphasises methods of modelling FC in order to better understand the mechanism and organisation of the human brain. Specifically, we investigate the application of machine learning techniques to connectivity data in order to gain insight into the effects of pharmacological intervention on the human brain. Machine learning is well suited for connectivity analysis, offering a multivariate framework for group comparisons sensitive to spatial covariance within the data, particularly important when considering the highly correlated nature of connectivity data.

The use of pattern recognition (PR) techniques applied to neuroimaging data has garnered much interest in recent years. PR techniques are a form of supervised machine learning and are used to predict class membership for unseen test data based on previously observed patterns within a training dataset. This provides a clinically relevant technique with the potential for aiding patient diagnosis or prognosis (Ecker et al. 2010; Gong et al. 2011; Nouretdinov et al. 2011). While considered an established technique within the field of neuroimaging (LaConte et al.

2005; Mourao-Miranda et al. 2005; Marquand et al. 2008; Orrù et al. 2012), it is only recently that these approaches have been applied to the study of connectivity in the brain. Initial applications of PR techniques to functional connectivity have yielded impressive results such as accurate differentiation of patient groups (Anderson et al. 2011; Chen et al. 2011; Richiardi et al. 2012), varying degrees of brain maturity (Dosenbach et al. 2010) and cognitive state (Richiardi et al. 2011; Shirer et al. 2012). These methods provide an elegant way of discriminating groups, identifying discriminating patterns and have further potential for individual predictions and pharmacological imaging.

Another focus of this thesis is the examination of network effect in the human brain. It has been demonstrated that the brain expresses consistent functional networks in both task-free and task-positive states (Damoiseaux et al. 2006). Given previously observed effects of ketamine on key hub areas of the brain (Scheidegger et al. 2012) we expect ketamine to have widespread effects on these task-free networks. In this thesis we will explore methods of investigating network effects using pattern recognition techniques with the aim of investigating these potential network effects of ketamine.

In addition to the application of machine learning techniques to connectivity analysis, this thesis is also concerned with the investigation of connectivity dynamics over time. Traditionally networks have been examine through the assumption of stationary connectivity within each experimental condition. Recent observations of connectivity fluctuations have challenged this assumption (Chang et al. 2010; Van Dijk et al. 2010; Hutchison et al. 2012), leading to the development of new analysis techniques which consider temporal variations in brain connectivity (Zalesky et al. 2010; Kiviniemi et al. 2011; Allen et al. 2014). These techniques, while in their infancy, show promise for providing new insight into the mechanisms of the human brain. We propose that analysis of the temporal dynamics of FC during the infusion of ketamine will present new insight into the profile of drug effects on the human brain. To this end, we develop new methods to assess the temporal profile of functional connectivity network effects as measured by fMRI. Through the application of these methods we reveal how acute ketamine infusion elicits changes in the modular structure of the brain.

1.1 Introduction to Neuroimaging Analysis

Imaging analysis of fMRI data has been historically dominated by the identification of regional effects between experimental conditions using mass-univariate statistical analysis. Most analyses are performed using techniques based on the general linear model (GLM), one of the most common being statistical parametric mapping (Friston et al. 1995). This method applies independent statistical tests to each voxel, assessing responses in the context of a stimulus

model, resulting in a statistical parametric map (SPM). This approach, illustrated in Figure 1, has been widely used to further our understanding of the human brain. It provides a robust method for localisation of regions differing between experimental conditions based on a neuroimaging measure. While providing an intuitive method for detecting regional group differences, it is based on the assumption that voxels are independent from each other. This however, is contrary to our understanding of the brain in which regions act in concordance to perform tasks or direct behaviour. Furthermore, the GLM approach does not directly allow for individual predictions of group membership.

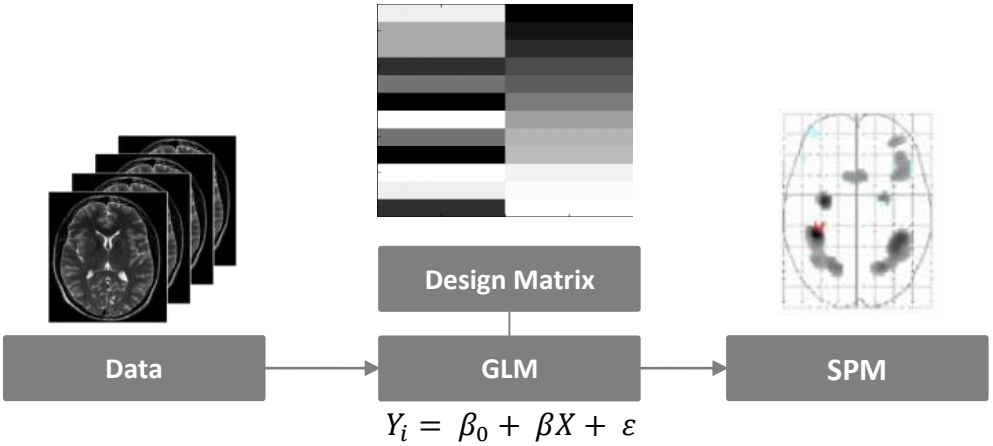

Figure 1 - Schematic of general linear model analysis as applied to neuroimaging data resulting in an SPM

Due to the large number of independent tests performed for a voxel-wise univariate analysis, in the order of hundreds of thousands for a whole brain analysis, correction for multiple comparisons is required to protect against false positives. Many mature solutions exist to correct this, such as the Bonferroni, false discovery rate correction (Benjamini et al. 1995) and random field theory (Worsley et al. 1996). These tests however, have the tendency to be conservative with small sample sizes, potentially increasing the false negative rate. This can result in decreased sensitivity of the GLM in identifying experimental effects. In an effort to overcome these limitations of the GLM, multivariate approaches, more specifically PR methods, have been applied to neuroimaging analyses (Mourao-Miranda et al. 2005; Kloppel et al. 2008; Marquand et al. 2010).

These PR approaches regard all voxels in unison as a pattern rather than testing voxels in isolation; as such, are sensitive to patterns of correlations between voxels. This provides increased sensitivity when compared to the GLM and affords a more biologically motivated representation of brain activity. These techniques are often used to perform classifications to compare groups, providing a method for predications of group membership on the individual scale. This is achieved with what can be considered a two stage approach. The first is the training phase, in which the algorithm optimises a set of parameters in order to adjust a classifier to

maximise the predictive accuracy of the model. This is followed by a test phase, where an independent data set can be used to test the generalizability of the classifier for predictions of class membership. This principle is illustrated in Figure 2. PR techniques discriminate groups based on patterns of data, identified from the training *samples.* Each sample is a vector of *features* representing some measure from the data; this may refer to raw values obtained from imaging. Alternatively features may be a higher level, more complex measurement such as Beta values (Figure 1) from the first level analysis, or the strength of connections between regions.

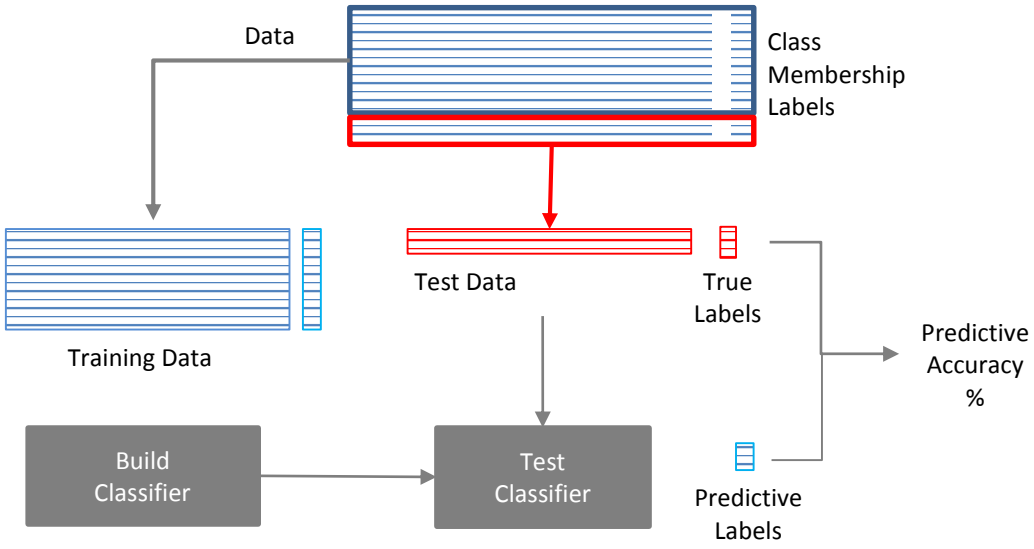

Figure 2 - Overview of training and test phases for machine learning

The ability to predict class membership for unseen test data makes PR an attractive option for the potential development of clinically applicable diagnostic and prognostic tools using neuroimaging data, something not directly possible using the GLM approach. Furthermore, a single outcome measure of predictive accuracy obtained from classification is advantageous as it avoids the issue of correcting for the large number of independent tests performed in the GLM. There have been several PR methods applied to neuroimaging but the most popular by far is the support vector machine (SVM)(Cortes et al. 1995) approach. This is an efficient, pseudo-probabilistic class of PR which has been successfully used in several neuroimaging studies (Mourao-Miranda et al. 2005; Wang et al. 2007; Klöppel et al. 2008). Another pattern recognition technique increasingly applied to neuroimaging analysis is Gaussian process classification (GPC)(Rasmussen 2006). This is a binary classification algorithm with a Bayesian framework allowing for probabilistic predictions of class membership. Furthermore, classification is driven by class typicality rather than support vectors which represent data on class boundaries. As such presents a more clinically appropriate method of pattern recognition. A summary of these methods is provided in Chapter 3.

1.2 Introduction to Functional Connectivity Analysis

Connectivity in the human brain has been widely studied and can be broadly dichotomised into two areas of study: 1) functional connectivity (FC), where the connections between regions are defined by temporal similarity of perceived brain activity, and 2) structural connectivity, where regions are connected by white matter tracts as observed in pathology and imaging. In this thesis we are exclusively concerned with FC.

In order to assess FC a temporospatial data acquisition is required, such as measurements of blood flow or electrical potentials across the brain. Connections are then inferred through similarity of regional time series data. This relational view is highly advantageous when looking at the mechanistic effects of neuro-active compounds on the human brain as well as providing insight into its fundamental organisation. Due to its relatively high spatial and temporal resolutions, fMRI has been the acquisition modality of choice for functional connectivity studies and will be the focus of this thesis; however other modalities such as PET (Friston et al. 1993), MEG and EEG (Fingelkurts et al. 2007) may also be used.

Several techniques have been proposed in order to assess the FC structure in the brain. The most commonly applied methods are blind source separation and graph theory methods. Of the former, independent component analysis (ICA) is the most prevalent. ICA seeks to decompose the data into a set of spatial patterns or time courses where the independence for spatial (spatial ICA) or temporal (temporal ICA) patterns is defined *a priori.* While temporal ICA is occasionally used (Biswal et al. 1999), spatial ICA is far more prevalent within neuroimaging analyses and has been used to identify consistently coupled regions over an entire acquisition (Damoiseaux et al. 2006; De Luca et al. 2006). These methods provide a readily interpretable view of connectivity in the brain, however they enforce assumptions of consistent intra-component connection strengths; furthermore selection of the optimal number of components can be problematic.

An alternative to blind source separation methods are graph theory techniques. This is a broad field with diverse applications to the study of FC; the connectivity in the brain is modelled as a graph consisting of nodes connected by edges. Nodes can then represent anatomical regions while edges inform the connections between respective nodes. These graphs can be interrogated to reveal specific topological or connectivity effects.

Most established techniques perform univariate statistical tests on the connections between regions in order to infer the statistical significance of a regional connection. One of the commonly applied methods to neuroimaging FC analysis is the *seed based* analysis which performs statistical testing on the regional connections to a seed region defined *a priori* (Biswal

et al. 1995). This provides an intuitive method for hypothesis testing, however limits the scope of investigation to the relationships related to the seed regions. Other methods have extracted regional summary statistics for a specific aspects of connectivity for regions of the brain and performed statistical testing on these summary measures (Schwarz et al. 2008; Lord et al. 2012). This provides a broader scope of investigation but precludes inferences on specific regional connections. Furthermore, these methods apply univariate statistics which enforce assumptions of statistical independence between edges, arguably inappropriate when considering the nature of connectivity data.

Pattern recognition (PR) techniques have been applied to graph theory analyses, circumventing many of these statistical limitations while respecting the correlations between connections (Shirer et al. 2012). This approach offers greater flexibility compared to blind source separation techniques, a plethora of different graph theory measures and node definitions may be used as a feature set. Furthermore, these techniques offer data driven, model-free approaches to whole brain connectivity analysis without the need to select components. Whilst a promising methodological advancement in the analysis of functional connectivity, further work is required to identify an optimal workflow.

The majority of FC analyses to date have assumed network configurations and effects are *stationary*. While this term has alternate definitions in different fields, for this thesis we define stationarity as temporal consistency for a given network configuration. However, more recent studies have demonstrated that connectivity exhibits temporal dynamics (Hutchison et al. 2012). These dynamics have been investigated revealing the occurrence of meta-stable network states (Smith et al. 2012). The existence of these states indicates the "resting state" may not be represented by a single connectivity configuration but rather as a collection of transitory states. This new insight into functional connectivity potentially offers a unique new perspective into the organisation of the brain. Furthermore, these dynamic states have been shown to be sensitive to disease states (Calhoun et al. 2014) indicating the potential applicability for pharmacological imaging. It is this potential sensitivity of functional connectivity dynamics to pharmacological intervention that we wish to explore as part of this thesis.

1.3 Thesis Outline

The work enclosed in this thesis is both methodological and applied, covering both the development of connectivity analysis pipelines and their application to pharmacological neuroimaging data. Early chapters are primarily focused on with the application of existing analysis approaches in order to better understand the stationary functional connectivity effects of our pharmacological imaging dataset and provide a foundation for later chapters. These later

chapters are dedicated to the development of methods to investigate specific network effects of pharmacological compounds and the dynamics of FC. The progression of presented work can be summarised in the flow diagram below (Figure 3):

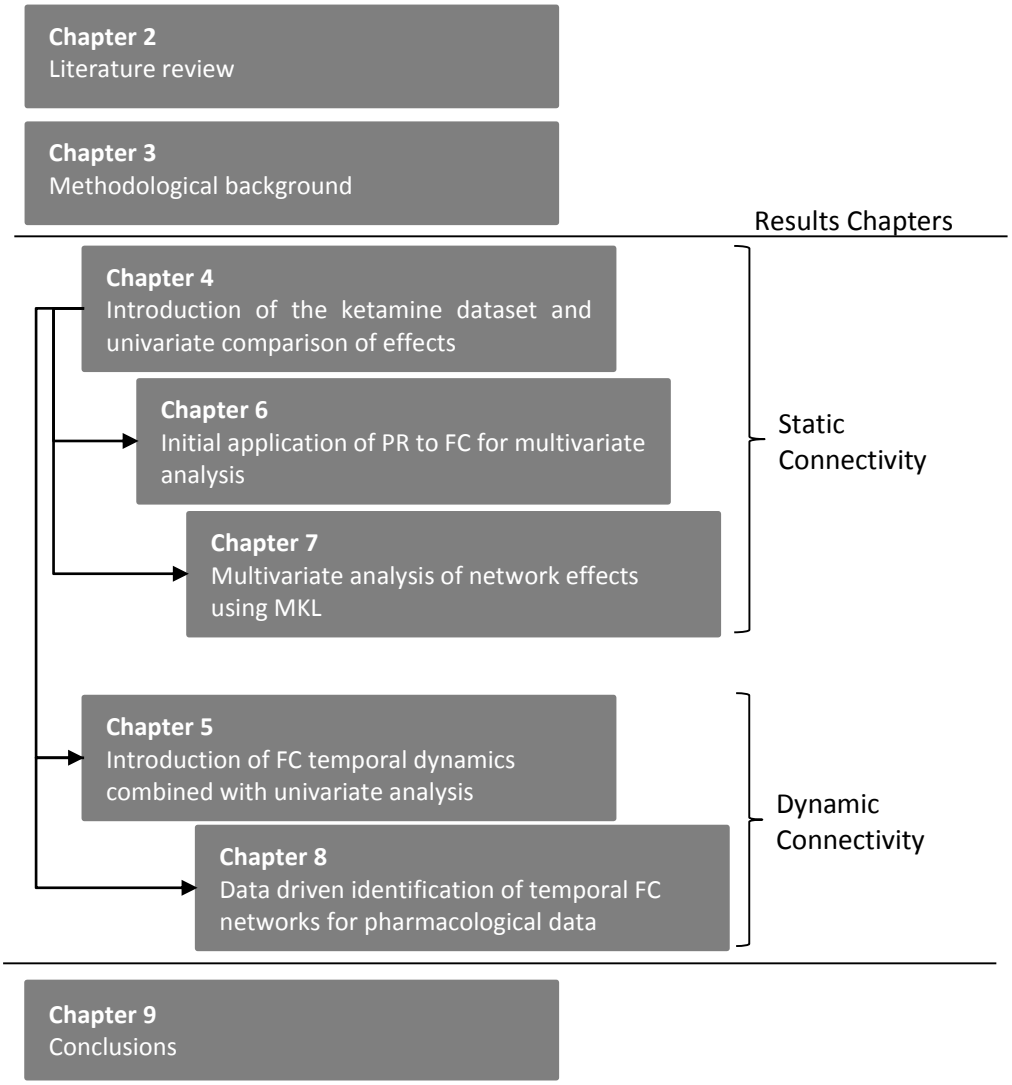

Figure 3 - Flow chart layout of thesis chapters, Arrows indicate dependencies between results chapters

A more detailed breakdown of chapters is as follows:

In Chapter 2 we present a brief overview of the literature concerning FC analysis. We attempt to provide context and outline the motivation of this work by highlighting key milestones in the development of FC analysis methodology and applications. We provide a brief summary of the expansive connectivity literature from its beginnings to the current state of the art while highlighting potential benefits and problems.

Chapter 3 provides an overview of functional connectivity principals and machine learning techniques which are necessary for the understanding of later chapters. In this chapter we explore the basics of graph theory, its application to neuroimaging data and the variety of metrics and measures available. We also provide an overview of supervised learning techniques

and introduce important concepts such as probabilistic prediction, generalizability and over fitting.

In Chapter 4 we introduce a ketamine pharmacological imaging dataset. We provide a brief background on the compounds administered and describe the pre-processing performed on the data. We subsequently apply traditional graph theory analysis to the data to investigate the connectivity effects of the compound, as observed with standard analysis techniques.

In Chapter 5 we apply PR techniques to analyse the connectivity effects in our dataset. We demonstrate the sensitivity of graph theory metrics and windowing procedures to the group discrimination using PR.

In Chapter 6 we apply multi-kernel learning to generate a principled view of network interaction effects within our dataset. This novel approach to network analysis provides a principled means of investigation for non-uniform network effects elicited by our experimental conditions.

Chapter 7 introduces functional connectivity dynamics as perceived through a windowing approach. We perform univariate analyses on the rate of these temporal dynamics to demonstrate sensitivity to pharmacological intervention.

Chapter 8 describes a novel application of multi-slice community detection to the identification of temporospatially dynamic networks in the brain. Clustering is subsequently applied to extract meta-stable connectivity states. Through statistical testing we identify states sensitive to our experimental conditions and provide insight into the effect of pharmacological intervention on the modular connectivity structure of the brain.

In Chapter 9 we summarise the work undertaken, offering conclusions regarding the methodology presented and the effects of the compound challenged used throughout this thesis. We suggest potential applications and further areas for research based on the work presented here.

Chapter 2: Literature Review

Functional connectivity (FC) has gained much interest in the field of neuroimaging and has become an increasingly preferential method of analysis supplementing and expanding upon more traditional forms of analysis. FC analysis can be considered advantageous over traditional blood oxygenation level dependant (BOLD) amplitude analysis methods as it incorporates relationships between regions, providing a more biologically motivated view of brain function and organisation. There are many forms of connectivity analysis each with advantages and limitations. This chapter, rather than providing an in-depth review of the expansive literature on the subject, will instead provide an overview of the key developments in the field of FC and outline the context and motivation for the work in this thesis; namely the application of pattern recognition (PR) to FC and the investigation of dynamic connectivity as observed with fMRI. For a more in depth review of the field in general, we direct the reader to the excellent review articles (Damoiseaux et al. 2009; van den Heuvel et al. 2010; Keilholz 2014).

2.1 The rise of functional connectivity

The concept of networks in the human brain originated with anatomical observations of brain structure. Early work examining basic neurons from the 1950's (Hodgkin et al. 1952; Eccles 1964) enabled the conception of complex networks arising from the interactions between simple neuronal elements. It was suggested that behaviours were controlled by specific neuronal circuits (Bentley et al. 1978). In order to understand the functional mechanisms of the brain it would first be necessary to understand these networks. Early work attempting to map the neuronal circuits in relatively simple organisms was hampered by the vast complexity of neuronal interactions and the tools available at the time (Selverston et al. 1983).

Prior to the early 1990's the study of FC was primarily concerned with the cross correlation of spike trains from separate brain areas (Palm et al. 1988; Aertsen et al. 1989; Gochin et al. 1991). These early studies shaped the field and resulted in the generally accepted definition of FC as the temporal correlation of functional measurements from spatially separated regions. These techniques were limited by the then achievable spatial resolution and coverage, furthermore the techniques used were highly invasive and generally only suitable for animal studies.

The development of new technologies and techniques enabled further in-depth investigations into functional connectivity. In 1993, Friston et al applied principal component analysis (PCA) to the study of functional connectivity in positron emission tomography (PET) data. This was one of the earliest investigations into in-vivo whole brain connectivity in humans and paved the way

for later studies investigating whole brain connectivity and studies using independent component analysis (ICA) methods. This technique presented many clear advantages over previous analyses of spike trains, namely the ease of interpretation of results, the non-invasive acquisition and the ability to cover the whole brain rather than sparse, discrete spatially sampling, as common with EEG analyses. However, the study of functional connectivity with PET is also highly restrictive due to low temporal and spatial resolution.

An advance in functional connectivity analysis came with the advent of functional magnetic resonance imaging (fMRI). It was observed that robust spatiotemporal patterns could be observed at low frequencies in the BOLD signal (Biswal et al. 1995). Due to the infancy and inherent technical issues of this method, the reported results were greeted with scepticism. Subsequent work attempted to validate the patterns of regional coupling observed with BOLD fMRI (Biswal et al. 1997; Biswal et al. 1997; Lowe et al. 1998). As evidence to the uncertainty that this technique was observing true functional connections, the authors provide an in depth discussion on possible confounds which may have spuriously produced the observed patterns of spatiotemporal correlations. These included correction methods for head motion, physiological effects and other noise sources. Whilst the optimal procedure for addressing these issues is still currently a source of contention in the literature (Glover et al. 2000; Lund et al. 2006; Chang et al. 2009), it has since been accepted the observed connections between regions are generally neuronal in origin. This has been further re-enforced by simultaneous EEG and fMRI connectivity studies showing overlap between resting state networks (Jann et al. 2009).

Since Biswal's early observations, fMRI has become the tool of choice for studying the functional connectivity of the human brain. The popularity of fMRI over competing data acquisition methods can be attributed to its non-invasive acquisition and its good spatial and temporal resolution providing advantages over both PET and electrophysiological measurements in terms of resolution. Electroencephalography (EEG) and magnetoencephalography (MEG) have also proved popular for functional connectivity analysis (Stam 2004; Brookes et al. 2012). This is primarily due to the fine temporal resolution achievable and reasonable spatial coverage. While this allows for investigation into functional connectivity over the order of microseconds, these techniques have relatively poor spatial resolution and present significant and present challenges when imaging deep cortical and sub-cortical regions.

Initial methods for examining functional connectivity in fMRI data have predominantly used correlation between brain regions to identify connected regions. This allowed for the identification of signal changes in relation to a task but was also sensitive to noise. In the late 1990's independent component analysis (ICA) was demonstrated as a viable alternative method

of connectivity analysis (Biswal et al. 1999). This allowed for a better understanding of signal sources as well as improving the reliability of extracted networks.

In order to compare the functional connectivity differences in disease populations or task groups it is often necessary to identify a baseline for comparison. A consistent baseline for the task free state, a *default mode network* (DMN), was identified in several studies (Gusnard et al. 2001; Raichle et al. 2001; Greicius et al. 2003). It was initially treated with scepticism due to demonstrations that physiological noise can affect the data low-frequencies from which connectivity is calculated (Cordes et al. 2001; Birn et al. 2006). It has also been shown improper post-processing can strongly affect measures of connectivity (Hallquist et al. 2013). Despite this, the DMN has been consistently identified in subsequent studies (Damoiseaux et al. 2006; De Luca et al. 2006; Smith et al. 2009) suggesting a strong degree of credibility and an underlying biological origin.

The DMN is a task-free network (TFN) exhibiting spontaneous correlated activations at low frequencies (<0.1Hz). It has proven to be of great interest due to its simplicity and potential applications to the clinical environment which has led to a plethora of research studies. This is evident in studies showing TFNs affected by Alzheimer ’s disease (Rombouts et al. 2005; Sorg et al. 2007) and ADHD (Uddin et al. 2008; Konrad et al. 2010), two clinical groups in which task based paradigms are highly challenging. Pursuit of mapping the DMN has led to the discovery of other TFNs (Damoiseaux et al. 2006; De Luca et al. 2006; Smith et al. 2013) as well as task specific networks.

Alterations in TFNs have been observed in autism (Assaf et al. 2010), schizophrenia (Whitfield-Gabrieli et al. 2009) and depression (Greicius et al. 2009). It is also important to note in many of these populations, participants exhibit increased head motion and other physiological confounds which may influence the measure of connectivity. Whilst effects of motion and physiological noise are minimised they cannot be entirely ruled out, as such the perceived connectivity change may not be entirely neuronal in origin.

2.2 Challenges in the data

Here we will discuss some of the challenges involved in preparing fMRI data for functional connectivity analysis. Task-free fMRI has a low signal to noise ratio and is susceptible to physiological effects and motion artefacts which can strongly influence connectivity measures; introducing spurious connections or resulting in overly optimistic connection strength. To combat these confounding effects, images often require several post processing steps in order

to minimise the non-BOLD contribution to estimation of connectivity strength. However, the optimal processing pipeline has been hotly contested within the literature.

Band-pass filtering with a pass band in the range of ~0.01Hz – ~0.1Hz is a widely used processing step for connectivity analysis. This has the effect of minimizing the contribution of low frequency confounds such as scanner drift and higher frequency physiological noise such as respiratory (~0.3Hz) and cardiac noise (~1Hz) (Biswal et al. 1995; Birn et al. 2006; Chang et al. 2009). Further support for band-pass filtering is present in recent work which has looked at performing group comparisons. It has been demonstrated that connectivity, primarily at frequency bands in the range of 0.03-0.11Hz provides robust distinctions between cognitive states corresponding to movie viewing and rest (Richiardi et al. 2011). However, discriminating information was present in frequencies up to 0.23Hz suggesting the standard band pass frequency range may be overly conservative. Higher frequency bands (>0.23Hz) were not found to significantly contribute to group comparisons, it was suggested the signal in this range is predominantly noise associated with the HRF, alternatively it may be this range was not sensitive to change in the experimental conditions.

Due to the low sampling rate of fMRI, usually two seconds (approx.), the effects of physiological noise are not completely removed by filtering; cardiac noise has been shown to alias into lower frequency bands (Lund et al. 2006). This has motivated further physiological correction algorithms such as retrospective image correction (RETROICOR)(Glover et al. 2000) and respiratory variations (RV) and heart rate correction (RVHRCOR)(Chang et al. 2009) which attempt to model the cardiac and respiratory signal and regress them from the data. These methods have been shown to reduce vascular related BOLD variations (Glover et al. 2000; Khalili-Mahani et al. 2013). Studies which do not perform specific physiological correction but rather apply global signal regression or regress out the cerebrospinal fluid (CSF) and/or white matter (WM) signal have identified similar consistent resting-state and task positive networks (Damoiseaux et al. 2006; De Luca et al. 2006). This raises questions regarding the necessity of physiological correction for identifying connectivity patterns. Furthermore, it is unclear whether it is correct to treat these physiological signals as noise, especially in the case of pharmacological imagining where cardiovascular effects may be an important aspect of the drug profile (Iacovella et al. 2011; Khalili-Mahani et al. 2013).

Standard connectivity pre-processing steps include regressing out non-BOLD signal, specifically motion parameters and mean CSF and WM signals, using linear regression. Furthermore, changes in the global BOLD signal are generally considered a nuisance parameter and are often removed using linear regression, however it is unclear whether the global signal is principally neuronal or not. A comparison of these processing procedures reveals linear regression of

motion parameters, CSF and WM parameters increases connectivity specificity; the addition of global signal regression was found to double this specificity (Weissenbacher et al. 2009). Whilst regressing CSF, WM and motion parameters are considered good practise, there is much debate about the use of global signal regression. The global signal contains not just noise, but BOLD signal as well, regression will remove nuisance confounds in addition to a portion of the signal of interest. Furthermore, regressing the global signal results in the mean of the distribution of connection strengths centring around zero, artificially creating negative correlations (Murphy et al. 2009). These negative correlations are not uniformly distributed but will vary regionally based on the unknown underlying connectivity structure (Saad et al. 2012). While there may be a neural origin of anti-correlated networks in the brain as suggested in (Fox et al. 2009); data for which global signal regression has been applied should not be considered evidence for the existence of these anti-correlated networks. Moreover, results of studies using global signal regression which report anti-correlations should be carefully interpreted with the caveat that these anti-correlations may be an artefact of the processing rather than biologically motivated (Weissenbacher et al. 2009).

The correct procedure for motion regression has also been the subject of contention within the literature. Head motion is estimated using the realignment parameters obtained during standard pre-processing, regressing these estimated motion parameters from the time-series data reduces the effect of spurious activations observed due to motion (Friston et al. 1996). At the most basic level, motion is represented by a spatial and a rotational parameter for each of the three spatial axis. Recent studies have suggested only regressing these six parameters is sub-optimal for removing motion related artefacts (Power et al. 2014). It has been shown that inclusion of the temporal derivatives and squares of the motion should also be regressed to reduce the effect of inter-session variance explained by motion (Lund et al. 2005; Satterthwaite et al. 2013).

This procedure of motion correction, while providing superior reduction of motion effects, may also reduce the signal of interest. Furthermore, it has been shown that head motion is related to signal changes in brain regions and networks (Pujol et al. 2014). It has also been asserted that regressing the motion will also remove additional variance at random which may contribute to the interesting “signal” under investigation (Bright et al. 2015). Bright demonstrates a worrying similarity between spatial connectivity patterns in motion regressed data and the noise removed, this may suggest established resting state connectivity patterns may be in some part artefactual. However, Bright also shows established connectivity patterns occurring using in the noise variance for data regressed with randomised noise parameters suggesting that applying any set of noise regressor may leave the same spatial structure in both the noise and cleaned

components. Interestingly Bright also shows that inclusion of additional nuisance regressor to the basic 6 parameter model does not account for more variance than randomised parameters. It must be noted that this work was performed with only 160 time points, as such more complex regressor models have may have a greater effect when considering longer acquisitions. Overall the choice of motion regression procedure remains a complex issue requiring careful consideration dependent on the length of the data acquired and the experimental procedure.

A promising alternative to multiple processing steps is the use of multi-echo echo-planar imaging (EPI). It has been demonstrated that independent component analysis (ICA) applied to multi-echo EPI data can effectively separate BOLD and non-BOLD components of the data (Kundu et al. 2012) potentially offering an alternative to multi-stage post-processing. However removing all neurovascular effects may be counterproductive for pharmacologic imaging as these effects may be related to the administered compound and potentially provide insight into compound effects.

2.3 Methods of functional connectivity analysis

Traditionally, functional connectivity in the human brain has been studied using one of two approaches, either blind source separation methods such as Independent Component Analysis (ICA) or a graph theory based methodology. While these methods are dissimilar in their execution, they have been shown to yield similar results (Beckmann et al. 2005; Bluhm et al. 2008; Van Dijk et al. 2010) suggestive of a consistent underlying connectivity structure.

Blind source separation provides a model free method for investigating whole-brain patterns of connectivity. Several different methods have been applied to connectivity such as principled component analysis (PCA)(Friston et al. 1993) and ICA (Damoiseaux et al. 2006; Calhoun et al. 2012) which is by far the more prevalent method showing high levels of consistency across studies. ICA provides an elegant solution for identifying spatially (McKeown et al. 1998) or temporally (Biswal et al. 1999) independent regions without prior knowledge of the data. In the presence of structured noise ICA is robust (Thomas et al. 2002) and has been demonstrated to reliably identify consistent networks across multiple studies (Biswal et al. 1999; Beckmann et al. 2005). ICA can be performed at the voxel level and provides an intuitive view of brain connectivity, identifying independent networks. Furthermore it is possible to see the weights of each spatial component in the temporal domain making ICA an attractive and versatile method of connectivity analysis.

One of the limitations of ICA is the need to select the number of components to extract. It is considered good practice not to compress the data too much, ideally maintaining the majority

of the information in the original data (e.g. 99% of the variance). This however can result in an impractically large number of components. Several heuristics can be applied to select the optimal, but not the minimal, number of components; these include the Akaike's information criterion (Akaike 1981) or the Bayesian information criterion (Schwarz 1978). Once extracted, meaningful components must be identified from the noise components, this is often performed visually. The biological validity of components may be ambiguous; as such it is possible meaningful components are excluded whilst noise may be retained.

Traditionally ICA applied to brain imaging has been interpreted using a single pass. However, given the fact that many implementations of ICA are stochastic and results may differ between multiple runs and are dependent on random sampling of the data. As such, the output of a single run should be treated with due consideration. A solution to these issues considered good practise (and readily accessible through the software package ICASSO) is to perform multiple runs of an ICA with differing parameters; by clustering results it is possible to statistically assess the reliability of independent components (Himberg et al. 2004).

An additional consideration for ICA is the association of significance levels to thresholded maps (Ma et al. 2007). ICA component maps are converted to z-scores as described in (McKeown et al. 1998) however these IC maps are not normally distributed and as such this conversion can result in a slightly overestimated false positive rate (Ma et al. 2007). Furthermore, when interpreting networks obtained by ICA, it is necessary to set a significance level which is often arbitrary and may potentially ignore network members. These ICA networks assume a uniform (binary) network topology and do account for varying connection strengths between network members.

Graph theory is the other commonly applied methodology for network analysis. This technique models connectivity between regions as graphs. Regions are modelled as graph vertices and edges inferred based on the temporal coherence between regional time courses. The use of graph theory can be said to encompass a spectrum of methods, the most straightforward and prevalent amongst them is seed based analysis (Biswal et al. 1995; Cordes et al. 2000). In this analysis a graph is computed from the relationship between every brain region and an *a priori* defined seed region, providing a robust means for hypotheses testing on the connectivity effects of a specific regions. This however, is blind to regional couplings not directly connected to the seed regions, unlike ICA which provides a whole-brain perspective on connectivity. Similar to ICA these seed based connections must be arbitrarily thresholded to facilitate interpretation which may result in an overly optimistic or conservative view of network effect. This technique is well suited to hypothesis testing and has been shown to perform well in assessing the connectivity effects to a region of interest (Ebisch et al. 2011; Scheidegger et al. 2012). Independent statistical

tests are then performed on each connection to assess significance, due to the high dimensionality of the data multiple comparisons testing should be performed. In practice this has the result of potentially reducing sensitivity and makes the use of many seed regions prohibitive as #voxels x #seed tests are required.

Rather than mapping connectivity to a single region, as with seed based analysis, it is possible to use graph theory measures to produce summary statistics of the connectivity of each region with the rest of the brain (Buckner et al. 2009). This circumvents the limitation of seed based analysis for investigating multiple seeds as only #voxel independent tests are required to access significance across the whole brain. These types of measures, often referred to as node-wise measures, have been used to study a range of connectivity effects for controls and disease populations (Lohmann et al. 2010; Lynall et al. 2010; Zhang et al. 2011). These analyses reveal whole brain connectivity effects and provide a great deal of flexibility allowing for the use of a range of metrics to investigate different network properties, however they are naïve to localised regional coupling effects which may describe key network effects. In a similar manner to node-wise measures, connectivity can be further abstracted to represent aspects of network connectivity as a single measure (Supekar et al. 2008). This allows for a high level comparison of connectivity traits, such as network efficiency and density (Rubinov et al. 2010), however these measures do not provide any insight into localised network or mechanistic effects. Furthermore, it is generally not possible to confidently attribute changes in this single summary statistic of an entire network to a group or task effect rather than one of many possible confounds.

A common approach to reduce the dimensionality and to improve interpretability is to parcellate the data into functionally or structurally homogenous regions. The signal from all voxels within each parcellated region is averaged and used as a node within the graph analysis. This dimensionality reduction allows for statistical testing on the edges between all nodes, allowing for interrogation of connectivity effects between all brain regions (Honey et al. 2007; Lynall et al. 2010). Summary node-wise metrics can also be applied to the parcellated brain regions allowing for the group comparisons to be performed based on regional connectivity effects (Lord et al. 2012). Parcellation allows for the whole brain connectivity analysis, identifying localised and regional coupling effects. However, it also introduces challenges in terms of defining regions. For group comparisons there is no guarantee that the same regions are consistent between groups. Furthermore, the results of connectivity analyses can vary depending on the scale of the parcellation scheme used (Craddock et al. 2012) further confounding the methodology.

Thus far we have discussed methods of representing the connectivity in the brain, most significance testing is performed using mass-univariate tests performed on individual edges or

measures or regional connectivity. This imposes an assumption of independence between regions, however network members by their very definition are not independent. More recent studies have applied multivariate pattern recognition methods, increasingly used for fMRI analysis (Mourao-Miranda et al. 2005; Ryali et al. 2010) to functional connectivity analysis to investigate cognitive states (Richiardi et al. 2011; Shirer et al. 2012) and disease populations (Chen et al. 2011; Lord et al. 2012; Richiardi et al. 2012; Zeng et al. 2012). This change from a univariate approach to a multivariate one was a significant development in connectivity analyses. These approaches are data-driven, sensitive to the spatial covariance of the data and produce single outcome measures providing greater sensitivity and avoiding issues of multiple comparisons. Furthermore, these techniques allow for predictions of class membership at the subject level, highly relevant for clinical applications. However, these methods are limited to group comparisons, and are unable to identify significant patterns of activations for a single group only.

An additional limitation of this approach is interpretability; classifications using graph edges will have N(N-1)/2 features, where N is the number of graphs nodes. A coarse granularity whole brain atlas has around 90 nodes, resulting in 4005 edges which can prove challenging to interpretation. In order to aid interpretability, feature sparsity can be introduce to reduce dimensionality. Shirer et al (2012) induced sparsity prior to classification through thresholding, however this imposes a univariate assumption on a multivariate dataset. Applicable alternate approaches are the use of threshold consensus functional connectivity (Dosenbach et al. 2010; Zeng et al. 2012) or permutation testing to remove connections which don't significantly contribute to group discrimination (Richiardi et al. 2012). These have been shown to yield interpretable maps in a principled manner however still require the setting of arbitrary thresholds or significance levels.

Interrogating the network structure of the brains functional connectivity offers an alternate perspective on the modular organisation of the brain. There has been much interest in functional connectivity at a network level. As discussed earlier, several consistent resting-state and task positive networks have been identified. These networks are shown to exhibit altered configurations for disease states (Greicius et al. 2004; Uddin et al. 2008; Assaf et al. 2010; Luo et al. 2011) and pharmacological interventions (Nagano-Saito et al. 2009; Minzenberg et al. 2011). These networks have been primarily detected using ICA, however graph theory provides an alternative perspective on the modular organisation of brain networks through the use of community detection algorithms. The most commonly applied form of community detection applied to functional connectivity is Newman's modularity metric (Newman et al. 2004). This measure has been used to identify the effect of depression (Lord et al. 2012) and aging (Schwarz

et al. 2008) on the community structure of the brain. The other form of modularity detection which is gaining popularity is the random walker algorithm (Rosvall et al. 2008), this has also been applied to functional connectivity in the brain revealing an underlying modular structure (Power et al. 2011). In a qualitative comparison of methods the random walker method was shown to outperform Newman's method (Lancichinetti et al. 2009). While this is an excellent step toward evaluating the best practice in modular connectivity analysis, the benchmarks used involve simulated networks which while informative are not representational of the biological networks in the brain, as such further work is required.

The use of community detection allows for partitions of connectivity to be identified, resulting in a topological network view similar to spatial ICA. Unlike ICA the number of modules is not required *a priori*, furthermore modules can be related back to the original graph providing measures of regional coupling, intra and inter module connectivity (Meunier et al. 2009). Furthermore, compared to ICA, graph theory provides greater flexibility in terms of a diverse range of measures available, different connectivity scales and applicable group comparison methods. However, Graph theory is more susceptible to structured noise and is unable to simply replicate the dynamic network view ICA provides.

Investigation into the network topology of the brain has revealed consistent network structures and communities. Whilst this provides some insight into the mechanisms and organisation of the brain, it also raises questions on how these networks interact. A naïve approach is to correlate the average signal between known networks (Jafri et al. 2008; Deco et al. 2011), similar analysis has revealed the effects of psilocybin on the coupling between the DMN and the salience network (Carhart-Harris et al. 2013). This principle can also be applied to community structures identified through graph theory to reveal sub-graph interactions (Deco et al. 2011). These investigations into network interactions provide insight in brain function, however are based on the supposition of network homogeneity. This assumes networks are uniformly and completely connected and does not account for a variable relationship between networks. Furthermore, overlapping networks will share a common signal which will strongly influence the measured relationship between two networks. Thus far, no principled methodology has been developed to address these issues.

2.4 Network Dynamics

Typically it has been assumed the connection strengths between regions is constant during the resting-state, this has the effect of dramatically reducing the complexity of connectivity analysis. As such, traditional methods used to analyse connectivity are naive to temporal dynamics. These include spatial ICA (Calhoun et al. 2001) which does not account for network changes over time

and seed based analyses which obtain a single correlation value for regional connections by correlating regional signals for the entire acquisition length (Biswal et al. 1995).

Changes in the pattern of regional couplings have been shown to occur in long time scales (> days-years) such as in development (Uddin et al. 2011) and aging (Dosenbach et al. 2010); macro time scale, in the order of hours, where consistent resting state networks are effected by learning (Sun et al. 2007) and cognitive load (Esposito et al. 2006). More recent work has demonstrated that network dynamics are present in the resting state networks, occurring over the course of a single scan (Chang et al. 2010; Kiviniemi et al. 2011; Hutchison et al. 2012).

Investigating these spontaneous fluctuations in the resting state presents challenges such as inter-subject variation, the lack of ground truth and the unpredictable nature of the network change. Most studies investigating these dynamic connectivity changes have used the sliding window approach to investigate changes in estimated connections over the length of the acquisition (Kiviniemi et al. 2011; Hutchison et al. 2012; Allen et al. 2014). In effect, this acts as a low pass filter for network changes, where increasing the window length reduces the pass band (Leonardi et al. 2015). In this approach a window, usually boxcar or possibly tapered, is passed over the entire acquisition in pre-defined increments, data within the window is then used to evaluate the connectivity for each window position. This requires the *a priori* definition of the window length and increment parameter. This can lead to issues if the window length is too small, introducing spurious connections and lowering the SNR, or too long and thus insensitive to network temporal dynamics. It has been reported that network states stabilise at ~4min (Van Dijk et al. 2010); moreover, it has been demonstrated window lengths of >30 seconds are sufficient to identify robust network effects (Shirer et al. 2012). It is important to note however the SNR decreases as the window length decreases (Van Dijk et al. 2010), while the overall variability in estimated connections increases (Hutchison et al. 2012). In effect there is little concurrence within the literature on the optimal window length for dynamic connectivity analysis, however, empirically lengths of 30sec – 4min have been shown to produce robust results. While many studies use a single length, others have demonstrated connectivity dynamics over a range of window lengths providing a more comprehensive view of network dynamics (Hutchison et al. 2012).

The sliding window approach estimates each graph independently of each other, as such there is no constraint on temporal homogeneity between temporally adjacent graphs. Pio Monti et al (Pio Monti et al. 2013) has suggested a modification of the sliding window approach for estimating sparse graphs at a high temporal granularity whilst enforcing dependency between temporally adjacent windows. The window length and measure of sparsity are set using a tuning

parameter. As such graph estimation can be optimised based on a criterion rather than arbitrarily selected, providing a more principled method for estimating temporal graphs.

Estimation of temporal connectivity has enabled the investigation of network changes over time, however methods for modelling and testing theses dynamic effects are lacking. Generally, studies examine the spatiotemporal variability of connections during the resting state (Chang et al. 2010; Kiviniemi et al. 2011; Liu et al. 2013) reporting various cortical areas exhibiting high and low stability across the whole brain, in relation to stable networks. More recently clustering has been applied to windowed network matrices identifying reoccurring stable network states (Allen et al. 2014) suggesting the DMN is a modular network state and with dependant probabilities of state transitions. This work represents a transition to a principled analysis of network dynamics as opposed to the traditional static view of connectivity, however further development is needed for the identification of network structures and metrics sensitive to temporal variations.

Temporal community detection is a promising new area of dynamic network analysis, this type of analysis seeks to identify evolving communities over time. A popular approach for investigating temporal communities is to identify communities within each instance of the temporal network and to match them across instances (Palla et al. 2007; Rosvall et al. 2010). However methods for static community detection are very sensitive to changes in the network and may result in the poorly or mis-matched communities. An alternative is to use multi-slice community detection (Mucha et al. 2010; Liu et al. 2013) where the temporal domain is included within the community identification algorithm in order to enforce consistency between communities at each graph instance over time. One such approach to multi-slice community detection is estrangement confinement (Kawadia et al. 2012) which has been empirically shown to outperform graph matching for identifying temporal communities. These forms of analysis offer a promising means of identifying evolving brain networks however has yet to be applied to functional connectivity in the brain.

While spatial ICA can be applied using the sliding window approach (Kiviniemi et al. 2011), it is possible to investigate temporal dynamics using a purely ICA approach, thus avoiding the need to select a window length. Temporal ICA can be applied to patterns of regions identified using spatial ICA (Smith et al. 2012). This reveals patterns of temporally independent network modes, referred to as temporal functional modes (TFMs). While this provides an elegant means for investigating modes of brain function it is noted that it is fundamentally less stable than spatial ICA and seed based analysis. This is due the lack of sampling in the temporal domain compared to the spatial, in which the number of voxels is many times greater than the number of volumes.

Chapter 3: Methodological background

In this chapter we will provide a brief overview of methods used within this thesis for mapping the functional connectivity of the brain. Specifically, we introduce graph theory measures for connectivity analysis, statistical tests and the pattern recognition techniques applied to assess functional connections. The functional connectivity (FC) of the brain, as estimated from temporal similarity of fluctuations in the blood-oxygen-level dependant (BOLD) signal, can be examined using a variety of approaches, some of which will be explored in this thesis. We also provide an introduction to pattern recognition techniques and their application to neuroimaging.

3.1 Functional Connectivity Analysis

There are two categories of connectivity analysis within the field of neuroimaging, structural and functional connectivity analysis. Structural analysis is primarily concerned with the mapping of anatomical white matter tracts using methods such as diffusion imaging (Gong et al. 2009). This type of analysis infers connectivity between regions through their physical connections with each other and has promising applications in the study of stroke (Moller et al. 2007; Schaechter et al. 2008), trauma (Niogi et al. 2008), and disease groups (Concha et al. 2005; Catani 2006; Lin et al. 2007). Structural connectivity is effectively a 'bottom up' approach, for further information regarding tractography and diffusion imaging we refer the reader to the review (Ciccarelli et al. 2008). In contrast, FC is top down approach which infers connectivity through similarity of perceived brain activity. This thesis is primarily concerned with the study of function connectivity. While there are many approaches to FC analysis, here we consider a branch of methods generally known as graph theory.

3.2 Basic Graph Theory

Graph theory is a mathematical framework used to model the relationships between objects as a graph, such as in Figure 4. Objects are represented as *nodes* or *vertices* in this graph and their relationship as *edges* connecting each vertex. Formally a graph can be described as $G(V, E)$ where V and E are sets of vertices and 2-element edges respectively.

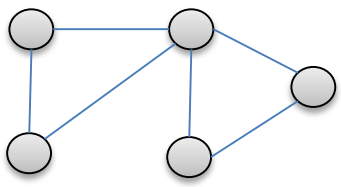

Figure 4 - Example of a graph model of 6 vertices (circles) connected by 6 edges (lines)

Graphs are most commonly represented through adjacency matrices, ***A***, as shown in Figure 5, allowing for compact intuitive representations of large complex networks. Elements in these matrices represent the connection strengths between nodes, denoted by the element's row and column indices. Graphs can be *directed* or *undirected*, a directed graph is asymmetric and denotes a causal relationship between a vertex pair through the use of directional edges. Undirected and symmetric graphs signify only that a connection exists between a vertex pair. Additionally, graphs can also be described as *weighted* or *binary*. A binary graph has edges with values of either 1 or 0, denoting the presence or absence of an edge between a vertex pair. Weighted graphs however, inform the strength of connection between nodes, edges can take any value usually between 1 and 0, although inverse relationships can be depicted using negative weights $\in \{-1, 1\}$. Binary graphs are often preferred due to their computational simplicity and ease of interpretation and are often obtained by thresholding weighted graphs. For highly connected biological systems such as the brain, weighted networks are generally deemed more appropriate.

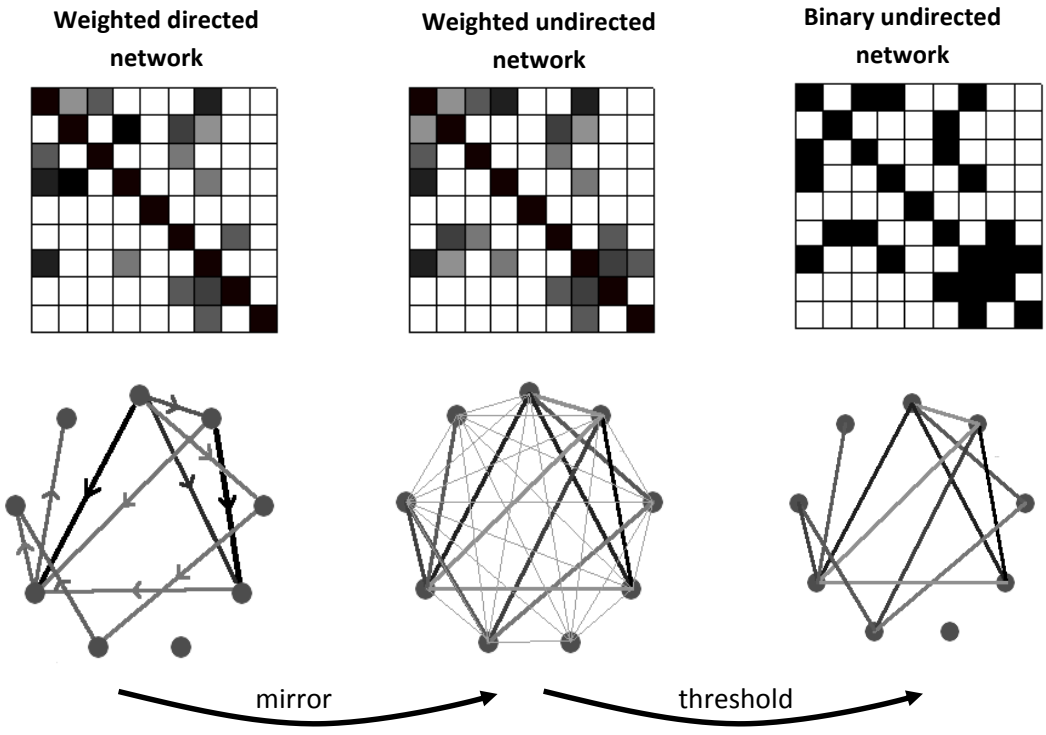

Figure 5 - Example of adjacency matrices and graph structure for a weighted directed network, a weighted undirected network and binary undirected network.

In the context of connectivity analysis using neuroimaging data, nodes represent anatomical regions of the brain and edges either the perceived connection due to similarity in temporal activation or the anatomical connection inferred through density or coherence of white matter tracts.

The definition of nodes based on brain regions is a crucial step to functional connectivity analysis. There are two approaches commonly applied in functional connectivity analysis relating to node definitions, namely the seed based approach and the whole-brain approach. The former refers to a type of hypothesis testing analysis. A region, or collection of regions, are selected *a priori* as *seeds*, graphs are then constructed based on the relationships between all brain regions (usually voxels) and these seed regions. This results in an asymmetric graph of low dimensionality in one direction and very high dimensionality in the other (Uddin et al. 2009).

The whole brain approach aims to generate a graph which contains all relationships between all brain regions. Due to the high dimensionality of neuroimaging data, in the order of hundreds of thousands of voxels, it is often not feasible from a computational point of view to construct this graph in a voxel-wise manner; Instead dimensionality reduction is undertaken by grouping either functionally or topologically homogenous voxels together in larger regions to use as nodes.

3.2.1 Graph Estimation

Graphs are generally constructed based on measured temporal similarities in regional time series. Through measuring the similarity between a pair of brain regions we infer the strength of the connection. Here we provide a brief overview of several commonly used methods for graph estimation.

Parcellation

Depending on the analysis being performed, parcellation may be a necessary step in order to reduce the dimensionality of the data. This is particularly relevant when performing whole-brain connectivity analysis where computation of the connections between voxels, in the order of magnitude of 2e5, is computationally prohibitive.

Parcellation is akin to down sampling, voxels within homogeneous regions are averaged to produce a mean signal for that given region. These regions are then used to define nodes within a graph analysis. In the context of neuroimaging analyses, parcellation is often performed using an atlas to define these homogeneous regions. Atlases can be defined anatomically such as the automatic anatomical atlas (AAL) (Tzourio-Mazoyer et al. 2002), Brodmann (Brodmann 1909) or Talairach atlas (Talairach et al. 1988). Alternatively regions may also be defined by functional homogeneity (Fischl et al. 2004; Craddock et al. 2012). Comparison of atlases reveal no significant differences between anatomical and coarse grain functional atlases (~100-200 nodes) of the same granularity. However, finer grain functional atlases (>~200 nodes) can facilitate more accurate representations of connectivity (Craddock et al. 2012). While finer grain parcellation can offer more accurate estimations of connectivity, this comes at the cost of

interpretability which becomes more challenging with higher dimensionality. The choice of atlas should be informed based on the hypothesis under question and should represent a compromise between interpretability, granularity and functional or structural parcellation.

Correlation

The most prevalent method used in functional connectivity analysis is Pearson's correlation coefficient (Biswal et al. 1995; Assaf et al. 2010; Hutchison et al. 2012). This is an attractive method as it is normalized, $r \in (-1, 1)$, and is sensitive to both phase and amplitude difference between signals. Furthermore, correlation reveals inverse relationships between time series which, if valid, have profound implications in the context of biological systems such as the human brain.

$$r_{xy} = \frac{\sum_{i=1}^{n}(\boldsymbol{x}_i - \overline{\boldsymbol{x}})(\boldsymbol{y}_i - \overline{\boldsymbol{y}})}{\sigma_x \sigma_y} = \frac{\sum_{i=1}^{n}(\boldsymbol{x}_i - \overline{\boldsymbol{x}})(\boldsymbol{y}_i - \overline{\boldsymbol{y}})}{\sqrt{\sum_{i=1}^{n}(\boldsymbol{x}_i - \overline{\boldsymbol{x}})^2 \sum_{i=1}^{n}(\boldsymbol{y}_i - \overline{\boldsymbol{y}})^2}}$$

The correlation between any two nodes can be influenced by other nodes within the network. In order to minimise this effect, partial correlation can be applied to remove the common effects of all other nodes. This allows for the investigation of the relationships between regions, minimising common dependencies between brain regions and has been applied in several FC studies (Marrelec et al. 2006; Marrelec et al. 2007). Minimising common dependencies allows for analysis using direct connections, furthermore the application of regularization can induce sparsity in the adjacency matrices (Monti et al. 2014). By direct connections we refer to a connection which exists directly between nodes rather than through a common dependency, as shown in Figure 6.

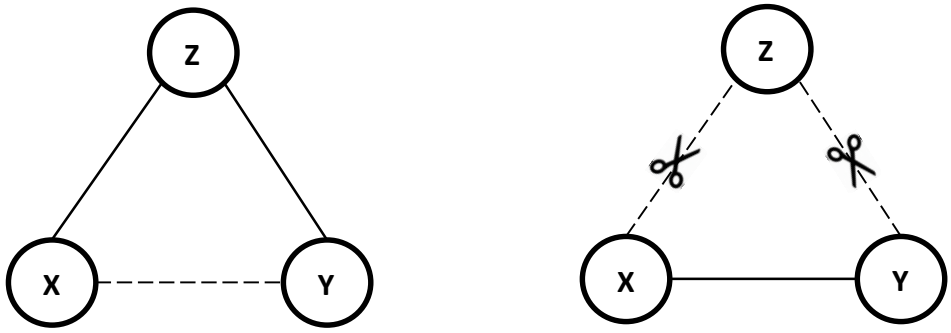

i) In-direct connection between X and Y through Z

ii) A direct connection between X and Y

Figure 6 - Illustration of an (i) in-direct connection where node X and Y are not directly connected but may report a connection through a shared dependency of Z and (ii) direct connection between nodes X and Y with no shared dependancy

Partial correlation is commonly calculated using linear regression or matrix inversion. Linear regression arguably provides the simplest and most intuitive implementation of partial

correlation. The correlation between X and Y, accounting for Z, is calculated by correlating the residuals of linear regression of Z with X and Y respectively:

$$p_{xy} = \frac{N\sum_i^N \boldsymbol{r}_{x(i)}\boldsymbol{r}_{y(i)} - \sum_i^N \boldsymbol{r}_{x(i)}\sum_i^N \boldsymbol{r}_{y(i)}}{\sqrt{N\sum_i^N \boldsymbol{r}_{x(i)}^2 - \left(\sum_i^N \boldsymbol{r}_{x(i)}\right)^2}\sqrt{N\sum_i^N \boldsymbol{r}_{y(i)}^2 - \left(\sum_i^N \boldsymbol{r}_{y(i)}\right)^2}}$$

where r_x and r_y are the residuals of the linear regression of Z with X and Y respectively and N is the number of nodes. This must be calculated for each node pair at a time and can be computationally expensive. Matrix inversion however, allows for the calculation of the partial correlations between all node pairs simultaneously. We define the correlation (or covariance) matrix between all nodes as $\boldsymbol{\Omega} = (\omega_{ij})$ where ω_{ij} is the correlation (or covariance) between nodes i and j, the inverse of this matrix as $\boldsymbol{\Omega}^{-1} = (\widehat{\omega}_{ij})$. The correlation matrix for an undirected network will be symmetric around the diagonal and the inverse will also be symmetric. The diagonal in the inverse, $\boldsymbol{\Omega}^{-1}$, inform the correlation for each node with all other nodes. The partial correlation between any node pair can be obtained using:

$$p_{xy} = -\frac{\widehat{\omega}_{ij}}{\sqrt{\widehat{\omega}_{ii}\widehat{\omega}_{jj}}}$$

This metric can be further modified to induce sparsity, such that only informative connections remain; all other connections are set to zero. This can be achieved using regularization, as discussed later**,** to calculate the inverse matrix $\boldsymbol{\Omega}^{-1}$.

3.2.2 Network measures

Networks can be interrogated in multiple ways through the use of network metrics to extract different aspects of connectivity from graphs. In relation to functional connectivity these measures can be used to assess functional segregation and integration, identify anatomical circuitry within the brain, localise key network hubs and test the modularity of the human brain.

Network measures can be applied at different spatial scales interrogating edge, node, sub-graph and global network effects. These measures often have variants for directed, undirected, weighted and binary graphs. Here we will cover a range of network measures applicable for functional connectivity analysis in the human brain, primarily using weighted undirected graphs.

Path Length

Path length measurements inform the functional integration of a network. The ease with which nodes can communicate is assessed using the shortest path between nodes. Paths between nodes are defined as a sequence of connected nodes across a network which facilitates a flow

of information. Paths with fewer intermediary nodes or strongest connections are assumed to have the greatest functional integration. Shortest paths between nodes in a binary graph are obtained through minimising the number of intermediary nodes. This can be achieved using one of several standard search algorithms such as a breadth-first search. For a weighted graph the shortest path is the one of least resistance, and as such the path with the strongest connections. There several methods which attempt to identify the shortest path in a weighted network (Dijkstra 1959; Yang et al. 2001). In most cases the edge weight is inverted to represent the cost of transmission, such that strong connections have low cost. We note these algorithms do not penalise intermediary nodes, only the final cost of the connection. Therefore the shortest paths may not be those with fewer edges, and as such may not be biologically accurate.

The *characteristic path length* is one of the most commonly used measures of functional integration and is defined as the average shortest path length between nodes (Watts et al. 1998). This measure uses only the average of the shortest path lengths and does not account for multiple paths between nodes. As such it may not accurately reflect the true integration of a network.

Node Centrality Measures

Network measures of centrality assess various criteria of individual nodes. These are particularly informative when considering hubs which communicate with many other nodes and are usually anatomically significant.

The most basic and commonly used graph vertex measure is the node strength (NS), occasionally referred to as *degree centrality*. This is a node measure which reflects the 'connected-ness' of a node, which is interpreted as its importance within a network. For a binary network it is simply the number of connections on a given node. For a weighted graph this becomes the sum of the weights of all connections on a node.

$$NS(i) = \sum_{j}^{N} a_{ij} \qquad (3.2.1)$$

here a_{ij} is the adjacency between nodes i and j and N is the number of nodes. For networks which aren't fully connected it may be necessary to normalize node NS values by the number of connections on each node to account for varying connected-ness of nodes.

$$NS(i) = \frac{1}{N}\sum_{j}^{N} a_{ij} \qquad (3.2.2)$$

NS is often used as a measure of network density and can used to calculate the strength distribution which is simply the distribution of NS across all the nodes in the network. Both the density and node strength distribution can heavily influence other network measures and are commonly used for null hypothesis testing. One of the most common tests of topological significance is to compare a network against a graph of the same size, density and distribution but random topology (Rubinov et al. 2010).

Network density is a measure of the overall connectedness of a graph. It is the ratio of possible edges to actual edges. For a complete graph this is effectively the average node strength of all nodes within a graph.

Betweenness centrality (BC) is another measure of node importance within a network, arguably more informative than NS. It is a measure of how important a node is for information routing through a network. The BC of a node is given by the proportion of shortest paths between node pairs that pass through a given node, formally:

$$BC(i) = \frac{1}{(N-1)(N-2)} \sum_{\substack{h,j \\ h\neq j, h\neq i, j\neq i}}^{N} \frac{\rho_{hj}(i)}{\rho_{hj}}$$

where ρ_{hj} denotes the number of shortest paths between node *h* and *j*. The number of shortest paths that pass through node i is given by $\rho_{hj}(i)$. When applied to neuroimaging, this measure is weighted toward subcortical structure and hub structures rather than cortical regions which are not present in the majority of shortest paths.

Local efficiency (LE), is another measure concerning the importance of a node for the transmission of information between vertices within a network. The LE coefficient for a node is related to the cost of transmitting information between a vertex pair through a given node. Rubinov et al (2010) define the efficiency of a node for a weighted network as:

$$LE(i) = \frac{1}{2} \frac{\sum_{j,h,j\neq h}^{N} \left(a_{ij} a_{ih} \left[\rho_{jh}^{a}(N_i) \right]^{-1} \right)^{\frac{1}{3}}}{NS_i(NS_i - 1)}$$

where $\rho_{jh}\ (N_i)$ is the shortest path between the nodes j and h which includes only neighbours of node i. The strength of node *i* is define as $NS_i$and the connection between nodes j and h as defined by the adjacency matrix is indicated by a_{ih}.

The *Clustering Coefficient* may be calculated for multiple levels of a network, in relation to an individual node, it is a measure of node segregation and quantifies the level of clustered connectivity around a node. More generally it is a measure which assesses tendency of nodes

to group together, providing a value of *clique-ness* for a single node and its neighbours. The clustering coefficient of a single node is defined as:

$$C(i) = \frac{1}{n}\sum_{i}^{N}\frac{2t_i}{DC_i(DC_i - 1)}$$

A triangle is defined as a closed loop of three nodes each interconnected by an edge. Here, the t_i is the number of triangles around node i, and for a binary network is defined as:

$$t_i = \frac{1}{2}\sum_{j,h,j\neq h}^{N} a_{ij}a_{ih}a_{jh}$$

in a weighted network this becomes:

$$t_i = \frac{1}{2}\sum_{j,h,j\neq h}^{N} (a_{ij}a_{ih}a_{jh})^{\frac{1}{3}}$$

A measure of segregation across a network can be expressed using the average clustering coefficient which reflects the average amount of connectivity clustered around nodes. For information regarding other graph theory metrics, we direct the reader to (Rubinov et al. 2010).

Global network measures

Networks can be summarised using global measures which assess aspects of the network as a whole and can facilitate a high level comparison between networks. (Supekar et al. 2008; Deuker et al. 2009). Aspects of a network are expressed using a single value and may provide some insight into a general effect of an experimental condition (eg reduced average connectivity for a compound). However, these measures are topologically insensitive and may ignore finer scale mechanistic effects. Furthermore, as average measures, global statistics are sensitive to strong values skewing results. Interpretation of these global values can also be challenging, as effects can be driven by multiple sources it can therefore be difficult to confidently attribute an effect to a given cause.

The functional integration across an entire network or *global efficiency* is defined to be the average inverse shortest path length. This can be interpreted as the average cost of transmitting information across the network, formally (Rubinov et al. 2010):

$$E = \frac{1}{N}\sum_{i}^{N}\frac{\sum_{j,j\neq i}^{N}(\rho_{ij})^{-1}}{N-1}$$

where ρ_{ij} is the shortest path between node i and j. This is effectively the average normalised efficiency across all nodes within a network. The global efficiency relates the average ease of transmission across a network.

Another commonly used global measure within the neuroimaging literature is *Small Worldness*. This measure relates to the topology of connections between nodes. A small world network has a short average path length between any two nodes, similar to a random network but exhibits a high level of clustering (Watts et al. 1998) as shown in Figure 7.

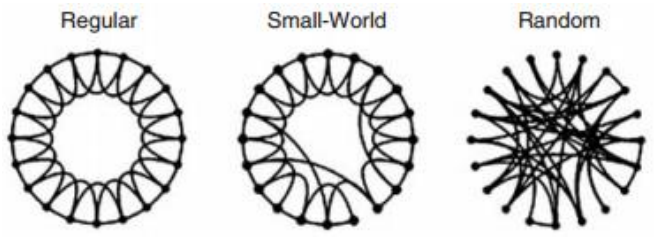

Figure 7 - Illustration of network organisation from (Watts et al. 1998)

Specifically, small-worldness as proposed by (Humphries et al. 2008) captures the statistical measure of simultaneous functional integration and separation within a network as given by:

$$S = \frac{C/C_{rand}}{L/L_{rand}}$$

Where C and C_{rand} are the clustering coefficients for the network under investigation and a network with the same size and density but random topology. L and L_{rand} represent the characteristic path lengths of the network to test and a random network respectively. A typical small world network will have a larger number of hubs and small interconnected clusters where most nodes in the small world network are connected by a shortest path.

Small worldness measures have been applied to neuroimaging and have demonstrated sensitivity to disease state (Micheloyannis et al. 2006; Stam et al. 2007) as well as informing brain organisation (Achard et al. 2006; Bassett et al. 2006), however interpretation of small worldness was found to vary across studies.

Sub-graph Measures

A graph may contain sub-graphs (self-contained circuits within larger networks) examination of which can be highly informative in the understanding of network mechanics. These self-contained *sub-graphs* can be defined in several different ways. A complete, independent sub-graph where all nodes are mutually connected is defined as a *clique*. More formally a clique is a subset of G, such that each node pair in the clique C is connected by an edge. Communities are more flexible definitions of sub-graphs. The community structure of a graph generally refers to

the partitioning of vertices, such that each vertex belongs to a community. Furthermore, it is not necessary for communities to be complete, where each node is mutually connected within the community, or non-overlapping. An example of a clique and community structure within a graph is shown in Figure 8.

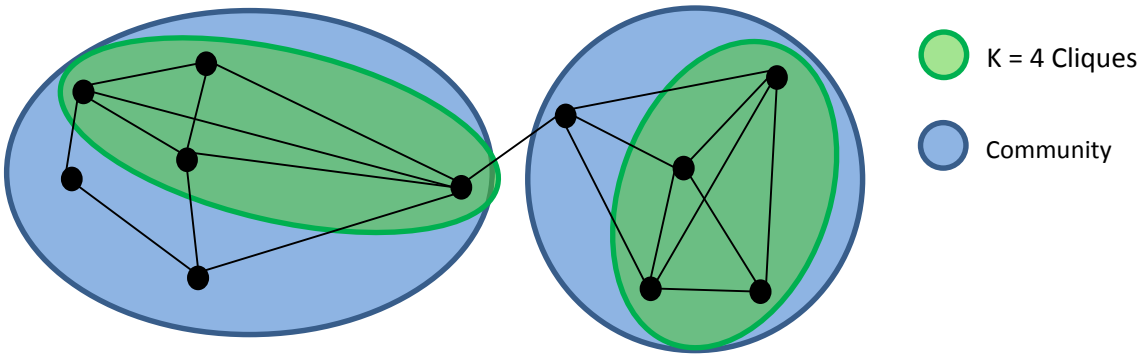

Figure 8 - Illustration of k = 4 clique and community structure within an exemplar graph. Cliques (of four nodes) are represented in green and communities in blue

This thesis will explore the use of community detection to identify communities, clusters or modules within a graph. There are several methods for community detection, though modularity maximisation introduced by Newman et al (Newman 2006), is the most prevalent. In direct comparison to other methods, optimizing modularity over possible partitions was found to outperform other forms of community detection in many situations (Danon et al. 2005). The modularity parameter Q, defined by Newman, is given as:

$$Q = \frac{1}{4m}\sum_{i,j}^{N}\left(a_{ij} - \frac{DC_i DC_j}{2m}\right)\cdot\delta(l_i, l_j)$$

where m is the total weight of the network $m = \sum_{i,j=1}^{N} a_{ij}$, l_i and l_j refer to the module membership labels of node *i* and *j*. Here, δ represents Kronecker's delta, where $\delta(l_i, l_j) = 1\ iff\ l_i = l_j$ and 0 otherwise. The value of Q relates to how well the partitioning of nodes describes the community structure of a given graph. The most commonly used algorithm for modularity optimisation is the Louvain method (Blondel et al. 2008). This greedy agglomerative algorithm is an iterative two stage approach. The data is initialised such that each node is assigned to a unique community. In the first stage of the algorithm, vertices are re-assigned to a community based on the largest gain in modularity, ΔQ. The second phase of the algorithm re-formulates the network such that communities found in the first stage are represented as nodes in a new graph. At this point the algorithm iterates until no improvement to the overall modularity can be made.

3.2.3 Windowing

Real-world and biological networks can exhibit temporal dynamics. This is particularly pertinent to neuroimaging where recent work has demonstrated the non-stationary of resting state networks (Chang et al. 2010; Deco et al. 2011; Hutchison et al. 2012; Allen et al. 2014). Sliding windows have been applied to the estimation of connectivity allowing for analyses to account for these temporal dynamics (van den Heuvel et al. 2010; Kiviniemi et al. 2011).

In this approach, a moving window of length L, is applied to the time-series data of each node. Convolving the window with the node signal results in a truncated time-series representing the activity of a node for the temporally discrete period, defined by the window position. The connectivity between all node pairs is estimated using these truncated time series, resulting in a connectivity graph for the window position. The window is then incremented to its next position and the process is repeated. This results in a collection of connectivity matrices, referred to as a multi-slice graph, representing the connectivity in discrete periods over the length of an acquisition. A visual representation of this process can be found in Figure 9.

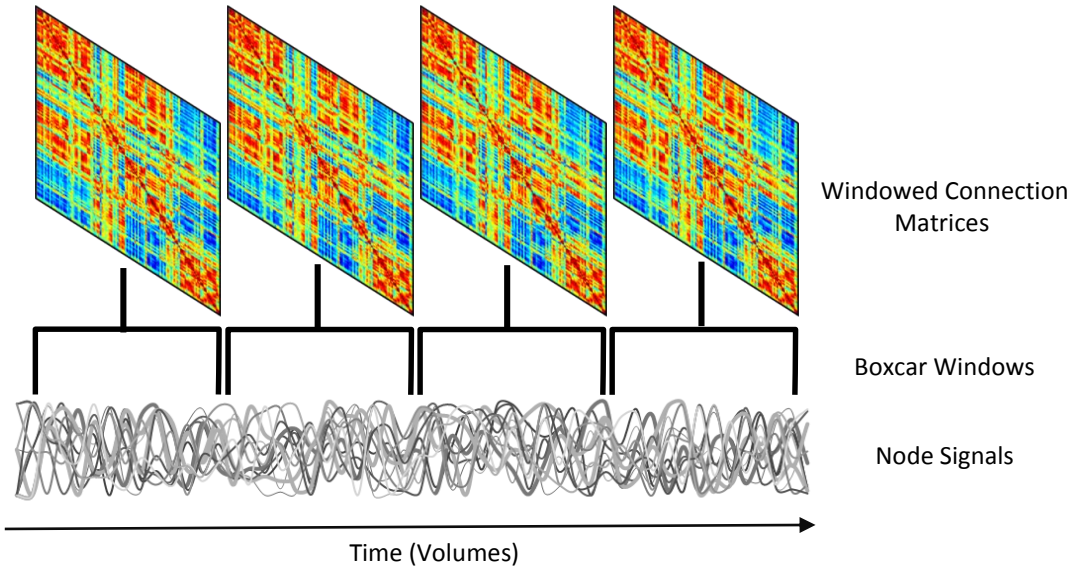

Figure 9 - Visual schematic of a sliding window procedure using a box car window to estimate the multi-slice connection matrix of an acquisition

Generally, sliding windows applied to neuroimaging studies employ non-overlapping box car windows (Van Dijk et al. 2010; Kiviniemi et al. 2011; Allen et al. 2014). However, boxcar windows offer relatively coarse temporal sensitivity, can be heavily influenced by outliers and arguably should not be overlapped. All samples within the window period are equally weighted. If overlapped, multiple windows may be driven by a single outlier effect. More recent studies have employed tapered windows (Monti et al. 2014; Zalesky et al. 2014), providing increased

temporal sensitivity and robustness to outliers and arguably may be overlapped as shared information between windows is reduced due to tapering.

In this thesis we employ a Gaussian window to estimate temporal connectivity, as illustrated in Figure 10. This provides a tapered window resulting in increased temporal sensitivity as compared to the boxcar. Windows of length T were estimated with a full width of 6 standard deviations (σ); the effective length, 2s, of the window is then given as T/3.

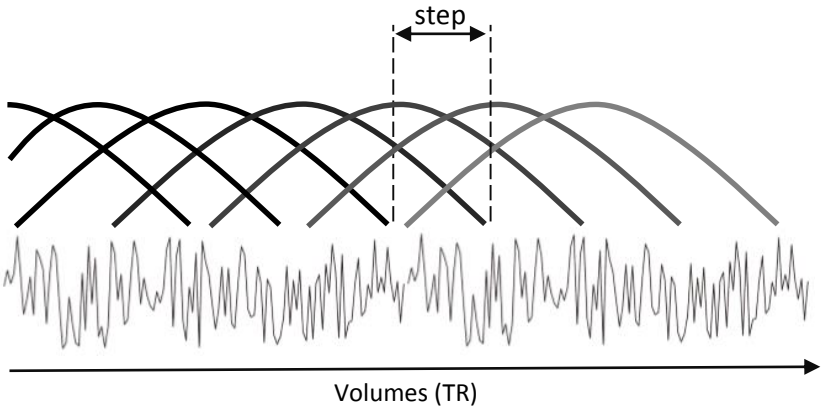

$$y = \exp\frac{-\left(t - \frac{T-1}{2}\right)^2}{2s^2}$$

$$s = \frac{T}{2\sigma}$$

Where:

$$\sigma = 3$$

Figure 10 - Illustration of application of tapered window to time-series data. Gaussian windows are formulated using the formula displayed. The entire window, of length T, expresses a 3σ Gaussian distribution and has an effective length of 2s = T/3.

When applying a sliding window one must be careful when selecting a window length. If the length is too short spurious correlations may occur resulting in a noisy estimations of connectivity. Alternatively window lengths that are too long are insensitive to connectivity dynamics (Hutchison et al. 2012). Currently there is little consensus on the optimal window length. Empirical evidence suggests connectivity can be robustly estimated and sensitive to temporal changes with windows of 30-60 seconds up to 5 minutes (Van Dijk et al. 2010; Whitlow et al. 2011; Shirer et al. 2012). This however was for a box car window, further analysis is required to compare the effects of different windowing shapes and lengths.

3.3 Statistical measures

Here we will briefly describe some of the statistical methods applied within this thesis.

3.3.1 The general linear model

The general linear model (GLM) is often applied for the testing of a statistical models. It is a generalisation of a multiple linear regression model and can be expressed as:

$$\boldsymbol{Y} = \boldsymbol{X\beta} + \boldsymbol{\varepsilon}$$

where **Y** represents a collection of data samples, in a neuroimaging context, this is typically the signal for each voxel across subjects. The design matrix is given by **X**, and the regression coefficients relating **X** to **Y** are defined by **β**. The residual error is defined by **ε**. The values of **β** can be obtained through solving:

$$\boldsymbol{\beta} = (\boldsymbol{X}'\boldsymbol{X})^{-1}\boldsymbol{X}'\boldsymbol{Y}$$

To assess the significance of the fit to the model, one sample t-tests are commonly applied to $\boldsymbol{\beta}$ values.

3.3.2 Intra class correlation coefficients

The intraclass correlation coefficient (ICC) provides a quantitative statistic describing the similarity of measures within a group. This measure is often perceived as akin to correlation performed on a group scale rather than paired observations. ICC's have several formulations, as discussed in (Shrout et al. 1979; McGraw et al. 1996). In this thesis we apply ICC as a measure of reproducibility and as such we use the definition of ICC formularised as:

$$ICC(3,1) = \frac{MSR - MSE}{MSR + (k-1)MSE}$$

Here correlation between repeated measures is modelled by a repeated measures ANOVA, where MSR is the between mean square measure and MSE the mean square error. The value of k is given as the number of measurements. In order to test the significance of the ICC in relation to a hypothesis, we compute the F-statistic; which is simply MSR /MSE for a two-way design.

3.4 Regularisation

We define situations where the dimensionality of data, *D*, is much greater than the number of samples, *N*, as ill-posed problems. Ill-posed problems can render some traditional statistical methods unsuitable. Regularisation may be applied to solve these types of problems. This involves applying a penalty for model complexity or alternatively, rewarding smoothness. This allows for the predictions and statistical inferences to be made on datasets where $D \gg N$ by selecting preferred levels of model complexity and optimising the generalizability of the model.

3.4.1 Ridge Regression

Also known as Tikhonov regression, this is one of the earliest and simplest regularisation methods (Tihonov 1963). It is a modification of the least squares estimator which introduces a penalty on the square of the coefficients.

The least squares (LS) method, most commonly applied to linear regression, allows for the selection of regression parameters, w, by minimising the sum of squared residuals, R, for a set of data, **X**. This is also the penalty minimised by the GLM mentioned above. For example

$$R(\boldsymbol{w}) = \sum_{\boldsymbol{i=1}}^{\boldsymbol{N}} \left(y_i - \boldsymbol{w^T x_i}\right)^{\boldsymbol{2}} \qquad (3.4.1)$$

Where y_i is the true target for the data point. Applying the regularisation penalty, λ, to the squared coefficients of the LS method we obtain the residuals of ridge regression as:

$$R(\boldsymbol{w}) = \sum_{\boldsymbol{i=1}}^{\boldsymbol{N}} \left(y_i - \boldsymbol{w^T x_i}\right)^{\boldsymbol{2}} - \lambda \sum_{j=1}^{D} w_j^2 \qquad (3.4.2)$$

Here λ determines the model complexity, compromising between small weights and goodness of fit. The above formulation employs an L2 norm, the Euclidean norm. Other types of norms will be discussed below.

3.4.2 Lasso

The least absolute shrinkage and selection operator (LASSO) is a commonly used alternative to the ridge regularisation. Unlike the ridge regularisation, Lasso employs the L1 norm(Tibshirani 1996) which enforces sparsity, i.e forces some coefficients to zero where possible.

$$R(\boldsymbol{w}) = \sum_{\boldsymbol{i=1}}^{\boldsymbol{N}} \left(y_i - \boldsymbol{w^T x_i}\right)^{\boldsymbol{2}} - \lambda \sum_{j=1}^{D} \left|w_j\right| \qquad (3.4.3)$$

The greater the value of λ more of the coefficients will be set to zero. When applying the Lasso to neuroimaging data we must be wary of correlation in the data. Presented with highly correlated data, the LASSO will tend to favour one of the variables while setting the rest to zero without regard to which variable is retained. This is undesirable and particularly pertinent to neuroimaging data where voxels tend to be highly correlated.

3.4.3 Elastic Net

Elastic net is an extension of the Lasso and can be considered a convex combination of ridge and lasso penalties. It employs both the L2 and L1 norm which are controlled by the λ term which regulates the trade-off between each norm (Zou et al. 2005).

$$R(\boldsymbol{w}) = \sum_{\boldsymbol{i=1}}^{\boldsymbol{N}} \left(\boldsymbol{y_i} - \boldsymbol{w^T x_i}\right)^{\boldsymbol{2}} - \sum_{j=1}^{D} \left(\frac{(1-\lambda)}{2} w_j^2 + \lambda \left|w_j\right|\right) \qquad (3.4.4)$$

When λ = 0, the elastic net uses an L2 norm and when λ = 1, it is equivalent to the Lasso. The elastic net helps to overcome some of the limitations of the Lasso and is capable of selecting

groups of correlated variables. Indeed the elastic net has been shown to often outperform LASSO regression in terms of prediction accuracy (Zou et al. 2005).

3.5 Pattern Recognition

3.5.1 Probability Theory

Probability theory provides a mathematical framework for dealing with uncertainty and probability. In the context of neuroimaging and pattern recognition we are primarily interesting in predicting the probability of class membership for groups of participants or patients, for instance classifying based on drug response or disease diagnosis.

Uncertainty in this situation may relate to noisy data or varying confidence in regard to group labels, such as disease diagnosis or varying effects of drug response. Probability theory allows us to form probabilistic models in order to assess the probability of a prediction of class membership. Probabilities are used to quantify the chance of a given outcome or set of outcomes occurring from random variables based on a set of possible or observed outcomes. All probabilities must be positive and the sum of the probabilities for all outcomes of a random variable must sum to 1, formally $\sum_{x \in X} p(\boldsymbol{X}) = 1$.

Given a dataset, $\boldsymbol{X}$, of m samples $\boldsymbol{X} = \{\boldsymbol{x_i}\}_1^m$ of d-dimensional data $\boldsymbol{x_i} = [x_1, \dots x_d]$ and corresponding set of class labels $\boldsymbol{Y} = [y_1, \dots y_m]$, $y \in$ [-1, 1], we wish to make target predictions, y*, given new samples $\boldsymbol{x}$* of unknown class membership.

3.5.2 Kernel Machine Learning Algorithms

Pattern recognition (PR) algorithms are a subset of machine learning methods; these powerful techniques are becoming increasingly popular in neuroimaging. They exploit kernels which efficiently represent the similarity between data samples. Kernel sizes are determined not by the dimensionality of the data, but by the number of samples, m. This representation is advantageous in neuroimaging analyses where the dimensionality of the data is usually several orders of magnitude greater than the sample size. Using kernels it is possible to represent the similarity between the samples of a $m \times d$ dataset as an $m \times m$ kernel. Importantly, kernels also enable non-linear mappings of data, however these are not always tractable. Computations can be performed directly in the kernel space, affording a substantial computational advantage over using the feature space. Here we provide a brief overview of two kernel methods often applied to neuroimaging data, namely support vector machines (SVMs) and Gaussian process classifiers (GPCs).

3.5.2.1 Support Vector Machines

First introduced in the 1990's, SVMs have emerged as one of the most commonly employed supervised learning methods for linear and non-linear classification of high dimensional data (Cortes et al. 1995). The details provided here are intended to familiarise the reader with the methodology used in this thesis, for a more detailed account refer to Cortes et al (1995).

In general terms, SVMs seek to identify a hyperplane, or decision plane, which optimally separates data points of differing classes. Optimal separation is achieved through maximising the distance between the hyperplane and the closest training samples (i.e. the support vectors). A large distance, or functional margin, implies a model with low uncertainty and potentially higher generalizability.

More formally, given a dataset $\mathcal{D}$ with class labels $\boldsymbol{y}$, where $y_i \in \{-1,1\}$ the hyperplane can be written as a set of point which satisfy the equation:

$$\boldsymbol{w^T x} + b = 0 \qquad (3.5.1)$$

Where **w** is the weight vector normal to the hyperplane and b is a bias term where $b/\|\boldsymbol{w}\|$ is the offset of the hyperplane to the origin. The distance of any point to this hyperplane is given by:

$$\frac{\boldsymbol{w}^T\boldsymbol{x} + b}{\|\boldsymbol{w}\|} \qquad (3.5.2)$$

For data that is linearly separable there are infinite possible hyperplanes, the SVM method seeks to find the optimal hyperplane which maximises the margin. It is conventional to scale **w** and b such that the distance between margins is $2/\|\boldsymbol{w}\|$, Figure 11.

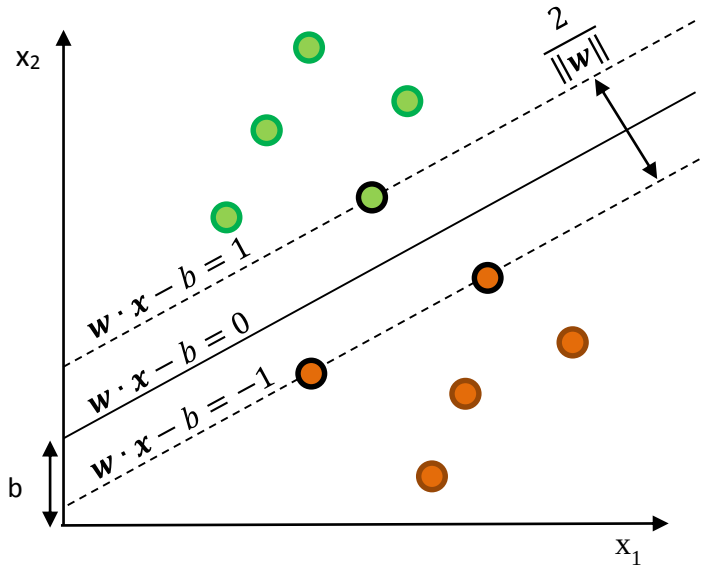

Figure 11 - SVM hyper plane separating classes of two dimensional samples, hyperplane is indicated by solid line, margins by dotted lines and support vectors are outlined in black.

For linearly separable data the hyperplane can be found minimising $\frac{1}{2}\|\boldsymbol{w}\|^2$ subject to $y_i(\boldsymbol{w}^T\boldsymbol{x}_i + b) \geq 1$ where maximising the margin is equivalent to minimising the weight vector. For data that is not linearly separable it is necessary to incorporate a vector of slack variables, **ξ** which permit a degree of misclassification. Regularization is employed to facilitate compromise between margin width maximisation and misclassification, this is controlled by the hyper parameter C. The resultant *primal* form is given as:

$$\min_{w,b} \frac{1}{2}\|\boldsymbol{w}\|^2 + C\sum_{i=1}^{n}\xi_i \qquad (3.5.3)$$

Subject to: $y_i(\boldsymbol{w}^T\boldsymbol{x}_i + b) \geq 1 - \xi_i$

$$\xi_i \geq 0$$

for: $i = 1,2,\ldots n$

This can be solved efficiently using Lagrange multipliers. We introduce **α** and **β** which correspond to the constraints of the primal above. From this, the Lagrangian can be expressed as:

$$\arg\min_{w,b}\max_{\alpha,\beta\geq 0}\{L(\boldsymbol{w}, b, \boldsymbol{\alpha}, \boldsymbol{\beta}, \boldsymbol{\xi})\} \qquad (3.5.4)$$

$$L(\boldsymbol{w}, b, \boldsymbol{\alpha}, \boldsymbol{\beta}, \boldsymbol{\xi}) = \frac{1}{2}\|w\|^2 - \sum_{i=1}^{n}\alpha_i[y_i(\boldsymbol{w}^T\boldsymbol{x}_i + b) - 1 + \xi_i] + C\sum_{i=1}^{n}\xi_i - \sum_{i=1}^{n}\beta_i\xi_i$$

for: $i = 1,2,\ldots n$

The motivation of this is to find a saddle point at which α_i and β_i are set to zero for all points which can be distinguished as $y_i(\boldsymbol{w}^T\boldsymbol{x}_i + b) - 1 > 0$. The non-zero values of α correspond to samples which lie on the margin, satisfying $y_i(\boldsymbol{w}^T\boldsymbol{x}_i + b) = 1$. These are known as support vectors and contain all the information pertaining to the definition of the hyperplane. For an optimal solution only a subset of samples will be support vectors. The weight vector for the training data can be expressed as:

$$w = \sum_{i=1}^{n}\alpha_i y_i \boldsymbol{x}_i \qquad (3.5.5)$$

And the bias can be obtained for a given support vector using:

$$b = y_i - \sum_{i=1}^{n}\alpha_i y_i \boldsymbol{x_i^T}\boldsymbol{x_i} \qquad (3.5.6)$$

Differentiating the Lagrangian with respect to the variables of the primal form results in the *dual form:*

$$\max_{\alpha} \tilde{L}(\alpha) = \sum_{i=1}^{n} \alpha_i - \frac{1}{2} \sum_{i,j=1}^{n} \alpha_i \alpha_j y_i y_j k(\boldsymbol{x}_i, \boldsymbol{x}_j) \quad (3.5.7)$$

Subject to: $0 \leq \alpha_i \leq C$

$\sum_{i=1}^{n} \alpha_i y_i = 0$

for: $i = 1,2, \ldots, n$

where $k(\boldsymbol{x}_i, \boldsymbol{x}_j)$ defines the kernel function. We focus on the linear kernel, $\boldsymbol{x}_i^T \boldsymbol{x}_j$ **,** for neuroimaging applications as it presents a compact representation of the high dimensionality. Furthermore the linear kernel is tractable, aiding interpretation and visualisation of results.

This dual form offers significant advantages: the slack variables have disappeared and C is only present in the form of a constraint on the Lagrange multipliers. Furthermore, under linear constraints, the objective function has a unique minimum (i.e. is convex) so long as $y_i y_j k(\boldsymbol{x}_i, \boldsymbol{x}_j)$ is positive semi-definite. Solving can be achieved using quadratic programming for which several efficient solutions exist (Platt 1998).

Classification can now be performed using:

$$y^* = sign\left(\sum_{i=1}^{n} \alpha_i y_i k(\boldsymbol{x}_i, \boldsymbol{x}^*) + b\right) \quad (3.5.8)$$

Where **x*** represents the test data and y* the predicted class label.

3.5.2.2 Multi-kernel Support Vector Machines

Kernel methods such as SVMs, discussed above, are powerful tools for discriminative analysis. By considering multiple kernels it is possible to extend these methods allowing for learning across multiple heterogeneous data modalities. Here we discuss a method of identifying an optimal kernel from a weighted combination of "base kernels" as described in (Lanckriet et al. 2004; Sonnenburg et al. 2006). This optimal kernel can be achieved using a convex combination of *K* kernels such that:

$$k(\boldsymbol{x}_i, \boldsymbol{x}_j) = \sum_{k=1}^{K} \beta_k k_k(\boldsymbol{x}_i, \boldsymbol{x}_j) \quad (3.5.9)$$

Where each kernel k_k uses distinct features and is associated with a weight β_k where $\beta_k \geq 0$. In order to fairly combine kernels, it is necessary to ensure all kernels are of the same scales, as such kernel normalisation is necessary, as introduced in chapter 6. Inspection of kernel weights

can provide insight into the varying degrees of importance of each kernel for class discrimination.

Here we provide a basic overview of the binary classification multi–kernel learning (MKL) technique as described in (Sonnenburg et al. 2006). For a MKL SVM classification, data points $\{\boldsymbol{x}_i\}$ must be translated from the input space to *K* feature spaces before optimization. The primal form of the MKL SVM then becomes:

$$\min_{w,b} \frac{1}{2}\left(\sum_{k=1}^{K}\|\boldsymbol{w}_k\|_2\right)^2 + C\sum_{i=1}^{n}\xi_i \qquad (3.5.10)$$

Subject to: $y_i\left(\sum_{k=1}^{K}(\boldsymbol{w}_k^T\boldsymbol{x}_{k\,i}) + b\right) \geq 1 - \xi_i$

$$\xi_i \geq 0$$

for: $i = 1,2,\ldots n$

Thus, the weight vector can be expressed as:

$$\boldsymbol{w_k} = \beta_k \sum_{i=1}^{n} \alpha_i y_i \boldsymbol{x}_{ki} \qquad (3.5.11)$$

Subject to: $\beta_k \geq 0$

for: $k = 1,2,\ldots,K$

and the dual form:

$$\min \frac{1}{2}\sum_{i,j=1}^{N} \alpha_i\alpha_j y_i y_j k_k(\boldsymbol{x}_i, \boldsymbol{x}_j) \qquad (3.5.12)$$

3.5.2.3 Gaussian Process Classification

Gaussian process classification (GPC) is an extension of the Gaussian process regression introduced by Rasmussen (Williams et al. 1996) in 1996. The details provided here are intended to familiarise the reader with the methodology used in this thesis, for a more detailed account refer to (Rasmussen 2006).

The Gaussian distribution is one of the most commonly used continuous probability distribution in modern mathematics and statistics. The probability density function (pdf) of a Gaussian distribution is defined by its mean, μ, and its variance, σ^2:

$$\mathcal{N}(\boldsymbol{x}|\mu,\sigma) = \frac{1}{\sigma\sqrt{2\pi}}\exp\left(-\frac{(\boldsymbol{x}-\mu)^2}{2\sigma^2}\right)$$

For multivariate variables, the Gaussian distribution is defined by a mean vector, **μ**, and covariance matrix, **Σ**. The distribution is given by:

$$\mathcal{N}(\boldsymbol{x}|\boldsymbol{\mu},\boldsymbol{\Sigma}) = \frac{1}{\sqrt{(2\pi)^D|\boldsymbol{\Sigma}|}}\exp\left(-\frac{1}{2}(\boldsymbol{x}-\boldsymbol{\mu})^T\boldsymbol{\Sigma}^{-1}(\boldsymbol{x}-\boldsymbol{\mu})\right)$$

A Gaussian process (GP) is a stochastic process which can be considered an infinitely-dimensional generalization of the Gaussian distribution. The GP is constrained such that a finite set of random variables are multivariate Gaussian distributions. As before, the GP is defined by its mean (*m)* and covariance (*K*), in this case given as functions, $\mathcal{GP}(m,K)$.

GPC is performed using a Bayesian framework and hence intrinsically probabilistic in contrast to SVMs. GPC models the latent function, f(***x***), which describes the mapping of the data, ***x***, to the class labels, ***y***. Classification is performed by placing a zero mean GP prior over this latent functional. The covariance function of the GP prior plays a similar role to the kernel in the SVM framework, and informs the smoothness. In this body of work we employ linear functions. The computed posterior distribution is then squeezed through a function to map values to the unit interval. This constrains the values of the latent function between 0 and 1, denoting the probabilistic state; this is then thresholded to generate a predictive class label of either 1 or -1.

We reframe the classification problem in a Bayes framework as "finding the probability of a given class label, where $y \in (-1,1)$, based on the data, ***x****. In this thesis we are primarily concerned with binary classification, for which $p(y^*=1|\boldsymbol{X},\boldsymbol{y},\boldsymbol{x}^*) + p(y^*=-1|\boldsymbol{x}^*,\boldsymbol{X},\boldsymbol{y}) = 1$, furthermore the marginal likelihood can be written as $p(\boldsymbol{y}|\boldsymbol{x}) = \sigma(\boldsymbol{y},f)$, where σ maps the values of the latent function to the unit interval. The GP prior over the latent function is written as $p(f) = \mathcal{N}(f|0,\boldsymbol{K})$, the marginal likelihood for the given training data as $p(\boldsymbol{y}|\boldsymbol{X})$, using Bayes rule this leads to:

$$p(f|X,y) = \frac{p(\boldsymbol{y}|f)p(f)}{\int p(\boldsymbol{y}|f)p(\boldsymbol{y}|\boldsymbol{X})df} = \frac{p(f)}{p(\boldsymbol{y}|\boldsymbol{X})}\prod_i^n \sigma(\boldsymbol{y}_i,f_i)$$

Where the marginal likelihood is denoted by $p(\boldsymbol{y}|\boldsymbol{X})$ and $p(f)$ is the prior over the latent function. When making predictions about a test set, we consider the test latent variables, f^*, where the joint prior is given by:

$$p(f\ f^*|\boldsymbol{X}^*\ \boldsymbol{X}) = \mathcal{N}\left(\begin{bmatrix} f \\ f^* \end{bmatrix}\middle|\, 0, \begin{bmatrix} \boldsymbol{K} & \boldsymbol{K}^* \\ \boldsymbol{K}^{*T} & \boldsymbol{K}^{**} \end{bmatrix}\right)$$

Where, for a given kernel function k(φ,φ) we define:

$$\boldsymbol{K} = k(\boldsymbol{x}, \boldsymbol{x})$$
$$\boldsymbol{K}^* = k(\boldsymbol{x}, \boldsymbol{x}^*)$$
$$\boldsymbol{K}^{**} = k(\boldsymbol{x}^*, \boldsymbol{x}^*)$$

As described in (Nickisch et al. 2008) the posterior for f^* can be obtained by:

$$p(f^*|f, \boldsymbol{X}\ \boldsymbol{x}^*\ \boldsymbol{y}) = \mathcal{N}(f^*|\mu^*\ \sigma^{*2})$$
$$= \mathcal{N}(f^*|\boldsymbol{K}^{*T}\boldsymbol{K}^{-1}\boldsymbol{f}, \boldsymbol{K}^{**} - \boldsymbol{K}^{*T}\boldsymbol{K}^{-1}\boldsymbol{K}^*)$$

Predictions of class membership are then given by the probability value:

$$p(y^*|\boldsymbol{x}^*\ \boldsymbol{y}\ \boldsymbol{X}) = \int \sigma(f^*)\, p(f^*|\boldsymbol{x}^*\ \boldsymbol{X}\ \boldsymbol{y}\ )df^*$$

A threshold is then applied to this probabilistic value in order to obtain class labels [-1,1] .

3.5.3 Model evaluation

Here we will briefly discuss some of the key issues involved in model evaluation.

3.5.3.1 Overfitting

Overfitting is one of the most important considerations in pattern recognition. It occurs when an overly complex model is selected in the training phase. Overfitting occurs as the criteria for the training of the model is not the same as the criteria for accessing the performance of the model, i.e. generalizability as measured by performance on an independent test set. Models which overfit will generally have a low residual error on the training set but will generalize poorly. The possibility for overfitting is related to the flexibility of the model, this is illustrated in Figure 12.

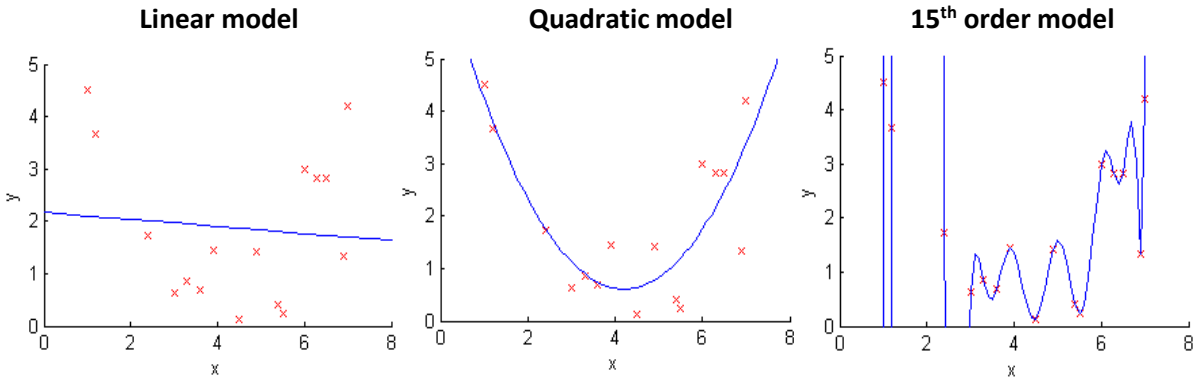

Figure 12 - Examples of polynomial fits to a dataset. The left pane shows an example of under fitting using a linear model which is too rigid and fits the data poorly. The central pane illustrates a quadratic model which provides a reasonably good fit to the data. The right hand pane depicts overfitting using a high order polynomial, which is overly flexible represents the data perfectly but will generalize poorly.

As illustrated the linear function *underfits,* as such is a poor fit to the training data and generalizes poorly. The high order model fits the training data perfectly but will generalize poorly, as such *overfits*. The low order model provides the best compromise between accuracy of fit for the training data and generalisability out of all three models highlighting the need for careful model selection.

3.5.3.2 Cross validation

Ideally the generalizability of a model is tested using an independent data set which was not involved in the model estimation. However in the context of neuroimaging, datasets are generally small, typically 15-50 subjects and in most case an independent validation set is often not available. To alleviate this issue, cross-validation approaches are employed to estimate the generalisation error of a particular model.

This method, divides the data into *k* partitions where the model is trained using k-1 partitions and tested using the remaining partition. This processes is repeated so that each fold is used as a test set; the reported accuracy of the model is the average accuracy for all folds. In this manner it is possible to estimate the generalizability of the model in a principled fashion. The above procedure is known as k-fold cross validation where k is the number of data partitions, in cases where an individual subject is excluded from the training data and used as a test set the process is known as leave one out cross validation (LOOCV).

3.5.4 Clustering

Clustering is a general term for a group of unsupervised learning algorithm which seek to identify some grouping of samples into clusters, in a way which minimises the within cluster difference while maximising the distance between clusters. Clustering methods are generally unsupervised, where partitions are data driven and no prior information is given. Semi-supervised implementations exist; these still seek to identify data driven groupings within the data however the initial seeds are define *a priori*.

Many implementations of clustering algorithms exist, differing in their definitions of a cluster and methods for cluster detection. Generally most clustering methods are an iterative optimisation of data partitions in order to maximise the partition fit to the data.

Clustering is inherently dependant on data pre-processing and model parameters which must be selected for specifically for each clustering problem. Here we outline one of the most common clustering algorithms, K-means clustering (Lloyd 1982).

3.5.4.1 K-Means Clustering

This is one of the most commonly used centroid clustering algorithms, it is a two-step iterative procedure which partitions data into a fixed number of clusters, *k*. The number of clusters is often select *a priori* which can introduce erroneous partitioning in the data if not appropriately selected.

The algorithm initialises by randomly selecting *k* samples as initial centroids. In the first phase of the algorithm, observations are assigned to their closest centroid, as measure by a given metric, often the Euclidean distance. Once all observations are assigned to one of k centroids, new centroids are calculated from the mean of all observations assigned to each cluster. These steps are repeated until a maximum number of iterations is achieved or until there is no change in observation assignment between iterations.

Optimisation is an NP-hard problem so it is common to search for approximate solutions; this often results in local optima. It is often necessary to repeat the clustering multiple times and select the optimal result due to inherent variability introduced with random initialisation.

Chapter 4: Functional Connectivity Effects of Ketamine

In this chapter we examine the functional connectivity (FC) effects of ketamine on the human brain using traditional approaches to connectivity analysis. Ketamine modulates glutamatergic release and has been widely used within the field of neuroimaging to facilitate the study of glutamatergic dysfunction in the human brain. We suggest connectivity is a highly suitable measure to investigate these widespread glutamatergic effects. Additionally we study the effect of pre-treatment with pharmacological probes on this ketamine induced connectivity to investigate potential modulation or attenuation of this state. The motivation for this work is to provide a foundation for later chapters, providing an initial insight into the effects of ketamine on localised connectivity within the brain.

4.1 Ketamine background

The N-methyl-d-Aspartate receptor (NMDAR) antagonist ketamine has been shown to elicit psychomimetic symptoms which can resemble schizophrenia (Krystal et al. 1994; Goff et al. 2001; Corlett et al. 2011). Furthermore acute ketamine administration has been shown to cause an increase in both positive and negative symptom scores (Honey et al. 2008). While not a phenocopy of the disorder, ketamine has commonly been used as a model for schizophrenia to investigate the glutamate hypothesis of psychosis (Deakin et al. 2008).

Robust ketamine-induced effects on the blood oxygenation level dependent (BOLD) signal have been observed in healthy volunteers (Deakin et al. 2008; De Simoni et al. 2013; Driesen et al. 2013). These BOLD effects have been investigated primarily in terms of amplitude (Deakin et al. 2008; De Simoni et al. 2013; Doyle et al. 2013). Furthermore, it has been demonstrated that the ketamine-induced BOLD response is attenuated by pre-treatment with compounds theorised to reduce glutamate release (Deakin et al. 2008; Doyle et al. 2013).

To date there has been little investigation into the effects of ketamine on the functional connectivity in brain. It has been shown that functional connectivity is altered by acute NMDAR blockade in both humans (Niesters et al. 2012; Driesen et al. 2013) and rodents (Gass et al. 2013). While it is not understood what mechanism is responsible for this effects, it is theorised that the connectivity change is driven by downstream glutamatergic effects.

Previous work using the dataset presented here has demonstrated an attenuation effect on the ketamine-induced BOLD response by pre-treatment with clinically effective doses of either lamotrigine or risperidone in healthy volunteers (Doyle et al. 2013). These compounds exhibit different mechanisms of action; the atypical antipsychotic, risperidone, is assumed to indirectly

reduce glutamate levels as a downstream effect of 5-HT_{2A} receptor antagonism (Meltzer et al. 2011). Furthermore, risperidone having been observed to directly potentiate NMDARs (Konradsson et al. 2006), possesses an additional mechanism of action to attenuate the ketamine response. In contrast, the anticonvulsant Lamotrigine, directly attenuates glutamate release pre-synaptically through sodium ion channel modulation, (Large et al. 2005).

Recent studies have begun to investigate the effect of ketamine on the functional connectivity in the human brain. This type of analysis which is sensitive to correlation between regions, is well suited for the study of ketamine which elicits widespread glutamatergic effects. Indeed sub-anaesthetic dosages of ketamine have been demonstrated to robustly alter the global functional connectivity in the human brain (Driesen et al. 2013). In an attempt to describe this modulatory effect of ketamine, studies have demonstrated robust effects between network hubs (Scheidegger et al. 2012) and seed regions (Anticevic et al. 2012). These studies however have been limited in their scope of investigation, restricting their investigations to connectivity effects associated with few a priori selected seed regions.

In this chapter we provide a comprehensive investigation into the functional connectivity effects of ketamine across the whole brain using the standard univariate approaches. Moreover we investigate the modulation of any ketamine effects through pre-treatment with risperidone and lamotrigine. The motivation for this analysis is to reveal the effects of ketamine on functional connectivity across the whole brain. This analysis will provide an initial univariate understanding of the effects of ketamine and its modulation by lamotrigine or risperidone which shall be expanded upon in later chapters. The secondary aim of this chapter is to highlight the limitation of traditional univariate analysis and the need for method development for the study of whole brain connectivity.

4.2 Introducing the Ketamine Dataset

Data collection for this study was performed by Dr Sara De Simoni (s.de-simoni@imperial.ac.uk). This was funded by a grant by Eli Lily. Further details of this dataset can be found in (Doyle et al. 2013).

4.2.1 Ethics

Data collected in this study was approved by the Wandsworth Research Ethics Committee (09/H0803/48). All participants provided written informed consent and their GP was notified of their participation in the study.

4.2.2 Participants

Twenty healthy right handed male volunteers were recruited using flyers and advertising across campuses of King's College London as well as local (Camberwell, London) and web-based advertisements. Participants of a departmental (Neuroimaging, Institute of Psychiatry) database were also contacted regarding study participation.

Participants were screened for any physical, neurological or psychiatric illness as well as standard haematology and urinalysis screenings. Additional exclusion criteria included the presence of drugs of abuse or excessive alcohol, cigarette (>5 cigarettes/day) or caffeine (>5 caffeinated drinks/day) consumption. From the 20 participants who passed screening, complete data was collected from only 16. One participant withdrew due to fainting upon cannulation in the first session. In the third session a participant withdrew due to nausea, two other participants were withdrawn due to compromising study lifestyle restrictions.

4.2.3 Study design

In this randomised, placebo-controlled, cross-over design study, data was collected over four sessions. Each session was separated by a period of at least ten days. During each session, participants received an oral pre-treatment followed by an intravenous infusion of Saline or ketamine, to a target plasma level of 75 ng/ml. Treatment combinations were oral placebo (ascorbic acid) followed by intravenous saline (PLA-SAL), oral placebo (ascorbic acid) followed by intravenous ketamine (PLA-KET), oral lamotrigine (300mg) followed by intravenous ketamine (LAM-KET) and oral risperidone (2mg) followed by intravenous ketamine (RIS-KET). Intravenous infusions were timed to occur during the broad maximum plasma exposure for risperidone and lamotrigine. At 30mins, 1, 1.5, 4 and 8 hours following the administration of the oral compounds, blood samples were taken to measure ketamine, risperidone and lamotrigine concentrations in plasma. The typical day schedule of session is illustrated in Figure 13.

4.2.4 Data acquisition

Gradient-echo echo-planar imaging (EPI) was used to acquire 15 minutes of task-free eyes-open BOLD phMRI images using a 3T GT HDx scanner. Participants were instructed to lie still and think of nothing in particular, a fixation cross was presented throughout. This resulted in 450 volumes of 38 near-axial slices (3mm thickness, 0.3mm inter-slice gap) per scanning session (TE = 30ms, TR = 2000ms, FA = 75°, in-plane resolution = 3.3mm, matrix size = 64x64, field of view = 21.1x21.1cm). In addition, a high resolution gradient echo volume or 43 near-axial slices was acquired 3mm thickness, 0.3mm inter-slice gap, TE = 30ms, TR = 2000ms, FA = 75°, in-plane

resolution = 3.3mm, matrix size = 64x64, field of view = 21.1x21.1cm). Intravenous infusions were administered 5 minutes into the 15 minute EPI sequence.

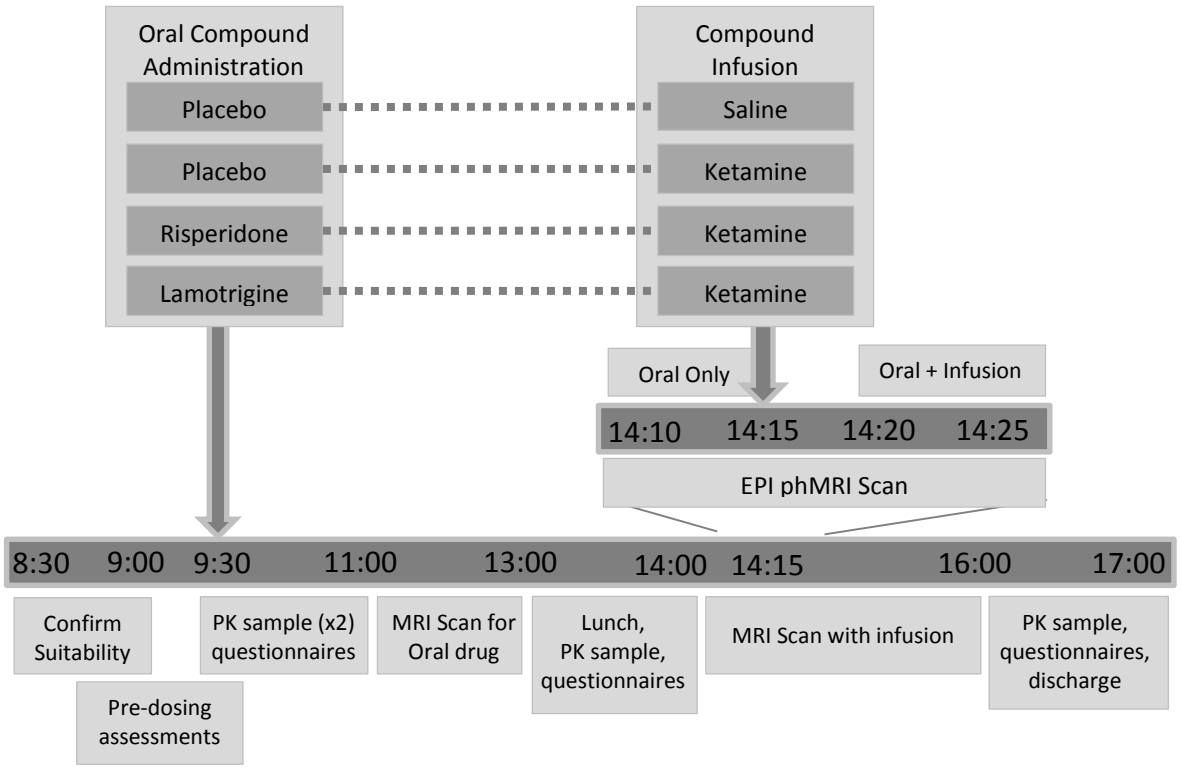

Figure 13 - Ketamine study design for a single session over the course of a day

4.2.5 Compound administration

Racemic ketamine was intravenously administered to a target plasma level of 75ng/ml (weight and height adjusted) using a Graseby 3400 pump based on the Clements 250 model implemented in Stanpump (http://www.opentci.org/doku.php). The administered sub-anaesthetic dose, equivalent to 0.12 (±0.003 SD) mg/kg was administered in during the first minute of the task-free acquisition followed by a pseudo-continuous infusion of 0.31 mg/kg/h.

4.2.6 Experimental Conditions

The experiment was designed such that the last 5 minutes of the EPI scan achieved a steady-state infusion. The acquired time series was divided into two conditions corresponding to the first and last 5 minutes (150 volumes). The first condition, the pre-infusion state, corresponds to the period where participants had only the oral compound present. The second condition represents the last 5 minutes or post infusion condition, here both of the session compounds are present. While this study employed a task-free paradigm, the expectation of the compound infusion likely induces presumed subjective effects in both pre-infusion and post infusion conditions.

We define experimental sessions as the four compound combination acquisitions: PLA-SAL, PLA-KET, RIS-KET and LAM-KET. Conditions are defined as the two experimental states within each of these sessions. For clarity we define our experimental conditions explicitly as:

Name	Description
Placebo (pre Saline)	Placebo prior to ketamine
Saline	Saline subsequent to placebo
Placebo (pre Ketamine)	Placebo prior ketamine
Ketamine	Ketamine subsequent to placebo
Risperidone	Risperidone prior to ketamine
Ris + Ketamine	Ketamine subsequent to risperidone
Lamotrigine	Lamotrigine prior to ketamine
Lam + Ketamine	Ketamine subsequent to Lamotrigine

4.3 Functional connectivity effects of ketamine

SPM 5 (www.fil.ion.ucl.ac.uk/spm) was used to slice-time correct, realign images, initially to the first volume and then to the mean, co-register to the hi-res image, spatially normalise to the MNI template and smooth the images using a Gaussian kernel of 8mm at full-width half-maximum. The data pre-processing was executed by Dr Sara De Simoni and Dr. Owen O'Daly (o.o'daly@kcl.ac.uk) and was provided to the student pre-processed using SPM5 and QC checked. All subsequent processing and analysis, unless otherwise stated, was performed by the doctoral candidate Richard Joules.

4.3.1 Post processing

Data were post-processed to enable connectivity analysis; linear regression was applied to minimise the effect of nuisance parameters, specifically the six motion parameters, mean cerebrospinal fluid (CSF) and white matter (WM) signal. CSF and WM were identified using thresholded a priori masks, provided in SPM 5, the applied masks are presented in Appendix A.

Ketamine is an anaesthetic and may introduce a systematic bias due to a reduction in head motion, potentially driving artefactual group differences. To test for differences in motion between experimental conditions, the mean, median and maximum frame-wise displacement were computed for each subject, Figure 14, and compared using paired t-tests. We note significant differences ($p<0.05$; Bonferonni corrected) between the saline (PLA+SAL post infusion) and the ketamine (PLA+KET post-infusion) and ris+ketamine (RIS+KET post-infusion) conditions for comparisons of the mean and median frame-wise displacement comparisons. This suggests that comparisons between these condition should be treated with caution as any

identified difference may be artefactual driven by motion effects. Motion was regressed from the data using the 6 motion parameters estimated during the realignment pre-processing.

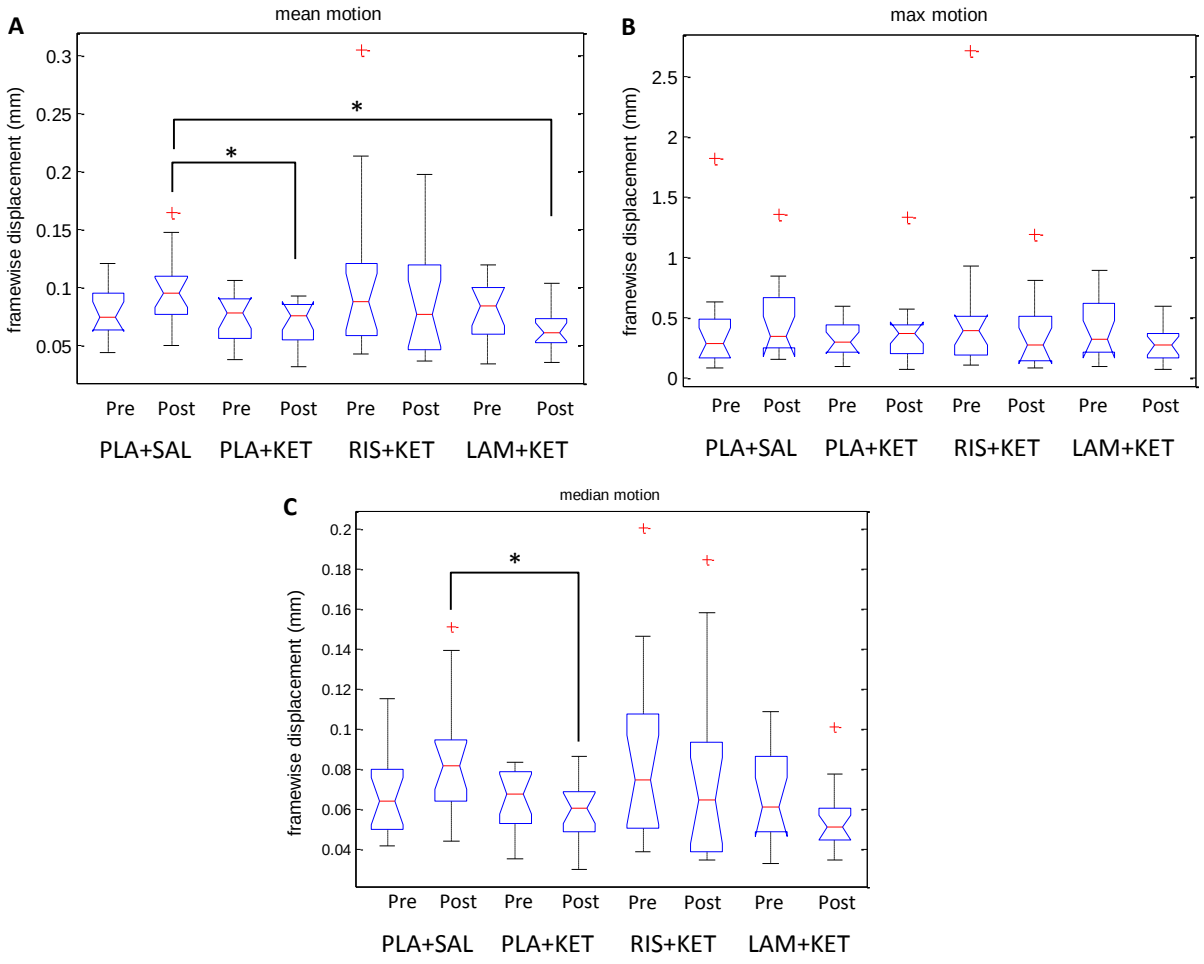

Figure 14 – Summary motion measures for each experimental condtion. Box and whisker plots show A) mean, B) maximum and C) median frame-wise displacements for the pre-infusion (pre) and post-infusion (post) conditions in each experimental session. * indicates significance after multiple comparisons correction

Subsequent to regression, band pass filtering was applied with a pass band of $0.01Hz < f < 0.1Hz$ to reduce the effect of low frequency scanner drift and high frequency physiological noise, for further discussion on the effects of post-processing we refer the reader to Chapter 2.

4.3.2 Graph Estimation

To investigate the connectivity effects, a graph, G(V,E), was formulated. Brain regions were represented as graph vertices or *nodes* where the connections between regions were given by the indices or *edges*. Data were parcellated into 90 anatomical regions covering all cortical and subcortical areas, as defined by the automated anatomical labelling (AAL) atlas (Tzourio-Mazoyer et al. 2002). Other atlas' have been shown to perform as well, if not better, in comparative connectivity analysis (Craddock et al. 2012) and may provide superior regional homogeneity in regards to function. However this comes at the cost of interpretability and

increased dimensionality which can potentially reduce sensitivity in univariate analysis due to the need for multiple comparisons correction. As such, the AAL was chosen as compromise between accuracy of parcellation, interpretability and granularity of parcellation. Furthermore due to its prevalence with connectivity studies it allows for some measure of comparison of results. Regions were used to define nodes within our graph analysis and the mean time course of each atlas region was computed from its voxel members. Edges between nodes were computed by the application of Pearson's correlation coefficient to the mean time series of all node pairs. Correlation measures were converted to z-scores using the Fisher r-z transform as an approximate for a variance stabilizing transform. This results in a fully connected, undirected, weighted graph for each subject representing the functional connectivity between the 90 AAL regions over the 5 minute period of each condition.

4.3.3 Graph Theory metrics

To investigate the effect of experimental conditions on the functional connectivity in the brain, graph edges and graph theory summary statistics were compared using paired t-tests. These comparisons were performed at the micro, meso and macro spatial scales to respectively investigate effects on individual connections, regional connectivity and effects across the whole brain network. This provides a multi-scale perspective on the effect of ketamine and the administered pre-treatments, across micro (edge), meso (nodal) and macro (global) connectivity scales.

*Edge diffe*rence

The effect of each experimental session on individual connections was investigated by comparing the lower triangle of the signed weighted adjacency matrices computed for the pre and post infusion conditions. In order to reduce false positives and to remove weak connections associated with noise, a connection mask was generated for each session. A thresholding procedure was applied where one sample t-tests were performed on each edge within each session's condition across all participants. Edges were retained if they were significant in any condition, as suggested in (Shirer et al. 2012). Significance was defined as $p < 0.01$ and Benjamini-Hochberg correction was applied to correct for multiple comparisons. This has the effect of removing all weak connections, the resultant masked edge connections were compared between experimental conditions using paired t-tests revealing connectivity effects on the micro scale of functional connectivity.

Node measures

To investigate the effect of pharmacological intervention on regional connectivity, graph theory centrality measures were computed and compared, again using a paired t-test. We define these node-wise measures as meso-scale metrics. The node strength (NS), betweenness centrality (BC) and local efficiency (EF) were calculated for each node to investigate any regional effects. These measures were computed on connection matrices prior to the thresholding procedure. NS is the simplest and most intuitive measure, related to the overall connectedness of a node. BC quantifies the importance of a node for the transmission of information across a network and EF relates the ability of a node to transfer information to other all nodes. We estimate BC measurements using MATLAB functions extracted from the Brain Connectivity Toolbox (BCT; http://www.brain-connectivity-toolbox.net), all other measures were implemented by the student in Matlab.

While insensitive to changes in individual regional couplings, these node measures provide insight into regional integration with the rest of the brain. For a summary of these measures and their interpretation we refer the reader to Chapter 3.

It has been suggested that nodal measures should be normalised by the network density; any change in density between conditions will impact nodal measures. This can result in significant group difference in nodal measures that are due entirely to a change in density, as opposed to any topological differences. Density normalisation can present challenges in interpretation especially if an experimental condition induce non-uniform density changes over a network. This is particularly relevant for pharmacological imaging studies where pharmacological intervention may elicit regionally specific changes which, when density normalised may result in spurious network changes. However, due to the nature of paired comparisons, it is likely any change in density is a result of the experimental condition rather than subject differences. Thus, effects of density on the functional topology may prove highly informative.

The legitimacy of density normalisation should be determined by the hypothesis under investigation. It is likely that administration of ketamine will result in a change in network density. In order to generate an informed view of the topology of node-wise functional connectivity effects of ketamine, we compare NS measure both with and without density normalisation. This will provide insight into how density alters the regional topology as measured by NS. Density normalisation was not considered for EF and BC measures as the formulation of these measures includes a normalisation term generating measures comparable between networks of different densities.

In order to correct for multiple comparisons across each meso-scale measure we applied the Benjamini-Hochberg (BH) correction (Benjamini et al. 1995) with an error rate of $\alpha = 0.05$, similar to Lord et al (2012). This provides a principled method for controlling the false discovery rate without imposing the extreme restrictions of the Bonferroni, furthermore this has method has been demonstrated appropriate for corrections of meso-scale connectivity.

Global connectivity effects

Connectivity statistics can be abstracted to the macro spatial scale, providing a single value representation of whole brain connectivity. Network density and global efficiency, as described in Chapter 3, were calculated and compared between session conditions using paired t-tests.

While comparison of whole brain connectivity measures provide perspective on general effects of experimental conditions, global metrics must be treated with caution. Values may be overly influenced by strong regional connections and influenced by a myriad of potential confounds; as such it is difficult to be confident in the interpretation of any change in global statistics.

4.3.4 Results

Conditions were compared using paired t-test, applied to connectivity measures at different spatial scale in order to assess the connectivity effects across the whole-brain. For comparisons of edge effects (micro-scale), we display both t-statistics and p-values in a single figure where the upper triangle displays the t-statistics while the lower triangle illustrates the p-values. Connections excluded in the initial one-sample t-test masking procedure are reported as having a t-statistic of 0 and a p-value of 1. Definitions of regional indices, as given by the AAL are provided in Appendix B.

Connectivity effects of Saline

To investigate the functional connectivity effect of saline on the human brain, univariate micro, meso and macro scale comparisons were performed between saline and placebo conditions. The saline condition was found to exhibit increased network density and global efficiency in relation to placebo, suggesting a more highly connected and efficient network state. Only increases in global efficiency reached significance ($p<0.05$), however this did not pass multiple comparisons correction. This trend of increased connectivity was consistent in both micro and meso-scale analyses. No active pharmacology was present in either condition compared, suggesting this subtle global increase in connectivity may be due subjective effects of anticipation of the blinded infusion.

The effect of saline, as compared to placebo, can be summarised as a trend-level ($p<0.05$; uncorrected) increase in functional integration of the frontal cortices. Comparison of individual connections reveal increases in connection strengths in the frontal cortices and the connections between frontal regions and the rest of the brain for the saline condition. This suggests a state of greater frontocortical functional integration in the saline condition. Meso-scale comparisons of NS and LE reveal a similar pattern of saline-induced increased frontal, parietal and temporal connectivity, supporting the suggestion of increased functional integration in these regions. This increased integration of regions associated with cognitive processing may potentially represent a change in many aspects of cognitive state such as alertness or anticipations.

Density normalisation was found to have a large effect on the relative topology of NS values for the comparison of placebo and saline. Saline exhibited relatively reduced occipital connectivity, primarily in V1 and V2 visual region, while NS for ventrolateral frontal regions was found to increase. Results of BC comparisons reveal a different pattern of effects indicating a reduction in the BC of most regions. This may be a result of the increased functional integration resulting in shorter "shortest paths" thus reducing the presence of intermediary nodes and reducing BC. While these effects indicate a subtle change in connectivity between conditions, no effect passed multiple comparisons testing. Lending confidence to the suggestion of within session stability.

Ketamine induced modulation of functional connectivity

Conditions in the PLA+KET session were compared to PLA+SAL conditions to reveal the effect of ketamine on the human brain across multiple spatial connectivity scales. The main effect of ketamine, in contrast to placebo, was found to most notably reduce connectivity in the brain. Comparisons of global metric report a trend level reduction in network density and efficiency. This general trend of ketamine induced decreased connectivity is also present in macro-scale measures of connectivity.

Micro-scale trend-level ($p<0.05$; uncorrected) can be summarised as wide spread distributed ketamine-induced decreases in cortical connectivity. Notably medial-temporal connections and connectivity between temporal regions were found to decrease under ketamine, while temporal-striatal connectivity was observed to increase. Furthermore, ketamine decreased connectivity between visual regions and the precuneus, an important hub region within the brain.

Comparison of meso-scale NS and EF changes for ketamine > saline and ketamine > placebo (pre ket) report similar patterns of change, indicating a common effect driving both comparisons. An

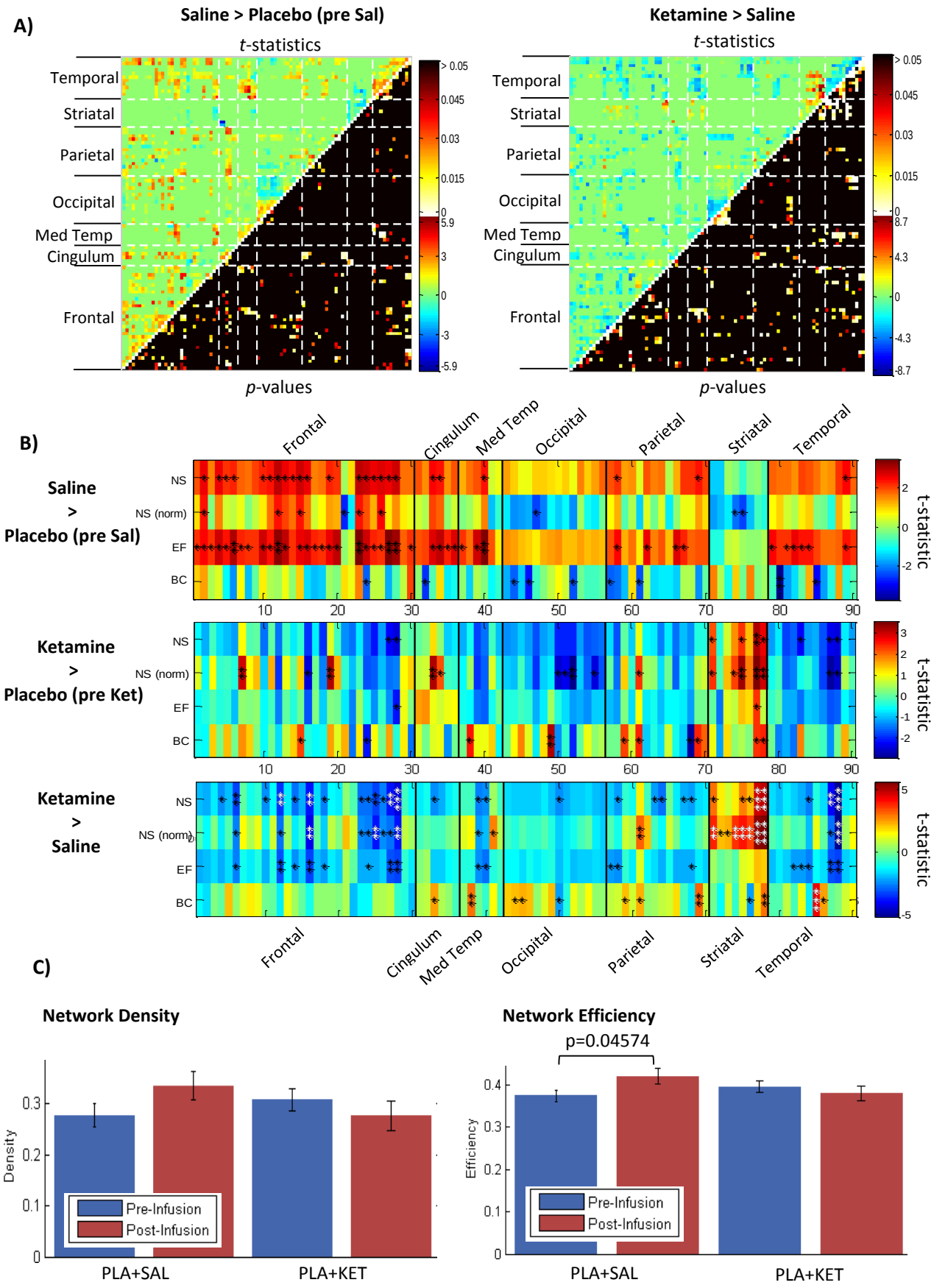

Figure 15 - Univariate comparison of functional connectivity effects for PLA+KET and PLA+SAL sessions, revealing A) micro-scale effects on regional coupling B) meso-scale comparisons of NS, EF, and BC, stars indicate statistical significance * p<0.05, **p<0.01,*p<0.001. Comparisons which pass the BH test are indicated in white. C) macro-scale comparisons of Network density and Network efficiency values**

effect we attribute to ketamine, however only effects for the comparison of ketamine and saline achieved significance, suggesting while the spatial pattern of change may be similar but the magnitude of change is not.

When compared to saline, ketamine was observed to significantly decrease NS measures of connectivity in the orbital frontal cortex (OFC), the right ventrolateral frontal cortices as well as the mid temporal pole. These effects may contribute to the memory deficits and perceptual distortions that occur as a result of acute ketamine. However, the sparsity of subjective reports precludes specific testing of this hypothesis.

Significant increases in NS measures were observed in the thalamus, left pallidum and right putamen. Additional significant increases in the left pallidum and right putamen for comparisons of normalised NS values. The thalamus has been implicated in mediating cortical circuits, the observed increased thalamic-cortical connectivity is likely the result of decreased integration of cortical networks. No significant effects were observed in EF and BC comparisons, although a similar pattern of trend level localised effects were observed between EF conditions. Normalised and non-normalised NS measurements reported a similar distribution of localised effects indicating any density related changes occur uniformly over regions.

Comparison of BC values between ketamine and saline reveal ketamine induced subtle, trend-level increases in thalamic, right hippocampal, primary visual and paracentral lobule BC. This is likely a result of the observed decreased cortical integration resulting in an increase presence of these key areas on shortest paths between regions.

The differences between ketamine and saline should be treated with caution due to the difference in motion parameters between these conditions. However, the spatial similarity in results for the ketamine condition compared to the saline and placebo (pre ketamine) conditions lend confidence to these effects being driven by the experimental condition rather than an artefact of motion.

Effects of lamotrigine pre-treatment

Conditions within the LAM+KET session were compared to those in PLA+KET and PLA+SAL sessions, Figure 16. A trend level reduction in network density ($p=0.049$) and global efficiency ($p=0.0222$) were observed between lam+ketamine and saline conditions, however these effects did not pass multiple comparisons testing.

Lamotrigine pre-treated ketamine was observed to significantly differ from the saline conditions when compared using EF and NS measures. Widespread decreases efficiency were observed for

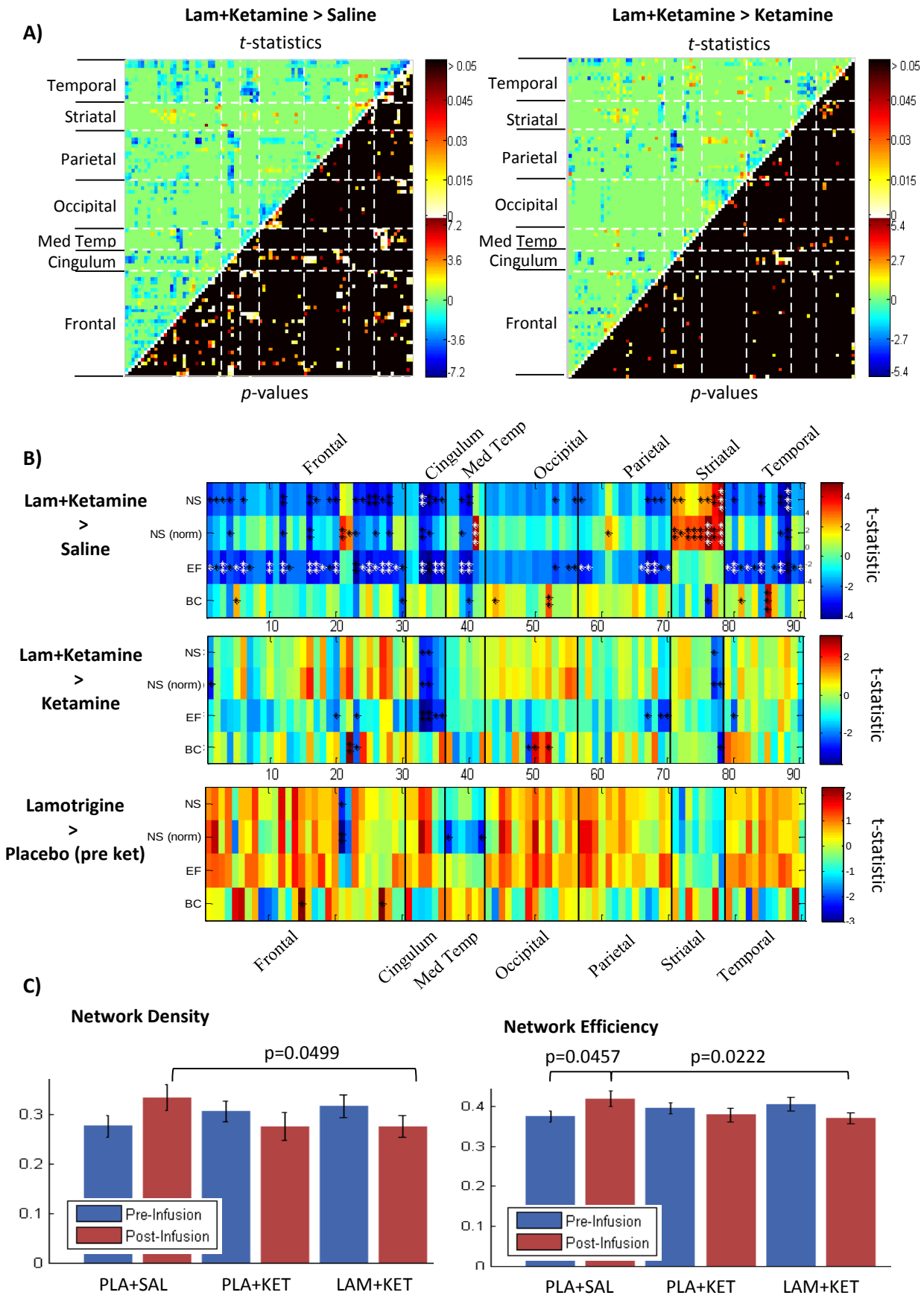

Figure 16 - Univariate comparison of micro, meso and macro-scale connectivity effects for LAM+KET, PLA+KET and PLA+SAL sessions. A) micro-scale effects on regional coupling B) meso-scale comparisons of NS, EF, and BC, stars indicate statistical significance * p<0.05, **p<0.01,*p<0.001. Comparisons which pass the BH test are indicated in white. C) macro-scale comparisons of Network density and Network efficiency values**

the lam+ketamine condition compared to saline, this is surprising as lamotrigine is hypothesised to attenuate the effects of ketamine resulting in a more saline state, however comparisons of efficiency reveal a contrary pattern of localised effects. A significant decrease in regional efficiency was observed in the obPFC, right superior temporal cortices, the posterior cingulate (pCC), parahippocampus, post central gyrus and the precuneus. Notably, many of these regions are associated with the DMN (introduced in Chapter 2), suggesting a reduced integration of the DMN for lamotrigine pre-treated ketamine compared to salience.

A similar trend of reductions was observed for comparisons of NS effects, however these changes were less pronounced with significant reductions reported in the right mid cingulate (mCC), right frontal inf operculum and right mid temporal pole only. No significant effects were reported for comparisons of BC measures. Furthermore we note the increases NS in the thalamus and obPFC failed to reach significance, unlike the comparison of ketamine and saline, suggesting a weak attenuative effect of lamotrigine in these regions.

Localised changes between lam + ketamine and saline were highly similar to that of ketamine and saline however much more pronounced. This suggests that lamotrigine does not significantly alter the topology of the ketamine induced state, rather it elicits further reductions in cortical efficiency resulting in a more pronounced ketamine induced connectivity sate, as measured by EF.

No significant effects were observed for the comparison of lamotrigine and placebo suggesting lamotrigine, at the administered dosage, does not robustly alter connectivity at baseline. Additionally, no significant effects were reported for the comparison of lam + ketamine and ketamine conditions also, suggesting lamotrigine, at the given dose, does not significantly alter the ketamine induced connectivity state. However, statistically notable, trend-level ($p<0.05$; uncorrected) effects were observed for this comparison, revealing a reduction in the ketamine-induced mCC and thalamus NS and EF values; Notable as this may suggest a weak, non-significant attenuative effect of lamotrigine in the thalamus and cingulate.

Effects of risperidone pre-treatment

To investigate the modulatory effects of risperidone on the ketamine induced connectivity, we compared conditions in the RIS+KET session to PLA+SAL and PLA+KET sessions, Figure 17. Significant (uncorrected) effects were observed on the global scale metrics with comparisons of pre and post infusion conditions in the RIS+KET session, decreasing both efficiency and density for the post-infusion ($p = 0.0093$ and $p = 0.0129$ respectively). This change in global metrics between pre and post ketamine infusion states with risperidone pre-treatment was more

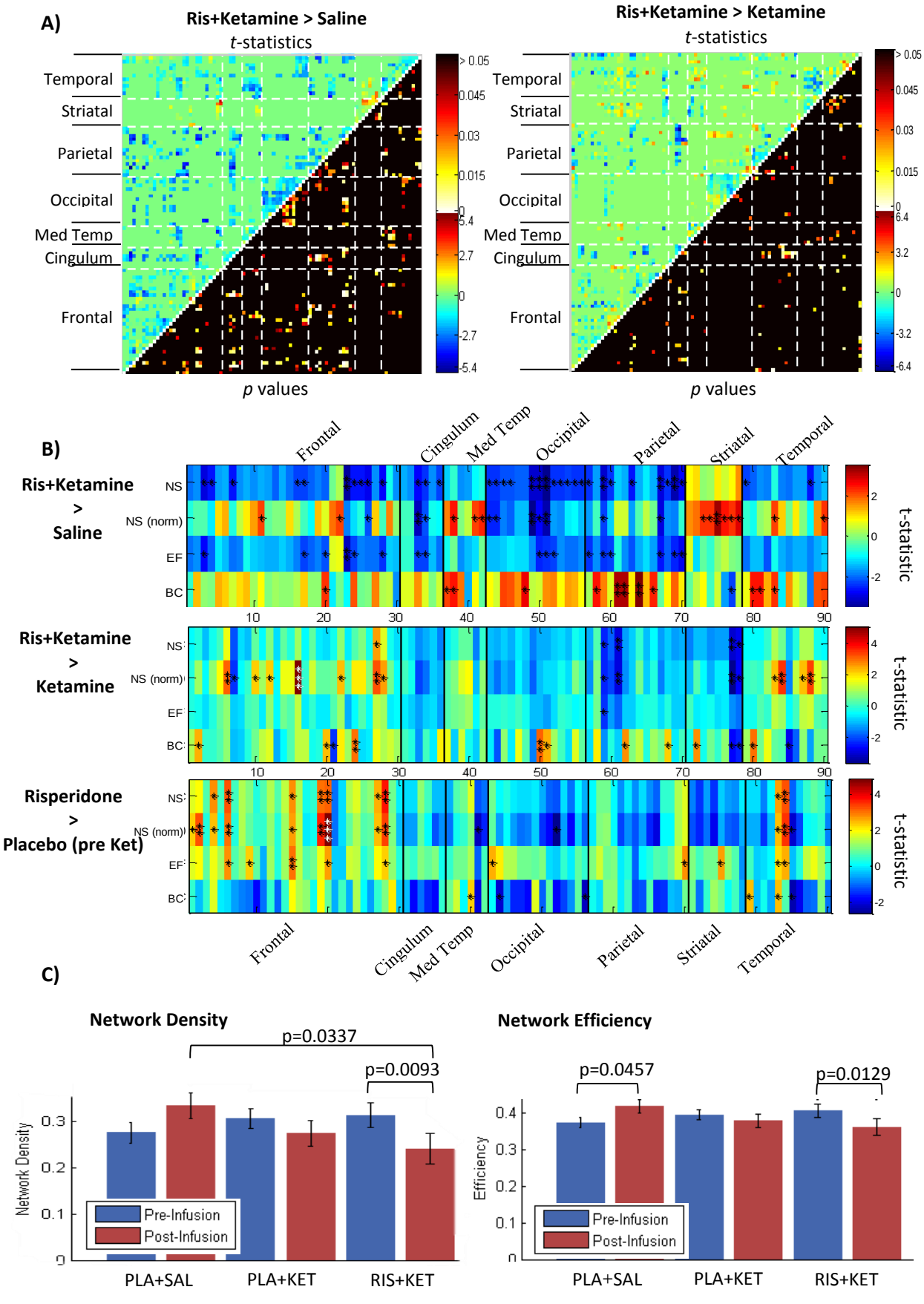

Figure 17 - Univariate comparison of micro, meso and macro scale connectivity measures for RIS+KET, PLA+KET and PLA+SAL sessions. A) micro-scale effects on regional coupling B) meso-scale comparisons of NS, EF, and BC, stars indicate statistical significance * p<0.05, **p<0.01,*p<0.001. Comparisons which pass the BH test are indicated in white. C) macro-scale comparisons of Network density and Network efficiency values**

pronounced than the change observed in PLA+KET and LAM+KET comparisons. This indicates risperidone globally alters network connectivity and to a greater extent than placebo or lamotrigine. This did not pass multiple comparisons.

No significant effects of risperidone were observed in micro-scale comparisons. When comparing meso-scale effects of ris + ketamine and saline, no significant effects were observed. This is notable as comparisons of ketamine and saline reported significant differences. Indeed comparisons of thalamic regions failed to report any statistically notable effect for ris + ketamine > placebo, a region strongly effected by ketamine.

This suggests either a protective effect or attenuative effect of risperidone on the ketamine state. Statistically notable, trend level ($p<0.05$; uncorrected) effects were observed in visual regions which were not present in comparisons between the saline condition and ketamine and lam + ketamine conditions. This indicates risperidone may have a weak effect in these regions however the lack of statistical evidence means this is supposition. The pattern of localised changes between ris + ketamine and placebo is noticeably different between NS and normalised NS measurement suggesting the risperidone induced change in density has localised effects, resulting in topological changes.

This modulation effect of risperidone on ketamine is most discernible through direct comparison of ris+ketamine and ketamine conditions, however only a single significant effect was observed. It was found risperidone significantly increases the normalised NS of the right inferior orbital frontal gyri. Trend-level ($p<0.05$; uncorrected) effects were also observed, namely an increase in NS in the gyrus rectus, and a decrease in thalamic NS and BC. Together this suggests a potential attenuation effect of risperidone on the ketamine state, particularly in the obPFC and thalamus, areas associated with network mediation and cognition.

Comparisons of risperidone to placebo reported a single significant effect at baseline, namely an increase in the Right supplementary motor area, as measure by NS (nom). Several trend-level changes were reported and can be summarised as an increased orbital frontal, supplementary motor, superior temporal pole and precentral cortical NS. This pattern of effects was notably different from that of lamotrigine suggesting differential mechanisms of action for pre-treatments.

Differential pre-treatment effects

To investigate differential connectivity effects of risperidone and lamotrigine, we directly compare both the baseline (main effects of pre-treatment) and post infusion (pre-treatment effects of ketamine) conditions in the LAM+KET and RIS+KET sessions, as shown in Figure 18.

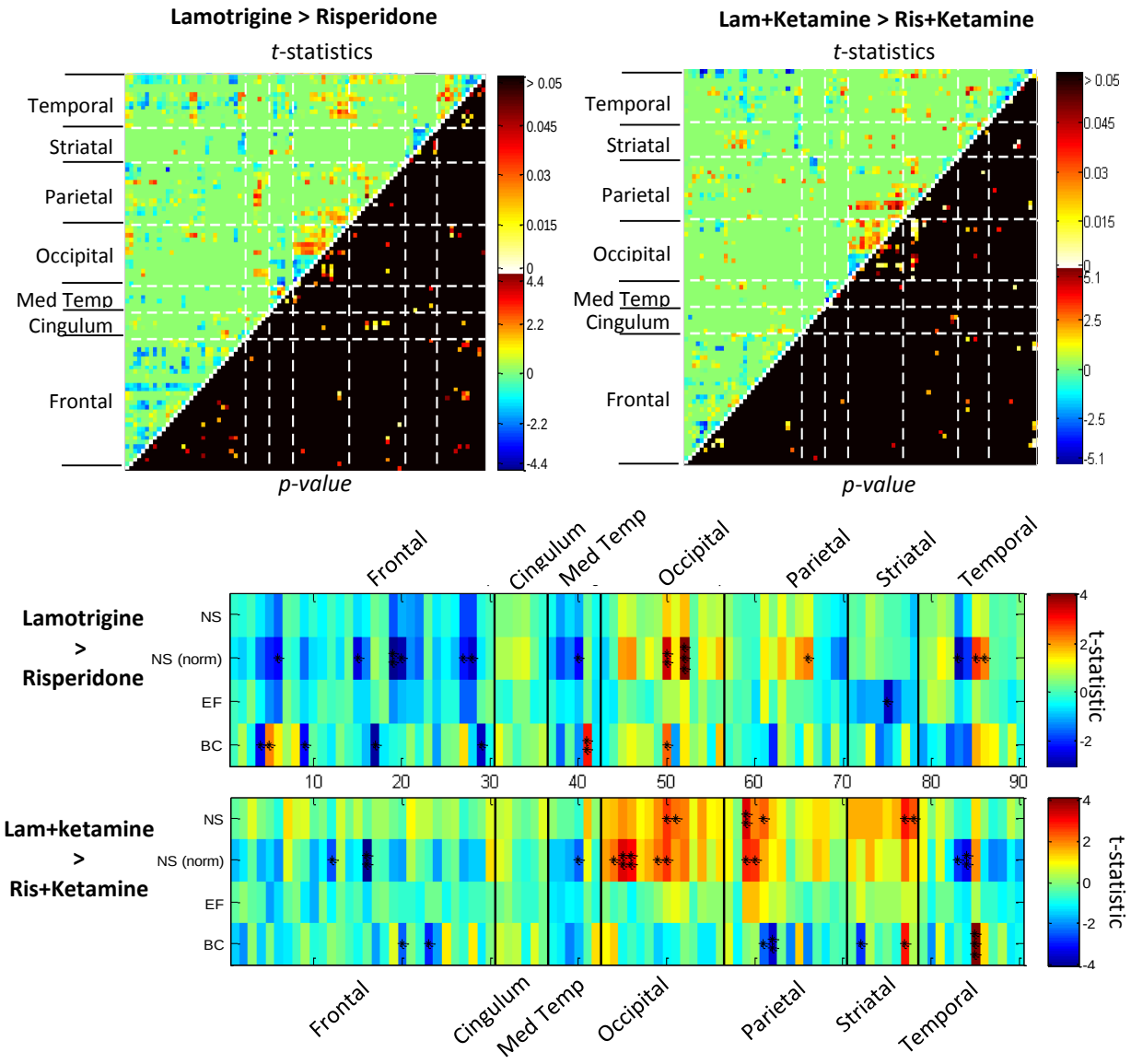

Figure 18 - Comparison of differential effects of risperidone and lamotrigine on micro, meso and macro-scales of connectivity. Stars indicate statistical significance * p<0.05, **p<0.01,*p<0.001**

No significant differences in macro-scale measures between lamotrigine and risperidone pre-treatments at baseline were reported. Statistically notable trend-level effects however were reported in micro and meso-scale connectivity comparisons, primarily in visual and supplementary motor areas as measured by normalised NS, and left insula, amygdala and thalamus as measured by BC.

Similar to baseline comparisons, no significant effects were for the comparison of the ris+ketamine and lam+ketamine however, trend-level (p<0.05) effects were also observed. These can be summarised as a risperidone induced increase in NS for primary and secondary visual regions, the thalamus and the superior parietal gyri. Also notable were decreases in BC values for superior frontal medial, pre-central and inferior parietal regions, and BC increases in left thalamus and angular gyrus.

The existence of these trend level effects leads to the supposition that lamotrigine and risperidone have subtly different mechanisms of actions both at baseline and on the ketamine response, however the limitations of this approach prohibit firmer conclusions to be drawn.

4.3.5 Discussion

Using commonly applied connectivity analysis methods, ketamine was observed to elicit distributed connectivity effects across various connectivity measures and spatial scales. A direct modulation effect of risperidone on the ketamine induced connectivity state was observed, however lamotrigine failed to yield any significant attenuation effects in direct comparisons. Taking the results as a whole we infer that both compounds affect a change in ketamine induced connectivity. The moderately high dimensionality of connectivity data and the need to correct for multiple independent statistical tests means that the sensitivity of this approach to detecting changes is reduced.

Effects of Saline

No significant effects changes in connectivity measures were observed between placebo and saline conditions, suggesting between session stability. However a range of statistically notable effects were observed ($p<0.05$). Most noteworthy was an increase in density and global efficiency, for saline compared to baseline. This is notable as all ketamine infused conditions were found to elicit a decrease in density, suggesting a differential change in relation to baseline for saline and ketamine conditions.

Examination of regional connectivity effects reveal a trend level increase in connectivity between cortical regions, most strongly in those regions associated with cognition within the saline condition. A topological change in connectivity was also observed resulting in a relative increase connectivity for ventrolateral frontal regions while decreased connectivity in visual areas. Further inspection of trend-level effects reveal widespread increases in NS and EF measures across the frontal cortex under saline, indicative of a session timing effect. While acquisition is akin to the resting state in so much as it is task free, we expect putative subjective effects due to the expectation and of ketamine infusion and the subsequent cognitive effects following the infusion period. It is these putative effects likely driving the observed differences. This presents an additional confound to be considered in comparisons of pharmacologically active conditions as observed effects may be influenced by both active pharmacologically and subjective cognitive state.

Interestingly, micro scale comparisons reveal weak differential connectivity effects of saline within visual regions. A trend of increased connectivity was observed between striate (V1) and

pre-striate (V2) visual regions, however saline was found to decrease V1 and V2 connectivity with extrastriate visual regions (V3-V5). While these effects are weak and non-significant they are notable as a consistent pattern of opposing connectivity effects within the visual cortex was consistent for all micros scale comparisons. This suggests the existence of a consistent connectivity structure in the visual cortex, the organisation of which is unaffected by the experimental condition.

Effect of Ketamine

Ketamine was found to decrease NS in the frontal and temporal regions. Furthermore, a non-significant decrease in network density was also observed. This is inconsistent with the findings in (Driesen et al. 2013), where ketamine was found increase global connectivity in comparison to saline. This disparity is likely due to methodological differences such as the thresholding procedure and fixed order sequential task design employed by Dreisen. This fixed order design represents a departure from the blinded randomised design implement in this study. This would likely cause a significantly different saline connectivity state. The reported increase in global connectivity reported by Driesen et al (2013) were particularly prominent in the thalamus and striatal circuits, which are consistent with our findings where we observe significant ketamine induced increases in striatal and thalamic connectivity.

Decreased NS was observed at the trend-level in the anterior prefrontal cortex, consistent with findings in (Scheidegger et al. 2012). This consistency in findings with our study however should be treated cautiously due to methodological differences. Most notably the disparity in administration and acquisition timings. Additionally, decreased connectivity was observed in OFC and frontal ventrolateral regions, areas strongly associated with cognition and sense of self. Significant effects of ketamine were observed in the gyrus rectus and mid temporal pole (mTP), reporting a decrease in connectivity compared to saline. The gyrus rectus has been linked to cognitive function, specifically executive tasks (Elderkin-Thompson et al. 2009), which may contribute to the cognitive deficits observed in ketamine. While these areas are notoriously difficult to image and often suffer from signal drop out (Ojemann et al. 1997); however, they are not significantly effected in the PLA-SAL session, lending credibility to the suggestion of ketamine specific effects in these areas. We note ketamine-induced reduction in ventrolateral NS values are lateralised toward the right hemisphere. It has been shown the right ventrolateral PFC has a dominant role in response inhibition (Garavan et al. 1999), the effects observed here may contribute to the deficits in response inhibition induced by ketamine (Morgan et al. 2004). Specific testing would be required to confirm this however.

Edge-wise comparisons suggest that these regional effects may be driven by trend-level decrease in connectivity between these regions and occipital cortices. The mTP has been implicated in linking of emotional response to sensory stimuli (Olson et al. 2007) and has been shown to contribute to sensory processing, disconnection of the mTP and visual areas is likely associated with the perceptual distortions, impaired memory and contextual processing that is experienced under ketamine.

We note significant differences between ketamine and saline conditions were observed in the mean motion parameter. As such any results between these conditions should be treated with caution. However given the similarity in the pattern of results for ketamine compared to saline and compared to placebo (where no significant motion effects were observed) we are inclined to believe the observed effects are primarily due to the experimental condition rather than driven by motion artefact.

We can summarise the functional connectivity effects of ketamine as a reduction of connectivity in the mTP, obPFC and right ventrolateral frontal cortices and an increase in sub-cortical connectivity. It is feasible that disruption of connectivity in the frontal cortices would lead to the disrupted cognitive processing, memory impairment and perceptual deficits observed with ketamine. Increased striatal connectivity, particularly in the thalamus, may be the result of a compensatory mechanism as the posterior pulvinar of the thalamus may play a significant role in synchronising pyramidal neurons (Shumikhina et al. 1999). Indeed the observed increased connectivity of the thalamus suggests an increased functional integration with the rest of the brain and may be a result of the thalamus compensating for ketamine-induced disruptions in pyramidal synchrony.

Modulation by Lamotrigine

Lamotrigine is theorised to attenuate the ketamine effect through reduction in glutamate release, achieved via Na^{2+} channel modulation. This may, to some extent, counter downstream effects of ketamine. A general trend of increased connectivity was reported across meso-scale measures for lamotrigine at baseline, as compared to placebo. Decreases in connectivity were also observed in the olfactory bulb (left) and anterior and posterior cingulate reporting statistically notable trend-level effect ($p<0.05$ uncorrected).

No significant effects were reported when investigating the modulation of the ketamine induced connectivity by lamotrigine. However the contrast of lamotrigine pre-treated ketamine against saline yielded distributed significant reductions in node efficiency, effects that did not reach significance for the comparison of ketamine and saline. The direction of change was consistent

between both comparisons however the significant results suggest lamotrigine pre-treatment alters the magnitude of ketamine induced efficiency changes resulting in more pronounced decreases in EF. Significantly decreased EF was observed in the OFC, mid frontal cortex, pCC and precuneus, areas associated with the so called default mode network (DMN). If lamotrigine truely enforces the ketamine reduced integration of regions of the DMN, this would be consistent with observations in (Scheidegger et al. 2012).

While the changes in EF values were increased with lamotrigine pre-treatment, the spatial distribution of effects in normalised NS values, with the exception of the cingulate, were highly similar for the saline condition contrasted to placebo and lamotrigine pre-treated ketamine. Considered as a whole, our results suggest lamotrigine does not have a robust attenuation effect on ketamine. The differential pattern of effects between contrasts suggest lamotrigine may induce a further decrease in ketamine-induced network efficiency, resulting in reduced integration between regions, most notably in frontal cortices. Furthermore this reduced efficiency likely effects the network uniformly, as revealed by similar patterns of normalised NS between contrasts; suggesting lamotrigine does not significantly not significantly altering the topology of ketamine-induced regional NS.

Modulation by Risperidone

Risperidone is expected to attenuate the ketamine induced connectivity through occupancy of 5-HT_{2A} and D_2 receptors (Nyberg et al. 1999) reducing glutamate levels downstream through 5-HT_{2A} antagonism. Risperidone has also been reported to potentiate NMDAR function directly (Konradsson et al. 2006). This presents a two mechanism of action by which risperidone may affect the ketamine response.

Few significant effects were observed for risperidone contrasts. In the comparison of saline and risperidone pre-treated ketamine states, no significant effects were observed. This is noteworthy given the contrasts of saline with lamotrigine and placebo pre-treated ketamine states both yielded widespread significant effects. Indeed while trend level-effects were observed in frontal and temporal cortices, similar to ketamine compared to saline, we did not observe any indication of an effect in striatal regions. This indicates an attenuation or protective effect of risperidone in this region. Decreases ($p<0.05$; uncorrected) in visual NS values were also present in the comparison of saline with risperidone pre-treated ketamine but not the comparison with placebo pre-treated ketamine. Furthermore the comparisons of network density suggest risperidone pre-treatment further reduces the network density of the ketamine infused state. This reduction in density does not affect all regions equally, topological changes

in trend-level effects were for normalised NS values between comparisons of saline contrasted with risperidone pre-treated ketamine and placebo pre-treated ketamine.

Inspection of direct modulatory effects of risperidone pre-treatment on the ketamine state reveal a single significant effect. An attenuative effect of risperidone in the right frontal inferior orbital region, as measured by normalised NS was reported. Trend-level ($p<0.01$) attenuation effects were also observed in normalised NS measures of the right frontal superior orbital region, the gyrus rectus, the thalamus and right temporal pole. This coupled with global measures and qualitative comparison of contrasts suggests that risperidone effects a reduction in network connectivity, further enforcing the ketamine induced reductions. Furthermore the results suggest, these reductions in connectivity do not occur uniformly over the network but rather elicit topological changes which to some extent attenuate the effect of ketamine. This is indicated by the comparison of risperidone and placebo pre-treated ketamine states and the differential pattern of normalised NS for saline contrasted to risperidone pre-treated ketamine and placebo pre-treated ketamine. This suggests the effects of risperidone differ from that of lamotrigine, and has implications regarding the effects of glutamate and NMDA blockade on functional connectivity in the brain.

Differential pre-treatment effects

Both lamotrigine and risperidone are theorised to reduce glutamate release, and thus attenuate the ketamine effect on the connectivity in the brain. Indeed, both pre-treatments have been shown to effectively modulate the ketamine BOLD amplitude response at the administered dosage (Doyle et al. 2013). The results presented here suggest differential modulatory effects of pre-treatments, implying down-stream glutamate release is not the sole driver of modulation of ketamine induced connectivity.

No significant effect was observed when directly comparing lamotrigine and risperidone pre-treated ketamine states. Statistically noteworthy effects ($p<0.05$) were reported for NS and BC comparisons. Taken together, our results suggest that risperidone and lamotrigine have subtly different effects on connectivity. Both compounds were found to strengthen ketamine induced reduction in network efficiency, however lamotrigine pre-treated ketamine did not exhibit substantially altered topological changes, unlike risperidone. Furthermore risperidone was found to significantly attenuate the effects of ketamine as measured by normalised NS, albeit in a highly localised manner. This considered with differential effects when contrasted to the saline state, suggest that both compounds elicit a weak magnitude modulation on connectivity and attenuate to some degree the ketamine induced thalamic connectivity. Risperidone however, exhibits trend-level topological effects not observed with lamotrigine pre-treatment resulting in

a more robust modulation of the ketamine state. This is surprising given results of previous study suggest lamotrigine has increased efficacy in attenuating the ketamine BOLD response when compared to risperidone (Doyle et al. 2013). This complex pattern of effects is likely due to the additional mechanism of action of risperidone, namely the ability to potentiate the NMDAR directly. This also demonstrates that functional connectivity analysis of ketamine reveals effects not observed when considering BOLD-amplitude only.

In summary, ketamine was found to reduce connectivity in the orbital frontal cortex and temporal pole while increasing the connectivity of the thalamus with the rest of the brain. We suggest that glutamatergic effects of ketamine are not solely responsible for the induced connectivity changes, but instead the blockade of the NMDAR likely has notable effect on functional connectivity in the brain.

Limitations

The analysis performed here, while informative, has limitations which must be considered. Firstly we note a general limitation of univariate analysis performed on high dimensional data, the need to correct for multiple comparisons. In this study we apply the BH test to correct for multiple statistical tests of a single measure within each comparison. This provides a principled means for correcting for false positives, however is insensitive to correlations between results and enforces a restrictive threshold potentially increasing the false negative rate. Furthermore, these univariate tests are not ideally suited for the analysis of connectivity data due the multivariate nature of the data. Arguably a much fairer form of analysis would be to compare patterns of connectivity while accounting for covariance within the data.

A consistent challenge when interpreting the results presented here has been the implementation of normalisation. Differences in network densities can drive regional measures of connectivity resulting in statistical differences in network topology; as such normalisation is often applied to correct for inter-subject differences in densities facilitating fair comparisons. In this study however, where we have paired pharmacological imaging data, it is arguably these very changes in overall connectivity that are of interest. Furthermore though the use of statistical testing which respects pairings in the data, we minimise the effect of inter-subject differences. One situation in which density normalisation may be appropriate is the comparison of subjects' connectivity between sessions where density differences may not relate entirely to the experimental condition and thus confound comparisons. The necessity for normalisation in pharmacological imaging remains contentious and further work is required to investigate the effects of comparisons with and without density correction.

When forming conclusions about the differences between groups or states based on graph theory measures, one must be cautious regarding the accuracy of a measure. Global measures, based on the accumulation of connections across the entire network, are subject to a myriad of confounds and must be treated with caution. Meso-scale connectivity measures also suffer the same limitations, albeit to a lesser extent than global measure. The summation of connectivity effects on a node provides an informative indication of regional connectivity effects, however may be skewed by outlier effects. There are also advantages to meso-scale measures, such as the reduction of dimensionality of the data and the ability to extract specific aspects of connectivity such as the integration or farness of a region. While all scales of connectivity measures are potentially informative, meso-scale measures, particularly the NS and EF, yielded the most significant results. This is due to the compromise in data dimensionality and sensitivity that these measures provide.

Further work is needed to examine the applicability of the graph theory metrics to neuroimaging data. Several studies have applied different metrics such as node strength, betweeness centrality and local efficiency (Sporns et al. 2007; Buckner et al. 2009; Rubinov et al. 2010; Lord et al. 2012), however many applied measures are highly correlated; such as efficiency and clustering coefficient. Currently these measures are purely interpreted in a context of network analysis however further work is required to develop an understanding of these measures in a biological context.

Chapter 5: Graph Theory and Machine learning

This chapter introduces the application of pattern classification to functional connectivity (FC) data for group comparison. This relatively new advance in the field of functional connectivity has shown a great deal of promise, however as yet little work has been applying this methodology to pharmacological imaging studies. In this chapter we demonstrate the use of pattern recognition (PR) applied to FC in order to discriminate between effects of different pharmacological compounds. We test the hypothesis that functional connectivity offers increased sensitivity to the effect of ketamine on the human brain. The secondary aim of this chapter is to investigate the applicability of multi-slice graphs as a feature set for group discrimination.

The work presented here consists, in part, of a paper published in the Journal of Psychopharamcology (2015).

5.1 Introduction

Ketamine, an N-methyl-d-Aspartate receptor (NMDAR) antagonist, has been demonstrated to induce glutamatergic dysfunction in healthy humans, as discussed in chapter 4. This has been linked to the acute onset of psychomimetic symptoms which resemble schizophrenia (Krystal et al. 1994; Goff et al. 2001; Corlett et al. 2011). While not a phenocopy of the disorder, ketamine has been used to investigate the glutamatergic hypothesis of schizophrenia (Lahti et al. 1995). It has been shown that acute ketamine elicits an in an increase in positive and negative symptom scores for schizophrenia, additionally has been shown to impair cognition (Dsouza et al. 1994; Honey et al. 2008).

Robust ketamine-induced effects on the amplitude of the blood oxygen level-dependent (BOLD) have been observed in healthy volunteers (Deakin et al. 2008; De Simoni et al. 2013; Driesen et al. 2013). Furthermore it has been demonstrated that this ketamine-induced BOLD effect is attenuated by pre-treatment with compounds theorised to reduce glutamate release (Deakin et al. 2008; Doyle et al. 2013). Indeed, a previous study employing the dataset used here, has demonstrated that the ketamine-induced BOLD response is attenuated by pre-treatment with clinically effective does of risperidone or lamotrigine in healthy volunteers (Doyle et al. 2013).

The functional connectivity in the brain has been shown to be altered as a result of acute NMDAR blockade in both and humans (Niesters et al. 2012; Driesen et al. 2013) and rodents (Gass et al. 2013); However it is not fully understood how this is achieved. It is theorised that this may be

the effect of downstream increased glutamate release, however evidence for this is lacking and may similarly be the result of NMDAR blockade.

In this chapter we investigate how acute ketamine affects the pattern of functional connectivity across the whole brain in healthy volunteers. Moreover we explore how this pattern of connectivity is affected by pre-treatment with the pharmacological probes lamotrigine and risperidone. The changes of these compounds on the ketamine induced connectivity reveals the effect of different modulatory mechanisms. If both compounds are found to modulate the ketamine-induced connectivity we would presume attenuation via glutamatergic systems. However if the ketamine connectivity effects result primarily from NMDAR blockade then we hypothesise lamotrigine will have little effect on the connectivity while risperidone may elicit attenuation effects.

We apply functional connectivity measures across the whole-brain in combination with PR techniques to compare experimental conditions and identify spatial patterns of whole-brain connectivity underlying the effects of acute ketamine. Multivariate pattern recognition techniques were favoured over standard univariate approaches due to the increased sensitivity that results from considering covariance between features. Furthermore these techniques provide a single outcome measure from each comparison, alleviating the issues associated with multiple comparisons testing, such as a potential increased false positive rate in the standard univariate framework. Moreover, pattern recognition provides a clinically relevant framework, allowing for classifications to be performed on a subject level, highlighting the potential of such techniques in aiding diagnosis and prognosis.

We favoured GPC over the commonly used SVM as the GPC weights samples by class typically, in the SVM framework, samples are weighted by distance from the margin and as such are not necessarily the most typical representatives of each class. This is important in the context of medical imaging where we have heterogeneous groups and wish to classify based on a typical class response.

Through comparison of conditions pre-treated with lamotrigine and risperidone, we investigate the effects of these pre-treatments on the ketamine-induced pattern of connectivity. As discussed in Chapter 2, PR techniques have recently been employed to perform single subject inference using measures of FC over the whole brain to investigate the effect of age (Dosenbach et al. 2010), cognitive processing (Richiardi et al. 2011; Shirer et al. 2012) and disease states (Zhang et al. 2011; Richiardi et al. 2012). Given findings of previous investigation into the BOLD signal amplitude effects within this dataset (Doyle et al. 2013), it is expected that both risperidone and lamotrigine pre-treatment will modulate the ketamine connectivity response.

Furthermore, we predict that the pattern of connectivity effects and discrimination accuracy for these modulatory effects will provide insight into the mechanisms underpinning ketamine's effect on the connectivity in the brain.

5.2 Materials and Methods

Data acquisition

In this chapter we investigate the application off functional connectivity analysis using PR, as applied to a ketamine dataset. Data was acquired and processed as described in Chapter 4.

Data preparation

As described in Chapter 4, data were pre-processed and normalized to standard MNI space. Nuisance parameters such as the mean CSF and WM signal and motion parameters were regressed from the data prior to band pass filtering with a pass band of 0.01Hz – 0.1Hz. The optimal choice of motion regression is an area of discussion within the literature, in this body of work we have favoured the regression of 6 motion parameters, R = [X Y Z pitch yaw roll], obtained from the detrended realignment estimates in the pre-processing. It has been suggested that this may be insufficient to remove all effects of motion and as such more complex models are required (Satterthwaite et al. 2013). Satterthwaite proposes a 24 regressor model, $R = [R\ R_{t-1}\ R^2\ R^2_{t-1}]$, where R_{t-1} refers to the temporal derivative of the regressor parameters (computed backwards) in order to more effectively remove the effects of motion.

Conversely, it has also been demonstrated that using more than the six parameters provides little advantage over randomised regressors for short time-series (Bright et al. 2015). Furthermore, it may be possible that the 24 parameter model may reduce the signal of interest and remove signal correlated with motion but neuronal in origin (Bright et al. 2015). In this work we have favoured the 6 parameter model however, to confirm such a motion correction procedure is sufficient for this dataset, we also consider the 24 parameter model used in (Satterthwaite et al. 2013).

Parcellation

To facilitate a graph theory analysis and reduce the dimensionality of the data, images were parcellated such that each parcellated region represents a node in a graph. The brain was divided into 116 anatomically homogeneous regions, as defined by the automated anatomical labelling (AAL) atlas (Tzourio-Mazoyer et al. 2002), providing complete coverage of cortical and sub-cortical structures. The AAL was chosen due to its prevalence within neuroimaging studies

(Zalesky et al. 2010; Braun et al. 2012), to some extent facilitating a qualitative analysis between connectivity analyses. The connectivity within the brain was modelled as a graph, *G = (V, E)*, consisting of a collection of nodes, V, here defined by the AAL, and a collection of edges between nodes, E. Each node in V is represented by the mean signal of all voxel members of the corresponding AAL atlas region.

Graph estimation

Task-free networks have been demonstrated to exhibit spatiotemporal dynamics, as discussed in Chapters 3, 7 and 8. In order to capture these dynamics, we compute multi-slice connectivity graphs using a Gaussian windowing approach (Chapter 3) over a range of temporal scales.

It has been demonstrated that connectivity states can be robustly separated with as little as 30-60 seconds of data (Shirer et al. 2012), these short window lengths reveal connectivity effects at higher frequencies. Networks derived from longer window lengths provide insight connectivity effects at lower network frequencies, with increased stability. In order to investigate the effect of ketamine on different network frequencies we applied a moving window procedure using window lengths (w) of 90, 180 and 360 seconds, with respective effective lengths of 30, 60 and 120 seconds. This provides a broad coverage of the available frequencies of connectivity variation. Gaussian windows, computed to have six standard deviations width where σ=T/6, were applied to the time series in discrete intervals of 2σ = T/3, the effective length. The rationale was to minimise overlap of the central portion of the window which predominantly drives the correlation. The temporal positioning of these windows, with an effective length of 30 seconds is illustrated in Figure 19.

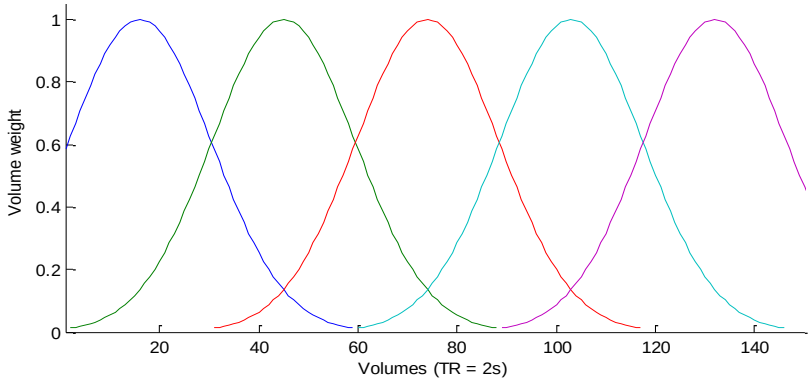

Figure 19 - Windowing procedure used to truncate time series for estimation of windowed correlation using a Gaussian window of full length 180 seconds, effective length 60 seconds (30 volumes)

For each window position, the weighted truncated time series as obtained and the connections between each node pair were estimated using Pearson's correlation coefficient. We also estimate connectivity using the conventional *single-pass* approach, where the entire time series

for a given condition is used to compute the correlation coefficient. This resulted in a collection of connection matrices, representing the connectivity at each window position.

Nodal Measures

The functional connectivity network of the brain is highly dimensional as such, interpretation can present challenges. In order to aid interpretation, we abstract networks to a collection of summary statistics representing an aspect of functional connectivity for each node. In this work we compute the node strength, NS, as defined in Chapter 3. This is an intuitive representation of the *connectedness* of a region with the rest of the brain, resulting in a measure of node importance with respect to a given network.

The NS values at each graph slice were calculated for each graph and were centred by the respective graph density, this allows for comparisons of network topology between conditions with differing densities. Furthermore, this necessary for topological comparisons between subjects and conditions where subjective responses to compounds elicit changes in network density.

This process resulted in a collection of NS measures representing discrete periods of connectivity for each subject in each condition. The number of samples of whole brain NS measures are dependent on the length of the window used, with shorter window lengths resulting in more discrete representations of connectivity per subject in each session. These NS samples were then used as a feature set for Gaussian process classification.

Pattern Recognition

Comparisons between session conditions was performed using Gaussian process classification (GPC), as described in Chapter 3. Condition comparisons were performed separately for each window length employed. As such each subject had multiple samples of subject-wise mean centred NS values, used as feature set for each condition comparison.

Leave one out cross validation (LOOCV; Chapter 3) was employed to estimate classification accuracy and permutation testing (Chapter 2) the significance of a comparison. In this application each subject was represented by a collection of samples, as such for each “hold out” subject, all NS samples computed for different window positions were used in the test case to avoid introducing bias. The obtained accuracies and significance values were then used to quantitatively compare condition similarities where a high significant accuracy suggest a robust difference between classes, while a chance level (50%) accuracy indicates an inability of the classifier to distinguish classes.

We performed classification in two configurations; 1) conditions in the PLA+SAL and PLA+KET sessions were classified to investigate the effect of ketamine on whole-brain connectivity. 2) To investigate the effects of pre-treatment using lamotrigine and risperidone on the ketamine induced pattern of connectivity, conditions in LAM+KET and RIS+KET sessions were contrasted to conditions in the PLA+KET and PLA+SAL sessions. Multiple comparisons testing was applied using the Benjamini-Hochberg procedure at a level of $\alpha=0.05$ in order to account for the number of statistical tests performed.

To investigate the existence consistent robust motion effects, motion parameter summaries namely the mean, maximum and median framewise displacements were used as a feature set to compare experimental conditions using a GPC. Significant discriminations based on motion would indicate a robust, predictable noise structure in the data and would indicate the need for caution when interpreting any observed difference in connectivity. Furthermore, to confirm the applied motion regression procedure is not insufficient we repeat the classifications performed in configuration 1) from above with data regressed the using the additional motion regression models discussed in the pre-processing section, namely the 12 and 24 parameter models.

In order to investigate ordinal trends between experimental conditions, we applied ordinal regression using Gaussian processes (ORGP)(Doyle et al. 2013). The existence of an ordinal progression between rank ordered classes may be reveal by accurate discrimination of classes, if not ordinal trend is present then a poor class discrimination may be observed. For further details on this multi-class classification algorithm, we refer the reader to (Chu et al. 2005).

Classification Maps

To visualise the spatial covariance's driving the classifications, multivariate maps (g-maps) were generated for significant comparisons ($p < 0.05$). In these maps, we render graph nodes as spheres spatially centred on their corresponding AAL region in the brain, the colour of the sphere indicates the class membership and the radii the relative weight in relation to its class typicality. These weights are interpreted such that features with positive weights reported a greater weighted average node value for the class with the positive class label, and vice versa for the negative class label, recalling that classes are encoded with the labels ±1, for example placebo = +1 and ketamine = -1. Due to the multivariate nature of this analysis, the sign of a nodes weighted average within a these maps is determined by the change in node strength as well as its variance the classification parameterisation. To confirm the direction of change for a given node, t-tests were performed on node deltas; these were only used qualitatively to avoid imposing any univariate assumptions on the data.

To confirm the consistency between g-maps between classifications performed using different windowing parameters, the intra class correlation coefficient (ICC(3,1)) was applied, as described in Chapter 3.

5.3 Results

Comparison of motion summary parameters

Motion parameter summary values namely the mean, maximum and median frame-wise displacement values were compared between experimental conditions to confirm motion robustness. No significant differences were observed, Table 1, this suggests the lack of robust predictable structure in the motion parameters as represented by the summary statistics, lending confidence to conclusion that any observed effects are due not due to motion artefacts.

Table 1 - Results for the comparison of experimental conditions in the PLA+SAL and PLA+KET sessions using motion summary parameters as a feature, specifically mean, maximum and median frame wise displacements

Comparison			Accuracy (%)	p-value
Placebo (pre Sal)	v	Placebo (pre Ket)	43.75	0.942
Placebo (pre Sal)	v	Saline	56.25	0.288
Placebo (pre Ket)	v	Ketamine	56.25	0.224
Saline	v	Ketamine	59.38	0.121
Risperidone	v	Placebo (pre Ket)	56.25	0.430
Risperidone	v	Ris+Ketamine	53.12	0.167
Ris+Ketamine	v	Saline	53.12	0.341
Ris+Ketamine	v	Ketamine	46.88	0.862
Lamotrigine	v	Placebo (pre Ket)	43.75	0.928
Lamotrigine	v	Lam+Ketamine	56.25	0.250
Lam+Ketamine	v	Saline	59.38	0.124
Lam+Ketamine	v	Ketamine	65.62	0.061
Lamotrigine	v	Risperidone	53.12	0.451
Lam+Ketamine	v	Ris+Ketamine	53.12	0.189

Ketamine robustly alters the whole-brain functional connectivity pattern

Conditions with the PLA+KET and PLA+SAL sessions were compared in order to investigate the primary effects of ketamine on the pattern of NS in the human brain. We observed consistently high and significant classification accuracies for the comparison of saline and ketamine across all network parameters (87% < Acc < 94%) as shown in Table 2. The classifier was also able to accurately differentiate the pre and post infusion conditions in the PLA+KET sessions (75% < Acc < 82%); similar patterns of weights driving the classifications were observed for both

comparisons. Furthermore, similar accuracies were observed across comparisons using different window parameters, indicating a similar effect of ketamine across network frequencies.

We were unable to significantly separate pre-infusion conditions in the PLA+KET and PLA+SAL sessions (62% < Acc ≤ 75%) and between conditions within the PLA+SAL session (56% < Acc < 69%). This suggests a similarity between placebo states, akin to between session stability. Moreover, an inability to separate pre and post infusion conditions in the PLA+SAL session is considered akin to with-in session stability.

Table 2 - Classification accuracies for the comparison of PLA+KET and PLA+SAL sessions using GPC accessed using LOOCV and permutation testing over a range of network parameterisations, namely Gaussian window lengths of 60, 120 and 240 seconds. Comparisons were also performed using networks estimated from the entire condition time series, indicated by "All". Bold p-values indicate significance after multiple comparisons testing

Comparison	Window (sec)	Accuracy (%)	p-value
Placebo (pre Sal) V Placebo (pre Ket)	90	75.00	**0.012**
	180	68.75	0.036
	360	68.75	0.029
	All	62.50	0.154
Placebo (pre Sal) V Saline	90	56.25	0.261
	180	56.25	0.311
	360	68.75	0.075
	All	62.50	0.119
Placebo (pre Ket) V Ketamine	90	78.13	**0.016**
	180	75.00	**0.006**
	360	81.25	**0.007**
	All	75.00	**0.047**
Saline V Ketamine	90	90.63	**0.004**
	180	93.75	**0.002**
	360	90.63	**0.008**
	All	87.50	**0.015**

This configuration of classifications were repeated using data regressed with the 24 motion parameter model (Satterthwaite et al. 2013), Appendix C. A similar pattern of group discriminations were observed for comparisons between both sets of "cleaned" data however, we note a reduction in the accuracy of the comparison of placebo and ketamine conditions.

Examination of the discrimination map (g-map) driving the classification between ketamine and saline conditions reveals a distributed pattern of effects. Figure 20 depicts the g-map for this comparison performed on connectivity estimated with a window length of 180 seconds. The discrimination maps for this classification performed with different window lengths were compared to confirm the consistency of discriminating patterns. An ICC of r = 0.9769 was

reported for discrimination maps obtained for this comparison across different window lengths, indicating a strong consistency between the discriminating pattern of weights across windowing parameters.

Ketamine (depicted in Red) is strongly represented in predominantly sub-cortical and cerebellar regions, whereas saline (depicted in Blue) is represented by a pattern of weights most prominent in occipital, temporal and pre-frontal cortices. A similar pattern of effects was observed for the comparison of saline and ketamine, suggesting a common effect driving both classifications.

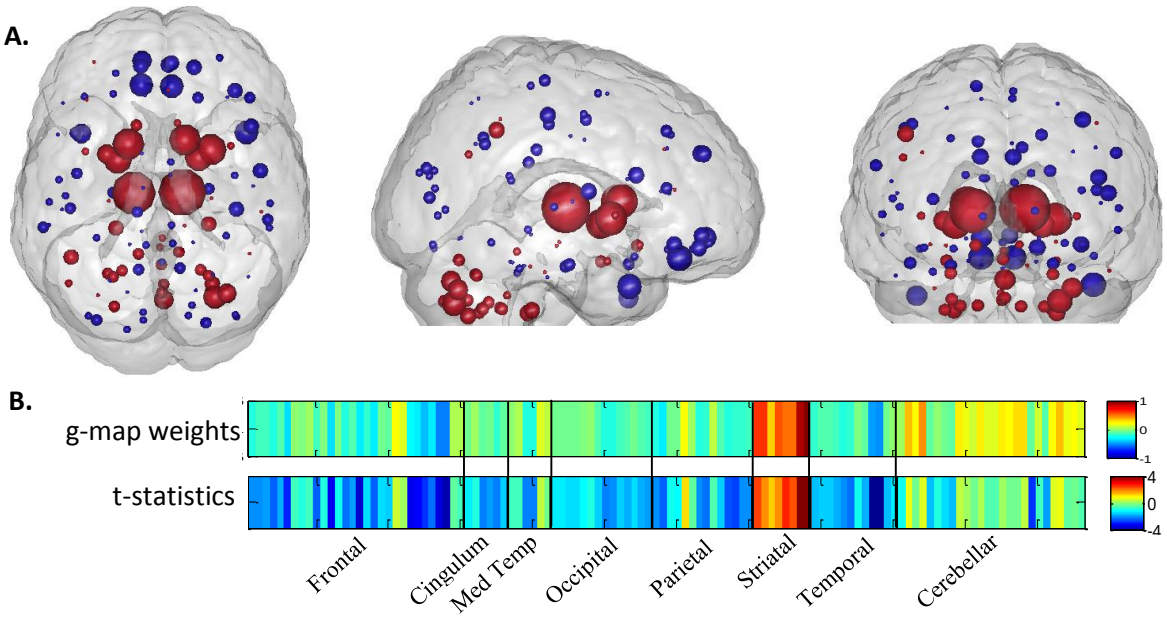

Figure 20 – A) Discrimination map for the classification of saline (Blue) against ketamine (Red) using NS measures computed using a 180 second sliding Gaussian window. Spheres represent weights where the radii of the sphere indicates the magnitude of the weight. Spheres were spatially positioned at the centre of their corresponding AAL region. B) g-map weights in matrix form and nodal t-statistics for ketamine > saline.

Additional t-tests were perform on windowed NS values directly to confirm the regions with increasing NS relative to placebo matched the pattern of weights favouring ketamine (red) and that the same was true for decreasing NS values and negative weights (blue), Figure 20B. While the direction of change is consistent between both univariate and multivariate tests, the amplitude is not. Striatal regions were strongly weighted in both analyses however in the pattern of node strengths in the cortical regions differed between in the multivariate approach likely reflecting the sensitivity of this approach to covariance in the data.

Effect of risperidone pre-treatment

The effects of risperidone pre-treatment were investigated by comparing conditions within the RIS+KET session with those of PLA+KET and PLA+SAL, as shown in Table 3. We observe consistent modulatory effects of risperidone across several comparisons.

The pattern of node NS for the risperidone condition was not significantly different from placebo (pre ket) when comparing connectivity estimated using the entire time series, however shorter window lengths (< 360 sec) reported significant effects ($p \leq 0.001$). Furthermore, we observe an ICC of $r = 0.93$ between g-maps from this comparison using window lengths of 90, 180 and 360 second. This may be due to risperidone having an effect on the temporal dynamics of connectivity in the brain at higher network frequencies, when compared to placebo. Examination of the pattern of weights driving these classifications, the g-map from this classification using a 180 second window is visualised in Figure 21, reveals the pattern of NS describing risperidone is strongly represented in frontal and parietal regions which corresponded to a univariate increase in NS when compared to placebo (pre Ket). The pattern of weights favouring placebo was strongly represented in occipital, temporal and subcortical regions which univariate tests confirmed exhibited decreased NS. These effects are opposite of those observed for ketamine in frontal and sub-cortical regions. Notably the univariate analysis did not reveal any notable effect in sub-cortical regions.

Table 3 - Results of GPC classifications for conditions in RIS+KET sessions against PLC+SAL and PLC+KET sessions using a range of window parameters, revealing modulatory effects of risperidone pre-treatment on the pattern of NS expressed in the brain. Bold p-values indicate significance after multiple comparisons testing. Bold p-values indicate significance after multiple comparisons testing

Comparison	Window	Accuracy (%)	p-value
Risperidone V Placebo (pre Ket)	90	87.50	**0.001**
	180	87.50	**0.001**
	360	71.88	**0.020**
	All	50.00	0.424
Risperidone V Ris+Ketamine	90	71.88	**0.020**
	180	78.13	**0.004**
	360	81.25	**0.004**
	All	81.25	**0.009**
Ris+Ketamine v Saline	90	78.13	**0.010**
	180	81.25	**0.002**
	360	87.50	**0.001**
	All	62.50	0.150
Ris+Ketamine v Ketamine	90	87.50	**0.001**
	180	93.75	**0.0001**
	360	93.75	**0.0002**
	All	75.00	**0.008**

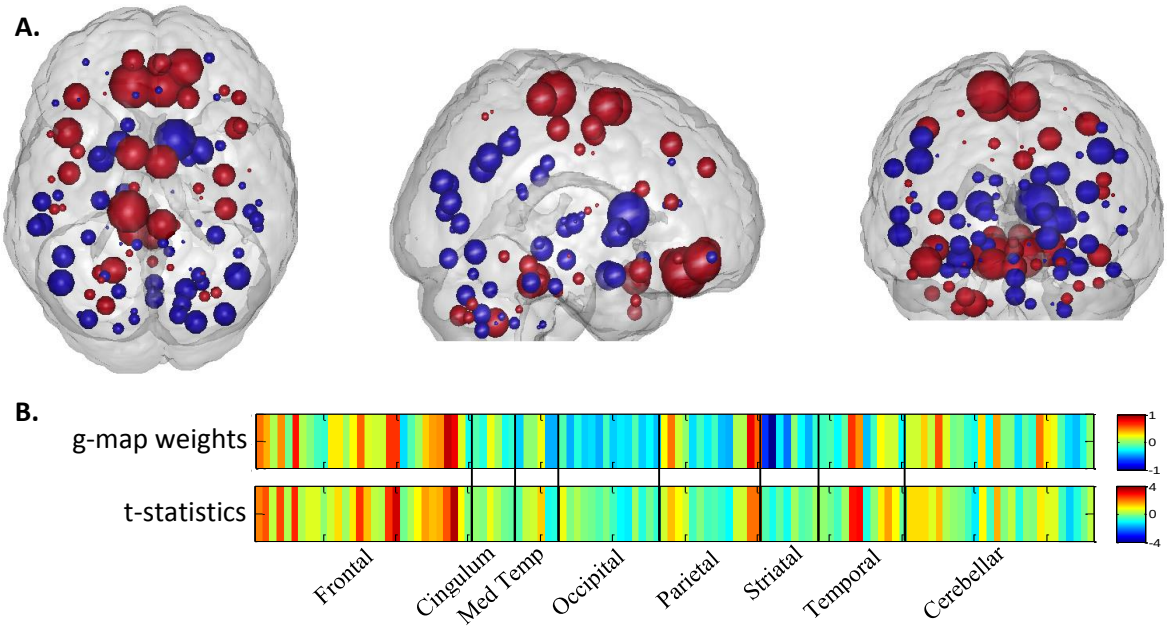

Figure 21 – A) g-map for the comparison of risperidone (Red) and placebo (Blue; pre Ket) compared using NS measures computed using a 180 second sliding window, revealing the effects of risperidone on the pattern of connectivity in the brain. B) g-map weights in matrix form and nodal t-statistics for risperidone > placebo.

The comparison of pre and post infusion conditions for the RIS+KET session yields significant difference between conditions (71.875% ≤ Acc ≤ 81.25%) indicating ketamine modulates the risperidone induced pattern of NS. Consistently high accuracies were observed across all tested window lengths suggesting a consistent effect across windowing parameters. Examination of the weight map for this comparison with a 360sec window length, shown in Figure 22A, reveals ketamine modulates risperidone NS patterns with the greatest effects in sub-cortical, occipital and cerebellar regions. Ketamine was found to cause a relative increase in sub-cortical and cerebellar NS while decreasing occipital NS. Comparing the g-maps for the windowed classifications of this comparison reveal an ICC of r = 0.9349, suggesting a similar effect driving all windowed comparisons. The low contribution from frontal and temporal cortices could indicate an attenuative effect of risperidone preventing ketamine effects in these regions, which ketamine is unable to modulate the risperidone induced NS pattern in these regions or that effects in these regions don't contribute to class discrimination.

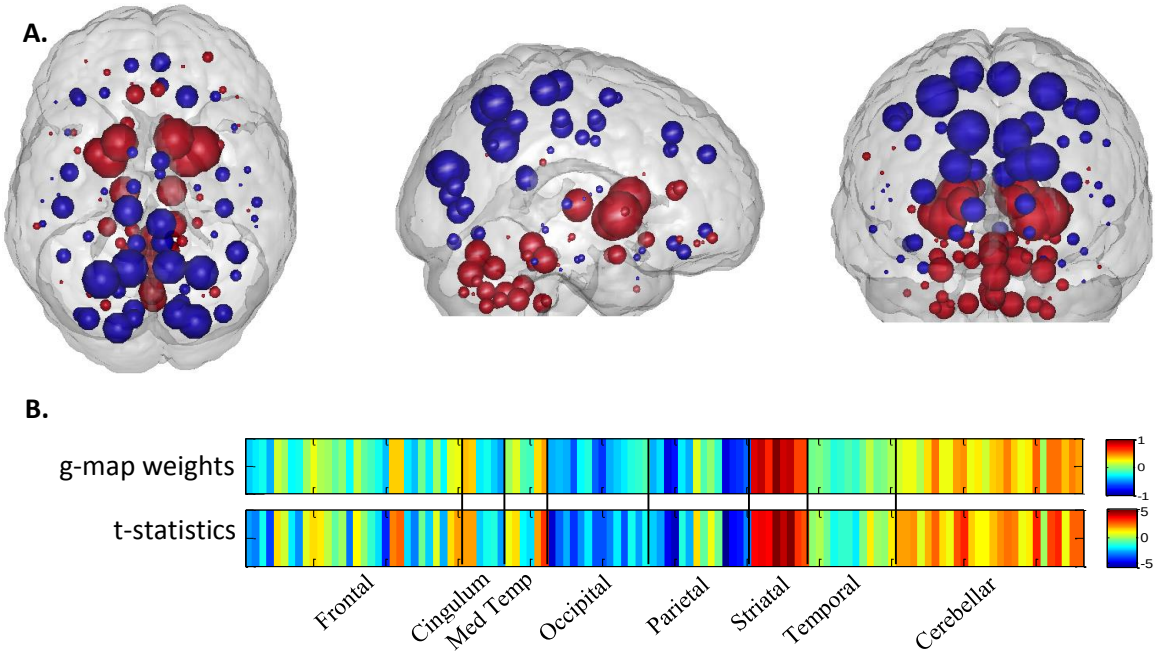

Figure 22 – A) Comparison of pre (Blue) and post (Red) condtions in the RIS+KET session, classified using NS measures copmputed using a sliding Gaussian window of length 360 seconds, revealing the main effect of ketamine on the risperidone state. B) g-map weights in matrix form and nodal t-statistics for risperidone Infusion > baseline.

Ris + ketamine was significantly discriminated from both ketamine and saline when using a windowing approach to estimate connectivity. This suggests the interaction between risperidone and ketamine results in a dissimilar pattern of NS to both saline and ketamine. The pattern of effects driving the classification of ris+ketamine and saline conditions, compared using connectivity estimated with a 360 second window length, is reveal by the weight map in Figure 23. This pattern contains a spatial similar distribution of weights to the comparison of ketamine and placebo Figure 20, suggesting a ketamine effect driving the classification. Ris+ketamine (depicted in Red) is represented strongly in the insula, sub-cortical and cerebellar regions, while saline (depicted in Blue) is characterised by a pattern of weights most prominent in occipital, parietal and pre-frontal cortices.

The main effects of risperidone on the ketamine infusion, as revealed by the comparison of ris+ketamine and ketamine (Figure 24; classified using NS measures obtained with window length of 180 seconds), suggest risperidone pre-treatment results in reduced thalamic NS and increased orbital pre-frontal and temporal pole NS. High accuracies were observed across all classifications for this comparison, however classifications using a windowing approach reported notably higher accuracies; the g-maps from these classifications were highly similar reporting an ICC of r = 0.9401. The pattern of weights describing the risperidone + ketamine condition are primarily distributed in frontal and temporal cortices; weights favouring ketamine were predominantly located in occipital, sub-cortical and cerebellar regions.

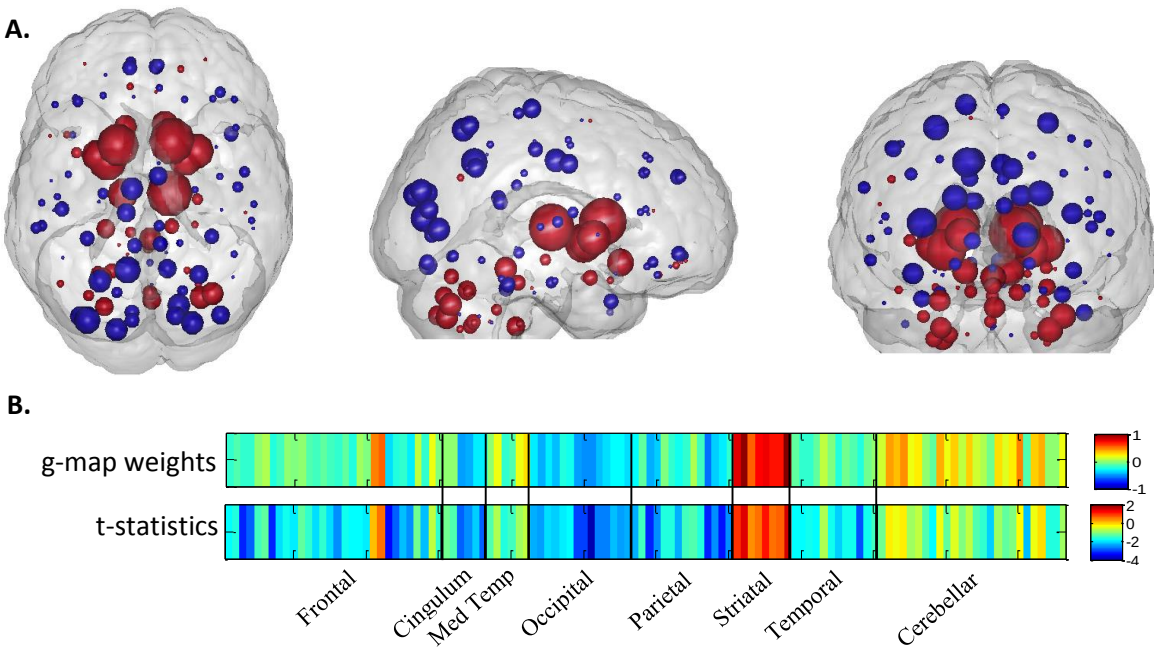

Figure 23 – A) Comparison of saline (Blue) and ris + ketamine (Red) condtions, classified using NS measures copmputed using a sliding Gaussian window of length 360 seconds, revealing the main effect of ketamine on the risperidone state. B) g-map weights in matrix form and nodal t-statistics for ris + ketamine > saline.

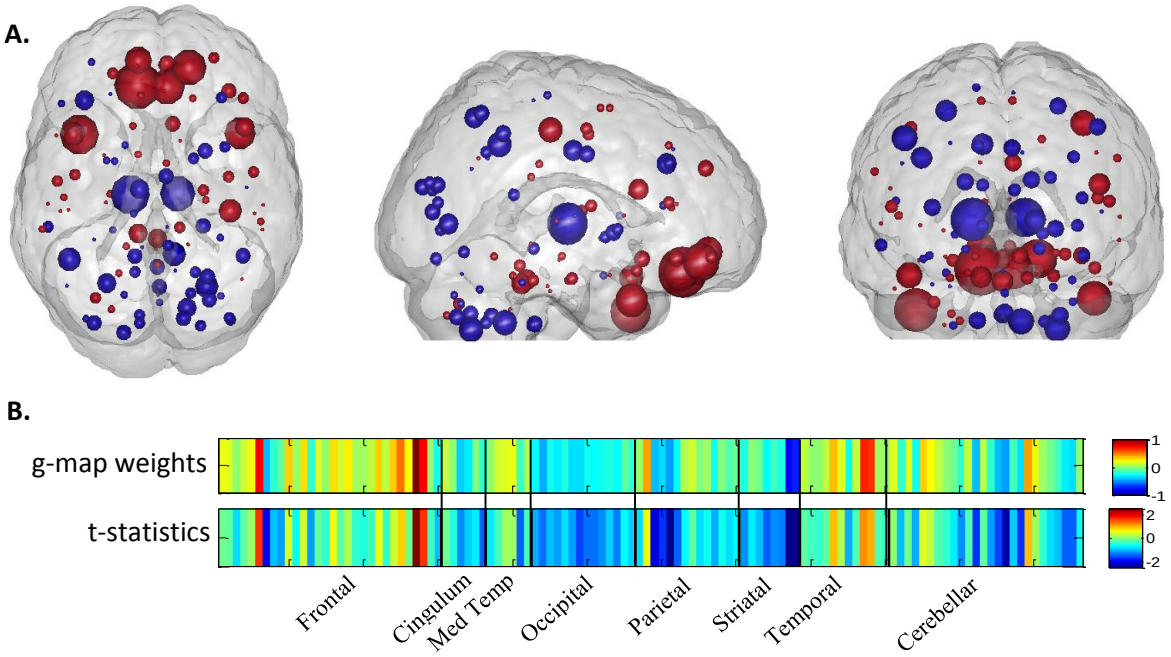

Figure 24 – A) Comparison of ris + ketamine (red) and ketamine (blue) conditions using NS measures computed using a window length of 180 seconds. This reveals attenuative effects of risperidone on the ketamine state. B) g-map weights in matrix form and nodal t-statistics for ris + ketamine > ketamine.

Effect of lamotrigine pre-treatment

To investigate the effect of lamotrigine pre-treatment on the ketamine induced NS patterns we compared conditions from the LAM+KET session with those in the PLA+KET and PLA+SAL sessions. Reported accuracies, as illustrated in

Table 4, were reasonably consistent across different window parameters suggesting lamotrigine doesn't differentially effect the temporal dynamics of brain connectivity.

Lamotrigine was not observed to have any significant effect on NS at baseline, as evidenced by the chance level accuracy for the comparison between lamotrigine and placebo across all windowing parameters (Acc < 69%). Furthermore, we found no evidence to suggest lamotrigine alters the ketamine induced NS patterns (Lam + Ketamine v Ketamine; Acc ≤ 50%). Indeed comparison of weight maps for the comparison between saline v ketamine and saline v lamotrigine + ketamine reveal a similar spatial distribution of weights, suggesting similar effects driving both classifications. Taken as a whole, these results suggest lamotrigine, at the administered dosage has little effect on the ketamine induced pattern of NS.

Table 4 - Classification results for comparisons of conditions in LAM+KET session against PLA+KET and PLA+SAL sessions over a range of windowing parameters, revealing modulatory effects of lamotrigine on the pattern of NS in the brain. Bold p-values indicate significance after multiple comparisons testing

Comparison	Window	Accuracy (%)	p-value
Lamotrigine v Placebo (pre Ket)	90	31.25	0.968
	180	37.50	0.990
	360	37.50	0.990
	All	68.75	0.014
Lamotrigine v Lam+Ketamine	90	87.50	**0.002**
	180	87.50	**0.005**
	360	90.63	**0.003**
	All	87.50	**0.011**
Lam+Ketamine v Saline	90	93.75	**0.001**
	180	93.75	**0.0014**
	360	93.75	**0.0016**
	All	100.00	**0.0002**
Lam+Ketamine v Ketamine	90	43.75	0.687
	180	43.75	0.641
	360	50.00	0.423
	All	37.50	0.845

Comparison of pre-treatments

Comparisons were performed between the LAM+KET and RIS+KET sessions for baseline and post infusion conditions to investigate differential modulation of the ketamine NS state. The results for comparison between pre-infusion and post-infusion conditions can be found in Table 8.

The classifier was unable to significantly discriminate conditions at baseline, suggesting a similar pattern of effects at baseline. However we observe a significant classification accuracy for the comparisons of lamotrigine and risperidone pre-treated ketamine conditions when compared using connectivity estimated using a windowing approach (75% ≥ Acc > 88%). Suggesting both compounds differently affect the pattern of ketamine induced centrality. Inspection of g-maps for the comparisons of lamotrigine and risperidone pre-treated ketamine conditions computed using a windowing approach reveal a similar pattern of effects, reporting an ICC of r = 0.9898. Inspection of weights for this comparison, as shown in Figure 25 reveal a spatial distribution of weights highly similar to that of risperidone + ketamine and ketamine. This further supports the finding that lamotrigine has similar effect on ketamine as placebo.

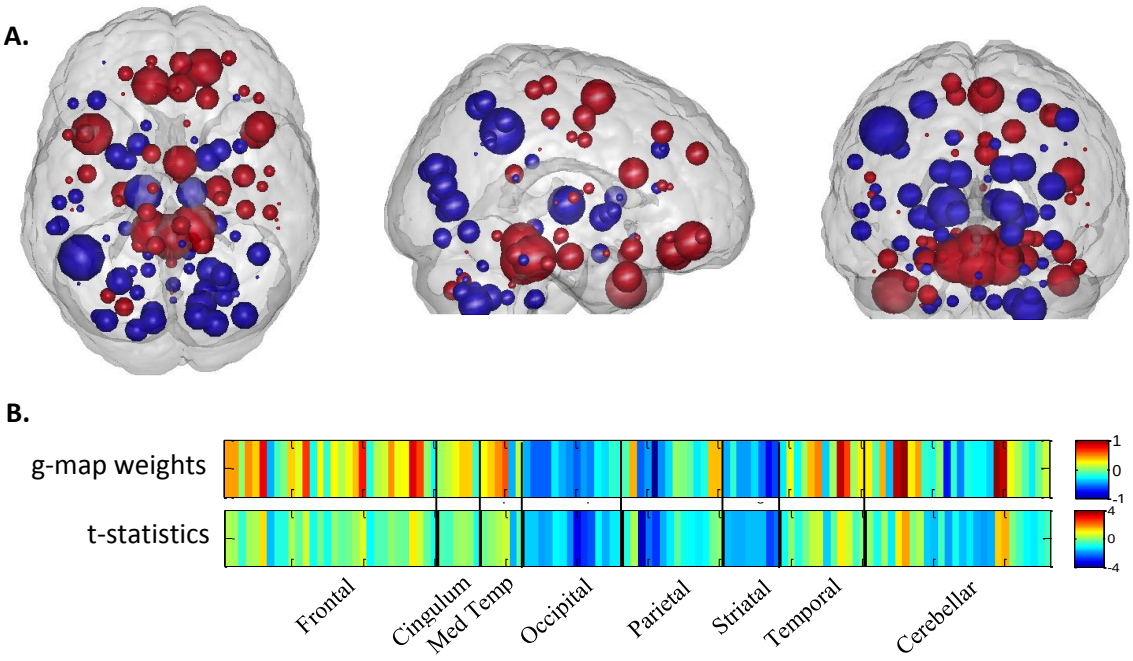

Figure 25 – A) g-maps for the comparison of ris + ketamine (Red) and lam + ketamine (Blue) classified using NS measures obtained with a windowing approach (window length = 360sec). This reveals the differential effects of lamotrigine and risperidone on the ketamine induced connectivity. B) g-map weights in matrix form and nodal t-statistics for ris + ketamine > lam + ketamine.

Table 5 – Results of GPC classifications for comparisons of RIS+KET and LAM+KET conditions over a range of window parameters. This reveals any differential of pre-treatments at baseline or on the ketamine-induced connectivity state. Bold p-values indicate significance after multiple comparisons testing

Comparison	Window	Accuracy (%)	p-value
Lamotrigine v Risperidone	90	68.75	0.058
	180	75.00	**0.006**
	360	62.50	0.120
	All	56.25	0.178
Lam+Ketamine v Ris+Ketamine	90	75.00	**0.016**
	180	84.38	**0.003**
	360	87.50	**0.0017**
	All	68.75	0.078

Ordinal regression

To investigate any ordinal attenuation effects of lamotrigine and risperidone on the ketamine-induced connectivity, we performed ordinal regression (Doyle et al. 2013). Two analyses were performed to investigate these possible attenuation effects, with conditions rank ordered: 1) Saline v Ris + Ketamine v Ketamine and 2) Saline v Lam + Ketamine v Ketamine.

Table 6 – Confusion matrix for ORGP of saline, ris+ketamine and ketamine conditions for classifications using NS values computed over a range of window lengths. For each confusion cell, the window length used to estimate the connectivity is shown on the left and the resultant confusion value on the right

Observed	Predicted: Saline	Predicted: Ris+Ket	Predicted: Ketamine
Saline	All 68.75	All 25.00	All 6.25
	W360 45.83	W360 45.83	W360 8.33
	W180 53.98	W180 37.50	W180 8.52
	W90 51.42	W90 38.35	W90 10.23
Ris+Ket	All 12.50	All 62.50	All 25.00
	W360 17.71	W360 53.13	W360 29.17
	W180 22.73	W180 51.14	W180 26.14
	W90 24.15	W90 46.31	W90 29.55
Ketamine	All 0.00	All 50.00	All 50.00
	W360 10.42	W360 57.29	W360 32.29
	W180 6.25	W180 43.18	W180 50.57
	W90 9.09	W90 43.75	W90 47.16

Total Accuracies

All: 60.42

W360: 43.75

W180: 51.89

W90: 48.30

Table 7 - Results from ordinal regression of Saline, Lam+Ketamine and Ketamine conditions over a range of windowing parameters. For each confusion cell, the window length used to estimate the connectivity is shown on the left and the resultant confusion value on the right.

Observed	Predicted: Saline		Predicted: Lam+Ket		Predicted: Ketamine	
Saline	All	75.00	All	25.00	All	0.00
	W360	51.04	W360	42.71	W360	6.25
	W180	57.39	W180	35.23	W180	7.39
	W90	58.24	W90	36.36	W90	5.40
Lam+Ket	All	0.00	All	56.25	All	43.75
	W360	11.46	W360	54.17	W360	34.38
	W180	8.52	W180	52.27	W180	39.20
	W90	13.64	W90	47.16	W90	39.20
Ketamine	All	0.00	All	68.75	All	31.25
	W360	11.46	W360	58.33	W360	30.21
	W180	13.07	W180	53.41	W180	33.52
	W90	16.48	W90	49.15	W90	34.38

Total Accuracies

All: 54.17

W360: 45.14

W180: 47.73

W90: 46.59

As shown in Table 6, no ordinal trend was observed between saline and ris+ketamine and conditions. Unlike GPC results we observe conditions were most accurately identified using connectivity measures estimated over the entire time series, rather than through a windowing approach. While ketamine and saline were well separated, the ris+ketamine condition exhibited confusion with both saline and ketamine conditions. No ordinal trend was observed when comparing saline, lam+ketamine and ketamine conditions. The ketamine condition was strongly confused with the lam+ketamine condition.

5.4 Discussion

We have demonstrated that ketamine induces a robust changes in the functional connectivity patterns of the human brain using network centrality measures and a multivariate methodology. The effect of ketamine can be surmised as shift from a cortically centred to a sub-cortically centred connectivity state. Lamotrigine was not observed to induce any significant alterations to the ketamine induced pattern of NS, however risperidone pre-treatment was found to elicit wide spread effects on the functional connectivity, both at baseline and modulating the ketamine induced pattern of NS. Indeed, the different modulatory effects of risperidone and lamotrigine pre-treatment on the ketamine induced connectivity could be significantly distinguished from one another, contrasting with their similar effects attenuating the ketamine BOLD amplitude effects (Doyle et al. 2013).

The work presented here demonstrates the advantages of pattern recognition techniques, as applied to functional connectivity analysis, over more traditional analyses. The use of GPC offers the ability to make predictions on the subject level and is sensitive to not only amplitude changes but covariance's in the data. Furthermore, the single output measure presents a simple an intuitive measure summarising group discrimination and alleviates the need for correcting for the large number of statistical tests as with the univariate approach.

Furthermore, this work demonstrates the advantage for the use of windowing in group comparisons. Comparison of NS measures obtained using a windowing procedure provided equal or greater classification accuracies than comparisons using connectivity estimated using a single-pass approach and may reveal frequency dependant effects of risperidone pre-treatment of ketamine.

Motion robustness

It was observed in Chapter 4 that patients in the saline condition exhibited increased average head motion compared to placebo and lamotrigine pre-treated ketamine conditions. This is consistent with the anaesthetic effects of ketamine however, may potentially introduce spurious group differences due to consistent motion differences. When compared using GPC, no significant effects were observed for comparisons of experimental conditions using the mean, maximum and median frame wise displacement parameters. While this does not preclude the possibility of subtle consistent motion effects contributing to group differences, it does contribute to the belief that the observed effects are not significantly driven by motion artefacts. However it should be noted that while the mean, maximum and median provide intuitive representations of head motion during an acquisition, they do not capture more complex movements such as different frequency tremor which may systematically bias experimental conditions.

When comparing conditions in the PLA+SAL and PLA+KET sessions using data "cleaned" with either the 6 or 24 motion regressor we note a similar pattern of classification accuracies. However, it was noted that the reported accuracies were lower in comparisons of placebo and ketamine for data regressed with the 24 parameters compared to the 6 parameter regression. It may be the 6 regressor model is insufficient to remove all noise effects (Satterthwaite et al. 2013) and that a consistent structure remains in the residual motion contributing to group differences. Alternatively, it is possible that the 24 parameter model is removing part of the single of interest (Bright et al. 2015), resulting in decreased signal and reduced group discrimination. The lack of significant differences in either univariate or multivariate comparisons of motion summary parameters suggests the former is unlikely, however given the

motion summary parameters used are simplistic and do not describe different types of motion, further investigation is required to form a clear conclusion.

Effect of Ketamine Infusion

A distributed pattern of connectivity change across the brain was observed during a task-free acute ketamine challenge. In the pattern of effects describing the discrimination between ketamine and placebo conditions, nodes strongly favouring the ketamine class were reported in the basal ganglia and cerebellum. Nodes in the frontal, occipital, parietal, temporal and medial temporal lobe regions were found to be highly weighted for the placebo state. To confirm the directionality of these changes, post-hoc univariate tests were performed. The results of these tests confirmed a decrease in cortical centrality and an increase in centrality for the basal ganglia and cerebellum in the ketamine state relative to the control. Consistent classification accuracies were observed within ketamine comparisons using different windowing length parameters, suggesting ketamine conditions are consistent across network frequencies.

Previous studies, investigating the effects of ketamine on connectivity in the brain have reported findings consistent with effects observed here. Ketamine has been demonstrated to elicit connectivity effects, relative to a pre-defined network, in sub-cortical, somatosensory, auditory, visual and cerebellar regions (Niesters et al. 2012). The pre-frontal cortex (PFC), temporal cortex, cingulum and thalamus reported decreasing FC in relation to somatosensory and auditory networks when influenced by ketamine. Moreover, in relation to visual networks, the cerebellum exhibited increased connectivity as did the connectivity between visual networks.

Furthermore, it has been shown that ketamine infusion in healthy volunteers results in an increased “global connectivity” (Driesen et al. 2013). Of these regions reporting an increased connectivity under ketamine, the cerebellum, thalamus and parietal cortex all reported the greatest increase. The analysis presented in this chapter is multivariate, precluding a direct comparison of results; however it is noteworthy that these same regions are prominent in the pattern of features describing ketamine in relation to placebo and furthermore, exhibit increased centrality.

The results of the multivariate analysis presented in this chapter demonstrate acute ketamine radically alters the pattern of whole-brain node strength for healthy volunteers in the task-free state. This ketamine-induced alteration results in both increases and decreases in the patterns of NS across the brain. This is consistent with previous studies demonstrating long-range decoupling of neural population activity in mouse neocortical slices subsequent to ketamine administration, resulting in both increases and decreases in connectivity (Dawson et al. 2013).

The analysis presented here extends these previous studies providing new insight on the pattern of ketamine-induced connectivity changes over the whole brain.

The observed pattern of ketamine induced connectivity effects in healthy volunteers can be summarised as a shifting of cortically centred connectivity to a state that is more sub-cortically centred. This reduced cortical centrality may result from a widespread disconnection between cortical regions, alternatively ketamine may result in more specific effects on hub regions in the brain, resulting in widespread dysregulation of cortical circuits. Either mechanism may elicit the observed changes in centrality. The framework presented here precludes the identification changes on individual connections; instead the presented methodology is designed to reveal consistent regional changes in connectivity across the whole-brain.

This observed pattern of reduced centrality in cortical nodes is consistent with many of the experiential effects observed with ketamine; reductions in cortical connectivity is predicted to impaired memory, sensorimotor processing, contextual processing and spatial representation. Indeed schizophrenia has been shown to evoke similar connectivity changes, such as wide-spread disconnections between cortical regions (Liang et al. 2006; Lynall et al. 2010) and a reduction in cortical hubs reporting strong centrality (Rubinov et al. 2009).

Ketamine has a strong affinity for the D_2 and NMDA receptor with a lower affinity for the 5-HT_{2A} receptor, muscarinic and opioid receptors; however the latter are predicted to report notable effects only at high doses (Hirota et al. 1999; Narita et al. 2001). It is the NMDA blockade to which the main effects of sub-anaesthetic ketamine are normally accredited (Driesen et al. 2013). Ketamine is hypothesised to effect the functional connectivity through disinhibition of the parvalbumin-positive GABAergic interneurons (Homayoun et al. 2007), indeed it has been confirmed through microdialysis that the NMDAR antagonists MK-801 and PCP increase extracellular GABA levels. These interneurons synchronise pyramidal cell oscillations through inhibition (Moghaddam 2007); NMDAR antagonism may thus result in dysregulation of pyramidal synchrony, potentially reducing long range connectivity in the brain and resulting in the observed pattern of decreased cortical centrality. The lateral posterior pulvinar has been implicated in the regulation of pyramidal synchrony in the cat brain (Shumikhina et al. 1999). The observed increase in thalamic centrality under acute ketamine may thus result from a compensation mechanism attempting to correct the disrupted pyramidal synchrony via the NMDA antagonism.

The whole-brain pattern of centrality changes reported here, for a low dose ketamine challenge, have not been previously observed. These patterns of centrality effects suggest a complex connectivity change underpinning the ketamine response in healthy volunteers. These changes

in the connectivity organisation may explain the anhedonia, perceptual distortion and cognitive disorganisation effects produced by ketamine.

This work contributes new insight in the ketamine-induced re-organisation of connectivity in the human brain. Due to the constraints of the experimental design, specifically the multiple administrations, it was necessary to maintain a relative low dose of ketamine. This resulted in sparse and inconsistent subjective responses, precluding any further analysis correlating connectivity effects and subjective ratings. In order to test the relationship between the pattern of connectivity effects and subjective reports of drug effects, a replication of this study would be required with higher doses of ketamine eliciting stronger subjective responses.

Lamotrigine treatment

Lamotrigine is expected to counter the glutamatergic effects of ketamine through Na^+ channel modulation, resulting in reduced glutamate release. If the connectivity effects of ketamine are driven by the downstream glutamatergic effects as has been previously suggested (Duncan et al. 2011), then we would expect strong attenuation effects of lamotrigine on the ketamine response. Previous studies have demonstrated the effective attenuation of the ketamine BOLD amplitude response via lamotrigine pre-treatment (Deakin et al. 2008; Doyle et al. 2013; Doyle et al. 2013). However, in contrast to these previous BOLD-amplitude studies, we did not observe any significant effects of lamotrigine on the pattern of ketamine-induced centrality within the brain. Lamotrigine was administered at a clinically effective dose (300mg) which has been demonstrated to attenuate the ketamine-induce BOLD response (Doyle et al. 2013; Doyle et al. 2013) indicating the lack of significant effects is not due to low dose. When considered with the results of previous studies, our results suggest lamotrigine primarily induces changes in the amplitude of the BOLD effects rather than effecting wide-spread changes in regional coupling. It is possible localised regional connections were altered, to which the framework presented here would be insensitive.

We did not observe an ordinal trend between saline, lam+ketamine and ketamine conditions in the ordinal regression analysis, consistent with the suggestion that lamotrigine does not significantly attenuate the ketamine-induced connectivity. Indeed the strong confusion between lam+ketamine and ketamine conditions, particularly at longer window lengths, and in the binary classifications suggest a similarity between conditions.

Taken together these results suggest that lamotrigine has similar effect on patterns of ketamine-induced NS as placebo. Furthermore, the lack of modulation on the ketamine response by lamotrigine has implications for the mechanistic effects of ketamine, suggesting the

glutamatergic effects of ketamine are not the primary driving factor of the observed connectivity changes. Instead the connectivity changes likely reflect NMDAR blockade. This conclusion could be confirmed through preclinical experimentation using specific NMDA subunit antagonists and non-NMDA antagonists for the AMPA and kainate receptors.

Risperidone treatment

Risperidone (2mg) is expected to reduce downstream glutamate release through 5-HT_{2A} antagonism (Nyberg et al. 1999), thus attenuating the glutamate effects of ketamine. Risperidone has also been reported to directly potentiate the NMDAR (Konradsson et al. 2006), providing a secondary mechanism to counter the effects of ketamine. Given this dual mechanism of action we predict that risperidone will attenuate the ketamine induced connectivity effects.

Indeed, the results presented here indicate that risperidone, unlike lamotrigine, has robust modulatory effect on the ketamine induced pattern of centrality. This is indicated by the significant discriminations between risperidone pre-treated ketamine and placebo pre-treated ketamine (Table 3), indeed this comparison reveals a pattern of NS effects suggesting risperidone pre-treatment opposes the ketamine effect. Comparisons using NS values, estimated with a single pass approach, suggest risperidone pre-treatment of ketamine results in a more saline like pattern of NS, as indicated by the similarity between saline and risperidone pre-treated ketamine conditions (Table 3). However, classifications using connectivity estimated using a windowed approach reveal a robust difference between saline and risperidone pre-treated ketamine, indicating when accounting for temporal variations in connectivity, risperidone pre-treatment results in a pattern of NS distinct from the saline state. The classification maps for the comparison of saline and risperidone pre-treated ketamine (Figure 23) revealed a similar spatial distribution of weights, with the exception of visual regions, to the g-map for saline compared to placebo pre-treated ketamine. This is consistent with the suggestion of an opposing effect of risperidone on the ketamine response.

Taken together these results support the conclusion that risperidone may oppose the ketamine effect, resulting in a pattern of connectivity distinct from both the saline and ketamine. This conclusion of opposing modulation rather than attenuation is supported by observations from the ordinal regression, which suggest risperidone does not attenuate the ketamine NS in an ordinal manner.

We suggest it is the additional mechanism of action of risperidone that results in the effective modulation of the ketamine induced NS, as compared to lamotrigine. Indeed, given the

difference in effect of the two pre-treatments we suggest it is the potentiation of the NMDAR by risperidone that results in the opposing effects of the ketamine response. It is possible that the opposing effect of risperidone on ketamine may also be due to serotonergic effects, however further work using a compound with selective 5-HT_{2A} binding is required.

Stability of pattern recognition method in the absence of pharmacological intervention

The proposed framework did not report significant discriminations between patterns of centrality in session conditions with no active pharmacology (saline v placebo (pre sal)). Classifications between the pre-infusion scans of the two oral placebo sessions (PLA+KET and PLA+SAL) revealed no significant effects, however a high accuracy was observed at the shortest window length (90seconds). This may be a spurious result, alternatively may be due to a weak consistent effect in the connectivity dynamics between sessions. The non-significant nature of this effect however suggests reasonable rest-retest stability, instilling confidence that the observed effects connectivity reflect the pharmacological action of interventions.

Limitations

While the work presented here provides new insight into the effects of acute ketamine on the human brain in healthy volunteers, the limitations of this analysis should be considered. We have demonstrated a framework for analysis of pharmacological imaging data combining graph theory measures with PR techniques to compare groups, while respecting the temporal variations of connectivity. The use of windowing and centrality measures as a feature set for PR classifications of whole brain connectivity is a new contributions to the field.

The use of NS provides an elegant solution to the issues of interpreting spatial patterns of discrimination, however prohibits investigation into effects on specific regional connections. Alternative univariate approaches (Niesters et al. 2012) allow for hypothesis led testing of specific regional connections, however these analyses may also prove sensitive to non-pharmacological effects and enforce inappropriate assumptions of independence on the connections between regions. The choice of examining patterns of centrality change over the whole brain was motivated by the widespread expression of NMDA receptors.

An additional limitation of this analysis is the need to select window lengths. In this analysis we have selected a range of window lengths covering the range of possible values. However, further investigation into the temporal variations of connectivity is needed to identify an optimal windowing procedures. A promising alternative for future analysis is use of wavelet coherence to estimate temporal connectivity, allowing for classifications to be performed on the connectivity in different frequency bands.

Finally, the use of a single centrality measure as a feature set is further limitation, providing insight into only a single aspect of connectivity. In this analysis we compare patterns of node strength, this metric was selected as it provides a simple, intuitive measure of the connectedness of a region. However using multiple centrality measures such as local efficiency and betweeness centrality may provide a broader perspective on the connectivity effects elicited by pharmacological intervention and provide further insight in the mechanisms of action of these compounds.

Chapter 6: MKL and network interaction

In this chapter we present a method for examining the interactions within and between networks in a principled manner, sensitive to differential alterations in the pattern of regional connections within and between networks. We apply multi-kernel learning (MKL) to classify group difference based on network connectivity. Kernels are computed from connections within and between pre-defined networks of interest (NOI). Through inspection of each kernel's contribution to the class discrimination we can evaluate the effect of the experimental conditions on network interactions. Work from this chapter was presented as a conference poster (2014 Organisation for Human Brain Mapping).

6.1 Investigating network interactions

As previously discussed in Chapter 2, the interactions between functional networks are important for understanding the mechanisms in the brain. Studies investigating the interaction between networks and have compared the average network signals (Niesters et al. 2012; Carhart-Harris et al. 2013) and relationships between hub nodes in NOIs (Scheidegger et al. 2012). These comparisons make assumptions about the uniformity of functional connectivity within and between NOIs, which based on our understanding (van den Heuvel et al. 2011) of network organisations, are invalid. Indeed this is clearly evident through comparison of connections within the DMN (Fransson et al. 2008) which reveals an incomplete network mediated via the posterior cingulate/precuneus rather than complete network with uniform connection strengths. Furthermore, the existence of *hub* structures in brain networks which mediate connectivity (van den Heuvel et al. 2011) suggest a non-uniformity of regional connectivity effects within a network. This arguably invalidates the supposition that between network connectivity can be accessed purely by correlating mean NOI signals. Furthermore the functional hub structure of brain may be altered by experimental conditions such as the presence of a disorder or psycho-active compound. If true, this may void the assumption of consistent functional hub structures between pharmacological conditions.

Here we propose a methodology to compare groups based on the change in edge-wise connectivity within and between NOIs using MKL techniques. This provides a network scale perspective on functional connectivity effects and provides greater sensitivity to strong regionally specific coupling effects within or between networks which may be lost when comparing network global signals. Thus groups can be compared in a principled manner that considers all intra and inter network connections rather than an average signal, as illustrated in Figure 26. Such a methodology should be sensitive to small, but consistent, localised changes

which may be lost when computing a network mean. Furthermore, the proposed method does not enforce any assumption of with-in network structure.

6.1.1 Methods

Data was acquired and pre-processed as discussed in Chapter 4. Identical post-processing procedures were also performed to prepare the data for connectivity analysis. Specifically the mean CSF and WM signal were regressed out, as were the six motion parameters. Band pass filtering was applied in the range of 0.01Hz – 0.1Hz. Experimental conditions were also as defined as in Chapter 4.

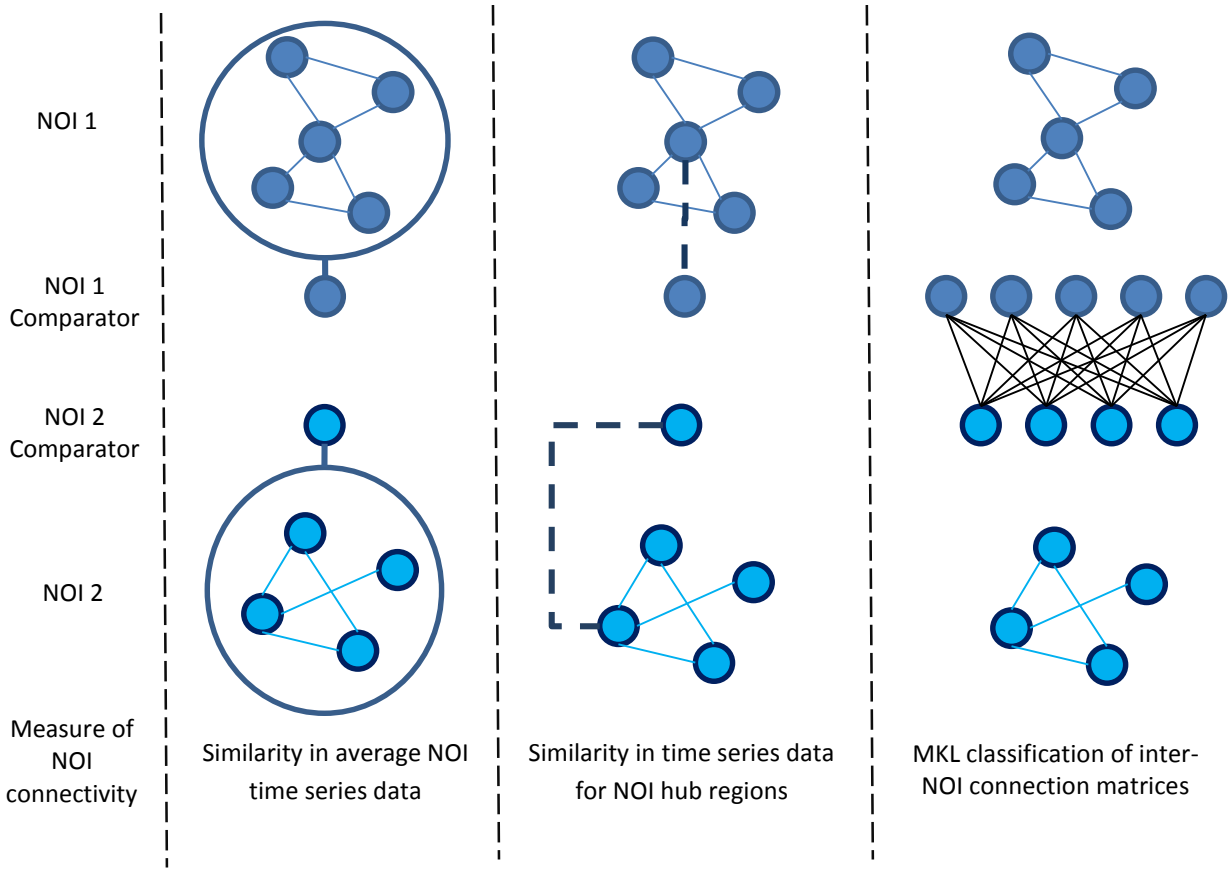

Figure 26 – Visualisation of methods for the comparison of NOI conectivity, NOIs are visualised at the top and bottom of the figure while the central section depicts the manner in which they are compareded, In the left pane, NOIs are represented by their mean signal which is then compared between regions. The central pane illustrates the network comparison through comparison of network hub regions, while the right pane represents comparison using the proposed method,

Graph estimation

The functional connectivity of the data was modelled as a graph, where nodes or vertices characterise spatial brain regions and the edges inform the perceived functional connection between node pairs. Data is parcellated using the AAL atlas and the mean time series of each atlas region computed from regional voxel members. We selected 90 atlas regions for use in this analysis, these represent complete coverage of the cortex and sub-cortical structures. Each

region, with its corresponding mean signal, is used to represent a node within each graph; for a more detailed explanation we refer the reader to Chapter 3.

In order to account for the inherent spatiotemporal dynamics of the resting state, connectivity between nodes was estimated using a sliding windowing approach employing Gaussian windows, as described in Chapter 3. A Gaussian window was chosen in order to achieve better temporal sensitivity than the traditional box-car window. We apply Gaussian windows of full length 90, 180 and 360 seconds incremented across the time series in steps equivalent to the effective length of window, 30, 60 and 120 sec respectively. These window lengths were selected to ensure a broad coverage of available connectivity frequencies were investigated. A minimum window length of 90 seconds was chosen based on empirical evidence that connectivity patterns can be accurately measured with as little as 30-60 seconds of data, as defined with a box car window, using multivariate measures (Shirer et al. 2012). This is also consistent with other studies demonstrating stable connectivity states in the order of ~100 seconds using univariate statistics (Chu et al. 2012). For each window position Pearson's correlation was applied to estimate the functional connectivity, resulting in a collection of multi-slice graphs for different windowing parameters.

Network interaction

In order to investigate the effects of ketamine on consistent resting state networks, we defined ten NOIs using the networks identified in (Smith et al. 2009), see Figure 27-A. These have been shown to be consistently identified across multiple studies (Damoiseaux et al. 2009; Menon 2011). These network maps were thresholded at $p < 0.05$, as recommend by Smith (2009) and then binarised to form an NOI mask. Each NOI mask was subsequently overlaid on the parcellation atlas, any region overlapping with the mask was defined as a member of that NOI; this resulted in a node-wise definition of each NOI. Multi-slice connection matrices were divided into NOIs based on the derived NOI node definitions, as illustrated for a single slice in Figure 27-B. We identify diagonal regions within these parcellated graphs as *within NOI* connections whilst the off-diagonal partitions describe the *between-NOI* connections.

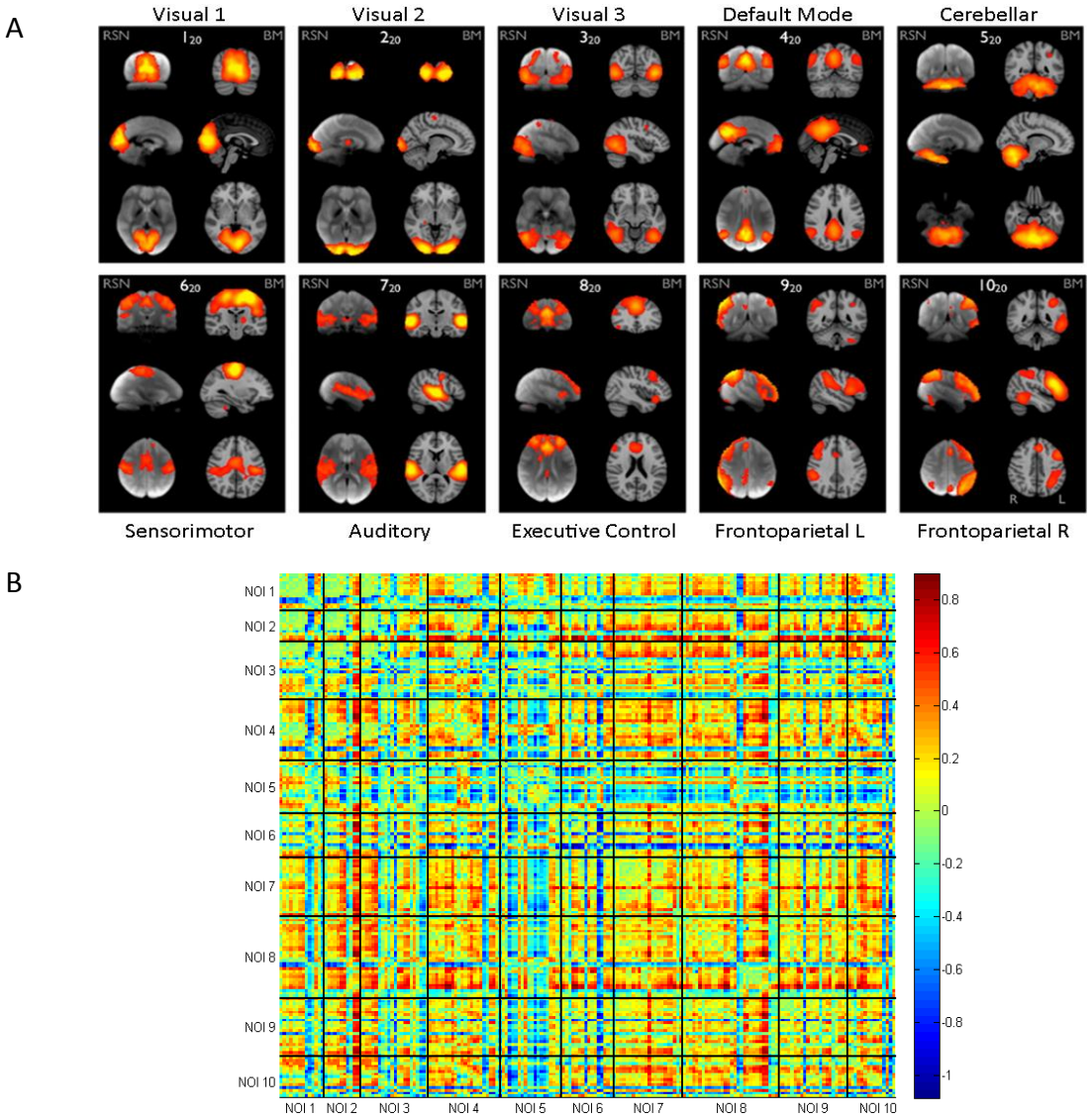

Figure 27 – Network definitions for network interaction analysis, A) Consistent resting state network z-scores, published by S Smith (2009), corresponding to 10 distinct resting state networks. B) Illustration of connection matrix for participant 1 in the saline condition, parcellated into NOI connections. Dark lines indicate NOI divisions with correlation values displayed in colour within each partition

Pattern Recognition

Group comparisons were performed using multi-kernel leaning (MKL) pattern recognition (SVMs), as introduced in Chapter 3. We employed the shogun toolbox (http://www.shogun-toolbox.org/)(Sonnenburg et al. 2006) implementation of multi-kernel SVM, using the MATLAB interface. This imple

mentation offers a flexible and efficient execution of MKL, providing options for different estimation procedures for kernel combinations and loss penalties incorporating regularisation.

This binary classification methodology allows for comparisons to be performed combining multiple sources of data as kernels. In the MKL problem these kernels may be weighted and linearly combined where:

$$k(\boldsymbol{x}_i, \boldsymbol{x}_j) = \sum_{k=1}^{K} w_k k_k(\boldsymbol{x}_i \boldsymbol{x}_j)$$

individual kernel weights are defined by w_k, where $w_k \geq 0$. Each sub-kernel, k_k, represents different feature sets. Inspection of kernel weights for the optimal combination of sub-kernels can quantitatively inform the contribution of each feature set to group discrimination. In order to assess the effect of ketamine on the connectivity within and between NOIs, we performed MKL where each within NOI and between NOI connection matrix was used as a feature set for a linear kernel. This resulted in 55 kernels representing the connections within each NOI and between all possible NOI pairs.

In order to perform fair classification and achieve good separation it is necessary to ensure all kernels are in the same scale. All kernels were normalised by the square root of the product of the diagonals, resulting in kernels having unit length in feature space, using the below, as discussed by Sonnenburg (2006):

$$K'(\boldsymbol{x}, \boldsymbol{y}) = \frac{K(\boldsymbol{x}, \boldsymbol{y})}{\sqrt{K(\boldsymbol{x}, \boldsymbol{x}) K(\boldsymbol{y}, \boldsymbol{y})}}$$

The Shogun toolbox employs regularisation for the estimation of kernel weights and to control the sparsity of the MKL. In this study we apply elastic net regularization (see Chapter 3) due to the highly correlated nature of data. This regularisation penalty is a combination of L1 and L2 terms, the balance of these terms is controlled by a tuning parameter$\lambda \in [0,1]$, allowing for varying degrees of sparsity to be enforced.

$$(1 - \lambda) \sum_{k=1}^{K} \|f_k\|_{Hk} + \lambda \sum_{k=1}^{K} \|f_k\|_{Hk}^2$$

when λ = 0, the penalty is entirely L1 and so the model is very sparse; setting λ = 1 results in a L_∞-MKL and a uniform weighting of kernels. The subscript Hk denotes the norm in Hilbert space and f_k is the kth member of the reproducing kernel Hilbert spaces. In addition to tuning the λ parameter, it is also necessary to select a C parameter, as discussed in Chapter 3.

We have selected the elastic net regularisation over the commonly applied LASSO regularisation. Not only has the elastic net been shown to outperform the lasso (Zou et al. 2005) it is the more appropriate choice given the manner in which the kernel weightings will be interpreted. In this

application we expect the occurrence of highly correlated representations of network connections; in such a scenario, LASSO tends to select only one of these highly correlated predictors, setting the rest to zero. Given that we wish to use the kernel weightings to inform the contribution of each network to the class discrimination, in the presence of highly correlated predictors Lasso may provide inappropriate variable selection resulting in erroneous conclusions of network connectivity effects. Elastic net however, retains or drops groups correlated predictors and is deemed the more appropriate method of regularisation.

To investigate the effects of ketamine on the network connectivity in the brain and its potential modulation by pre-treatment with lamotrigine and risperidone, we perform classifications in three configurations: 1) To investigate the main effects of ketamine we compare PLA+SAL and PLA+KET sessions. 2) The modulation effects of risperidone pre-treatment are investigated through classification of RIS+KET with PLA+KET and PLA+SAL sessions. 3) We classify LAM+KET with PLA+KET and PLA+SAL sessions to investigate the effects of lamotrigine on the ketamine network connectivity. In order to account for network dynamics, each classification was repeated using connectivity estimated with differing window lengths.

In order to access the generalizability of our trained model, we applied leave one out cross validation (LOOCV). This approach was chosen over k-folds cross validation due to the limited size of the dataset and the lack of an independent test set. In this iterative approach, a single subject is withheld from the data for use as a *test set*, the remaining data is used to train the model. The trained model is the applied to the test set and an estimate of class membership computed; this process is repeated until every subject has been employed as a test set. The reported accuracy is computed from the predictions across all test iterations. For each LOOCV fold, the feature data were centred using the mean of the training data, which was then applied to the test set in order to minimise any bias.

To select optimal parameters for C and λ we performed a nested grid search within each LOOCV fold. A nested instance of LOOCV was performed using the training data to ensure an unbiased parameter selection. The value of C was altered logarithmically over the range 1e-5 to 1e1 while λ was varied in the range [0 – 1] in 0.1 divisions and classification performed. Training parameters were subsequently selected from those which offered the best accuracy across all nested folds and applied to the parent LOOCV fold.

Permutation testing was applied for significance testing of model accuracies. For each comparison, class membership labels for the training data were randomly permuted N_{perm} times. At each permutation, classification was perform using LOOCV and an accuracy obtained for the true test labels. This resulted in a distribution of permuted accuracies. Significance was inferred

from the proportion of accuracies greater than or equal to the accuracies obtained using the true class labels.

In this analysis we collect kernel weights into a matrix. The row and column index for each cell contains a kernel weight revealing the importance of respective NOI to the class discrimination, akin to a network-level connection matrix. Henceforth we refer to this matrix of kernel weights as a *kernel weight map*. Inspection of these kernel weight maps for significant classifications provides insight into the effect of the experimental condition on NOI interactions for the given model. However, any interpretation must be treated with caution due to a number of confounds such as potentially differing model parameters and issues interpreting connectivity at high network frequencies.

Kernel weight maps, estimated using a range of window parameters, were correlated within each comparison to investigate the stability of network effects across windowing parameters. The similarity between these maps, produced from the classification of connectivity estimated over a range of window parameters, was quantified by the intra-class correlation coefficient (ICC), as described in Chapter 3. This may provide an indication of differential effects of the pharmacological intervention across network frequencies. The range of frequencies effects under investigation is limited by the selection of window lengths which enforces a low pass filtering effect. Here we employ a range of window lengths distributed amongst feasible values; providing a broad perspective of frequency effects on NOI connectivity. Here, to aid the reader, we visualise the mean kernel weight map across window lengths for each comparisons; the ICC was also reported to inform map similarity between models.

6.1.2 Results

Ketamine modulates network connectivity in the brain

To investigate the effects of ketamine on the interaction between regions in consistent resting state networks, classification was performed comparing conditions in PLA+KET and PLA+SAL sessions, Table 8. The classifier was unable to significantly distinguish between conditions with no active pharmacology, with classifications of placebo (pre sal) against both placebo (pre ket) and saline reporting chance level accuracies (Acc < 67% and Acc < 69% respectively). This is indicative of within and between session stability when compared within the proposed methodology. Ketamine was well separated from both placebo and saline conditions with the classifier reporting accuracies (Acc ≥ 67% and Acc > 82% respectively) indicating ketamine has a robust effect on the pattern of network connectivity, for networks as defined by Simth (2009).

Inspection of the kernel weight maps for the comparisons of ketamine and saline, Figure 28, reveal ketamine predominantly affects connections within the auditory network. Relatively high weights were also observed for kernels representing the interaction between auditory and executive control networks and between the right front parietal and visual1, visual2 and DMN networks. Furthermore ketamine was observed to affect the connections within the visual 2 network. We note the auditory network, identified by Smith (2009) has a high degree of overlap with the salience network (Menon et al. 2010).

The different window lengths were found to subtly alter the strengths of the kernel weights, however the relative spatial topology of the weight maps remained consistent across different window lengths. An ICC of r = 0.8862 was calculated for the weight maps computed using different window lengths, suggesting a similar effect driving the classification of ketamine vs saline across networks estimated at different frequencies.

Table 8 – Results from comparison of conditions in PLA+KET and PLA+SAL using MKL.

Comparison			Window (sec)	Accuracy (%)	C mean (±std)	λ mean (±std)	p
Placebo (pre Saline)	v	Placebo (pre Ketamine)	90	56.96	1 (4.24)	0.45 (0.37)	0.122
			180	59.09	1 (3.16)	0.2 (0.32)	0.083
			360	66.71	10 (4.61)	0.2 (0.22)	0.047
Placebo (pre Saline)	v	Saline	90	63.78	0.01 (0.04)	0.8 (0.29)	0.074
			180	68.31	0.01 (0.04)	0.8 (0.32)	0.042
			360	66.67	0.1 (0.32)	0.2 (0.31)	0.045
Placebo (pre Ketamine)	v	Ketamine	90	68.89	0.1 (0.04)	0.9 (0.24)	0.037
			180	71.31	0.1 (0.04)	0.45 (0.29)	0.007
			360	67.19	0.1 (0.46)	0.4 (0.32)	0.042
Saline	v	Ketamine	90	82.95	0.1 (0)	0.3 (0.15)	<0.001
			180	83.24	0.1 (2.4)	0.25 (0.2)	<0.001
			360	91.67	0.1 (0)	0.6 (0.19)	<0.001

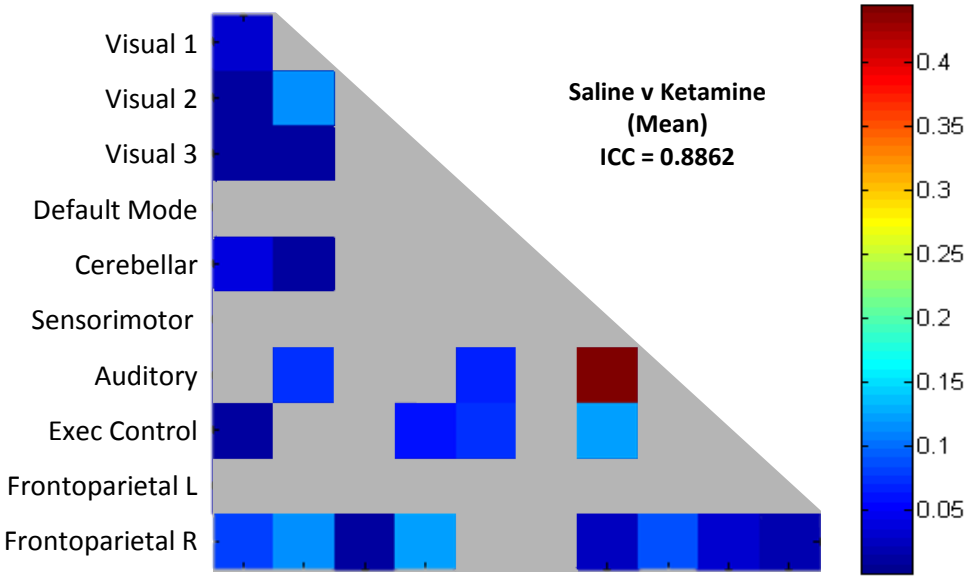

Figure 28 – Mean kernel weight maps for the classification of Saline and Ketamine using networks formulated from data windowed at 90, 180 and 360 seconds. Light grey region denotes kernels with weighting of zero.

Effect of Risperidone

To investigate the modulatory effect of risperidone pre-treatment on the ketamine-induce network connectivity, comparisons were performed between the RIS+KET and placebo pre-treatment sessions (PLA+KET and PLA+SAL), Table 9.

The pattern of network connectivity for the main effect of risperidone at baseline was not significantly discriminated from placebo (Acc < 64%), suggesting the pattern of NOI connectivity in risperidone cannot be distinguished from placebo. A similar result was also observed for the classifications of ris+ketamine v saline and for risperidone v ris+ketamine, (Acc < 69% and Acc < 65% respectively). This indicates that pre-treatment with risperidone may reduce ketamine induced changes in the pattern of connectivity within and between consistent resting state networks. Furthermore, the inability of the classifier to distinguish between ris+ketamine and saline conditions suggests that risperidone pre-treatment modulates the ketamine state resulting in a pattern of network connectivity resembling saline. This is supported by the discrimination between ris+ketamine and ketamine conditions (Acc ≥ 75%), indicating risperidone has a robust modulatory effect on the ketamine state. This is most likely due to an interaction effect between risperidone and ketamine as the main effects of risperidone did not result in a significant classification.

Table 9 – Classification accuracies for the comparison of RIS+KET, PLA+KET and PLA+SAL sessions using NOI connectivity as a feature set for SVM MKL.

Comparison	Window (sec)	Accuracy (%)	C	Λ	p
			mean (±std)		
Risperidone v Placebo (pre Ket)	90	63.35	1 (3.82)	0.8 (0.18)	0.032
	180	63.07	0.1 (2.45)	0.85 (0.26)	0.054
	360	59.09	0.1 (2.43)	0.85 (0.35)	0.091
Risperidone v Ris+Ketamine	90	59.94	0.001 (3e-3)	0.9 (0.02)	0.073
	180	61.94	0.001 (4e-3)	0.9 (0.2)	0.052
	360	64.06	0.001 (4e-3)	0.9 (0.06)	0.019
Ris+Ketamine v Saline	90	65.77	0.055 (0.33)	0.5 (0.32)	0.039
	180	62.50	0.55 (0.24)	0.65 (0.38)	0.064
	360	68.23	0.055 (0.049)	0.35 (0.35)	0.03
Ris+Ketamine v Ketamine	90	75.85	0.1 (0)	0.4 (0.17)	0.003
	180	81.53	0.1 (0.23)	0.55 (0.26)	<0.001
	360	80.74	0.1 (0.31)	0.7 (0.22)	<0.001

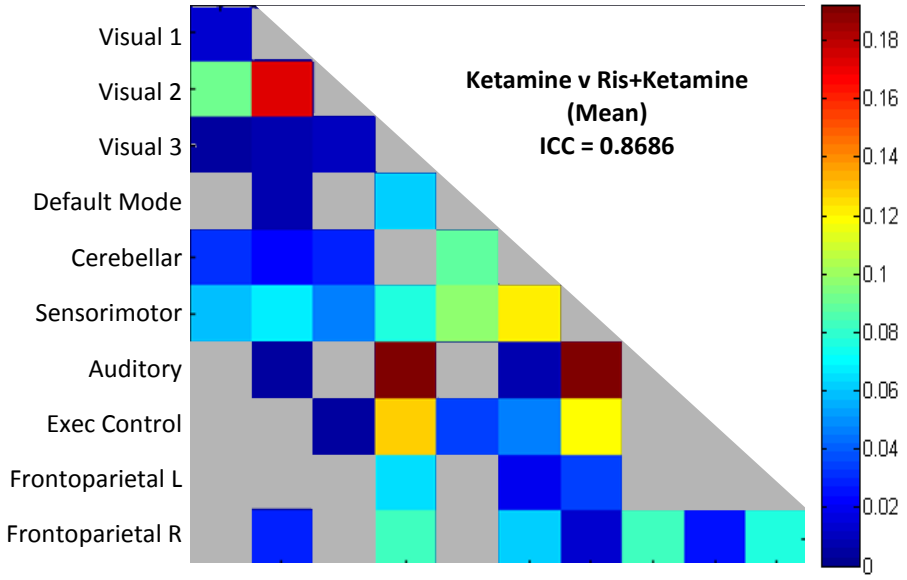

Figure 29 – Mean kernel weight maps for MKL SVM classification of ketamine compared to ris+ketamine for networks estimated using windows of 90, 180 and 360 seconds. Light grey region denotes kernels with weighting of zero.

Examination of the kernel weights for the comparison of ris+ketamine and ketamine reveals a distributed pattern of network effects; as illustrated in Figure 29. Kernel weightings for this classification compared using networks formulated over a range of window lengths, reported a high degree of similarity with an ICC of r = 0.8686. Kernel weightings were observed to subtly alter between classification using graphs estimated from different window lengths. The sparsity of the pattern of weights was found decrease at longer windows, resulting in a more widespread pattern of effects, possibly indicating risperidone has differential modulatory effects on the ketamine induced connectivity at different network frequencies. However, specific testing is required to confirm this.

Inspection of this pattern of kernel weights indicates risperidone modulates the ketamine-induced connectivity within the visual network, the auditory network and the relationship of the auditory network with the default mode network (DMN). Risperidone was also observed to modulate the ketamine induced network interactions within and between visual networks. High kernel weightings were observed for kernels representing interaction of the DMN with sensorimotor, auditory, executive control and frontoparietal networks. Effects were also observed for interactions between the sensorimotor network and the cerebellar, visual and the right frontoparietal network; for auditory-executive control connectivity, and for connectivity within the right frontoparietal network and the sensorimotor network. Modulation of the ketamine induced network state by risperidone may also alter the perceptual and cognitive deficits induced by ketamine, however the sparsity of subjective reports prohibits a quantitative analysis.

The lack of evidence of modulation for the main effects of risperidone suggest the pattern of change between ris+ketamine and ketamine can be seen as differential effects of ketamine on the risperidone state. However this does not preclude risperidone biasing the maps here through a subtle opposing effect. Together the pattern of observed effects suggest risperidone pre-treatment robustly alters the pattern of ketamine induced network connectivity as compared to placebo pre-treatment. The inclusion of similar network interactions between ris+ketamine v ketamine and saline v ketamine suggest risperidone may have an attenuative effect on ketamine. However it also elicits changes in NOI interactions not associated with the ketamine effect, suggesting a distinct network connectivity state for risperidone pre-treated ketamine.

Effect of Lamotrigine

Conditions in the LAM+KET session were compared against placebo pre-treated sessions (PLA+KET and PLA+SAL) to investigate modulation of the ketamine state by lamotrigine, Table 10. The classifier was unable to distinguish between lamotrigine and placebo (Acc < 47%) indicating lamotrigine does not alter network connectivity at baseline. Furthermore, there was no indication of significant modulation of the ketamine induced connectivity state by lamotrigine pre-treatment (lam+ketamine v ketamine Acc < 72%). The inability of the classifier to separate placebo and lamotrigine pre-treated ketamine conditions indicates lamotrigine, at the administered dosage, does not significantly alter the ketamine induced network connectivity.

The lamotrigine pre-treated ketamine infused states were well distinguished from saline (Acc > 75%) suggesting a robust connectivity effect between conditions. Inspection of the kernel weightings for the classifications of lam+ketamine and saline, Figure 30, reveals a widespread pattern of network effects. This pattern of effects was found to include regions effected in the comparison of ketamine and saline, Figure 28. Specifically high kernel weightings were observed for interactions of the auditory network and frontoparietal networks and between the default mode and executive control networks. Additionally high weightings were also observed in the DMN interactions with frontparietal and executive control networks; between the cerebellar NOI and sensorimotor, executive control and auditory networks and between the auditory and frontoparietal networks.

Taken together, our results suggest lamotrigine pre-treatment, at the administered dosage, does not have a significant effect on ketamine induced network connectivity patterns. As indicated by the non-significant comparison between lam+ketamine and ketamine. However we cannot preclude subtle effects of lamotrigine on the NOI interactions resulting in altered patterns of network connectivity.

Table 10 – Classification accuracies for SVM MKL comparisons of LAM+KET conditions with PLA+SAL and PLA+KET conditions

Comparison	Window (sec)	Accuracy (%)	C	λ	p
			mean (±std)		
Lamotrigine v Placebo (pre Ket)	90	39.77	0.01 (0.44)	0.5 (0.40)	0.883
	180	46.02	0.01 (0.25)	0.65 (0.36)	0.692
	360	46.35	0.01 (0.02)	0.7 (0.35)	0.732
Lamotrigine v Lam+Ketamine	90	65.20	0.055 (0.05)	0.85 (0.18)	0.037
	180	65.34	0.1 (2.4)	0.75 (0.21)	0.056
	360	72.40	0.1 (2.4)	0.8 (0.28)	0.009
Lam+Ketamine v Saline	90	75.71	1 (3.21)	0.3 (0.33)	0.011
	180	79.55	1 (4.44)	0.5 (0.27)	0.001
	360	85.42	1 (4.52)	0.65 (0.35)	0.001
Lam+Ketamine v Ketamine	90	67.90	0.1 (0)	0.4 (0.15)	0.032
	180	72.16	0.1 (0)	0.4 (0.15)	0.007
	360	76.04	0.1 (0.05)	0.35 (0.18)	0.002

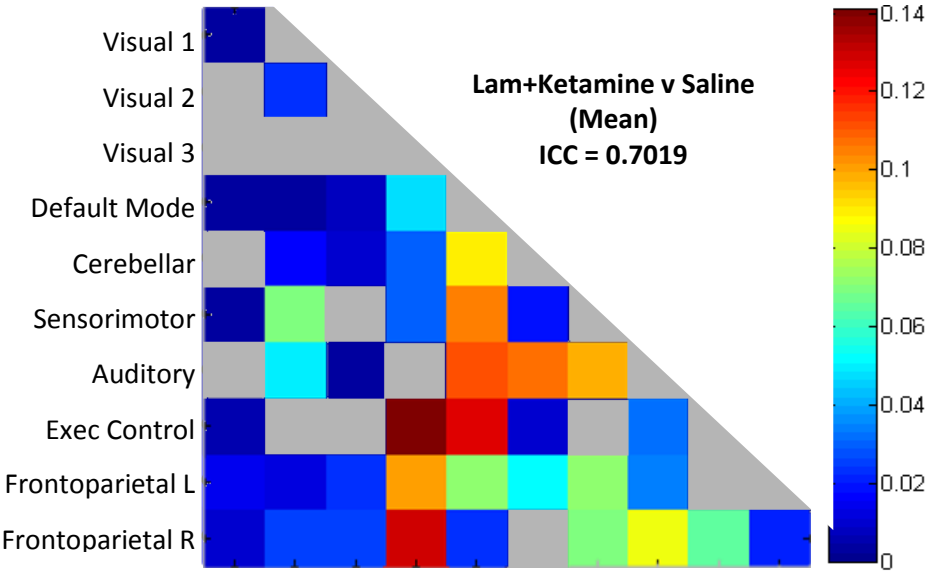

Figure 30- Mean kernel weight maps for the comparison of saline and lam+ketamine for classifcation of networks computed using different window parameters. Light grey region denotes kernels with weighting of zero.

Differential effects of pre-treatment

We were unable to distinguish between both lamotrigine and risperidone sessions when compared directly (lamotrigine v risperidone, Acc < 64%, p>0.05), Table 11. However, a moderately high classification accuracy was observed for the comparison between post-ketamine conditions following a pre-treatment of lamotrigine and risperidone (lam + ketamine v ris + ketamine, 72% > Acc). This suggests compounds differentially affect the pattern of ketamine induced NS.

Table 11 – Results of SVM MKL classification of LAM+KET and RIS+KET sessions using a range of windowing lengths to estimate network connectivity

Comparison	Window (sec)	Accuracy (%)	C mean (±std)	λ mean (±std)	p
Lamotrigine v Risperidone	90	62.93	0.1 (0.23)	0.8 (0.21)	0.054
	180	61.08	1 (3.26)	0.8(0.31)	0.051
	360	63.02	1 (3.67)	0.7 (0.25)	0.047
Lam+Ketamine v Risp+Ketamine	90	64.06	0.1 (4.39)	0.3 (0.21)	0.013
	180	71.31	0.1 (0.02)	0.25 (0.21)	0.001
	360	71.87	0.1 (3.89)	0.7 (0.31)	0.006

6.2 Discussion

We have demonstrate ketamine robustly alters the relationship between connections within consistent resting state networks. The effects of ketamine can be summarised as modulation of the visual and auditory networks, as well as the interaction of the auditory network with the executive control, cerebellar and visual 2 networks. Risperidone was observed to significantly modulate this pattern of network effects in line with predicted attenuation effects of ketamine. However, lamotrigine was not observed to significantly modulate the ketamine connectivity.

Ketamine modulate network connectivity

Consistent with previous chapters and related studies, ketamine was observed to effect a distributed pattern of network alterations. Ketamine was well separated from the placebo (pre Ket) and saline conditions, suggesting a robust predictable network connectivity effect of ketamine. We note highly similar accuracies were reported for each comparisons performed over a range of windowing parameters. For comparisons of ketamine the largest difference in accuracy observed was ~9%. Such a small change may be due to a myriad of confound factors and does not provide any indication of differential effects of ketamine effects on different network frequencies.

When contrasting ketamine with saline we observe relatively high kernel weightings for NOIs representing connectivity in the visual, auditory networks as well as those representing the connections between auditory and the cerebellar, visual and executive control networks. A similar effect of modulated cerebellum and auditory-visual network connectivity was observed by (Niesters et al. 2012). This network connectivity effect of ketamine on cerebellum was attributed to high expression of NMDAR in the cerebellar regions. Connectivity effects with the cerebellum may contribute to disassociative effects observed with ketamine. The cerebellum has been associated with sensorimotor processing models which, if disrupted might predict dissociative symptoms, or aberrant perceptual experiences (Blakemore et al. 2003; Walsh et al. 2014).

Ketamine was also observed to consistently affect the connectivity of the auditory network and its interaction with cerebellar (weakly), executive control and visual networks. The visual, auditory and cerebellar networks have all been implicated in sensory processing. The modulation of these network interactions may be due to ketamine's effect on perceptual processing. The strongest effects of ketamine were observed within the network containing the primary auditory processing regions. The degree to which this reflected perceptual distortions of the scanner environments auditory input is not known. Furthermore, the constraints of the

applied NOIs must also be considered. The auditory network also contains multiple regions, such as the insula and areas of the ventrolateral frontal cortex which are involved in other functional processes. Thus, observed effects may also relate to altered processing of body perception or social cognition through altered insula connectivity.

Alternatively, these effects may represent ketamine modulating the salience network. We note the auditory network as defined by Smith (2009), while containing key auditory regions, also extends to ventrolateral prefrontal regions including the insula cortex. As such, this network can be considered a combination of the salience network (Seeley et al. 2007) and auditory networks.

The salience network has been implicated in the mediating of DMN and executive control networks (Bressler et al. 2010; Menon et al. 2010; Bonnelle et al. 2012), furthermore it has been suggested that the salience network is involved in the orientation of attention (Seeley et al. 2007; Eckert et al. 2009). Ketamine induced modulation of the auditory networks may then be interpreted in terms of salience modulation which may result from ketamine induced attentional control and cognitive processing deficits.

Comparisons of lamotrigine effects

As discussed in Chapter 4 and 5, lamotrigine is theorised to modulate ketamine induced connectivity effects through a reduction in ketamine-induced glutamate release. While lamotrigine, at the administer dose, has been observed to attenuate the ketamine-induced BOLD amplitude response (Deakin et al. 2008; Doyle et al. 2013), no evidence was observed in this study for significant modulation of ketamine induced network connectivity by lamotrigine. Indeed, we were unable to distinguish lamotrigine from placebo nor lam+ketamine from ketamine. We conclude lamotrigine has no significant effect on network connectivity either at baseline nor on the ketamine induced network connectivity, however we cannot disqualify more subtle modulatory effects. We also cannot preclude network connectivity effects for alternate network definitions or parcellation schemes, not included in this analysis. While the networks investigated in this study represent repeatedly identified resting state networks, alternate network configurations have also been presented (Menon 2011; Smith et al. 2012) which may reveal connectivity effects of lamotrigine.

The lack of connectivity effect of lamotrigine has implications for the mechanisms by which ketamine alters functional connectivity. The observation that lamotrigine pre-treatment was indistinguishable from placebo suggests that direct modulation of glutamate release does not significantly alter the network configuration in the brain. This, when taken in context of the observed connectivity effects of ketamine, suggests NMDAR blockade is primarily responsible

for the alteration to the connectivity structure of the brain, as opposed to the downstream glutamatergic effects.

Risperidone modulates network connectivity

Risperidone affects the human brain through different mechanisms to lamotrigine and ketamine, as discussed in Chapters 4 and 5. It is known to achieve high occupancy 5-HT_{2a} and D_2 receptors (Nyberg et al. 1999) the former leading to reduced downstream glutamate release. Moreover, risperidone has been shown to directly potentiate the NMDAR (Konradsson et al. 2006). As such risperidone has two mechanism of action theorised to counter the ketamine effect.

Our observations indeed indicate risperidone modulates the network connectivity effects of ketamine. We were able to accurately distinguish risperidone pre-treated ketamine from the placebo pre-treated ketamine state suggesting a robust modulation of network connections (Table 9). Furthermore we could not separate saline from the ketamine state following a risperidone pre-treatment (Acc < 69%) indicating that risperidone modulation of the ketamine effect may result in a more saline-like network connectivity pattern. We note a similar classification accuracies and kernel weight maps across window lengths suggesting consistent network connectivity effects across connectivity frequencies.

Inspection of the kernel weight maps for the comparison of risperidone and placebo pre-treated ketamine states (ris+ketamine v ketamine) reveals risperidone modulates the ketamine induced connectivity in auditory and visual 2 networks. These kernels were also highly weighted for classification of ketamine and saline. This considered with the classification accuracies suggest that risperidone may attenuate the connectivity effects of ketamine in these networks creating a more saline-like state.

Risperidone was also found to alter the ketamine induced connectivity within and between DMN, sensorimotor and right frontoparietal networks in addition to the connectivity between auditory, executive control and the DMN. This pattern of effects represents network interactions associated with sensory processing (visual, sensorimotor and frontoparietal) and cognitive processing (salience/auditory, frontoparietal and DMN). Risperidone however did not produce any significant effects at baseline, suggesting these modulations are not simply risperidone effects still present under ketamine. Instead we speculate that the effects of risperidone and ketamine interact, resulting in a distinct sate of network connectivity, more similar to that of saline than ketamine.

Taken as a whole, our results suggest that it is the dual mechanism of action of risperidone on the ketamine response that affects this pattern of network connectivity changes. Given the lack of effect of lamotrigine we hypothesise that the NMDAr potentiation of risperidone plays a key role in this connectivity modulation as opposed to the downstream glutamatergic effects. This hypothesis is supported by the comparison of lamotrigine and risperidone pre-treated ketamine conditions, reporting accuracies in the range 70% < accuracy < 77%, indicating differential connectivity effects of pre-treatment compounds on the ketamine state.

Limitations

In this study we compare the effects of pharmacological intervention on network connectivity in a principled and novel manner. While providing insight into effects of ketamine on consistent resting state, networks the limitations of this analysis must also be considered.

This methodology while identifying networks modulated by ketamine, does not inform the manner in which these networks are modulated. A I interpretation of network connectivity would be to assign increases or decreases in connectivity between these networks, this however would render the motivation for this study void through enforcing an assumption of network uniformity. We argue that networks may be differentially altered through pharmacological intervention, for example the network regions may express inversely altered connectivity as a result of a compound infusion. Such differential network effects present a challenges in terms of interpretation. In relation to the current analysis, the regional network modulations may be interpreted using post-hoc univariate statistics, this however enforces the assumption of independence between connections and is naïve to covariance's in the data. Future work will consider the principled investigation of network modulatory effects through the interrogation and subsequent analysis of weights obtained from projection of the combined kernel coefficients into feature space.

The work here considered networks formulated over a range of windowing parameters, the motivation for this was the investigation differential network frequency effects. We found no evidence to support the suggestion that either ketamine or any of the pre-treatments resulting in connectivity differences at different network frequencies. Generally classification accuracies for well differentiated conditions decreased with shorter window lengths, however this decrease was relatively small, in the order of ~4-8% between window lengths of 90 sec and 360 seconds. This decrease is most likely due to the inclusion of spurious correlation values at short window lengths resulting in increased noise and decreased classification accuracies.

The work here is also constrained by the *a priori* selection of NOI definitions. Furthermore, the applied NOIs were defined using regions implied in multiple networks. This is particularly evident in the defined auditory network which contains areas often associated with the salience network. Recent studies have isolated these network (Di et al. 2013) overcoming these issues of confounded network descriptors. Furthermore, these network descriptions often neglect the basal ganglia and thus we are blind to altered striatal-cortical effects elicited by ketamine. We suggest further work investigating the effect of ketamine on network connectivity using the Di (2013) NOI definitions with an additional basal ganglia NOI.

Chapter 7: Temporal variation in functional connectivity effects

As discussed in Chapter 2, investigating network dynamics provides new insight into the organisation of the brain. Traditional approaches to connectivity analysis have considered a single representation of the brain connectivity, computed from the entirety of the time series data. These analyses provide highly pertinent information regarding robust changes in connectivity dynamics, however are blind to temporal variations in connectivity.

The investigation of group differences in temporal variations of functional connectivity (FC) can provide additional information to aid the understanding of the organisation in the brain (Hutchison et al. 2012). Specifically, analysis of the temporal profile of connectivity provides insight into the temporal alterations in regional connections (Chang et al. 2010), the occurrences of discrete meta-stable states (Smith et al. 2012) and the variability of connections between regions (Zalesky et al. 2014). Here we wish to expand on the traditional approaches outlined in the Chapter 4 through investigation of the effect of ketamine, and its potential modulation via pre-treatment, on temporal variations of the observed FC.

The aim of this chapter is to provide empirical evidence toward the hypothesis that analysis of connectivity in the temporal domain provides additional insight into the organisation of the human brain and the effect of pharmacological interventions.

7.1 Introduction

Conventionally, FC is estimated using a “single-pass” approach, where connectivity is estimated through measures of signal similarity over the entire time-series. This enforces assumptions of both temporal and spatial stationarity on the estimated connectivity. While informative, this is likely an over simplification of the true underlying connectivity in the brain. Indeed, it has been shown that the connectivity between regions globally fluctuates during a resting-state scan (Chang et al. 2010; Hutchison et al. 2012; Zalesky et al. 2014). Furthermore, the organisation of topological networks has been shown to alter over the resting-state, resulting in discretely occurring meta-stable network states (Calhoun et al. 2014).

The sliding window approach (Chapter 3) has been widely employed to investigate time-varying connectivity in the brain (Sakoglu et al. 2010; Hutchison et al. 2012; Zalesky et al. 2014). An alternative approach for estimating time-varying connectivity is wavelet coherence (Chang et al. 2010). However, the inclusion of the frequency domain drastically increases the dimensionality of the estimated temporal connectivity. This presents challenges in concisely summarising the connectivity information for analysis. Windowing provides a proven, simple representation of

connectivity over time, where each discrete period is represented as a connection matrix. This allows for the statistical testing of temporal dynamics without the issues associated with increased dimensionality.

Windowing is akin to a low pass filtering (Van Dijk et al. 2010), short windows reveal higher frequency FC fluctuations, while longer windows reveal slower frequency changes in the connectivity profile. Thus, the selection of an appropriate window length should be carefully considered. Short window lengths (~<60 seconds) are prone to spurious correlations and a reduced signal to noise ratio (Van Dijk et al. 2010; Whitlow et al. 2011), however allow for investigation into higher frequency connectivity changes. Conversely, windows that are too long (>5 minutes) may not be sensitive to connectivity fluctuations (Hutchison et al. 2012) but are more robust to spurious correlations.

Here we examine temporal variations in the FC and assess the sensitivity of these fluctuations to the effects of ketamine (Chapter 4). We demonstrate the use of the sliding window approach to estimate temporal behaviour of connectivity and apply measures of connectivity dynamics to reveal the effect of neuro-active compounds on the temporal profiles of connectivity. Here we limit the investigation of connectivity dynamics to the PLA+SAL and PLA+KET sessions in order to demonstrate the applicability of this new investigate approach to phMRI data.

7.2 Methods

The participant recruitment, experimental design, image acquisition and pre-processing steps are described in Chapter 4. Identical post-processing procedures were performed to prepare the data for connectivity analysis. Namely the regression of CSF and WM parameters, the six motion parameters and band pass filtering in the range 0.01Hz to 0.1Hz.

Generation of a multi-slice graph

In order to investigate the FC effects of acute ketamine in healthy volunteers, we model imaging data as a series of graphs, defined as a multi-slice graph. Similar to Chapter 4, data is parcellated using the AAL atlas and the mean time series of each atlas region computed from regional voxel members. We selected 90 atlas regions for use in this analysis, these represent complete coverage of the cortex and sub-cortical structures. Each region, with its corresponding mean signal, is used to represent a node within each graph; the connections between those regions are denoted by edges, for a more detailed introduction we refer the reader to Chapter 2.

Multi-slice graphs were generated using a sliding windowing approach, as described in Chapter 3. Temporal connectivity was estimated using a Gaussian windowing (Chapter 3) procedure in

order to achieve better temporal sensitivity than the traditional box-car window. Windowing was applied in increments of a single volume (TR = 2seconds) along the length of the acquired time-series. In order to investigate the widest range of frequency effects possible we select a short window length of 90 seconds (effective length: 30 seconds). It has been demonstrated that graph theory measures can be accurately computed with as little as 90 seconds of data (Whitlow et al. 2011) and further empirical evidence suggests windows in the range of 30-60 seconds are also reasonable (Hutchison et al. 2012; Shirer et al. 2012).

Pearson's correlation was applied to estimate connectivity at each window step, s, generating a connectivity matrix, $\mathbf{A_s}$, for each window position. The Fisher r-z transform was applied to each correlation matrix to correct the distribution variance at extreme values. This resulted in a multi-slice graph per participant representing the temporal connectivity in each experimental condition.

Connectivity statistics

Regional connection strengths were computed using node strength (NS); computed as the normalised sum of the connections on a single node, *i*, in a graph slice, *s*:

$$NS_s(i) = \frac{1}{N}\sum_{j}^{N} \boldsymbol{A}_{ijs}$$

where N is the number of nodes within a graph (here 90, as defined in the AAL). This provides a regional-temporal view of the connectivity in the brain, facilitating interpretation of the complex temporal connectivity networks and providing insight into the connectivity hub effects. We refer to the collection NS values over graph-slices as the NS profiles.

Measures of Temporal Variation

Comparison of single-pass FC measures reveal the effect of the experimental condition on the changes in the value of connection strengths over the entire time-series. Here we propose a complementary analysis to investigate the effect of the experimental condition on temporal dynamics of the functional connectivity in the brain.

In order to investigate the effect of our experimental condition on the frequency profile of connectivity fluctuations, we calculate and the fast Fourier transform (FFT) using an NFFT=256, for the temporal profile of NS values. Each NS profile had a length of 150 samples and a sampling frequency of 0.5Hz. Windowing acts as a low pass filter, as such it is recommended to focus investigation to the pass-band frequency range. In the case of a boxcar this is [0-(1/w)]Hz where w is the window length (Leonardi et al. 2015). A Gaussian window however, affords a wider pass

band, as illustrated by the single-sided frequency response of the full width window of length 90 seconds, as shown in 31. Based on the pass band of this window, we limit the range of frequency investigations to 0-25mHz. The resultant single sided amplitude spectrum contained 129 bins for frequencies up to the Nyqusit, 0.25Hz. The pass band of 0-25mHz is represented by the first 14 frequency bins for the estimated frequency profile this range.

The amplitude in each frequency bin was compared between paired subjects using a paired t-test to assess the effect of the experimental condition. Low frequency comparison (0-2mHz) are akin to comparisons of using traditional single-pass approaches, indicating a change in the "stationary" connectivity (Leonardi et al. 2015). Higher frequency effects are indicative of changes in the temporal variations of connectivity values. These changes can be interpreted as changes in the amplitude of the oscillating connectivity at a given frequency.

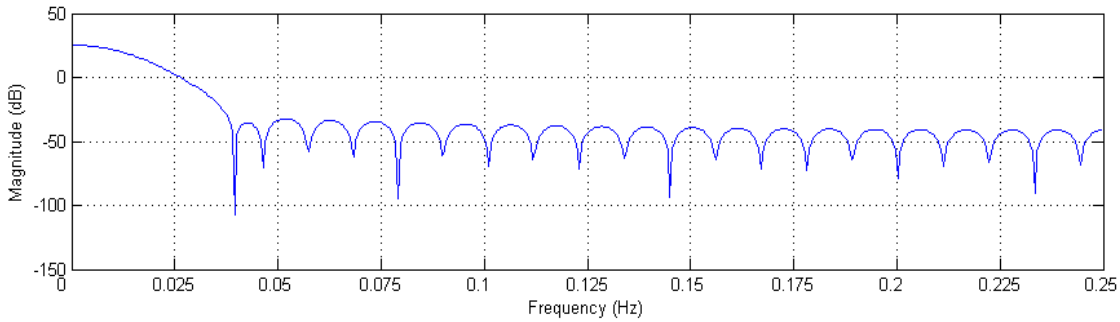

Figure 31 - Single sided frequency response of a 90 second Gaussian window at Fs = 0.5Hz.

Edge dynamics as measure by Zalesky's statistic

It has been suggested that the dynamics of the temporal connectivity can be quantified by the length of deviations from the median of each temporal connectivity profile (Zalesky et al. 2014). For the connectivity profile of a given edge, $\boldsymbol{e}$, median connectivity strength over all graph slices, μ, was computed. Median crossings are recorded as $\boldsymbol{t} = (t_0, t_1, \ldots, t_N)$, for each crossing the length of an excursion from the median is then given by $l_n = t_{n+1} - t_n$ and the height of this excursions is $h_n = \max(|\boldsymbol{e}_n - \mu| : t_n < t < t_{n+1})$. The dynamic connectivity statistic defined by Zalesky (2014) is then formulated as $T = \sum_{n=1}^{N} |l_n h_n|$. We compute this simple dynamic statistic for each edge and compare statistics between groups using a paired t-test. This test reveals changes in connectivity dynamics it terms of oscillations from the median.

Temporal synchronisation of regional connectivity

The similarity between the regional temporal profiles of connectivity reveals the synchronisation between connections, providing an alternate perspective on connectivity dynamics. The oscillation of connectivity over time is argued to represent periodic occurrences of meta-stable

states and connectivity reorganisation (Zalesky et al. 2014). Thus, change in the synchronisation between regions would represent alterations in the dynamic organisation of meta-stable states over time. To investigate this aspect of connectivity dynamics, we propose the application of the amplitude insensitive synchrony measure, the phase locking value (PLV)(Lachaux et al. 1999), to all pairs of NS profiles. The PLV informs the similarity of the phase at each time-point between two signals, regardless of the signal amplitude and is formulated as:

$$PLV(i,j) = \frac{1}{T}\sum_{t=1}^{T} \exp\left(real\left(\varphi_t^j - \varphi_t^k\right)\right)$$

Where φ_t^j is the phase of the NS profile at node j at slice t. We employ Hilbert transformation to compute the instantaneous magnitude and phase, as described in (Rosenblum et al. 1996)

If the correlation between nodes represents the intra-link connectivity, then the PLV between NS profiles would be the inter-region synchrony. This provides an alternate perspective on the temporal variations of connectivity, independent of amplitude. For effects between conditions which elicit consistent stationary changes in connection strengths, the relationship between NS profiles should remain the same. However, experimental conditions which afford a change in the dynamics of connectivity should also produce a change in the relationship between regional connectivity profiles, regardless of any amplitude change. To investigate these effects the PLV for all regional pairs is compared between conditions using a paired t-tests and the Benjaminni-Hochberg correction, at a level of α=0.05, applied to correct for multiple comparisons.

This is a fundamentally different comparison to that of the Zalesky statistic and the FFT measurements, revealing connectivity dynamics in terms of the temporal organisation of the brain rather than independent changes in rates of connectivity oscillation. This affords new insight into connectivity effects that arguably represent a more biologically motivated investigation of connectivity dynamics.

7.3 Results

As expected, examination of edge connectivity and node NS over time reveals globally coordinated connectivity fluctuations, as illustrated for an individual in Figure 32. We observe periods of globally organised high regional connectivity followed by bands of weak regional connectivity. Furthermore, we note qualitative differences in the synchrony between regional connectivity oscillations, indicating localised connectivity fluctuation effects and the possibility of dynamic organisation of regional connectivity.

To investigate regional connectivity synchronisation in the brain at rest, we perform a one-sample t-test on the difference in PLVs from the mean PLV for participants NS profiles in the placebo (pre sal) condition, Figure 33. This simple test allows for the testing of the null hypothesis that all regions are equally synchronised with each other, representing a globally synchronised state.

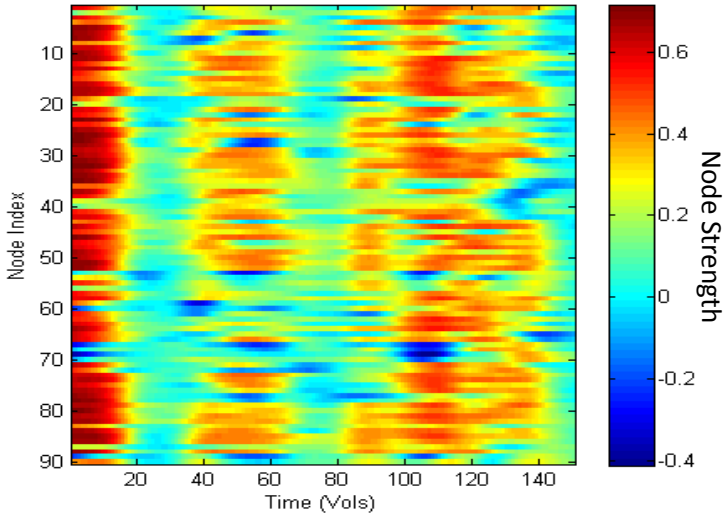

Figure 32 - Temporal NS profiles for the whole brain for a single subject in the Placebo (pre Sal) condition for a period of 5 minutes (TR=2sec). Obtained using moving Gaussian windows (90 sec : 45 vols) applied to data parcellated using the AAL atlas (90 nodes). Each horizontal line within each graph represents the correlation between a nodes pair calculated at each window position, figure illustrates globally synchronised epochs of high and low connectivity.

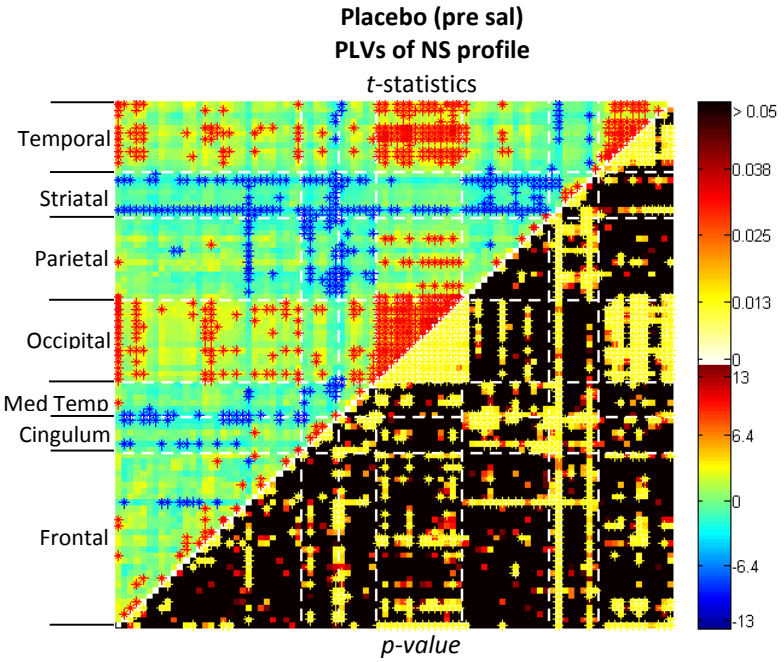

Figure 33 - Synchronisation of NS temporal profiles as measured by the PLV in the placebo (pre sal) condition. Upper triangle shows the t-statistic for one sample t-tests for PLVs (minus mean PLV), lower triangle reports p-values (thresholded at p<0.05 for visualisation). * indicates comparisons reporting a significant result after multiple comparisons correction (Benjamini-Hochberg, α=0.05), red and blue stars indicate significant positive and negative t-statistics respectively.

A differential pattern of regional synchronisation was observed, with many regional pairs reporting significant deviations from the mean PLV, suggesting regional deviations from the global synchrony. Furthermore, we observe a modular structure in regional synchronisations where a large cluster of regions were found to be significantly more synchronised than others. Most notably the visual, lateral temporal cortices and motor areas reported a significantly greater synchronisation that other NS profiles. This may indicate a preferential synchronisation between regions, such that the temporal variations in connectivity in these regions may be more strongly inter-dependent.

The PLV for NS profiles in the hippocampus, posterior cingulate (pCC), thalamus and caudate all reported significantly lower synchrony with other NS profiles than the global mean PLV. This may indicate either the relatively stationary connectivity in these regions, temporal connectivity of this region is less dependent on other regions or that connectivity alters with different modular organisations over, such as expected with a regulatory or mediatory region.

Effects of saline on connectivity variation

The effect of saline on connectivity temporal variations is revealed through comparison of measures of the NS frequency profiles, NS synchronisation and edge dynamics between the saline and placebo conditions.

For comparison of frequency profiles, Figure 34, no effects survived multiple comparisons corrections, akin to within session stability. Trend-level ($p<0.05$; uncorrected) low frequency (≤2mHz) increases in connectivity were reported across frontal, parietal and temporal cortices. These effects are akin to changes in connectivity as measured using traditional single-pass approaches. Increases in primary and secondary visual regions and the cingulate in frequencies less than 13.7mHz were also noted. This suggests that the transition between placebo and saline states may express subtle changes in NS at low frequencies.

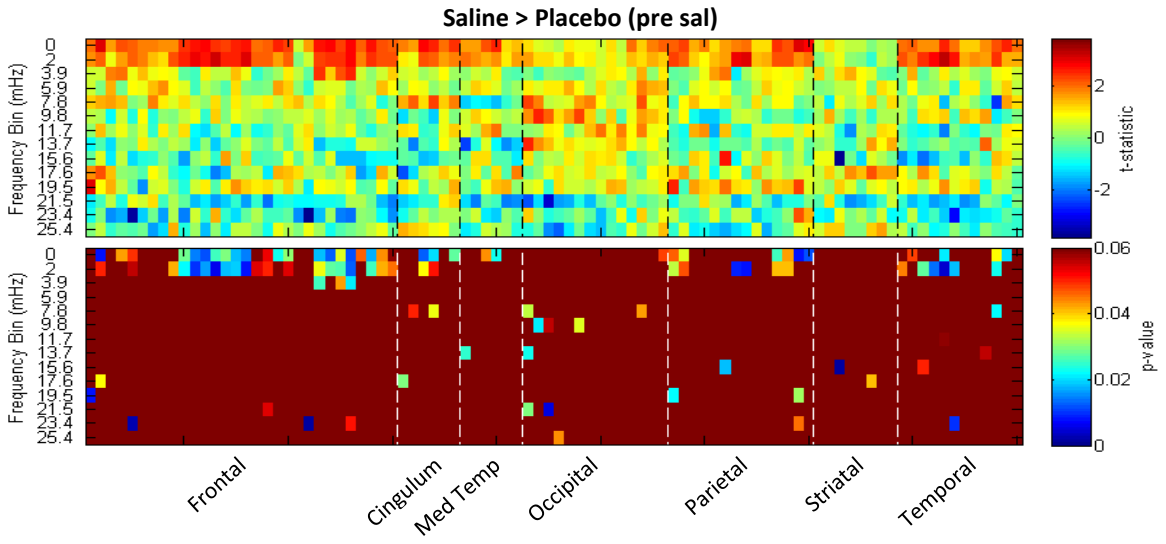

Figure 34 - Comparison of saline and placebo NS frequency profiles. The upper pane visualises t-statistics for frequency by node, the lower pane shows p-values (p<0.06 for visual contrast). No effect passed multiple comparisons correction

Comparisons of Zalesky's statistic, Figure 35, did not yield any significant effects after multiple comparisons correction. Results indicate a wide spread, trend-level reductions in the variability of connections. When considered with the comparisons of the frequency profiles of NS values, suggest this subtle effect is likely due to a reduction in the standard deviation in NS profiles.

Contrasting the synchrony between NS profiles for the saline and placebo conditions, Figure 36, also failed to yield any significant effects after multiple comparisons testing. Notable trend-level effects were observed, suggesting an increase in the synchrony of the NS within frontal regions and with the cingulum. Taken together these results suggest saline has no significant effect of the functional connectivity.

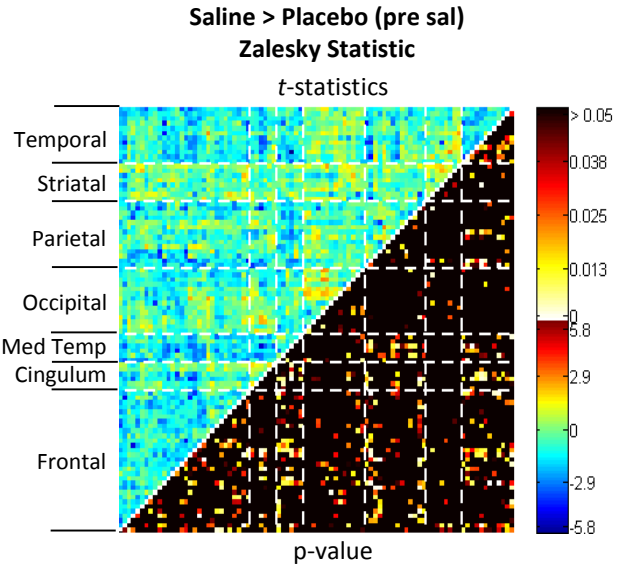

Figure 35 - Comparisons of Zalesky's statistic for connectivity dynamics between saline and placebo conditions. No effect passed multiple comparisons testing (Benjaminni-Hochberg, α=0.05)

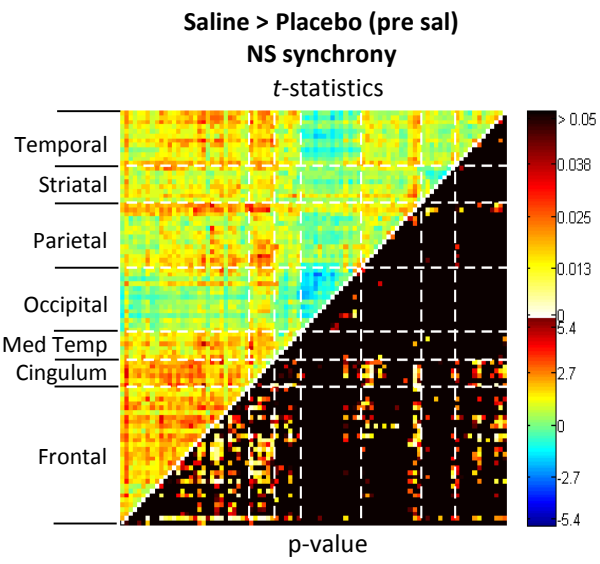

Figure 36 - Comparisons of NS profile synchronisation as measured by the phase locking value between saline and placebo conditions. No effect passed multiple comparisons testing (Benjaminni-Hochberg, α=0.05)

Ketamine elicits changes in connectivity variation

The effect of ketamine on temporal changes in FC is e through comparison of the ketamine condition with both placebo (pre ket) and saline conditions. Results for the comparison of frequency profiles reveals ketamine elicits few significant effects when compared to placebo and saline, Figure 37. A similar trend-level pattern of change in t-statistics was observed in both contrasts suggesting a consistent influence in both contrasts which we attribute to ketamine. Significant ($p < 0.05$; corrected) decreases in NS were observed at 11.7mHz in the right anterior cingulate (aCC) and left anterior frontal cortex for the main effect of ketamine (ketamine > placebo), suggesting ketamine decreases the strength of NS fluctuations at this frequency. For the between session comparisons (ketamine > saline), significant decreases were reported at low frequencies (0-2mHz) in the right mid temporal pole (mTP), right rectus gyrus and right supramarginal gyrus. Increases were observed in the left thalamus at 0mHz. These changes indicate ketamine induces changes in the overall magnitude of NS in these regions rather than effecting the regional connectivity fluctuations.

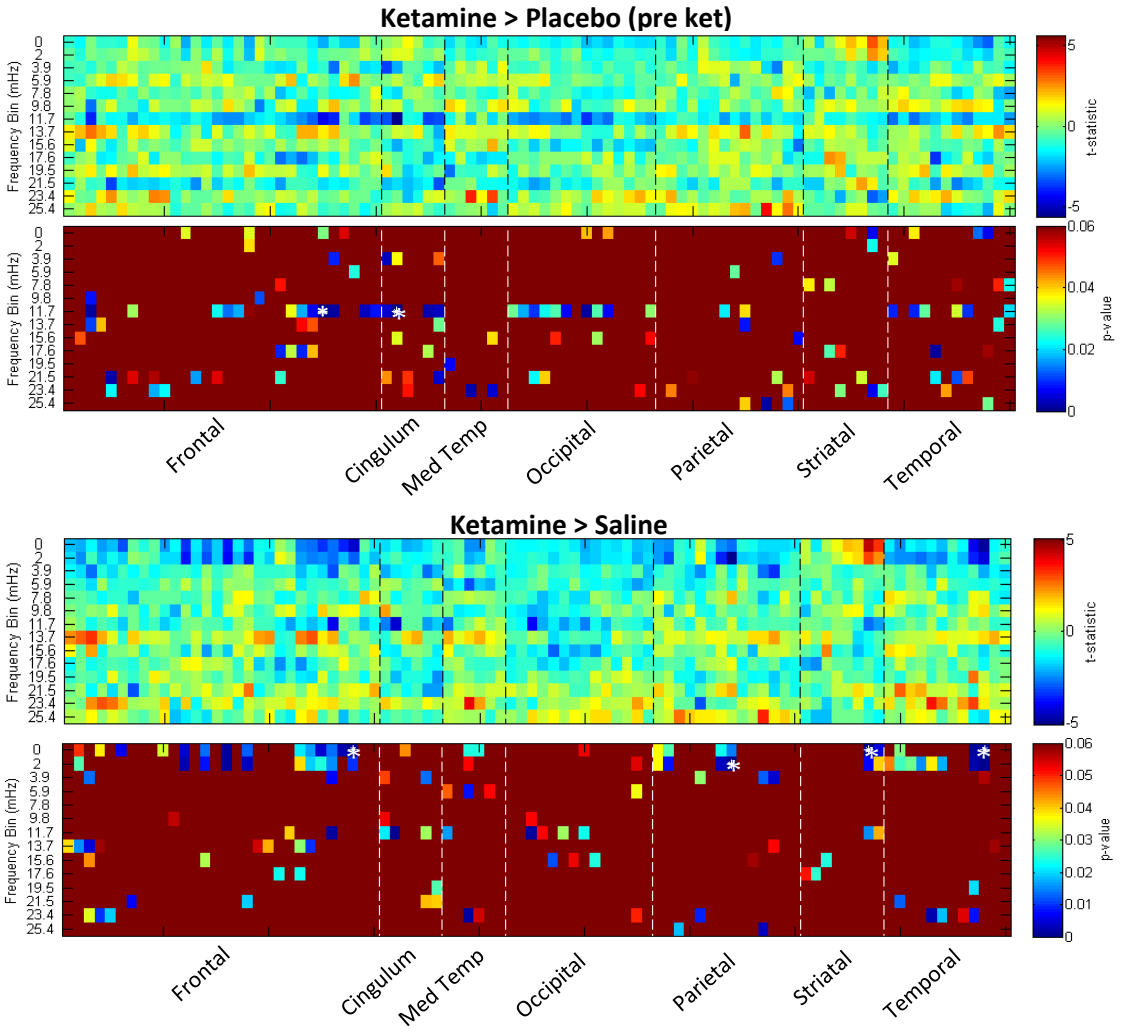

Figure 37 - Comparison of NS frequency profiles for ketamine, placebo and saline over the frequency range 0 – 25mHz. For each comparison we present both the t-statistics (upper pane) and p-values (lower pane). In order to improve visual constrast of p-values, only values <0.06 are displayed. * indicades a signifianct result after multple comaprisons correction at α=0.05.

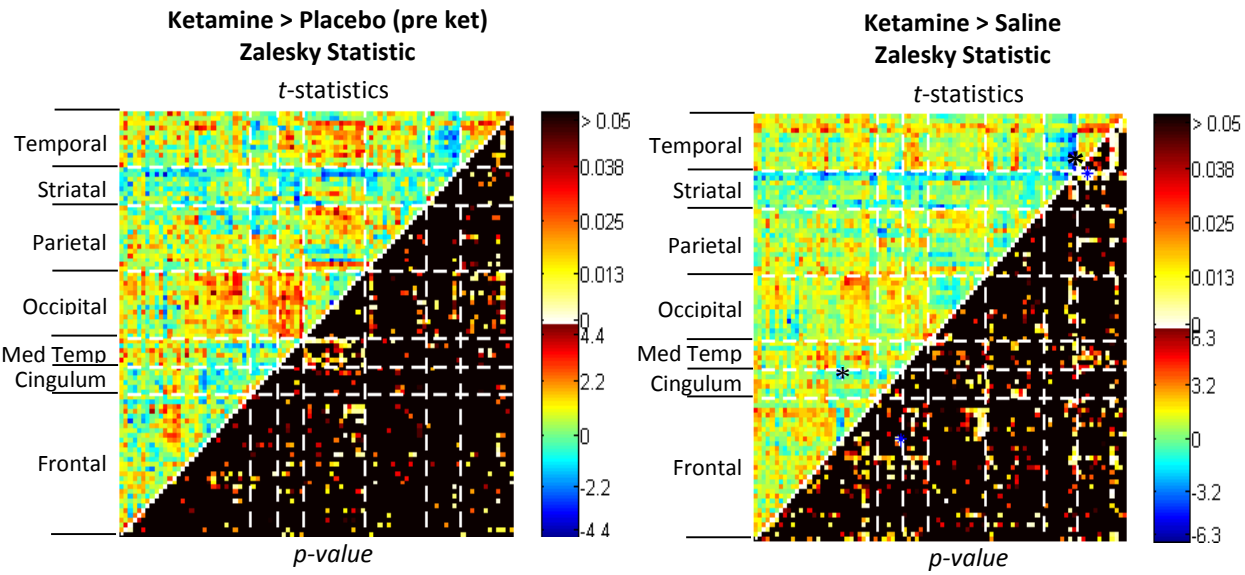

Figure 38 - Ketamine effect on connectivity fluctuations as measured by the Zalesky statistics compared between Ketamine and placebo and saline conditions. * indicades a signifianct result after multple comaprisons correction at α=0.05.

Comparisons of Zalesky's test statistic between ketamine and saline report a significant ketamine-induced reduction connectivity dynamics for the connection between the posterior cingulate (pCC) and olfactory bulb and between the thalamus and superior temporal gyri, Figure 38. The pattern of trend-level effects, as with frequency profile contrasts, was similar between comparisons; indicating a common ketamine effect. While similar to ketamine compared to saline, the contrast of ketamine and placebo did not yield any significant effects after multiple comparisons testing.

Finally, investigation of the synchrony between regional NS profiles reveals a highly similar spatial distribution of effects for ketamine compared to both saline and placebo (pre ket). Reported effects for the comparison to saline were far more prominent reporting multiple significant effects, Figure 39.

The NS profile in the thalamus was found to exhibit an increased PLV with all other brain regions, with the exception of the medial orbital frontal cortex. Significant ($p<0.05$ corrected) increases in PLV were observed between the left thalamus and lateral frontal cortex, the right fusiform, right inferior temporal gyri, left postcentral gyrus and right superior parietal gyrus. We interpret these effects as increased synchrony of the thalamic NS, perhaps indicating a ketamine-induced shift to subcortically driven connectivity. Significant ($p<0.05$ corrected) decreases in the PLV were reported between the right mid temporal pole and left inferior orbital frontal gyrus, the supplementary motor area, left frontal medial, left gyrus rectus, right Insula, left anterior cingulate cortex, right paracentral lobule and left mid temporal pole. Further significant reductions in PLV were reported between the gyrus rectus and frontal superior medial, medial

and inferior orbital areas. This suggests a reduced contribution of the gyrus rectus and medial temporal pole in the dynamic network organisation for the ketamine state.

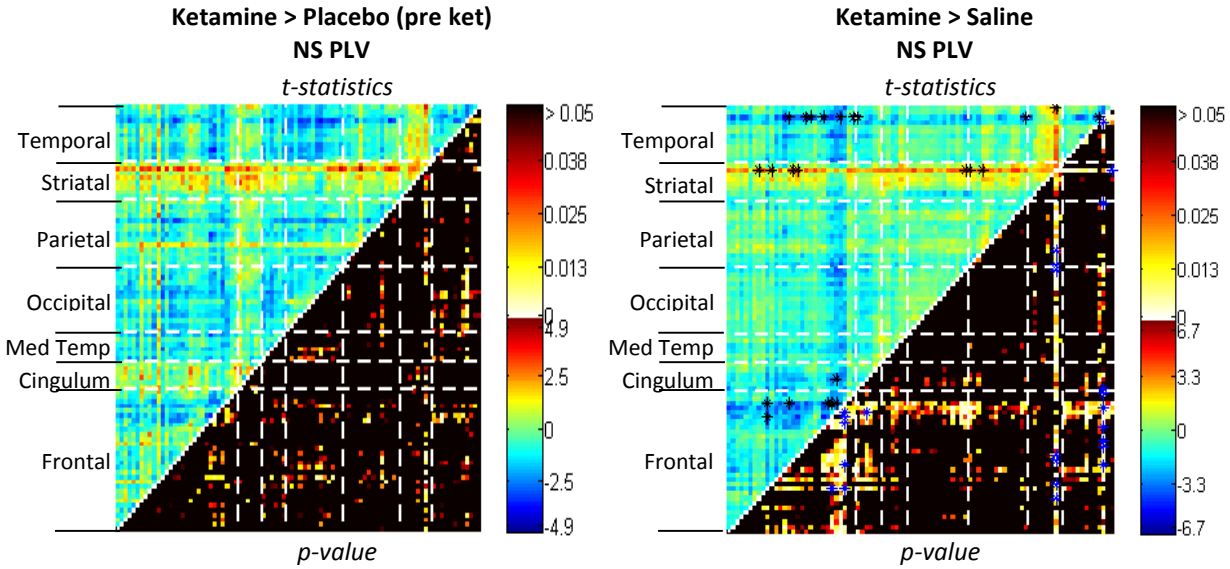

Figure 39 - Main effects of ketamine on the synchronisation of regional NS between brain areas, as revealed by comparison of ketamine with placebo (pre ket) and saline. * indicades a signifianct result after multple comaprisons correction at α=0.05

Taken together our results suggest ketamine has a differential effect on temporal connectivity across frequencies and significantly alters the temporal synchrony of connectivity between regions. These effects were most prominent in the orbital frontal cortex, temporal pole and thalamus where ketamine was found to alter both the stationary NS as well as the synchronisation of these regions with other brain areas.

7.4 Discussion

It is evident that functional connectivity in human brain is not static but exhibits temporal dynamics. We have observed coordinated fluctuations in regional connectivity values at baseline, Figure 32, consistent with other studies (Hutchison et al. 2012; Zalesky et al. 2014). Windowed connectivity reveals globally synchronous epochs of high and low connectivity followed by periods of low connectivity, Figure 32. It has been argued these oscillatory periods of synchronisation are necessary for normally segregated regions to cohere within a global workspace for effortful processing (Dehaene et al. 1998; Zalesky et al. 2014) and for the reconfiguration of meta-stable states (Van de Ville et al. 2010). However, this oscillating connectivity structure was also observed in the anaesthetised macaque brain (Hutchison et al. 2012). Thus indicating this periodic connectivity structure is not a result of cognitive, conscious or effortful processing but rather represents a fundamental process of the temporal connectivity in the mammalian brain. However, this does not preclude cognitive and effortful processing affecting a change in the organisation of connectivity in these periods of high connectivity.

Here we have demonstrated pharmacological modulation of the connectivity dynamics in the brain through investigation of the effects of ketamine on connectivity profiles. We have presented a comparison of frequency-amplitude profiles for connectivity values estimated over time. This provides an extension of traditional approaches comparing connectivity estimate over the entire time-series. Comparisons at low frequencies (< 2mHz) are akin to contrasting stationary effects while higher frequencies provide information regarding the effects of ketamine on the amplitude of connectivity oscillations.

We have also demonstrated that ketamine significantly alters the synchronisation of connectivity profiles between regions. When interpreted in the context of an oscillating connectivity structure, suggests ketamine alters not only the strength of connections but the dynamic topological organisation of connectivity in the brain.

Pharmacological effects on temporal connectivity profiles

Saline was not found to elicit significant effects in any of the connectivity dynamics metrics tested. This indicates either a within session stability or insensitivity of the presented approaches to changes in the temporal profile of connectivity. Given the observed changes in contrasts of ketamine and saline conditions we suggest the former is more likely.

Ketamine elicited significant effects across all measures when compared to saline. Investigations into changes in the frequency profile of NS values reveals low frequency changes (0-2mHz), consistent with comparisons performed in Chapter 4 comparing connectivity estimated using the whole time series. We equate these effects to a change in the stationary amplitude of the NS which can be summarised as increased thalamic NS and reduced medial orbitofrontal cortex, mid temporal pole and supramarginal gyrus NS. Comparison of frequency profiles also revealed higher frequency (11.7mHz) effects suggesting ketamine also reduces the strength of localised connectivity oscillations in the anterior cingulate (aCC) and medial orbital frontal cortex, Figure 37. This effect in the aCC was not observed in comparisons of stationary connectivity, demonstrating that consideration of connectivity dynamics provides new insight into pharmacological effects. Subtle changes were also observed at higher frequencies however these did not pass multiple comparisons testing.

Interestingly we note the thalamus, temporal pole and OFC were strongly implicated in comparisons of the PLV of NS profiles between ketamine and saline, Figure 39. This is interesting as synchronisation was measured using an amplitude insensitive approach however significant effects occur in similar regions as amplitude changes. The relationship between amplitude and synchronisation is as yet unexplored and it is uncertain whether a causal relationship exists.

Given significant amplitude effects were observed in areas reporting no effects in regional synchronisation, we suggest this is a distinct but connected mechanism effected by ketamine warranting further investigation. The observed decreases in PLV for the OFC and temporal pole were most prominent between areas in the frontal cortices and temporal regions suggesting a modulation of a localised circuit.

It has been suggested the oscillations in connectivity relate to the reorganisation of connective states (Van de Ville et al. 2010; Deco et al. 2013). As such changes in oscillations have implications for the dynamic occurrences of meta-stable states in the task-free state (Allen et al. 2014). Changes in synchrony, as measured by PLV on the NS profile, can thus be interpreted as modulation of the organisation of these meta-stable states.

The ketamine-induced decrease in synchronisation of OFC and temporal pole synchrony with the rest of the brain suggests reduced inclusion in transient connectivity states. Increased PLV for the thalamus suggests a shift from dynamic connectivity states synchronised with the OFC and medial temporal pole to states synchronised with the thalamus. This may indicate a more sub-cortically driven connectivity organisation in the brain.

Comparisons of the Zalesky statistic did not yield many significant effects, suggesting either the Zalesky statistic was not sensitive to changes in connectivity dynamics or that ketamine did not effect a significant change in the fluctuations of edge connectivity. When considered with the sparsity of significant effects in comparisons of frequency profiles of NS values, we suggest ketamine does not significantly affect the rate of connectivity fluctuations. Instead, ketamine affords a change in amplitude of connectivity amplitudes, Figure 37, and alters the synchrony between regional NS profiles, Figure 39.

The medial OFC was identified in comparisons of the ketamine frequency profiles and PLVs, a region implicated in social cognition and reward processing; specifically the representation and updating of possible future outcomes (Elliott et al. 2000; Ridderinkhof et al. 2004; Amodio et al. 2006), and thus is implicated in memory, emotional processing and social cognition. To date, there has been little investigation on the effects of ketamine on social and emotional cognition; while it may be that changes in the connectivity of medial OFC are associated with cognitive processing deficits observed with the ketamine state (Krystal et al. 1994; Lahti et al. 2001). However, the sparsity of subjective reports precludes testing for this. The temporal pole has also been associated with socioemotional processing and is suggested to play a role in the mediating of emotional response to sensory stimuli (Olson et al. 2007), reduced NS and disrupted synchronisation of connectivity in this region may also contribute to social and emotional deficits and the perceptual distortions which occur under ketamine. Replication of this study with a

higher dosage of ketamine, to elicit stronger effects, and full subjective ratings would be required to confirm this.

Methodological considerations

The work undertaken here provides novel perspective into the effects of ketamine and its effects on the functional connectivity dynamics over time. We suggest the comparison of the frequency profile of windowed connectivity estimations offers an advantageous extension to traditional comparisons of connectivity effects revealing both stationary changes in connection strengths and changes in the oscillatory connectivity. However, this additional information also results in increased dimensionality, potentially reducing sensitivity when applying multiple comparisons testing. Thus, may be more suitable for a multivariate rather than a univariate approach. The comparisons of regional PLVs also provides a novel insight into the synchronisation between regional connectivity profiles, an aspect of connectivity dynamics not commonly investigated.

The method presented here provides a simple extension on traditional univariate connectivity analysis allowing for new insight into the mechanisms of the human brain. However, further work is required to investigate the biological interpretation of these variations in temporal connectivity. Full subjective ratings for each subject in each experimental conditions would allow for an analysis relating localised temporal connectivity fluctuations to effects of each compound to changes. However due to the sparsity of subjective reports such analysis was not feasible. Furthermore the administered dose of ketamine is relatively low due to repeated administrations, also limiting analysis relating connectivity changes to cognitive effects.

The limitations and flaws of this approach should also be considered, foremost amongst which is the use of windowing to estimate temporal connectivity. The choice of window length results in a compromise between accuracy and frequency resolution. Short windows are vulnerable to spurious correlations while longer windows may be insensitive to temporal fluctuations. The choice of window length will determine the frequency spectra of the estimated connectivity as windowing generates a low pass filtering effect. One potential solution to this the recent work by (Monti et al. 2014) who presents a framework employing multivariate regularisation to enforce sparsity, temporal coupling and optimises the window length avoiding issues of manual selection. Another alternative is the use of wavelets to create a frequency-time perspective of regional coupling (Chang et al. 2010), this provides a plethora of information which then presents new challenges in terms of combining data into informative summary measures.

Another potential limitation of this analysis is the use of the AAL atlas to define graph nodes. Tis may be sub-optimal due to differential region sizes and the fact that regions are anatomically

defined rather than a functional parcellation. Larger regions may include multiple temporal profiles which may interfere when averaged. Further work is required to quantitatively assess the impact of the granularity of parcellation and compare functional and anatomically derived atlases for the investigation of connectivity temporal dynamics.

The most pressing limitation of this method however, is its univariate nature. Due to the dimensionality of the data and the number of univariate tests performed, we must apply highly restrictive thresholds to correct for multiple comparisons. This may result in reduced sensitivity for comparisons of high dimensional data in small populations. Furthermore univariate tests are insensitive to correlations in the data and enforce assumptions of independence between connections, arguably unsuitable considering the nature of connectivity data. This limitation is most evident in comparisons of PLVs, in this work PLVs were computed on the NS profile due to restrictions on the dimensionality. An edge-wise comparison however, may afford a finer scale insight into connectivity synchronisations, however the population size and dimensionality of the resultant PLV matrix precludes such a univariate analysis. While the current state of the art may be univariate tests applied to connectivity measures, it may be more appropriate to compare connectivity using multivariate statistics. Thus minimises the issues of multiple comparisons testing while also respecting the inherent correlated nature of the data.

We conclude that while the investigation of connectivity dynamics has limitations, especially when performed in a univariate fashion, it provides a unique insight into the connectivity effects of pharmacological intervention in the brain. Considering the connectivity frequency profile and the synchronisation between regional connectivity profiles we can draw new insights into connectivity organisations effects not previously observed.

Chapter 8: Temporally Dynamic Community Structures in Pharmacologic Imaging

This chapter will focus on the investigation of the temporal dynamics of functional connectivity in the brain and potential modulation of this organisation through pharmacological challenge. Here, we develop a framework for the data-driven identification of temporally constrained community structures in the brain using a graph-theory approach. Through the investigation of the temporal profiles of these identified communities we wish to gain insight into temporal variations in the modular structure of the brain. We predict that the mapping of these connectivity dynamics provides an alternate perspective into the effect of active pharmacological compounds on the organisation of the human brain.

In this chapter we apply the developed framework for dynamic connectivity investigation to the ketamine dataset to reveal the effects of ketamine on the temporal profile of connectivity organisation in the brain for healthy volunteers. The purpose of this is to gain insight into the spatiotemporal connectivity mechanisms of ketamine, and to investigate the temporal connectivity organisation during the ketamine infusion.

8.1 Motivation

As discussed in Chapter 2, analysis of functional connectivity (FC) has progressed from interrogation of single instance graphs to the investigation of temporal dynamics in multi-slice networks. It has been demonstrated that the brain exhibits globally co-ordinated oscillating functional connectivity (Zalesky et al. 2014). Furthermore, these oscillations have been observed in both conscious humans and anesthetised macaques (Hutchison et al. 2012), suggesting fluctuating connectivity is an intrinsic mechanism of the mammalian brain as opposed to the result of conscious or effortful processing. Zalesky (2014) argues that synchronised periods of low connectivity facilitate the transmission of information between normally functionally segregated regions and are necessary for the transition between meta-stable connectivity states. The motivation of this chapter is to investigate the dynamic occurrences of these meta-stable states and the modulatory effects of ketamine on their organisation. Given the work in previous chapters demonstrating the effect of ketamine on whole brain patterns of connectivity, we predict ketamine will also robustly alter the dynamics of the functional architecture in the brain.

In order to account for aspects of the connectivity dynamics, a framework combining temporal and spatial independent component analysis (ICA) has been presented to identify temporally

independent connectivity organisations (Smith et al. 2012). While providing a means for the identification of connectivity organisational modes, this does not inform about the connectivity dynamics. An alternative is the application of tensor based ICA approach which can decompose data into spatial temporal and subject dependent variables (Beckmann et al. 2005). This provides an elegant approach for the investigation of synchronised network occurrence over time within a group. However, for resting state scans where it is unlikely a group consensus of dynamic connectivity exists across subjects, analysis must be performed on a subject-level and resultant maps merged in order to form group-level inferences. This merging presents significant challenges due to differences in individual's maps. Moreover, statistical testing at localised time points across subjects is restrictive.

An alternate approach to assess connectivity dynamics is the use of graph theory measures applied to estimated profiles of temporal connectivity. This approach offers a highly flexible framework for the analysis of temporal variations in connectivity organisation. Sliding windows have been applied to estimate multi-slice connectivity graphs, representing temporal connectivity in the brain. Connectivity dynamics, as modelled by these multi-slice graphs, has been investigated in terms of node or edge stability (Van Dijk et al. 2010; Hutchison et al. 2012). More complex analyses have incorporated a network perspective of connectivity in order to identify temporally consistent states (Allen et al. 2014) or temporal dynamics in previously identified resting state networks (Chang et al. 2010; Kiviniemi et al. 2011). While these analyses provide new insight into the temporal organisation of the brain, they are reliant on the mapping of previously identified networks or spatially independent networks and lack framework for testing the effects of experimental conditions on the dynamic modular architecture in the brain.

Here we present a method for investigating spatially and temporally dynamic community structure of the human brain. This approach has the advantage of being data driven, as such no *a priori* definitions network are required. Furthermore, this provides a modular perspective on connectivity organisation. Through statistical testing of the temporal variations of identified community structures on a subject and group level, we infer the effect of an acute ketamine challenge on the dynamic modular organisation of the human brain.

8.2 Dynamic Community detection

Community detection has been previous applied to identify consistent sub-graphs in connectivity data estimated over an entire acquisition (Schwarz et al. 2008; GadElkarim et al. 2012). These analyses use methods as described in Chapter 3 and generally compute the community structure in single graph instance but are not sensitive to temporal consistencies. Real world networks such as the brain have been shown to exhibit topologies which change over

time (Uddin et al. 2011). Multi-slice community detection algorithms have been developed which are able to identify temporal community structure in multi-slice graphs (Mucha et al. 2010). Such methods are based on the Newman's modularity measure (Newman et al. 2004) with an additional temporal constraint. These algorithms have be primarily applied to simulated data and benchmark datasets (Carchiolo et al. 2011; Hu et al. 2012; Kawadia et al. 2012). There have been few studies to date using this methodology for the investigation of neuroimaging data.

Multi-slice communities may be identified through clustering edges both within each graph-slice and between neighbouring graph-slices. Here, we define a graph-slice as single graph instance representing a discrete time period within a series of graphs. The relationship between two nodes, *I* and *j,* within a given network slice, s are defined by the slice adjacency A_{ijs}. The relationship of each node *I* between slices *s* and *r* is defined by the inter-slice coupling C_{isr}. This coupling factor determines the possibility of consistent edges existing between neighbouring slices. Multi-slice community detection as defined in (Mucha et al. 2010) restricts graphs to undirected network slices where $A_{ijs} = A_{jis}$ with undirected inter-slice couplings $C_{isr} = C_{irs}$. Incorporating inter-slice coupling results in the modularity measure as derived in (Mucha et al. 2010):

$$Q = \frac{1}{2\mu}\sum_{sr}^{T}\sum_{ij}^{N}\left[\left(A_{ijsr} - \gamma_s\frac{k_{is}k_{js}}{2m_s}\right)\delta_{sr} + C_{jsr}\delta_{ij}\right]\delta(l_{is}, l_{jr}) \qquad (8.2.1)$$

In this equation the parameter γ_s can be tuned to allow for different resolution scales, k_{is} is the node strength of node *i* in slice *s*. Modularity is normalised by the sum of all strength values over all slices, $2\mu = \sum_{jr}(k_{jr} + c_{jr})$, where $c_{jr} = \sum_s C_{jsr}$.We define the slice wiring cost as $m_s = \sum_{i,j} A_{ij}$ which is the sum of all weights in a given slice, *s*. The community label of each node, *i*, in each slice, *s* is denoted by l_{is}. The function $\delta(l_1, l_2) = 1$ if and only if $l_1 = l_2$, otherwise $\delta(l_1, l_2) = 0$. This algorithm has been shown to perform well benchmark datasets and real world voting data (Mucha et al. 2010) revealing evolving, temporally dynamic networks.

Signed modularity

These network modularity measures assume unsigned, undirected network connections, while functional connectivity graphs used in this analysis are undirected, they are signed and may contain negative connections. This may be problematic as modularity uses the normalised product of node strength to denote the probability of nodes within a single slice being connected by chance, the null case, as given by:

$$p_i p_j = \frac{k_i k_j}{2m}$$

The inclusion of negative values in the calculation of node strength destroys the probabilistic interpretation of $p_i p_j$. A solution exists separating positive and negative edges, as described in (Gomez et al. 2009). This results in separate definitions for modularity computed from positive and negative weights, Q^+ and Q^- where overall modularity is given by $Q = Q^+ - Q^-$. Gomez (2009) formularizes this approach for estimating the single slice modularity by first separating weights:

$$A_{ij} = A_{ij}^+ - A_{ij}^-$$

where:

$$A_{ij}^+ = \max(0, A_{ij}) \qquad \text{and} \qquad A_{ij}^- = \max(0, -A_{ij})$$

The signed node connection strength is defined by:

$$k_i^+ = \sum_j^N A_{ij}^+ \quad \text{and} \quad k_i^- = \sum_j^N A_{ij}^-$$

and the signed densities are given as:

$$m^+ = \sum_i^N k_i^+ \quad \text{and} \quad m^- = \sum_i^N k_i^-$$

This leads to the single slice modularity definition:

$$Q = \frac{1}{m^+ + m^-} \sum_{ij}^{N} \left(A_{ij} - \left(\frac{k_i^+ k_j^+}{m^+} - \frac{k_i^- k_j^-}{m^-} \right) \right) \delta(l_i, l_j) \qquad (8.2.2)$$

This simple extension of modularity allows for the detection of communities in graphs with signed connections.

Signed multi-slice modularity

We further develop the existing measures of modularity for use in functional connectivity analysis with signed multi-slice temporal networks. As discussed in Chapter 2, the validity and interpretation of anti-correlations within functional networks is still a matter of contention. Nonetheless however it is important to allow for the possibility of these relationships within community detection. Modifying equation (8.2.1) in a similar manner to (8.2.2) results in a simple multi-slice modularity measure suitable for signed connections:

$$Q = \frac{1}{2\mu^{\pm}} \sum_{sr}^{T} \sum_{ij}^{N} \left(A_{ijsr} - \gamma_s \left(\frac{k_{is}^+ k_{js}^+}{m_s^+} - \frac{k_{is}^- k_{js}^-}{m_s^-} \right) \delta_{sr} + C_{jsr} \delta_{ij} \right) \delta(l_{is}, l_{js}) \qquad (8.2.3)$$

where $2\mu^{\pm} = \sum_s^T \sum_i^N \left(k_{is}^+ + k_{is}^- + \sum_r^T \sum_j^N C_{ijsr}\right)$

The node inter-slice coupling factor is designed to couple edges between slices, as such is usually set to 1 for neighbouring slices and 0 otherwise (Mucha et al. 2010). Here we suggest an intuitive weighted approach instead where edges with consistent strong connection values between slices will be highly weighted, while edges with highly variable values between slices will be penalised. One suggested inter-slice coupling measure is the square root of the product of edges, belonging to nodes in the same community, between neighbouring slices (Kawadia et al. 2012):

$$C_{ijsr} = \sqrt{A_{ij(s-1)}A_{ijs}}\,\delta\left(l_{i(s-1)}, l_{j(s-1)}\right)$$

This has the effect of coupling edges between neighbouring slices which have strong, consistent edges. While this is valid for unsigned, weighted networks, when applied to signed networks it may result in imaginary coupling values due to edges transitioning signs between slices. To rectify this we reformulate the inter-slice coupling factor using sign separated adjacency values:

$$C_{ijsr} = \left(c_{ijsr}^+ - c_{ijsr}^-\right)\delta\left(l_{is}, l_{js}\right)\delta(|s-r| \le \gamma_t)$$

where:

$$c_{ijsr}^+ = \sqrt{\left(A_{ijs}^+ A_{ijr}^+\right)} \quad \text{and} \quad c_{ijsr}^- = \sqrt{\left(A_{ijs}^- A_{ijr}^-\right)}$$

As with the with in slice community estimation, we must correct the inter slice coupling coefficient for edges coupled by chance. Thus the inter-slice coupling coefficient becomes:

$$C_{ijsr} = \left(\left(c_{ijsr}^+ - c_{ijsr}^-\right) - \left(\overline{c_{sr}^+} - \overline{c_{sr}^-}\right)\right)\delta\left(l_{is}, l_{jr}\right)\delta(|s-r| \le \gamma_t)$$

This allows for couplings between signed weighted networks, enforcing inter-slice coupling between edges with consistent high correlations only. Edges which transition sign between slices will have a coupling value of 0 while consistent negative edges will have a negative coupling coefficient. Here, the term $\delta(|s-r| \le \gamma_t)$ which controls the temporal resolution of the inter-slice coupling. The parameter γ_t, takes integer values and determines the distance of temporal coupling between edges. For $\gamma_t = 1$, edges will only be coupled between neighbouring slices, increasing γ_t will allow edges to be coupled to increasingly temporally distant slices. Adjusting this parameter will allow for detection across temporally distant consistent communities and improve robustness to noise and spurious connections, and will be explored in future work.

In order to identify communities within a multi-slice data set, we modify the node community labels in a manner which maximises the overall value of Q. There are many methods of optimisation for modularity, for an in depth review we refer the reader to (Fortunato 2010). For the work presented in this thesis we have selected a commonly used methodology which has been demonstrated to provide good results on large data sets, namely a greedy agglomerative search.

Greedy agglomerative search

Here we have opted for a greedy agglomerative search method for the optimisation of Q, as described above. This is due to the simplicity of implementation and the fact that this type of algorithm has been proven to perform well on large networks (Meunier et al. 2009). The algorithm developed by Blondel (Blondel et al. 2008), known as the Louvain method, has been shown to perform both efficiently and accurately. The Louvain method initialises each node to its own community, for every iteration the algorithm performs a two-step procedure. In the first step modularity is optimised by merging nodes which improve Q, in the second step, all node members of each communities are folded into a single node representation. As such the dimensionality of the network is reduced for each subsequent iteration. These steps are repeated until no further merging of nodes improves the overall modularity measure, an illustration of this node abstraction procedure is shown in Figure 40.

This algorithm can be extended to detect communities in multi-slice networks as described in (Carchiolo et al. 2011). Furthermore, the iterative merging of community folds provides an intuitive view of community hierarchy. We implemented an in-house version of this greedy agglomerative search with community folding using the modularity measure defined above, in Matlab 8 (http://www.mathworks.co.uk/products/matlab/). A promising application of this method would be to detect communities in the graph dual, thus defining communities in terms of edges rather than nodes, such an approach will be explored in future work.

From modularity optimisation we obtain a collection of node labels denoting node community membership at each graph slice which achieve a maximal value of modularity, Q_{max}. These are binary labels representing hard assignments of node membership, however it is possible to also compute a pseudo-fuzzy representation of node membership. This provides a more intuitive measure of the likelihood of node membership for a given community at a slice, but is pseudo-fuzzy as it is computed based the obtained binary labels.

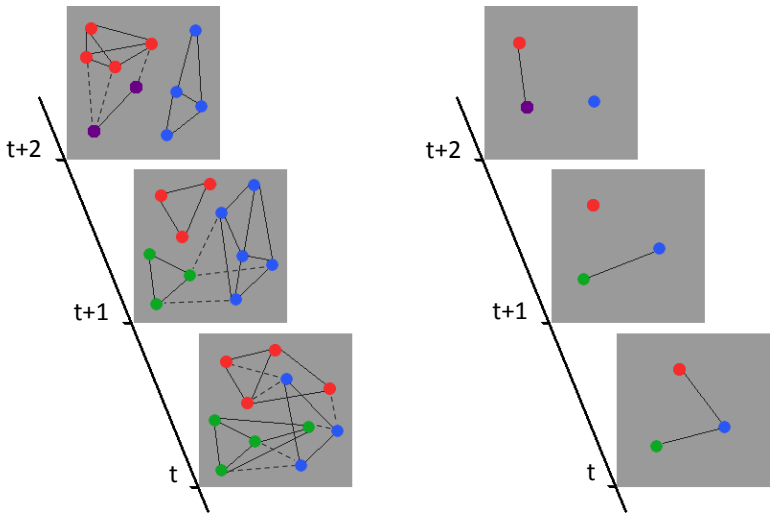

Step 1: Join all nodes which improve modularity into communities.

Step 2: Fold all nodes within a community into a single node.

Figure 40 - Steps of graph reduction in community detection, for each iteration of clustering, two steps are performed. Firstly community structure is identified, all nodes which when joined improve Q, are added to communities. In the second step, communities are folded into a single node. These steps are repeated for all iterations until merging nodes no longer improves Q.

Fuzzy community membership

The probability of a node being a member of its designated community, given an identified community structure, can be calculated by computing the distribution of all positive modularity values for each node at each time point for all identified communities. The probability that a node belongs to a community, which we refer to as fuzzy membership, for a given community structure is then simply given by the proportion modularity that a given community contributes to the total for that node. Simply:

$$p(n|c) = \frac{Q_j}{\sum_i^C Q_i}$$

Where C is the number of communities identified and Q_j is the value of modularity for node n belonging to a given community, j. This results in pseudo-fuzzy map for each community of node membership over time for a given community.

Identifying stable sub-states

Community detection using greedy agglomerative provides a perspective on the temporal community structure at the individual level. Such community structures may have high intra-subject variance and spurious community structures representative of communities in a state of transition. In order to identify recurring community structures both within and between subjects a second level of clustering was applied. This results in the identification of consistent, recurring community structures, likened to discrete sub-states. In a neuroimaging context these would be

considered modules of meta-stable network states and can provide insight into the organisation of the brain in relation to tasks or experimental conditions.

These stable sub-states can be identified by clustering the detected community instances on a group level. Specifically, we cluster community descriptors from each time point using k-means clustering, as described in Chapter 3, where stable community states are then defined by the cluster centroids. We employed the K-means function in Matlab 2013b to perform clustering of community descriptors. Furthermore, k-means randomly seeds each centroid during its initialisation. This can result in different solutions, in order to avoid the possibility of a local minima, clustering was repeated 100 times at each instance. The partition with the maximal inter-cluster distances and minimal intra-cluster distance is selected as the preferred solution.

Community descriptors, used as samples for the k-mean clustering, describe the nodes present across all slices for each community and can be represented as a collection, C, of Nx1 vectors where N represents the number of graph nodes. Here we use the pseudo-fuzzy community membership values from subject-wise modularity optimisation as community descriptors. This results in a collection of Ns clustering samples where the maximum value of *Ns* is given by N x (T x # communities x # Subjects).

In order to select the appropriate number of clusters, k, we compute the Bayesian Information Criterion (BIC) (Schwarz 1978) for each cluster partitioning over a range of k values, the selection of which is discussed below. The BIC is a goodness of fit term which consists of a loglikhood term and a penalisation term for model complexity, formally:

$$BIC = -2\log\big(p(\boldsymbol{x}|M)\big) + \ mlog(N)$$

Here $p(\boldsymbol{x}|M)$ is the likelihood of the data for a given model, M, with m free parameters and N data points. When applied to clustering communities, BIC can be defined as:

$$BIC = \ -2\sum_{i}^{k}\left(-n_{\mathrm{i}}\sum_{d}^{N}\log(\sigma_{id}^{2} + \ \sigma^{2})\right) + 2kN\ log(Ns)$$

Where k is the number of clusters, n_i the number of samples in cluster *i*. N defines the dimensionality of the samples, in this case the number of nodes and Ns is the total number of samples. The variance between samples is given by σ^2 and the variance within each cluster by σ_{id}^2.

The BIC was favoured over other goodness of fit measures, such as the Akaike information criterion (AIC), due to its strong penalisation on model complexity. This results in the BIC favouring solutions with fewer clusters and as such more interpretable solutions, and enforces

convergence, avoiding the possibility of an infinitely decreasing value with increasing number of clusters.

Clustering was performed over a range of k values, each clustering was replicated 100 times; the partition resulting in the lowest sum of distances was selected as the final partition for the clustering at the corresponding k value. The BIC was computed for each set of clustering performed and the resultant values plotted against the k parameter used. The k value at the minimum BIC, k_{min}, was selected as the optimal clustering parameter. The partitioning which occurs when clustering at k_{min} provides a set of community states representing recurring modular states within the brain during the period of acquisition, henceforth referred to as centroids. This collection of centroids that minimises the BIC will be used to define the communities present in the temporal connectivity profiles of the population.

Clustered community coherence

The clustering of centroids afford a high level perspective on the network configurations occurring in a multi-slice graph. While, this is informative in itself, it doesn't provide insight into the dynamic organisation of the brain over time. To investigate dynamic community organisation we can compute the distance between cluster centroids and each subject's temporal community structure. To do this we compute the subject-wise modularity profile individual communities, identified via clustering.

For each centroid **c**, consisting of an Nx1 pseudo-fuzzy descriptor of node members, we compute a community mask, **B**, representing the membership of each edge to the centroid **c**, where**:**

$$\boldsymbol{B} = \boldsymbol{c}\boldsymbol{c}^{\boldsymbol{T}}$$

Thus the value $\boldsymbol{B}_{ij}$ represents the pseudo-fuzzy membership of the edge between node *i* and *j* to the given community. The modularity of a community at a given slice is then defined as the proportion of graph vertices within the centroid **c**, minus the square of the fraction of edges which link **c** to the rest of the graph (Newman et al. 2004; Shi et al. 2013). We re-define Newman's (2004) measure of community modularity for use in weighted signed graphs in a similar manner to the modification of network modularity. We define the connections between members of the centroid **c**, as the Hadamard product between A and B:

$$\boldsymbol{A}' = \boldsymbol{A}\boldsymbol{B}$$

Separating this connectivity into signed matrices yields:

$$\boldsymbol{A}'^{+} = \max(\boldsymbol{A}', 0) \qquad \text{and} \qquad \boldsymbol{A}'^{-} = \max(-\boldsymbol{A}', 0)$$

The proportion of normalised signed connectivity within a centroid is then given by *e*. This is the proportion of edges which link a given community to itself, where:

$$e^{+} = \frac{1}{m^{+}} \sum_{i,j} A'^{+}_{ij} \qquad \text{and} \qquad e^{-} = \frac{1}{m^{-}} \sum_{i,j} A'^{-}_{ij}$$

Where $m^{\pm}$ is the total signed weighted of edges connected to nodes in **c**. The fraction of edges which link centroid **c** to the rest of the network are given as:

$$a^{+} = \frac{1}{m^{+}} \sum[\boldsymbol{A}'^{+} \cdot ((1-\boldsymbol{c})^{T}\boldsymbol{c})] \qquad \text{and} \qquad a^{-} = \frac{1}{m^{+}+m^{-}} \sum[\boldsymbol{A}'^{-} \cdot ((1-\boldsymbol{c})^{T}\boldsymbol{c})]$$

or graphically, where the blue area represents values $\in \{0,1\}$ and white indicates zeros:

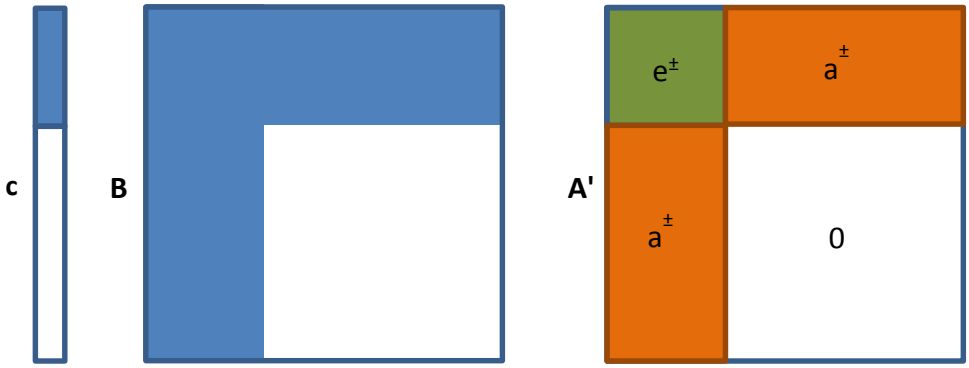

The strength of a given community at a slice is quantified as the normalised fraction of edges within a community minus the square of edges linking a community to the rest of a graph:

$$Q_c = (e^{+} - a_{+}^{2}) - (e^{-} - a_{-}^{2})$$

The value of Q_c then represents the modularity of a community in the context of a graph and takes values in the range [-2,2]. For clarity, we refer to this community specific modularity measure as community coherence. For random intra community edge values $Q_c = 0$; values approaching $Q_c = 2$ suggest a strong community structure anti-correlated with the rest of the brain. Values of Q_c approaching its minima at $Q_c = -2$ indicate anti-correlated community structure where community vertices are strongly connected to the rest of the network. In practise these extreme values are rare, Newman (2004) reports typical values of Q_c at 0.3 – 0.7, however it must be noted his approach was for unsigned graphs only.

This provides a measure of community modularity at every graph slice for each subject, resulting in a temporal-modularity view of the connectivity structure within a dataset. Furthermore, this measure relates community structure to the raw multi-slice adjacency, as such once communities are identified, community coherence can be computed for previously unseen data. This allows for the possibility of temporal community structure analysis on an individual subject scale in a clinical environment.

Statistical testing

The community modularity statistic provides a measure of the modularity of a given community structure within a network. Unlike the overall modularity value, this measure is based upon the ratio of connections and as such is normalised by density and thus is comparable between subjects and different sized communities.

The significance of the community modularity values at a given slice, across participants, can be assessed through comparison of the true modularity values to a null distribution. For a given community at each temporal slice, participant's adjacency matrices are randomised at N (1000) permutations and the community modularity value estimated for each permutation. At each permutation, the adjacency matrices are symmetrically permuted such that the mean, variance and density of the graph are the same but the topology is random. This results in a null distribution representing the range of modularity values for a given community that may occur by chance. The significance of the community modularity values obtained using the true connection matrices is then inferred through comparison to this null distribution using a z-test. Multiple comparisons testing using the Bonferroni is performed across all temporal occurrences and communities to correct for the large number of independent statistical tests. This provides a statistical framework for investigating community modularity at each volume, suitable for event related or block designs.

For task-free acquisitions however, there is no externally enforced temporal consistency between subjects, therefore it is necessary to compare entire task-free discrete temporal periods to draw statistical inferences. In this analysis we employ a non-parametric ANOVA, the Kruskal-Wallis (KW) test of variance (Kruskal et al. 1952), to compare the distributions of community modularity in task-free states, resulting in a Chi-square distance measure. To assess the significance of this difference we employ a permutation test, where at each iteration of 1000 permutations, participant group labels are randomly re-assigned and the KW re-compute for the new group definitions. This results in a null distribution from which we can infer the significance of the KW obtained using the true class labels.

8.2.1 Simulated Dataset

A challenge when testing a method for functional connectivity analysis in the human brain is the lack a of ground truth to compare against. In order to validate and optimise the presented methodology we generated simplistic synthetic ground truth multi-slice graphs each of 40 nodes and 70 slices. This sequence of graphs contains consistent clusters of interconnected nodes, communities, embedded in random graphs. Node members of simulated communities are

defined as temporally persistent with evolving membership, the ground truth simulated network is shown in Figure 41.

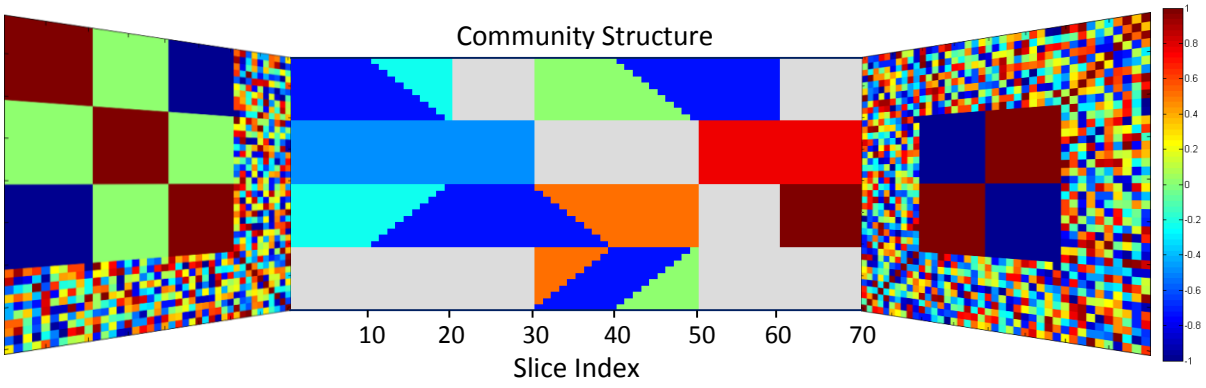

Figure 41 - Example of simulated multi-slice graph with ground truth community labels. Graph consists of 40 node slices with a dynamic community structure, main clusters are illustrated in the central panel while noise is represented as light grey blocks; community membership is indicated by colour. The first and last graph slice are presented either side of the main panel respectively, node connections values lie in the range -1 to 1.

This ground truth multi-slice graph contains 3 consistent stable network states, corresponding to node indices 1-10, 11-20 and 21-30 and a semi-stable state at nodes 31-40. Dynamic states were introduced with communities varying between network states, simulating the speculated meta-stable network structure of the brain (Kiviniemi et al. 2011; Allen et al. 2014).

To simulate the noisy nature of real data we combined each slice of ground truth graphs with random noise such that the resultant simulated network can be defined based on its percentage of noise G_{noise} and ground truth signal, G_{truth}, such that the final simulated multi-slice graph can be formulized as:

$$G_{sim} = (\xi - 1)G_{truth} + \xi G_{noise}$$

$$where\ 0 \geq \xi \geq 1$$

This allows for specifying the percentage of additive randomness in the graph by altering the value of ξ between 0 and 1. For ξ = 0, all intra-community edges will have values of 1 whilst between community edges have a value of 0 or -1. Edges between community nodes and non-community nodes (background noise) will take random values in the range of (-1, 1). As ξ approaches 1, the structure in the simulated graphs is reduced as graphs become more random. For a visual example of the effect of this additive white noise, see Figure 42.

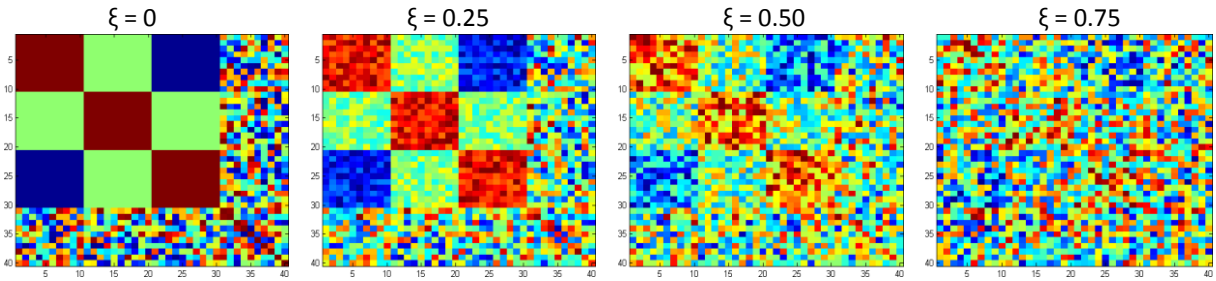

Figure 42 - Effect of combining noise with simulated ground truth adjacency matrix over a range of ξ values to achieve different degrees of graph randomness. At ξ = 0 graph has no additive noise, at ξ = 1, graph is random.

Varying the randomness of graphs will allow for simulations of multi-slice graphs with varying noise effects, such as those which can occur when calculating graphs from noisy data such as fMRI or by inclusion spurious correlations induced by methodological limitations in the graph estimation.

Detecting similarities between communities using Variation of Information

To quantify the similarity between our simulated data and the identified community structure obtained from the modularity maximisation procedure, we compute the variation of information (VI) measure, derived in (Meilă 2007; Good et al. 2010) . This is measure often used to quantify the similarity between clusters (Kawadia et al. 2012), and provides a distance measure between similar communities formularized as:

$$VI = -\frac{1}{N}\sum_{i,j}^{C} n_{ij} \log\left(\frac{n_{ij}^2}{n_i n_j}\right)$$

This measure computes the mutual information between two clusters, *i* and *j*. The number of nodes present across all slice for a given community, *i* or *j*, is denoted by n_i and n_j respectively. The total number of nodes present in both communities *i* and *j,* across all slices is denoted by n_{ij}. N is the number of all node-time occurrences. Highly similar communities have a low value of VI, a value of VI = 0 indicates community structures are identical. Clusters which are highly dissimilar, while still maintaining some intersection, will have a high value of variation between them. Clusters with no interception will report an infinite VI.

When calculating VI in relation to the simulated data, we are interested in the accuracy of the algorithm to detect the large communities in the ground truth data. As such communities representing the noise component in the ground truth data (grey areas in Figure 41) are excluded from calculations of VI.

Community detection on a simulated multi-slice network

To assess the ability of the presented modularity optimisation algorithm to detect the underlying community structure in the data, we apply the presented methodology to a simulated multi-slice graph with known ground truth, as discussed above and visualised in Figure 41. We quantitatively assess the accuracy of the proposed modularity optimisation by detecting the community structure of simulated data with varying degrees of randomness. The measures of VI and Q are used to quantify the quality of the detected communities.

We vary ξ from 0 to 1 in 0.1 increments. For each value of ξ, 100 simulated datasets were generated and community detection performed, gamma variables were maintained at $\gamma_s = \gamma_t = 1$ for all analysis. The modularity, Q, and variance of information value, VI, were recorded for each instance of the modularity optimisations, as shown in Figure 43. At low levels of randomness, community detection performs very well, reporting consistently low VI values. As the contribution of the noise component approaches and exceeds that of the true signal (ξ ≈ 0.5) the accuracy of the detected community structure rapidly declines. This indicates that the proposed community optimisation algorithm should perform well given connectivity data that contains a reasonable degree of structure.

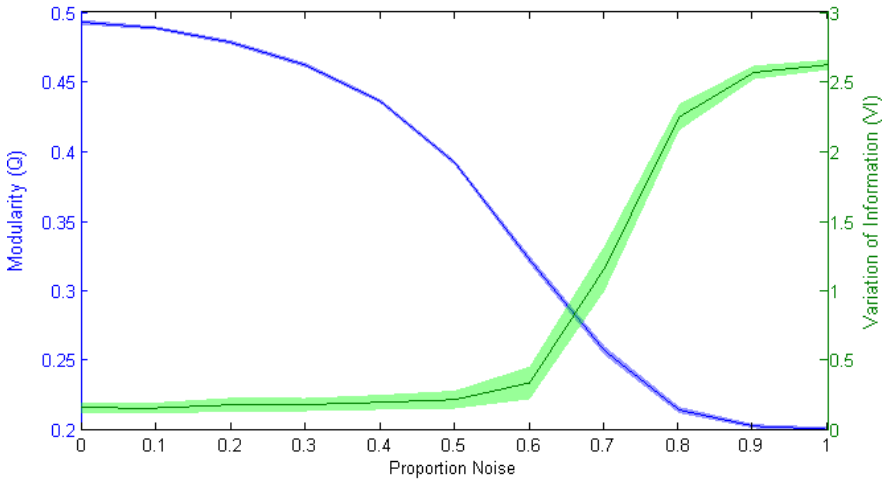

Figure 43 - Effect of noise on community detection, reported values of Q (blue) and VI (green) are the mean of 100 repeats of community detection using simulated data with an additive random noise. Plot of mean and standard error

We qualitatively inspect the community structure of the modularity optimisation for a single multi-slice simulated dataset at ξ = 0. As revealed by the low VI value in Figure 43, the proposed method accurately identifies all the ground truth communities, as illustrated in Figure 44. We note spurious node members are identified in the ground truth communities, this is due to inclusion of a random noise component of the ground truth data, best visualised in Figure 42. It are these spurious inclusion of noise connections into the ground truth communities that results in a VI value greater than zero.

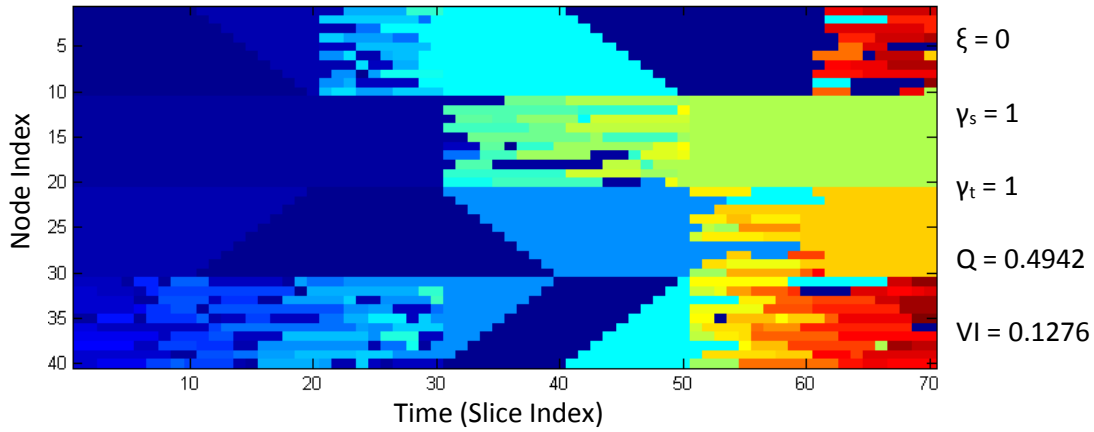

Figure 44 - Community structure in simulated data, community colours are assigned randomly and have no significance other than to identify consistent regions defined within the same community cluster. Simulated data set contained no additive noise

Consistent community state identification

Here we wish to demonstrate the use of clustering to identify consistent community states, given the detected community structure from the modularity optimisation algorithm. Firstly we examine community meta-states of the single subject case. We generate a simulated multi-slice graph with the ground truth as shown in Figure 44 and additive random noise with ξ = 0.5. Modularity optimisation was performed on this simulated multi-slice graph and the pseudo-fuzzy community membership extracted, an example of which is shown in Figure 45.

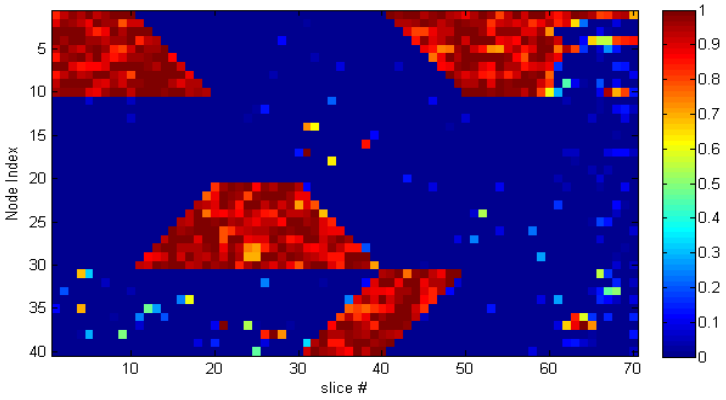

Figure 45 - Pseudo-fuzzy node membership obtained from modularity optimisation of a single simulated multi-slice dataset, ξ = 0.5.

The pseudo-fuzzy community membership values were used as samples for k-means clustering. Clustering was performed over a range of clustering parameters, $k \in (2,30)$ each with 100 replications. We recorded the BIC calculated for each set of model parameters, as shown in Figure 46, to select optimal clustering parameters. This shows a very clear vally at k = 4, suggesting a the presence of a robust optimal partition.

As discussed earlier, we use the minimum and maximum second derivative of the BIC values to idenitfy the prefered k parameters for clustering. For a single subject simulated data set, k_{min} =

4, with the centroids depicted in Figure 47. This partitioning correctly identifies the 3 consistent community states introduced in the ground truth (node groupings 1-10, 11-20 and 21-30). An empty cluster is also included which we define as a noise components. Samples used for clustering were fuzzy as such, the cluster centroids are also fuzzy resulting in a pseudo-probabilistic description of network states. The obtained cluster centroids were automatically cleaned, empty centroids or those containing a single node were removed as noise components. Results were presented using the cleaned centroid definitions and the original value of k used to partition the data.

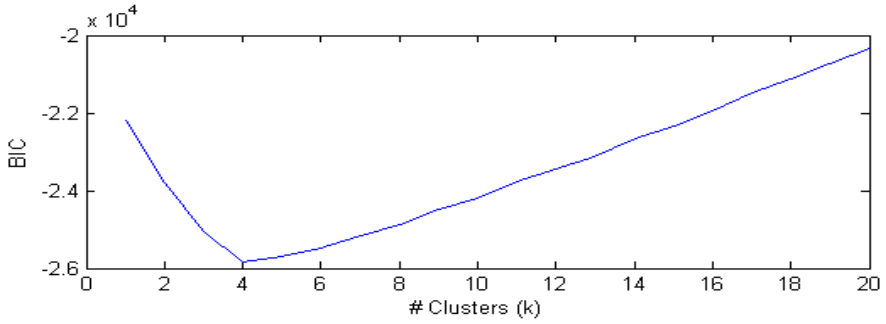

Figure 46 - BIC values for k-means clustering across different values of k, performed using 100 replications on fuzzy community memberships obtained from modularity optimisation of a single simulated multi-slice, ξ = 0.5.

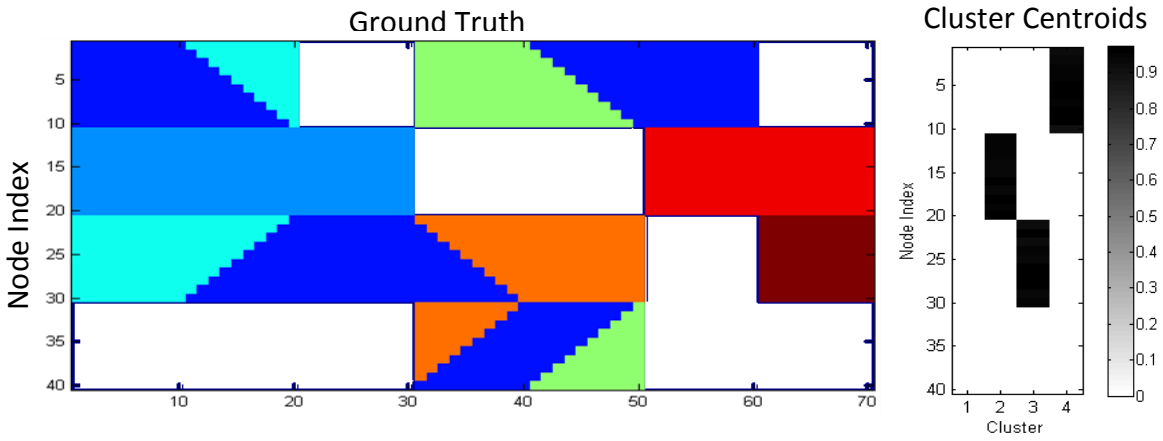

Figure 47 - Clustering results for models at minimum BIC (k_{min}=4) and simulated data ground truth

Here we have qualitatively demonstrates the use of clustering to accurately identify consistent community state in this single subject toy example. However, while this may prove informative for single subject analyses, in real neuroimaging studies we are interest in identifying consistent effects within groups of subjects.

Group level clustering

To identify consistent networks occurring in group data we perform k-means clustering on the combined fuzzy community membership data obtained from all subjects community detection. Combing data from multiple subjects also improves the generalizability of findings and increases the SNR, a necessity considering the inherently noisy nature of fMRI. However, as sampling sizes

increases, so does representation of 'noise' communities. These noise communities may arise from spurious connections, groupings of weak connections representing into a community or as an artefact of the community detection algorithm forcing each node to be a member of a community. Increasing the representation of these noise elements may potentially result in their combination as an additional centroid, confounding the results. Furthermore, due to increased repetition of community states and transitions, clustering using a larger k parameter obtained from the minimum BIC may include centroids representing consistent transitory configurations.

Clustering is initially performed using clustering parameters k in the range $\in$ E***rror***! ***Bookmark not defi***ned., however with increasing sample sizes, it is possible that k_{min} might not occur in this range. In order to ensure the minimum BIC is observed, the range of clustering parameters is incrementally extended while BIC values are observed to decrease below the current minimum and while the gradient of the BIC is negative. This extension of clustering parameters continues until either a maximum number of clusters has been reached or a BIC minima has been observed. This procedure avoids un-necessary computation clustering at large values of k, however it is possible that a local minima may be selected as an optimal solution before a global minima can be found.

Clustering was performed on different sized populations of simulated data to investigate the effect of sample size on the selection of clustering parameters. Simulated data, using the above ground truth and ξ=0.5, was generated for groups with population sizes 1 to 50 subjects. Data was clustered for each population with a 100 replications and k values at the BIC minima reported for each population size, Figure 48.

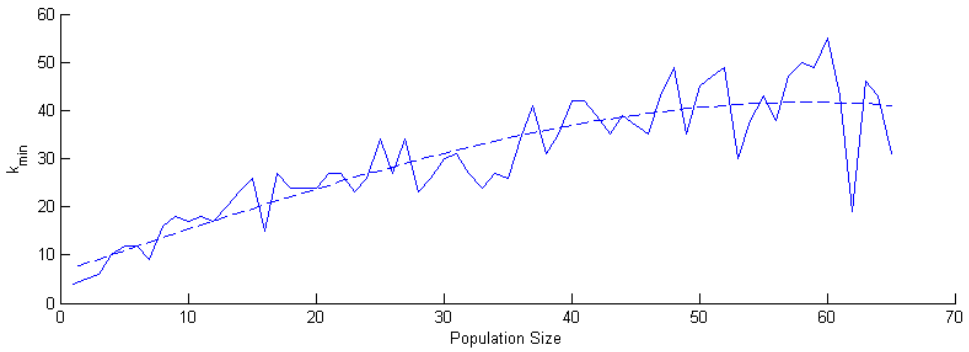

Figure 48 - Clustering parameter, k, at the BIC minimum as a function population size, demonstrating increased communities identified as population size increases

As expected, increases in population sizes resulted in the minimum BIC values occurring at larger values of K. This is due to the increased representation of transitional states in the sample pool which are assigned additional clusters. BIC values were found to plateau suggesting after a given population size no new information is gained from additional clusters. We note that the three core communities in the ground truth were obtained at every population size partition. However

the increased population size resulted in increased identification of clusters primarily associated with the transitional states between stable network occurrences and to a lesser extend identification of noise components. We argue that rather that the increased population size is beneficial as spurious centroids may be automatically removed with further processing, as discussed later in this chapter, and transitional states identified may provide insight into the temporal organisation of the brain.

Statistical testing of temporal modularity structure

Clustering identifies consistently recurring community states, however does not provide any insight into their temporal occurrence. Here we perform testing on the temporal occurrences of community states, as identified from a simulated dataset with ξ=0.5 and 15 subjects, chosen to represent a typical neuroimaging study.

Clustering over a range of k parameters revealed a minima in the BIC at k = 20, k_{min}. In this partition, six clusters were rejected having fewer than two nodes with a membership value of greater than 0.5, this resulted in 13 centroids of interest, Figure 49-B. The three core communities of the ground truth were identified at C1-C3, the transient community at c4 and community configurations representing the transition state between stable states at C5-C12. C13 was found to represent a spurious network configuration, likely a result of the additive random noise.

The modularity values of each centroid, Q_c, were at every slice of simulated connectivity graphs. The significance of each centroid was assessed through comparison to a null distribution of community coherence values obtained from randomised graphs. Obtained p-values, as depicted in Figure 49-C, were corrected for multiple comparisons both across time and communities using Bonferroni correction to a level α=0.05.

The significance profile of centroid modularity was found to highly correspond to the ground truth. Centroids C1-3 expressed significant modularity at periods corresponding to the occurrence of stable communities in the ground truth. C4-12 reported significant modularity values at periods corresponding to community transitions, as represented by each centroid. The centroid C13, representing a community structure identified as noise, did not report any significant occurrence.

This simulation instils confidence that the proposed workflow correctly identifies consistently occurring community structures and their temporal profile for a population with reasonable SNR. Furthermore, the algorithm was found to perform well in the identification of community

structures in simulated data, reporting low VI values for data less than 60% random and empirically identifying the temporal modular structure within a simulated multi-subject dataset.

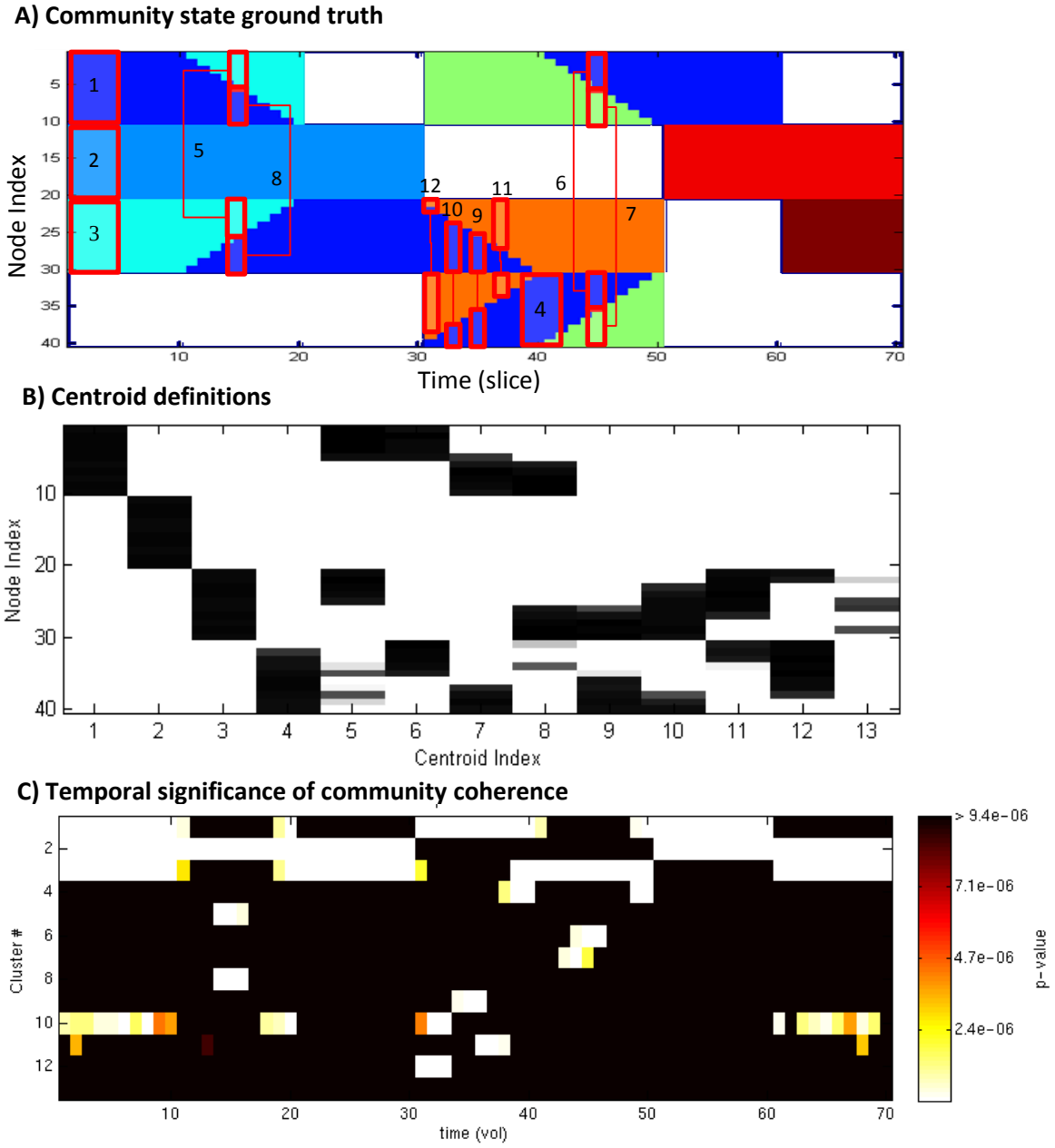

Figure 49 - Identified temporal community structure consistent across a population 15 simulated multi-slice graphs with and SNR of 1. Panel A) shows the ground truth community structure within the simulated data. Cluster centroids were labelled to corresponding community structures using red boxes. B) Visualisation of the retained centroids from the clustering procedure. Centroids were re-ordered for purposes of visualisation, however values were not altered. Centroid index is represented on the x-axis and node index on the y-axis. Black indicates a membership value of 1 and white of 0.

The statistical significance of each communities modularity across simulated participants at each graph slice is displayed in C). Values were thresholded if they failed to reject the null hypothesis after Bonferroni testing, α = 0.05. Centroid index is indicated on the y0axis and slice index on the x-axis.

8.3 Dynamic functional connectivity effects of Ketamine

Here we will demonstrate the application of the proposed dynamic connectivity analysis framework to a pharmacological imaging dataset. We identify consistent community states and their temporal profile for a phMRI dataset imaging an acute ketamine challenge in order to investigate the effects of ketamine on the temporal profile of connectivity organisation in the brain.

Previous studies have reveal robust effects of ketamine on the blood oxygen-level dependant signal (BOLD) in the brain (De Simoni et al. 2013; Doyle et al. 2013) and on regional connections (Scheidegger et al. 2012; Driesen et al. 2013). The work in Chapter 4-6 has also demonstrated that ketamine has wide-spread effects on the pattern of connectivity across the whole brain. Moreover, work presented in Chapter 7 suggests ketamine may additionally alter the localised temporal dynamics of connectivity in the brain. As such, we predict ketamine will elicit robust changes in the connectivity organisation which vary over time. We propose investigation of the temporal profile of connectivity organisations will afford a new perspective on the mechanisms of ketamine and provide insight into the temporal dynamics of functional organisation during the ketamine infusion. This chapter presents an additional investigation in the effects of ketamine, specifically in investigating the effect of ketamine on the temporally discrete periods of distinct connectivity organisations, referred to as meta-stable modular states.

8.3.1 Methods

Data Acquisition and processing

Data was acquired and pre-processed as described in Chapter 4. Identical post-processing procedures were performed to minimise the effects of noise and nuisance parameters. Specifically the regression of the mean CSF and WM signals and the six motion parameters and band pass filtering with a pass band of 0.01Hz-0.1Hz. For the purpose demonstrating this technique to pharmacological imaging data, we limit this analysis to the study of the ketamine sessions (PLA+KET).

Multi-slice Graph Estimation

To facilitate functional connectivity analysis using graph theory, we parcellate images into 90 nodes coving the cortex and sub-cortical structures as defined by the AAL atlas (Tzourio-Mazoyer et al. 2002). The AAL was chosen as it provides complete coverage of cortical and subcortical structures and its prevalence within the field (Zalesky et al. 2010; Braun et al. 2012) allowing for

some degree of comparison with results. Furthermore, the use of the AAL ensures consistency with other chapters in this body of work allowing for comparisons between findings.

Each atlas region was used to define a node with a graph, G; the mean time-series for all voxels in each atlas regions was computed. The computed similarity between these mean signals represents the connectivity between regions and are modelled as edges within a graph. In order to represent the temporal connectivity of imaging data, a multi-slice graph is required. To this end, we employ a sliding window approach using a Gaussian window, as described in Chapter 3, to estimate multi-slice connectivity graph for each experimental session. A short window length is preferred for increased temporal sensitivity to high frequency changes (Leonardi et al. 2015), however if the window length is too short the spurious connections may arise. Empirically a box car window of 30-60 seconds has been shown to provide reliable results (Shirer et al. 2012). In this analysis we employ a tapered window to achieve greater temporal sensitivity and robustness to outliers (Zalesky et al. 2014). Specifically, we employ a Gaussian window of 90 seconds (effective length 30sec) applied in 1TR (where TR = 2seconds) increments across time series data. For each window position connection matrices were computed using full Pearson's correlation, this resulted in a series of weighted adjacency matrices representing the functional connectivity over the length of each experimental session.

Community detection

To investigate the community structure of the functional connectivity in the brain and its alteration by acute ketamine, we apply the modularity optimisation algorithm discussed in section 8.2 to participant's multi-slice connectivity matrices in the placebo pre-treated ketamine (PLA+KET) session, as outlined in Chapter 4. This results in an estimation of community structure, with enforced temporal consistency, at each slice for every participant.

Consistent community structures across time or participants can be identified using clustering. To ensure the centroids identified are consistent across all subjects we propose a leave-one-out cross validated (LOOCV) approach to clustering. In this iterative framework, at each step data from a participant is withheld, the community definitions obtained from the modularity optimisations of the remaining participants are used as samples for k-means clustering. Clustering is performed over a range of k parameters, defining the number of clusters; the partition which minimises the BIC value is retained and stored. This process is repeated for each LOOCV fold such that every participant has been excluded once.

To assess the consistency and demonstrate the stability of the obtained partitions, we compare centroids obtained across CV folds. A greedy search was employed to match centroids matched

between folds, the ICC(3,1) (Chapter 3) was computed between matched centroids. Centroids were retained if a match exists across all LOOCV and a significant ICC reported, otherwise they were excluded. The mean centroid across LOOCV folds was computed for all retained, matched centroids, representing the recurring community structures occurring across all participants. Hence forth the resultant mean will be referred to as identified community states.

Community Modularity

The community modularity of the identified community states was computed for each slice of participant multi-slice connectivity graphs using the formula presented in section 8.1. This resulted in a collection of community modularity profiles for each participant representing the temporal community organisation in the brain over time and facilitating further statistical testing.

Modularity stationarity

To test where ketamine alters the overall modularity of the brain we apply the augmented Dicky-Fuller test (Fuller 2009) to test the stationarity of the participant modularity values, estimated at each slice of participant connectivity graphs as part of the modularity optimisation algorithm. Lag parameters were varied between 0 and 6, and the lag which minimised the BIC of the model was selected. This provides a measure of whether the profile of whole brain modularity, as defined by the detected community structure for each participant slice, is stationary or whether ketamine alters the properties of the connectivity organisation in general. This test does not inform whether ketamine alters specific connectivity organisations, rather indicates whether ketamine results in a more or less modular connectivity organisation.

PhMRI signal model

Based on the previous work of (Deakin et al. 2008) and (De Simoni et al. 2013), a gamma variate (GV) regressor was used to model the phMRI response to the ketamine infusion. The GV applied was allowed for independent parameterisation of time of peak amplitude, t_{max}, and model shape, b, formularised as:

$$y(t) = \left(\frac{t}{t_{max}}\right)^{bt_{max}} e^{((t_{max}-t)\cdot b)}$$

A GV has been previously applied to the BOLD amplitude response of the data used in this study (De Simoni et al. 2013), with the parameters t_{max} = 240s (post infusion) and b = 0.01. This resulted in the model visualised in Figure 50.

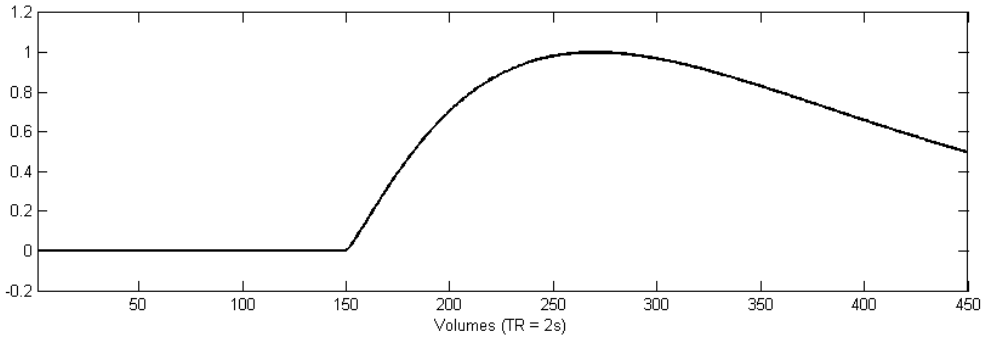

Figure 50 – Gamma variate model for the ketamine response

We apply this model to assess the fit of the community modularity profiles of the identified community states to the pharmacological response using a general linear model (GLM) framework. For each identified community state, the GV model is linearly regressed against the participant's community modularity profiles. A one sample t-test was applied to assess the fit of the expressed community structure to the modelled ketamine response. This provides an indication of whether the temporal profile of community modularity fits the predicted ketamine infusion model.

Conditional Comparison

The data analysed in this body of work was acquired using a task-free paradigm, as such there is no external stimuli (excluding the pharmacological infusion) enforcing temporal consistency between participants within each task-free block. To assess the effect of the pharmacological response in during the task free periods of the acquisition; the PLA+KET session was divided into three task-free periods, a baseline, compound-infusion and steady state infusion period defined as 0-5mins, 5-10mins and 10-15mins respectively; illustrated in Figure 51.

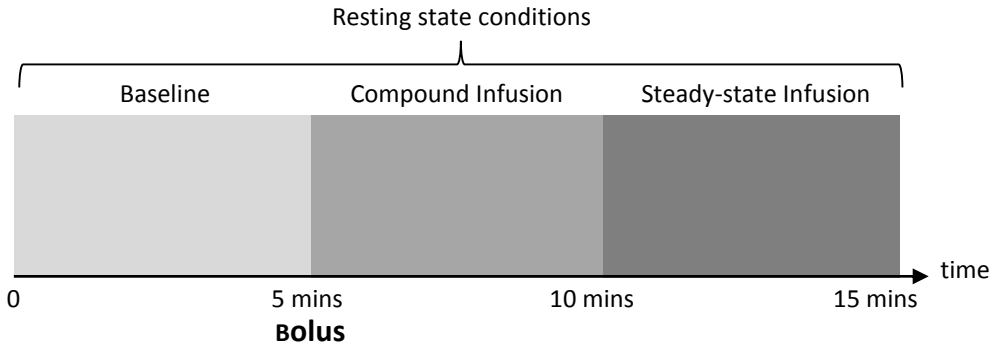

Figure 51 – Experimental conditions defined by temporally discrete resting-state sections of phMRI acquisitions used to define periods of the data for experimental conditions.

The modularity profiles of each identified community were compared between the baseline and steady-state infusion period using the Kruskal-Wallis test (Kruskal et al. 1952) to investigate the effects of ketamine. This non-parametric test is an extension of the Mann-Whitney U test and can be used to compare the distribution of community modularity values between states. We

assess the significance of this comparison using a non-parametric permutation test, as described in section 8.1. This provides an indication of whether ketamine alters the profile of modularity for the identified community structures in the brain during the task-free state.

Ketamine infusion connectivity dynamics

The ketamine bolus, administered at 5 minutes into the audition (150^{th} vol), represents a departure from the task-free state and arguably can be considered akin to a consistent event across participants. Thus the bolus and the immediately subsequent infusion period enable investigation into the temporal localised community organisation across participants.

In order to interrogate the modular organisation of the brain at each time point in the infusion period, we perform statistical testing at every graph slice for the modularity values of each community across participants. Significance is inferred through comparison of participant modularity values to a distribution of modularity values computed from random graphs, as described in section 8.2. Multiple comparisons testing was performed using the Bonferroni at a level of α=0.05. Inspection of significant modularity values within this infusion period offers insight into the ketamine-induced variations in functional organisations in the brain.

While this analysis is primarily concerned with the investigation of the community modularity profiles in the infusion conditions, we extend the statistical testing to include baseline and the steady state infusion conditions. Interpretation of effects within these periods however must be considered in the context of the task-free nature of the baseline and steady-state infusion conditions.

8.3.2 Results

Community Detection

Modularity optimisation, using the proposed method, was applied to the multi-slice connectivity of each participant in the PLA+KET session. We observe a highly complex pattern of temporal modularity, containing global oscillations in community structure as illustrated by the community profile of a single subject in Figure 52.

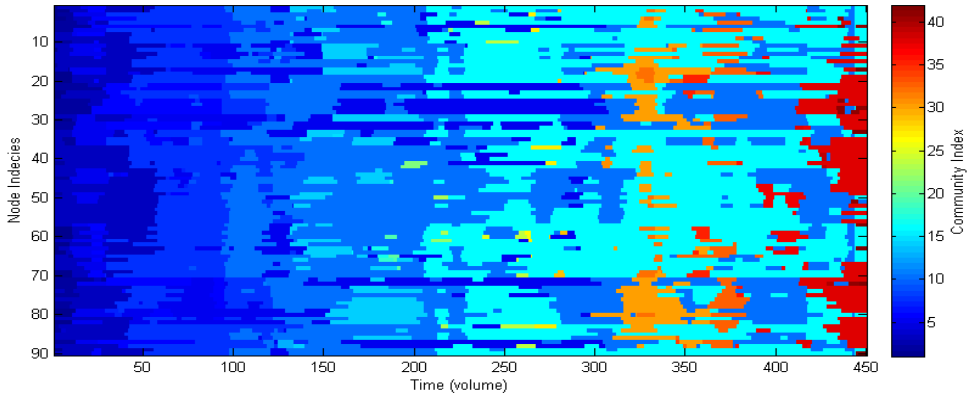

Figure 52 - Community structure over the course of a ketamine challenge as observed by optimisation of modularity (Q) using a Louvain search for participant 1 in the PLA+KET session. Time in volumes (TR = 2sec) is indicated along the x-axis and node index (defined by the AAL) shown on the y-axis. Colours indicate consistent community membership.

The modularity the whole brain was computed at each slice using the identified community structure at each participant. The temporal profile of whole brain modularity for each participant is visualised in Figure 53. To test the stationarity of the modularity profile of each participant, Dickey-Fuller tests were applied to each participant. No single subject rejected the null hypothesises of stationary, suggesting whole-brain modularity does not significantly change at the subject level, given the identified community structure. This does not however preclude the possibility of time varying modularity in individual modular structures. Furthermore, the presence of fast oscillations was observed within subject-wise temporal modularity values, consistent with earlier reports of periodic oscillations in functional connectivity strengths.

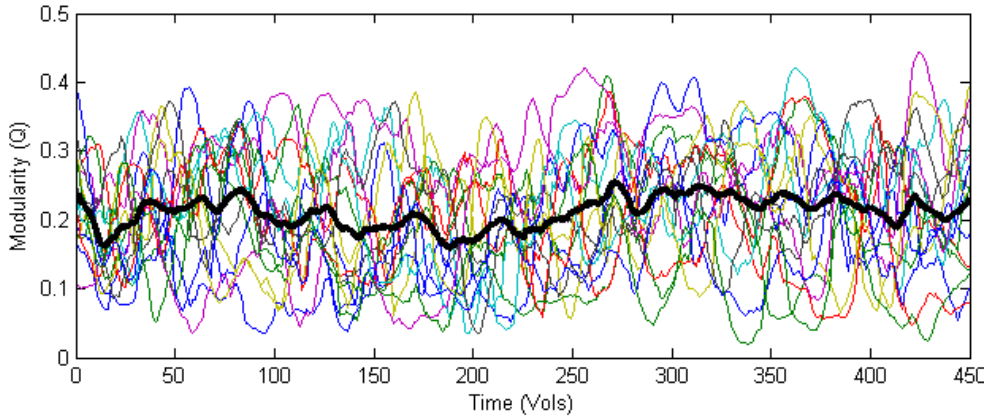

Figure 53 - Whole brain modularity at discrete temporal intervals, as detected by community modularity optimisation with temporal constraints. Mean modularity across subjects is shown by bold black line.

Community Clustering

A LOOCV clustering procedure, was applied to participant's community structures identified by modularity optimisation in order to identify consistent clusters across subject groupings to reveal consistent recurring community states. We observe a consistent trend of BIC values for different clustering parameters across LOOCV folds, as shown in Figure 54-A. Indicating a similar

quantity of centroids is required to represent the community states across folds. We note a shallow minima occurring after the elbow point of the curve suggesting that after a point additional centroids only offer a small contribution to the representation of information. This may indicate the presence of many consistent noise or transitory states within the data. We compute the BIC for increasing values of k. When a minimum BIC value is observed k is incremented by a further 10 values to reduce the risk of stopping in a local rather than the global minima. If no smaller value of BIC is observed, the search is stopped using the value of k at the BIC minima.

The centroids across LOOCV folds were matched by correlation using a greedy search. The ICCs were subsequently computed for each matched centroid as shown in Figure 54-B. On average the minimum BIC value was observed at k = 60.7 (±1.7), referred to as k_{min}. Inspection of ICC values for centroids matched across folds reveals the presence of several highly consistent community states as well as several variable states. Centroids were rejected where a consistent community could not be identified across all LOOCV folds and for matchings' reporting non-significant ICC values ($p<0.001$; Bonferroni correction at $\alpha=0.05$), marked with an x in Figure 54-B. Subsequent to this cleaning, 40 centroids remained, the mean community state was computed LOOCV fold resulting in a collection of mean centroids, rank ordered by ICC value, representing consistent community states.

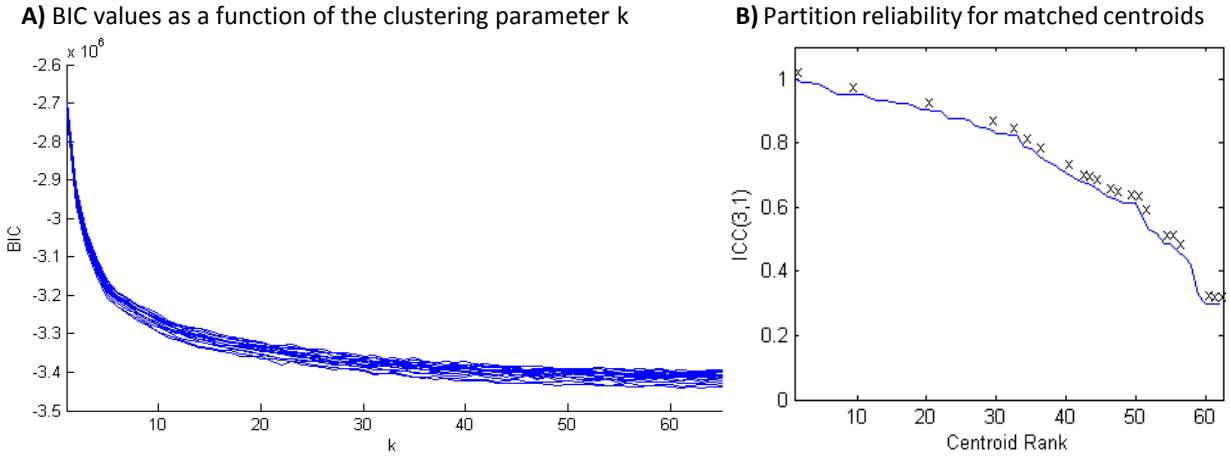

Figure 54 – Results of LOOCV clustering procedure, Panel A) depicts BIC values for partitions of modularity times eries data, performed over a range of k values in a LOOCV framework. Minimum BIC occurred at mean value of kmin = 60.7 (±1.7). B) Shows centroid consistency across LOOCV folds for partitions computed at the kmin parameter. Consistency for matched centroids across LOOCV folds was quantified using the ICC(3,1). Rejected centroids are denoted by x.

Inspection of these identified community states (mean centroids) reveals the community structures, as detected using the applied method, in the brain which occur during an acute ketamine challenge. A sub-set of the identified community states reporting ketamine effects or representing connectivity organisations similar to known networks are visualised at their most

informative angle in Figure 55, a visual representation of all centroids can be found in the Appendix D.

These identified community states were found to describe both spatially localised cortical communities as well as widely distributed networks. Community C1 expressed a high degree of similarity to the limbic/para-limbic system. C2 represented the medial orbital frontal cortex and caudate. The right superior lateral frontal cortex defined C22.

Furthermore, several community states resemble known consistent resting state networks, as identified in (Damoiseaux et al. 2009; Smith et al. 2009; Di et al. 2013); specifically C3 was found to resemble the visual network, C5 contained similar regions to the sensorimotor network, variations of the DMN were observed in community structures C6, C7 and C19. Several community structures (C12, C13, C15 and C16) resembled a network containing both elements of the salience and auditory networks. It was noted that in addition to these localised community states, several widespread communities were observed, such as C8 and C21, representing connectivity over large areas of the cortex.

The presence of these larger, more distributed communities, when considered with the observation of much smaller communities may suggests the presence of a hierarchical community structure. To investigate the relationship between these identified community states we compute the Jaccard distances between communities, expressed as a dendrogram in Figure 56.

Mapping of similarities between identified community states reveals combination of network representations. Several community structures were relatively dissimilar from all other communities such as the basal ganglia (C1) and visual community (C3). As indicated by a branching at a distance from leaf nodes in Figure 56. We note several communities identified are highly similar such as communities containing regions associated with the DMN and the executive control networks (C7 and C32) or the many communities representing widespread distributed cortical communities (C8, C20, C25, C26).

It may be that the more dissimilar community structures represent well defined networks in the brain, consistent across subjects and not notably altered by the acute ketamine challenge such as the orbital frontal cortex (C2) and limbic system (C1). The community states reporting a high degree of similarity to each other may represent poorly defined community structures in states of transition between meta-stable states, networks subtly altered by ketamine or noise structures.

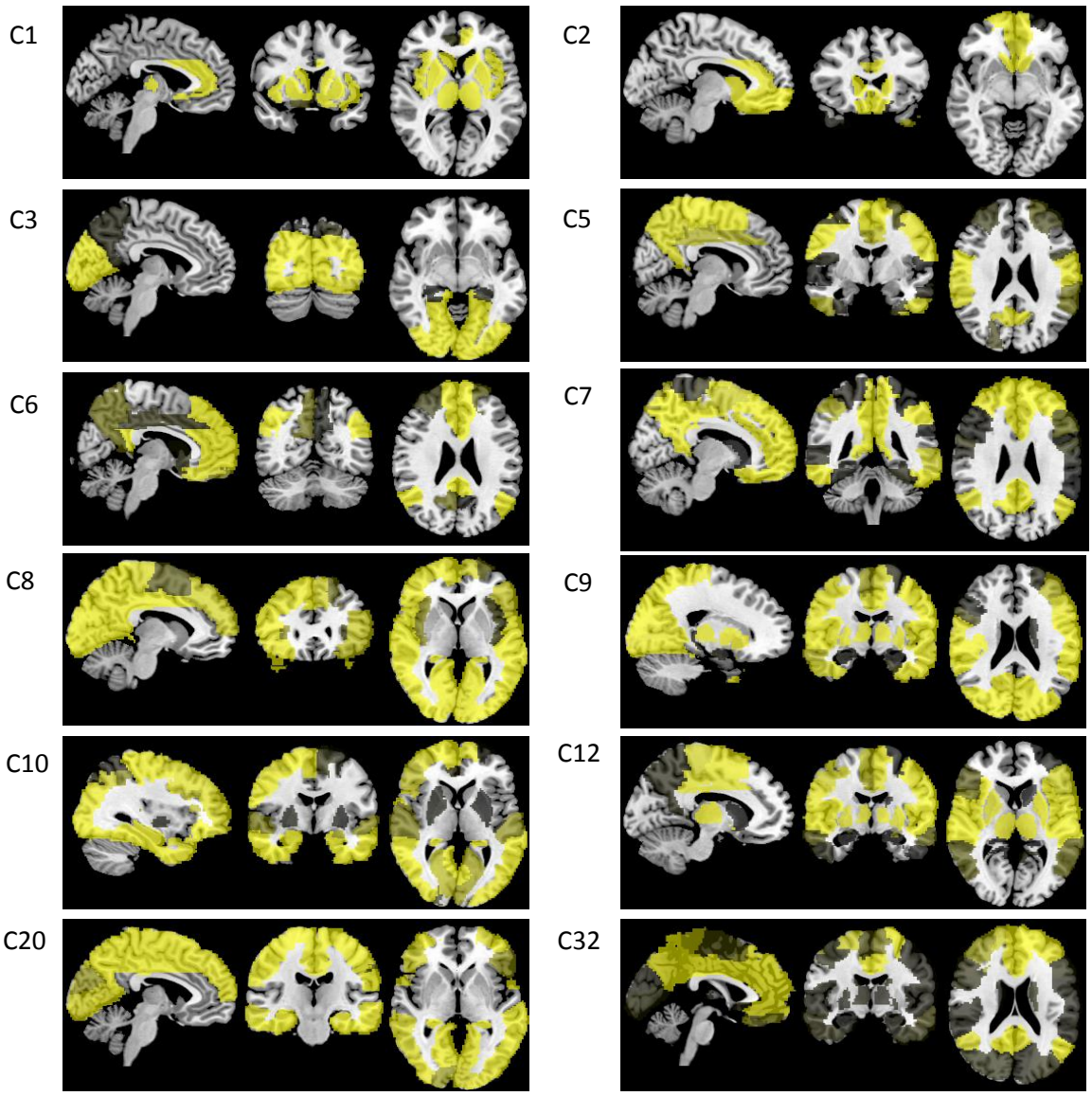

Figure 55 – Identified community states revealed by LOOCV clustering of participant temporal community structures obtained using modularity optimisation.

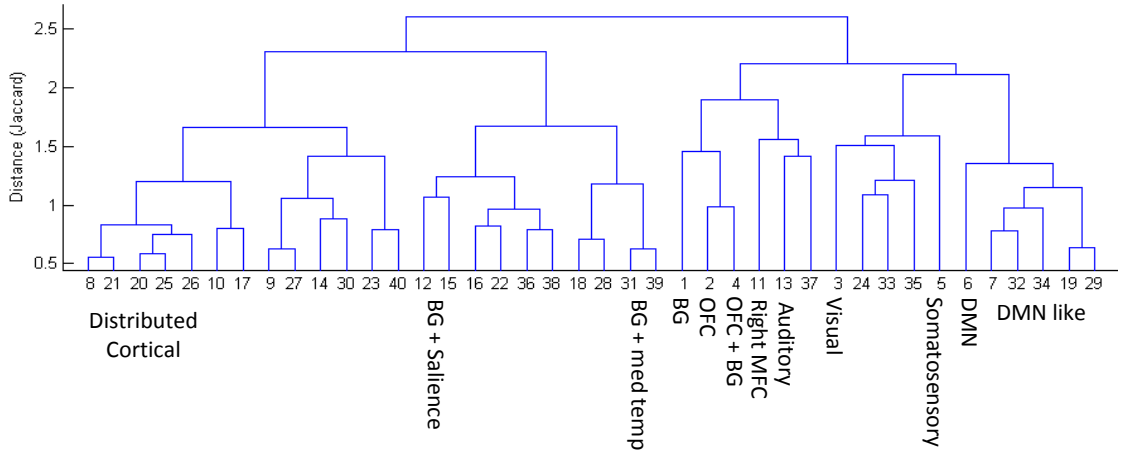

Figure 56 - Similarity of community states to each other, groupings lower in the tree represent higher degrees of similarity while merging of branches at higher levels of the tree indicate more dissimilar communities. Identified communities are noted by their index on the x-axis.

Conditional difference in community coherence

The main effects of acute ketamine on community modularity were investigated through comparison of the distribution of modularity values for each identified community state between placebo and ketamine conditions, Figure 57.

A significant ($p<0.05$; BH, $\alpha=0.05$) ketamine-induced reduction in the median community modularity of C10 was observed. This is a community comprised of regions associated with memory and vision. This reduction in community modularity may result from increased connectivity between a community members and the rest of the brain or decreased connectivity between regions within the community. Alternatively it is possible that ketamine does not affect the community organisation or modularity of C10, rather effects a change in the temporal processing in the brain such altering the occurrence of this community structure.

Several trend-level effects of ketamine in several identified community structures were also observed. Ketamine increased community modularity in communities comprising of regions associated with the visual network (C3) and the DMN (C6, C32), however these effects did not pass multiple comparisons testing. Furthermore, noteworthy increases in modularity were observed in C9 and C36, communities containing ventrolateral, striatal and motor regions, additionally C9 encompasses visual and temporal structures.

Noteworthy trend-level ketamine-induced reductions in the modularity of C8 and C21 were observed. These are wide spread inclusive communities representing large areas of the cortex. These reductions may indicate either increased occurrences of amplified connectivity with the basal ganglia, globally decreased connectivity or an increased occurrence of a modular connectivity structure of the brain.

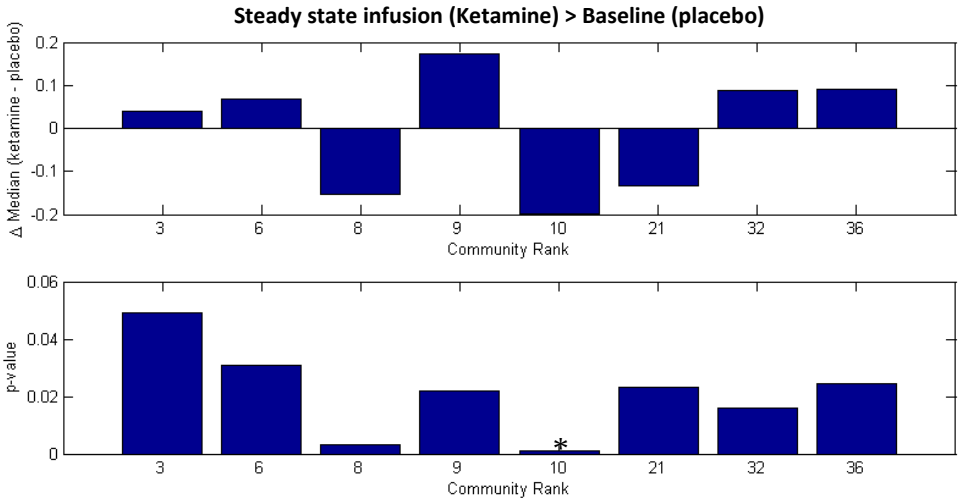

Figure 57 - Comparison of task-free community modularity values between ketamine and placebo conditions. Upper panel reveals the differences in medians for ketamine - placebo, indicating the direction of change. The lower panel reports the statistical significance of comparisons. * indicates comparisons which pass multiple comparisons testing at α= 0.05

Pharmacological mode Testing

Application of the GLM, using the GV pharmacological model, to the profiles of community modularity values yielded significant effects in several identified community structures, Figure 58. Strong positive values for the model fit indicate that ketamine induces increased community modularity in a manner similar to the predicated ketamine response; relatively strengthening within community connections and/or decreasing connections between the community and the rest of the brain. Strong negative values indicate an inverse response to the ketamine effect; namely increased integration of community regions with the rest of the brain and/or decrease within-community connectivity.

Significant model responses were observed in C9 and C3, both communities containing visual regions; C9 additionally includes striatal, sensorimotor and right ventrolateral regions. This suggests a ketamine induces increased in modularity in network configurations represented by these networks. Due to the overlapping nature of these communities, it is unlikely an increased in community modularity is expresses concurrently; instead increased modularity likely occurs in an asynchronous oscillatory manner within the task-free infusion period.

A significant inverse response was also observed for C10, a community encompassing primary visual, left frontal and temporal areas. Similarly, C8 also expressed a strong inverse response to the model, notable due to the similarity with community C10, however this effect did not pass multiple comparisons.

Statistical notable ($p<0.05$ uncorrected) model responses were observed in communities C32, containing regions associated with both the DMN and executive control networks, and communities C12 and C36, representing regions associated with sensorimotor and salience networks, suggesting an increased modularity for these communities in response to ketamine. The model also yielded a subtle inverse effect in C1, likely indicating a ketamine induced increase in striatal functional integration with the rest of the brain. These effects did not pass multiple comparisons correction.

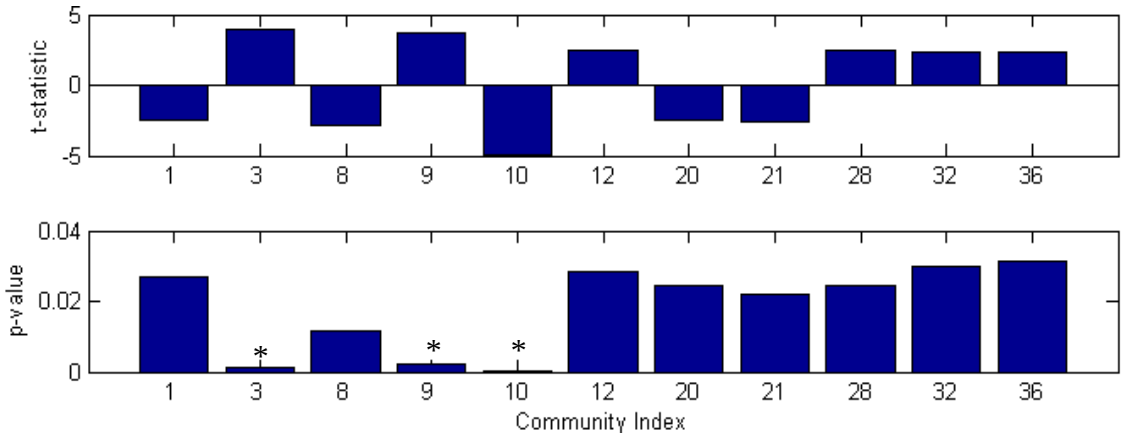

Figure 58 – Responses to the pharmacological model of ketamine infusion for community modularity profiles. The upper panel indicates the t-statistic for the model fit, the lower pane reports the significance. All communities were tested, however only communities reporting p<0.05 (uncorrected) are visualised here. * indicates results which pass multiple comparisons testing (α = 0.05).

Ketamine infusion results in altered connectivity dynamics

Ketamine was observed to have differential significant effects of community modularity profiles during an acute ketamine challenge. The resultant z-scores for each community coherence profile reveal a complex fluctuating pattern of consistent community organisations over time, as shown in Figure 59 - A. After multiple comparisons correction (Bonferroni α = 0.05), 15 community were states were found to exhibit significant modularity at any point during the ketamine challenge. The standardised score and significance values for these modularity profiles were extracted to aid visualisation in Figure 59-B and Figure 59-C respectively. Furthermore the occurrence of significant modularity values was binarised in a profile plot (Figure 59-D) in order to better visualise patterns of consistent modular organisations at the group level.

Visual inspection reveals the clear presence of a transitional period within the infusion condition occurring at volume 210 - 250 (2 - 3.5 minutes subsequent to the bolus). This likely represents the point at which the infusion of ketamine in the brain has reach sufficient levels to effect a connectivity change.

Communities C8, C10, C20, C21 and C26 reported significant modularity prior to this infusion period, but not subsequently and as such represent the connectivity organisation of the pre-ketamine infused brain. Furthermore, several of these communities, with the exception of C26, reported ketamine induced trend-level reductions in modularity, Figure 57. These communities represented widespread cortical networks specifically C8 and C21 covered almost the entirety of the cortex. C10 and C26 were found to include left lateralised frontal and parietal regions as well as visual areas. These communities were also found to express significance in the task-free baseline condition also. If indeed the period between 210-250 volumes represents the emergence of the ketamine effected connectivity, then these prior community occurrences are likely attributed to the task-free state rather than the ketamine driven connectivity.

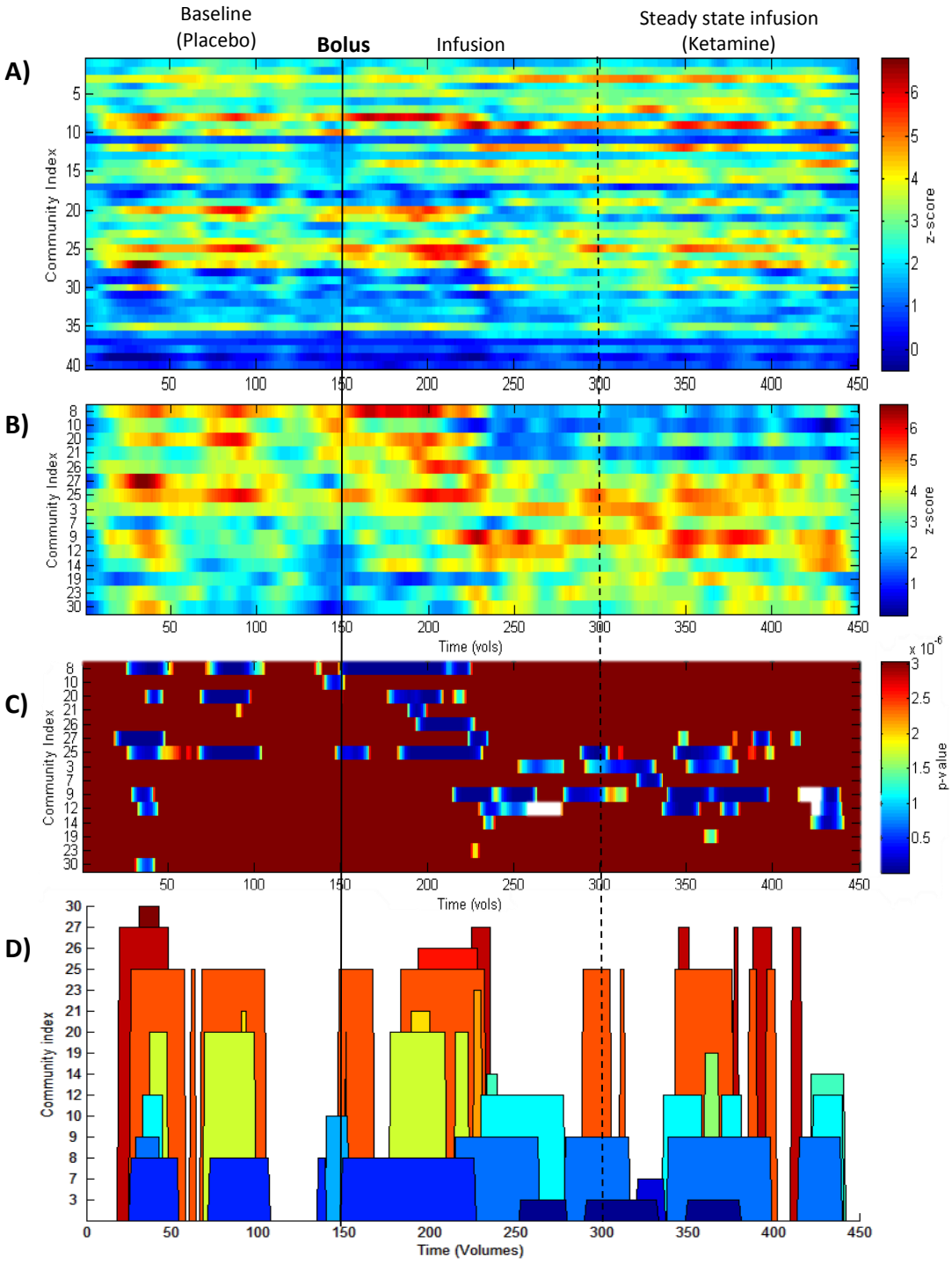

Figure 59 - Results of testing on community modularity values, A) Standardised group community coherence values over time. B) Z-scores for communities with a significant p-value (p<0.05; Bonferroni, α=0.05) during the aquistion, ordered to better visualise infusiooon effects. C) significance of each occurance, p values displayed passed multiple comparisons testing over all time points and communties (Bonferroni, α=0.05). D) State-level representation of community occurrence, community is deemed present at a group-level if a significant community coherence was observed.

Interestingly, inspection of modularity profiles in this period reveal subtle indications of oscillations in community coherence, suggesting epochs of high and low modularity. Given the inter-subject heterogeneities in connectivity organisation and synchronisation with in this task-free condition, we suggest these networks relate to the periods of relative low connectivity rather than any specific network occurrence.

Communities C3, C7, C9, C12 and C14 reported significant modularity subsequent to the period at 210-240 vols (2-3 minutes post bolus). These communities, with the exception of C7 and C14, were also implicated in comparisons of modularity distributions reporting significant relative increases in modularity for the ketamine condition compared to the baseline (Figure 58). The communities C7 and C19 contained regions associated with both the DMN and executive control networks. This network occurred only briefly, concurrent with community C3 representing the visual network. Investigation of these network dynamics on an individual subject scale is outside the scope of the work here, however represents a notable area for future study.

The profile of community modularity for C9, a network encapsulating somatosensory, visual, striatal and right lateral frontal regions, was observed to exhibit significant modularity. This significant modularity occurred in anti-phase with occurrences of significant modularity for C7 and C3. This is to be expected given the spatial overlap of C7 and C3 with C9. This effect is best illustrated on a participant level, as shown in Figure 60, where C3 and C9 report periods of anti-correlation. Overall these effects suggest ketamine induces a shift from a highly cortically connected organisation to a state of alternating modular networks inclusive of the striatum.

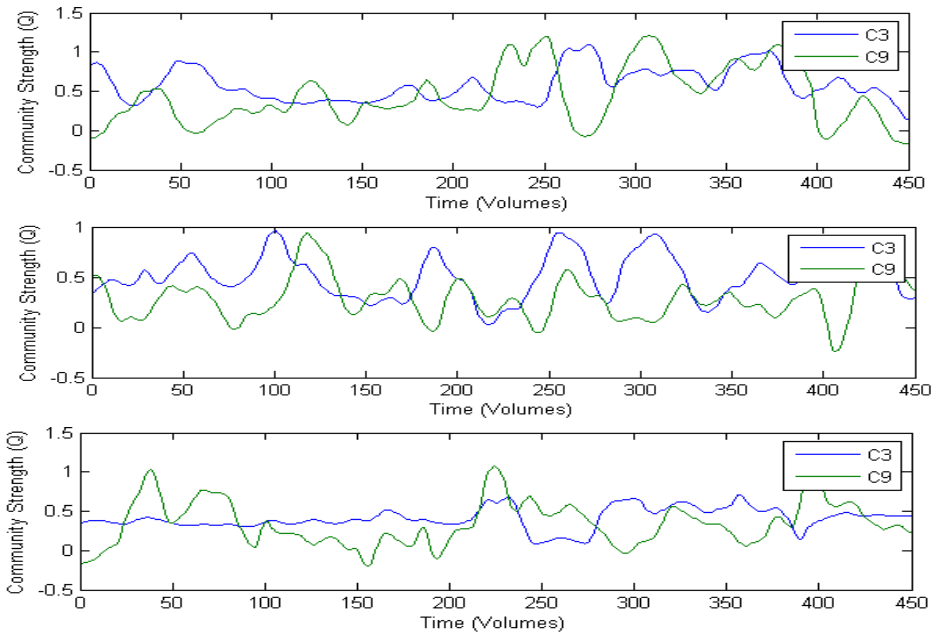

Figure 60 - Subject-wise community modularity values for C3 and C9 across 4 participants. Periods of correlation and anti-correlation were observed between networks indicating network organisational changes in the task-free period

8.3.3 Discussion

Here we have demonstrated acute ketamine alters the dynamic community structure of the brain. The proposed framework identified multiple modular structures occurring during the PLA+KET session. A range of community structures were observed ranging from large, widespread networks covering the majority of the cortex (e.g. C21) to highly localised networks such as the orbital frontal cortex (C2) and striatum (C1). Of the identified communities, many reported similar spatial configurations. This may represent the effect of ketamine subtly altering community organisation between conditions, however no statistically notable effects between conditions were observed across groups of highly similar communities between conditions this is unlikely. We therefore conclude these similar community states are instead likely due to noise or infrequently occurring weak community organisations which are consistent enough to warrant a separate centroid, yet are not so frequent or modular to yield significant effects in the proposed statistical testing. The identification of noise is an important issue, the proposed method allows for the identification of these spurious or weak communities through statistical testing of community profiles, thus eliminating the need for the user to visually inspect and remove community structures as with ICA.

Ketamine was found to elicit significant effects on the modularity profiles of these identified community states. Ketamine elicited a change in brain organisation resulting in a modular connectivity structure more inclusive of the striatum. However, no statistically notable effect of ketamine on the whole brain modularity dynamics was observed. Participant whole-brain modularity values revealed periodic oscillations consistent with observations in earlier chapters and with recent studies demonstrating the periodic nature of functional connectivity in the brain (Hutchison et al. 2012; Zalesky et al. 2014).

Ketamine Infusion

Statistically significant ketamine-induced alterations in the dynamic organisation of the brain were evident across all comparisons. Inspection of community modularity profiles reveal a clear transitory point of in the modular organisation of the brain at the period of 220-230 volumes (140-160 seconds post-bolus; Figure 59). This is consistent with previous work demonstrating a broad peak in the ketamine BOLD amplitude response at 240 seconds post bolus (De Simoni et al. 2013), contributing confidence that the observed changes in connectivity organisation are indeed driven by the ketamine response rather than a spurious effect. This transitory point is observed to occur prior to the reported BOLD amplitude peak and may suggest a greater sensitivity of connectivity to the effects of ketamine when compared to BOLD amplitude, as predicted in the aims of this thesis. Indeed, it indicates re-organisation of the functional

connectivity dynamics is achieved at a lower level of ketamine infusion. It may also be speculated that it is these connectivity changes that induce BOLD amplitude changes, however we have not specifically tested for this.

The observed effects of acute ketamine on the profile of connectivity organisation in the brain can be summarised as a reduction in the long-range, wide-spread cortical communities and the emergence of modular networks consistent across all participants. This suggests that the connectivity effects of ketamine are not uniform across the entire brain, but instead are localised resulting specific modular changes in connectivity.

The transition from the baseline task-free state was characterised by ketamine-induced reduction in modularity for widespread distributed cortical communities (C8, C10, C20 and C21). These modules represented connectivity across the majority of the cortex as well as a network consisting of left frontal, parietal, visual and temporal regions. These communities all excluded the striatum. Additionally, subtly decreased modularity was observed for the striatal community (C1; Figure 58), suggesting acute ketamine may increase in striatal integration with the rest of the brain however, this effect did not pass multiple comparisons testing. These findings are consistent with observations from Chapter 4 and 5 where ketamine was reported to decrease the connectivity of cortical regions with the rest of the brain while increasing thalamic connectivity.

The transition to the ketamine infused state is characterised by the increased modularity of communities associated with the visual network (C3), DMN/executive control networks (C7) and sensorimotor/auditory/striatal networks (C12). A large distributed community (C9) representing a combination of striatal, temporal, visual, auditory, sensorimotor and right ventrolateral cortices also report strong significant community coherence increases in response to the ketamine infusion. These observations are consistent with findings from Chapter 7 where ketamine was reported to increase the synchrony of the connectivity profile of the thalamus with other cortical regions. This is consistent with increased inclusion of the striatum in community structures present in the ketamine infused state.

It was noted increased modularity occurred prominently in communities representing combinations of sensorimotor, striatal, visual and auditory regions. This coupled with observations of reduced cortical connectivity are suggestive of reduced integration of the frontal cortices with regions associated with sensory processing and may contribute to the perceptual distortions and dissociative effects observed under ketamine. However, due to the sparsity of subjective reporting's it is not possible to confirm this in the current analysis.

Together these findings suggest an acute ketamine challenge induces a decrease in overall cortical connectivity and the emergence of a modular connectivity organisation. Moreover, this indicates that the ketamine does not act upon the connectivity in the brain in a globally uniform manner; rather, it elicits localised changes resulting in alterations to specific networks.

Ketamine is theorised to effect circuitry within the brain via the disinhibition of GABA interneurons resulting from preferential antagonism of the NMDAR (Krystal et al. 2003). It has been suggested that disinhibition of these GABAergic interneurons results in altered reduced BOLD responses through neuronal membrane hypo-polarization, meditated by GABA receptors (Minzenberg et al. 2011). Disruption of these inverse BOLD responses has implication for anti-correlated connectivity within neuronal networks. Indeed it has been demonstrated that task-free networks within the brain can be characterised by patterns of both correlations and anti-correlation (Smith et al. 2012). It has also been demonstrated that ketamine alters the relationship between anti-correlated networks within the brain, specifically the inverse relationship between the DMN and task-positive networks (Anticevic et al. 2012). Indeed it has been observed that sub-anaesthetic ketamine reduces the deactivation of the DMN during a working memory task, this failure to suppress the DMN resulted in decreased task performance suggestive of impaired working memory.

In this analysis we too noted a subtle ketamine-induced increase in DMN modularity, suggesting the activation of this network. We observe significant modularity in the ketamine state for a community (C7) consisting of regions associated with the DMN, the task positive network and the executive control network. This may indicate a ketamine-induced concurrent activation of the DMN with task positive networks, which could contribute to the memory deficits apparent under ketamine. It has been suggested hyperactivity of the DMN may result in a disrupted perception of the external environment and increased focus on internal thoughts and emotions, resulting in an inability to focus on external stimuli (Whitfield-Gabrieli et al. 2009). This is also consistent with perceptual distortion and depersonalisation effects observed under acute ketamine, however further study with higher dose ketamine and full subjective ratings would be necessary to confirm this.

Methodological considerations

The method proposed here enables investigation of changes in the dynamic network organisation within the human brain. It allows for the identification of recurring community states in the network organisation of the brain at both the individual and group level. This framework also offers a flexibility not available with blind source separation techniques, allowing the inclusion and testing of unseen data using the identified network states as well as

statistical testing on a range of connectivity metrics at localised time points. Here we have investigated the modularity structure of ketamine in a task-free design, however a task based design may provide richer results allowing for investigation into the temporal dynamics of modular networks across a group.

There are several limitations of this work, which should be noted. Firstly, the method of modularity maximisation using a greedy agglomerative search does not allow for overlapping communities within each graph slice for each individual, as such a single node may not belong to more than one community in a single slice. This may not be anatomically correct as it has been suggested that hub regions in the brain may mediate between networks and as such have multiple state membership. We have, partially successfully, attempted to circumvent this issue by using fuzzy descriptors of node membership to a community. However our search implementation uses binary assignment during the iterative optimisation rather than fuzzy assignments. A suggestion for future work which would address this would be to perform community detection, using a truly fuzzy framework, on the graph dual. This would thus define communities as a collection of edges rather than nodes; arguably a superior approach which we intend to pursue in the future.

Additionally, further work is required to develop an understanding of these connectivity fluctuations in a biological and functional context as the role of these connectivity fluctuations in the underling organisation of the brain is not understood. To provide insight into the functional role of connectivity dynamics in the acute ketamine challenge, rich moment-to-moment subjective reports are required. Such temporally rich data is generally not acquired during pharmacological imaging experiments. The findings reported here suggest this should be reconsidered in favour of increased recording of subjective responses when imaging functional connectivity dynamics. It is reasonable to assume the dynamic organisation of the brain may relate to subjective responses, if indeed the case, it may be possible to predict individual experiences based on the community organisation and modularity.

The frequency spectra of the time resolved connectivity estimated with a windowing approach is highly dependent of the length of the window applied. The windows enforce a low pass filtering effect inversely proportional to the window length, as such the choice of window length determines the maximum rate of connectivity fluctuations that can be studied (Leonardi et al. 2015). Ideally a window should be short enough to provide sensitivity to high frequency connectivity changes (15-30mHz) while not so short as to introduce spurious correlations. Empirically a rectangular window length of 30-60 seconds has been shown to produce robust results (Hutchison et al. 2012; Shirer et al. 2012). An alternative to windowed estimation of connectivity is the application of wavelet coherence, this is akin to “instantaneous correlation”;

however few methods exist to succinctly summarise the plethora of time-frequency information provided by this method.

Additionally, this method is also limited by the parcellation scheme applied. Here we consider the community structure of the brain using the AAL atlas in order to enforce consistency with other analyses within this body of work. However the coarse granularity of this atlas may not represent the true anatomy of the network in enough detail to allow for the differentiation of fine changes in resting state networks. As such further division of these regions or use of a finer grain atlas may yield superior results.

Chapter 9: Conclusions

In this chapter we bring together the various investigations performed within this body of work drawing conclusions about the field of functional connectivity (FC) and its applications to pharmacological imaging.

9.1 General conclusions

The purpose of the work has been to demonstrate the use of emerging functional connectivity approaches in the investigation of the effects of pharmacological intervention on the human brain. Through comparison of traditional approaches we have demonstrated the advantages of these emerging techniques for FC analysis. Specifically, we investigated the effect of sub-anaesthetic ketamine on the brain using pattern recognition (PR) to characterise whole brain patterns of centrality and network interactions. We also investigate the use of dynamic both connectivity to explore pharmacological imaging data. Through application of these methods we have exposed previously unobserved effects of ketamine and demonstrated the advantages of these approaches to the study of wide-spread glutamatergic dysfunction. Furthermore, we have shown that the inclusion of connectivity dynamics affords new insight into the effects of neuro-active compounds on the brain, furthering our understanding of the organisation of the brain. The work presented here is consistent with the suggestion that connectivity dynamics should be interpreted in terms of epochs of disconnection and stable connectivity organisation (Zalesky et al. 2014). This insight has motivated the novel approaches for investigating the network structure in the brain presented here.

The work here has presented a progression of functional connectivity analysis techniques, considering traditional “single-pass” univariate comparisons, introducing multivariate techniques and leading onto the investigation of network connectivity effects. The inclusion of temporal connectivity dynamics has been integral for understanding the organisation of the brain. This has led to a representation of functional connectivity in terms of not only fluctuation connectivity strengths but altered organisations and temporal occurrences of meta-stable states. This is particularly pertinent to pharmacological imaging, indeed the ketamine protocol presented in this body of work is designed to deliver a steady state infusion; however this does not necessarily translate into steady state pharmacological effects, as demonstrated in latter chapters.

This has obvious implications for the established understanding of stationary connectivity in the brain. Indeed traditional “single-pass” (correlation over entire signal) representations of connectivity likely represent a combination of the most commonly occurring connectivity

configurations in a given period. This is however, sub-optimal and does not represent the varying nature of connectivity in the brain. Indeed, it suggests changes in connectivity should be interpreted in the context of temporally discrete states rather than a stationary effect, potentially resulting in erroneous interpretation of stationary connectivity changes. Furthermore, this may be highly pertinent for pharmacological imaging where it is conceivable a compound may affect significant changes in the dynamics of connectivity which would be overlooked using the single pass approach. Indeed investigation of network dynamics has revealed significant effects of ketamine not observed in analysis using stationary connectivity estimations. Ketamine effects were reported on the frequency profile of connectivity fluctuations in the anterior cingulate and the synchrony of connectivity profiles in the thalamus, orbital frontal cortex and temporal pole (Chapter 7). Inclusion of connectivity dynamics also improved discrimination for patterns of connectivity between pharmacological conditions (Chapter 5) and revealed significant effects in the modularity profile of the visual networks (Chapter 8).

The representation of the temporal profile of connectivity has been fundamental to this work. We have focused on the use of graph theory to model connectivity estimated using a windowing approach, this affords a highly flexible and robust representation of the connectivity profile in the brain. A representation which, thus far has not been fully exploited in the existing literature. Other approaches have been suggested such as temporal ICA (Biswal et al. 1999), however this presents significant challenges in identifying consistent components between individuals. The advantage of windowed connectivity estimation lies in its flexibility and simplicity, however the disadvantages of this approach must also be considered. The most prominent amongst which is the need to select a parcellation scheme, connectivity metric and window length appropriate for the frequency range and spatial resolution under investigation. As such we should be mindful that connectivity effects must be interpreted in the context of the parcellation scheme, connectivity metric and windowing procedure applied. While advances in computational hardware may result in viable voxel-wise connectivity analysis incorporating temporal variations, the use of windowing still presents limitations regarding the choice of window lengths (Leonardi et al. 2015). An alternative method for temporal connectivity estimation is wavelet coherence (Chang et al. 2010). This provides a time-frequency estimation of connectivity however the increased dimensionality of the data generated with this approach presents new challenges in terms of analysis. As such, windowed correlation still provides the best compromise of computational efficiency, accuracy and flexibility.

To this end, we have employed windowed estimations of functional connectivity to account for the temporal dynamics within PR classification (Chapter 5 and 6). This resulted in equal or

superior classification accuracies compared to the single pass approach. For the comparisons of ketamine and control conditions windowed representation of connectivity resulted in a negligible increase of up to a 6% increase in accuracy. However, comparisons of risperidone to ketamine and control conditions using windowed connectivity resulted in classification accuracy increases of 12.5-37.5% compared to discriminations using connectivity estimated with the single-pass approach. This presents an important step toward the further development of PR approaches which are not simply black boxes but provide a rich interpretation of effects in addition to classification accuracies. Specifically, this highlights the importance of considering connectivity dynamics. However while this is advantageous, it may not be enough to correctly interpret dynamic connectivity effects. As such, we propose a graph theory framework identifying consistent community configurations and their variations over time (Chapter 8). This provides a principled method for the investigation of connectivity dynamics over time consistent with the understanding of connectivity dynamics a periodic occurrence of meta-stable modular states. This provides insight into the effects of ketamine on individual modular circuits and their temporal occurrence. Furthermore, testing at localised time points allows for the inference of connectivity organisation in the context of co-occurring modular circuits during the ketamine infusion period.

The main aim of this thesis is to demonstrate that the use of functional connectivity and the inclusion of connectivity dynamics offers new insight into the effects of ketamine on the human brain. We have demonstrated consistent effects of acute ketamine in modulating the topology of the brain, known network interactions as well as the temporal dynamics across the results chapters of this thesis. Furthermore many of these effects have not been previously reported, indicating the sensitivity of FC to the investigation of wide spread effects of ketamine within the human brain.

9.2 Novel Contributions

This thesis contains both methodological and pharmacological contributions to the field of neuroimaging. Specifically, we present new insights into the effects of ketamine on the functional connectivity within the human brain. We also demonstrate a novel application of MKL to investigate network connectivity, as well as novel approach to investigating dynamic connectivity. While the core methods employed are not novel, the framework presented and the translation of theoretical approaches for modelling brain dynamics represents a new contribution to the field.

Summary

The novel contributions of this work can be summarised as follows:

- This work provides one of the first whole-brain investigations into the functional connectivity effects of ketamine. We show that acute ketamine infusion can result in a reduction of cortical connectivity and an increase in sub-cortical connectivity. Our investigations of static and dynamic connectivity effects of ketamine also suggest a possible compensatory mechanism in corticothalamic connections in the ketamine state.
- We present previously un-observed effects of the anti-glutamatergic pre-treatments lamotrigine and risperidone on the ketamine state. We propose that NMDA blockade may be the dominant mechanism by which acute ketamine acts upon the functional connectivity in the brain rather than down-stream glutamatergic effects.
- We demonstrate the use of windowed correlation in combination with pattern recognition for whole-brain group discriminations of pharmacological imaging data. Results reveal the use of multiple windowed connectivity estimates provides increased classification accuracy over the traditional single pass approach when applied to whole brain node strength measures.
- A new approach to examine network interactions using multi-kernel learning with windowed parcellation is presented. Such an approach provides sensitivity to consistent changes in individual network connections offering an advantage over current methods for investigating changes in functional connectivity circuits.
- We suggest an extension for existing techniques for investigating dynamic connectivity using univariate statistics. We propose the use of the phase locking value as a measure of regional synchrony in temporal varying connectivity patterns.
- A new technique is proposed for the investigation of temporal changes in the community structure of the brain. Applied to a ketamine challenge acquisition it reveals a shift in the network organisation of the brain in relation to the compound infusion. Relating these connectivity changes to previously observed BOLD effects suggest that these connectivity changes may precede BOLD amplitude, an interesting effect not previously observed.

Whole brain connectivity classification

The work in Chapter 5 was undertaken early in my PhD in order to investigate the effects of ketamine in the brain. The methodological contribution of this chapter is a subtle extension of existing approaches to classifications of whole-brain (Richiardi et al. 2011; Shirer et al. 2012;

Zeng et al. 2012). Here we incorporate the dynamics of connectivity through the classification of regional connectivity measures estimated using a windowing approach. It was found that classifications of connectivity estimated using a windowed approach performed equally as well if not better than connectivity estimated using a single pass approach; thus, demonstrating the advantages of including temporal dynamics when comparing conditions. However, the use of windowing introduces the additional parameter of window length to consider. Our findings suggest the use of multiple window lengths may be the more appropriate than a single window lengths in order to investigate the effects of connectivity over multiple network frequencies.

We also demonstrate the use of a regional summary statistics, NS, as a feature set for classifications. The observed classification results indicate the use of regional summary statistics offers a viable alternative to classification of edge connections. The advantages of this approach are primarily a computational saving and the flexibility afforded by the range of regional connectivity measures available. This enables multiple classifications of groups using regional measures interrogating different aspects of connectivity, such as efficiency or small worldness. The downsides of this approach must also the considered, the foremost of these is the loss of sensitivity to subtle changes in regional couplings. As such, the use of regional statistics as a feature set is most suitable for the investigation of highly distributed effects, such as with pharmacological imaging. For the investigation of localised changes in connectivity, e.g. the analysis of trauma, the comparison of edges is likely the more appropriate tool.

Network interactions with MKL

The work presented in Chapter 6 was performed mid-way through my PhD and presents a new approach to group discrimination based on network connectivity effects. The framework presented affords the ability to perform group comparisons based on the interactions within and between multiple networks defined *a priori* within a multivariate framework. This provides a significant advantage over current methods of investigation of network interaction effects. As yet, no neuroimaging study has presented a similar method which allows for comparison of non-uniform connectivity effects within a network in a principled manner, allowing for individual-level predictions of class membership. Furthermore, the use of the sliding window approach for the estimation of functional connectivity in this approach can, to some degree, account for varying dynamic network states.

It must be noted that this method is computationally expensive and requires the tuning of regularisation parameters. Furthermore, the current implementation of this approach does not directly allow for inferences to be made on the direction of change in network connectivity from the kernel weight maps. The networks of interest used must also be defined *a priori*; if poorly

selected may limit the scope of investigation. Overall this presents a novel contribution to understanding the interactions between networks within the brain and the alterations of these interactions by an experimental condition.

Temporal Dynamics

The work in Chapter 7, specifically the univariate test of synchrony between profiles of regional connectivity, provides a new test for the investigation of temporal connectivity effects. This simple test, motivated by observations of connectivity fluctuations, enables investigation of connectivity covariance between regions. Results from this analysis revealed ketamine affects the synchronicity between regions, indicating a change in the dynamic organisation of the brain and motivates the work in Chapter 8. The work in this chapter, executed at the late stages of my PhD, provides some new methodological contributions to the field of FC as well as highlighting potential concerns with current FC investigations. Furthermore, this work provides novel insight into the effects of ketamine on the temporal FC organisation in the brain.

The main methodological contribution of Chapter 8 is a graph-theory framework for the investigation of consistent community states across subject and their temporal dynamics. Specifically, the novel aspects of this chapter are the application of clustering to temporally constrained community detection performed on the individual level. This allows for the identification of spatially overlapping community structures with incoherent temporal profiles across subjects, something not possible with tensor ICA techniques. This approach allows for the investigation of community state occurrences across subjects while accounting the lack of synchrony between subjects dynamic connectivity within task-free data. Moreover, this offers a flexible graph theory framework to investigate the dynamic modular structure of the brain without assumptions of temporal consistency between subjects. Through statistical testing we can compare the modularity structure of the brain between resting state conditions or in relation to a pharmacological infusion. This presents opportunities for the application of other graph theory measures to identified community structures enabling investigation of temporal dynamics through measures of differing aspects of connectivity.

Overall this chapter provides a preliminary contribution to the understanding of the dynamic community structure in the brain. This also illustrates the need for further work investigating dynamic alterations of brain modularity and to develop metrics and statistical tests to quantify and model these connectivity dynamics.

Effects of ketamine

While several studies have investigate the effect of ketamine on localised FC, there is a dearth of literature examining the effects of ketamine on whole-brain FC. The work present in this thesis provides a perspective into the spatial and temporal dynamics changes in connectivity elicited by ketamine. Significant previously unobserved effects of ketamine were reported for the functional connectivity organisation and dynamics, providing a novel contribution to the field regarding the understanding of ketamine.

Results from Chapter 4 indicate a ketamine induced a strong, stationary, topological effect resulting in a reduction of cortical connectivity and an increased striatal connectivity, as measured by NS. This was consistent with the pattern of effects observed in Chapter 5 where ketamine effected a pattern of change in centrality values across the brain, surmised as a decrease in cortical centrality and an increase in striatal and cerebellar connectivity. Classifications of pre-treated ketamine conditions performed in Chapter 5 and 8 are consistent with the suggestion that it is the NMDA blockade effects of ketamine primarily responsible for the observed connectivity effects, rather than the previously supposed downstream glutamatergic effects. These are novel contributions to the field and provide a new framework for the consideration of ketamine at a whole-brain level.

Investigations into the connectivity dynamics of ketamine also yielded novel insights into the effects of this compound. In Chapter 7, ketamine was found to elicit significant changes in the synchrony of connectivity profiles in the thalamus, orbital frontal cortex and mid temporal pole. Further investigation of the connectivity dynamics of ketamine suggest ketamine increases the segregation of the visual network with the rest of the brain. Moreover, the modularity of communities involving regions associated with the auditory network, salience and default mode was found to be strongly effected by ketamine, consistent with work in Chapter 6. Together, these findings reveal a widespread pattern of effects with altered network dynamics, previously not observed in ketamine.

Generally in phMRI, subjective effects of ketamine are not recorded at high temporal resolutions, thus precluding any association of subjective effects to profiles of temporal connectivity. The findings presented in Chapter 8 however, motivate the replication of this ketamine study with a higher dosage and the collection of subjective reporting's on a fine time scale, specifically with a focus on the period two minutes after the ketamine bolus. Given temporally rich subjective or objective data it may be possible to relate specific transient connectivity profiles and organisations to effects of ketamine potentially allowing for the prediction of subjective responses at an individual level.

9.3 Future directions

While functional connectivity is commonly used tool within the field of neuroimaging, current approaches are often limited in scope or sensitivity. At the time of writing, a current trend toward the investigation of dynamic connectivity exists in the literature being published. While current methods are limited, we expect the accuracy and understanding of dynamic connectivity to significantly improve in the next few years. The work presented here is a small step toward better understanding dynamic connectivity effects, however further work is required to address several limitations encountered in dynamic connectivity analysis.

Parcellation

The graph theory approaches to connectivity investigates presented here have all been constrained by the parcellation scheme employed. For the univariate comparisons in Chapters 4 and 7 and the multivariate comparison in Chapter 5, the AAL was appropriate in order to provide interpretable results. However, for the work in chapter 6 and 8 a finer parcellation scheme would be more appropriate. Several data driven parcellation schemes exist which allow for parcellation of the human cortex by functional homogeneity across multiple spatial scales (Craddock et al. 2012). This alleviates some of the limitations of the AAL, such as the dissimilarity in region sizes, limited spatial granularity and the fact regions are anatomically defined and thus may include multiple distinct functional regions. However, this comes at the cost of interpretability. These parcellation schemes represent a step toward the ultimate aim of voxel-wise analysis. The use of data-driven functionally defined atlases presents a promising principled approach to the problem of parcellation, however the use of an atlas is intrinsically limited by inter-subject variation in functional anatomy. A highly promising avenue of research is the use of *hyper-alignment* (Guntupalli et al. ; Hao et al. 2012) which allows for identification of functionally homogenous regions between subjects with differing functional topology. Such an approach to parcellation potentially avoids issues of variation in region size and location between subjects and affords a more biologically motivated parcellation.

Biologically motivated metrics

The vast majority of FC studies to date have primarily focused on the use of a few summary statistics to investigate the FC effects in experimental groups and disease populations. Previous studies have revealed changes in clustering coefficient and efficiency are exhibited in patients with Alzheimer's (Supekar et al. 2008), epilepsy (Liao et al. 2010) and correlate to illness duration for patients with schizophrenia (Liu et al. 2008). These metrics have an intuitive interpretations in regards to network effects, however the inference of these measure in a biological context is

often ambiguous. Furthermore many of the commonly applied graph theory measures are often highly correlated suggesting redundancy. A promising area of future inquiry is the association of specific graph theory measures to a biological context. The use of multi-modal connectivity investigation, such as DTI and fMRI, and the use of pharmacological imaging afford the potential investigations into the relationship between estimated graph theory measures and biologically informed measures.

Dynamic network Estimation

As discussed in Chapter 7 and 8, a promising avenue of research in the estimation of dynamic functional connectivity is the use of wavelet coherence (Chang et al. 2010). This provides a time-frequency perspective of connections between regions, circumventing the issues of selecting a window and window length in the sliding window approach. The use of wavelet estimated temporal connectivity would allow for the investigation of dynamic community structures at differing frequency bands. This would enable new investigations of frequency dependant dynamic effects between experimental conditions and disease populations, such as in schizophrenia where significant frequency dependant effects in temporal profile of regional connectivity has been observed (Sakoglu et al. 2010). A potential avenue of investigation would be the development of a spatiotemporal classification framework using wavelets estimations of connectivity combined with MKL. Where by kernels are generated for each frequency band of wavelet connectivity.

To date, studies have predominantly investigated dynamic connectivity states using modules defined by brain regions. A promising area for future research is the application of dynamic connectivity to the line graphs (Pandit et al. 2011). Such a framework would allow for the identification community structures as defined by connections between regions rather than regions themselves. This presents a more biologically motivated representation of connectivity in the brain, allowing for identification of communities where regions are not equally interconnected and with overlapping regional memberships. This would represent a significant increase in computational expense, however may prove highly advantageous over regional definitions of community structures.

Pharmacological imaging

The investigation of functional connectivity dynamics for an acute ketamine challenge has been limited by the lack of temporally rich subjective reports. A modification of the experimental protocol for future pharmacological imaging to include frequent reports of subjective effects will allow for analysis relating transient network configurations to subjective effects. This type

of analysis would be highly beneficial for rapidly acting drugs, such as anaesthetics where it may be possible to relate awareness ratings to connectivity dynamics. Investigations of compounds altering memory, learning and plasticity would also benefit from analysis of connectivity dynamics, presenting a rich area of future study.

In conclusion, the work presented here demonstrates the suitability of functional connectivity for the investigation of the distributed pharmacological of ketamine. We demonstrate that ketamine reduces cortical connectivity and increases striatal connectivity. Ketamine also induces a more modular connectivity structure with periods of integration and separation between regions associated with sensory processing. Differential results from classifications of ketamine pre-treated with risperidone and lamotrigine suggest the connectivity effects of ketamine likely result from NMDA blockade or serotonergic modulation rather than purely downstream glutamatergic effects.

This work also represents a preliminary contribution to a larger trend of the investigation of functional connectivity as a dynamic process rather than a static occurrence. We have confirmed the dynamic nature of connectivity as observed with fMRI and have presented a framework for its assessment using sliding windows and data-driven clustering. We reveal clear effects of pharmacological intervention on the modular structure of the brain, however without temporally rich subjective responses we are unable to relate connectivity dynamics to subjective effects. The present framework requires further development but presents promise for the investigation dynamic connectivity effects in pharmacological imaging.

Appendix A: Regression masks

Binary masks were used to identify CSF and WM regions from normalized images for use as nuisance parameters to be removed by linear regression. Masks were obtained through thresholding the probabilistic WM and CSF mask at 75%, selected based on visual inspection. Resultant binary masks were resliced to the normalised space.

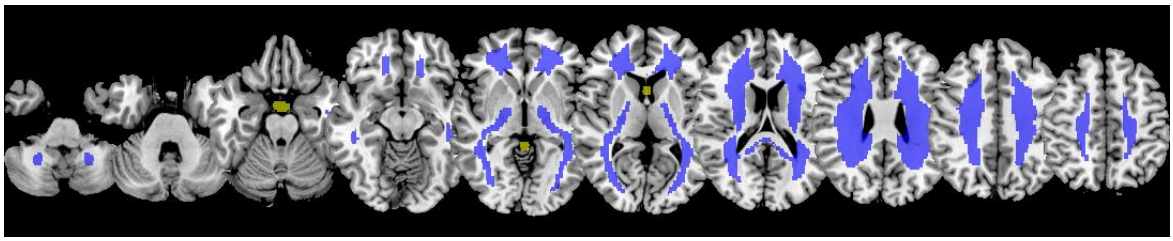

Figure 61 - Binary regression masks used to remove average CSF (orange) and WM (blue) signal

Appendix B: AAL region definitions

Index	Name	Regional Label
1	Precentral_L	Frontal
2	Precentral_R	Frontal
3	Frontal_Sup_L	Frontal
4	Frontal_Sup_R	Frontal
5	Frontal_Sup_Orb_L	Frontal
6	Frontal_Sup_Orb_R	Frontal
7	Frontal_Mid_L	Frontal
8	Frontal_Mid_R	Frontal
9	Frontal_Mid_Orb_L	Frontal
10	Frontal_Mid_Orb_R	Frontal
11	Frontal_Inf_Oper_L	Frontal
12	Frontal_Inf_Oper_R	Frontal
13	Frontal_Inf_Tri_L	Frontal
14	Frontal_Inf_Tri_R	Frontal
15	Frontal_Inf_Orb_L	Frontal
16	Frontal_Inf_Orb_R	Frontal
17	Rolandic_Oper_L	Frontal
18	Rolandic_Oper_R	Frontal
19	Supp_Motor_Area_L	Frontal
20	Supp_Motor_Area_R	Frontal
21	Olfactory_L	Frontal
22	Olfactory_R	Frontal
23	Frontal_Sup_Medial_L	Frontal
24	Frontal_Sup_Medial_R	Frontal
25	Frontal_Med_Orb_L	Frontal
26	Frontal_Med_Orb_R	Frontal
27	Rectus_L	Frontal
28	Rectus_R	Frontal
29	Insula_L	Frontal
30	Insula_R	Frontal
31	Cingulum_Ant_L	Cingulate
32	Cingulum_Ant_R	Cingulate
33	Cingulum_Mid_L	Cingulate
34	Cingulum_Mid_R	Cingulate
35	Cingulum_Post_L	Cingulate
36	Cingulum_Post_R	Cingulate
37	Hippocampus_L	Med Temporal
38	Hippocampus_R	Med Temporal
39	ParaHippocampal_L	Med Temporal
40	ParaHippocampal_R	Med Temporal
41	Amygdala_L	Med Temporal
42	Amygdala_R	Med Temporal
43	Calcarine_L	Occipital
44	Calcarine_R	Occipital
45	Cuneus_L	Occipital
46	Cuneus_R	Occipital
47	Lingual_L	Occipital
48	Lingual_R	Occipital
49	Occipital_Sup_L	Occipital
59	Parietal_Sup_L	Parietal
60	Parietal_Sup_R	Parietal
61	Parietal_Inf_L	Parietal
62	Parietal_Inf_R	Parietal
63	SupraMarginal_L	Parietal
64	SupraMarginal_R	Parietal
65	Angular_L	Parietal
66	Angular_R	Parietal
67	Precuneus_L	Parietal
68	Precuneus_R	Parietal
69	Paracentral_Lobule_L	Parietal
70	Paracentral_Lobule_R	Parietal
71	Caudate_L	Striatal
72	Caudate_R	Striatal
73	Putamen_L	Striatal
74	Putamen_R	Striatal
75	Pallidum_L	Striatal
76	Pallidum_R	Striatal
77	Thalamus_L	Striatal
78	Thalamus_R	Striatal
79	Heschl_L	Temporal
80	Heschl_R	Temporal
81	Temporal_Sup_L	Temporal
82	Temporal_Sup_R	Temporal
83	Temporal_Pole_Sup_L	Temporal
84	Temporal_Pole_Sup_R	Temporal
85	Temporal_Mid_L	Temporal
86	Temporal_Mid_R	Temporal
87	Temporal_Pole_Mid_L	Temporal
88	Temporal_Pole_Mid_R	Temporal
89	Temporal_Inf_L	Temporal
90	Temporal_Inf_R	Temporal
91	Cerebelum_Crus1_L	Cerebellar
92	Cerebelum_Crus1_R	Cerebellar
93	Cerebelum_Crus2_L	Cerebellar
94	Cerebelum_Crus2_R	Cerebellar
95	Cerebelum_3_L	Cerebellar
96	Cerebelum_3_R	Cerebellar
97	Cerebelum_4_5_L	Cerebellar
98	Cerebelum_4_5_R	Cerebellar
99	Cerebelum_6_L	Cerebellar
100	Cerebelum_6_R	Cerebellar
101	Cerebelum_7b_L	Cerebellar
102	Cerebelum_7b_R	Cerebellar
103	Cerebelum_8_L	Cerebellar
104	Cerebelum_8_R	Cerebellar
105	Cerebelum_9_L	Cerebellar
106	Cerebelum_9_R	Cerebellar
107	Cerebelum_10_L	Cerebellar

50	Occipital_Sup_R	Occipital	108	Cerebelum_10_R	Cerebellar
51	Occipital_Mid_L	Occipital	109	Vermis_1_2	Cerebellar
52	Occipital_Mid_R	Occipital	110	Vermis_3	Cerebellar
53	Occipital_Inf_L	Occipital	111	Vermis_4_5	Cerebellar
54	Occipital_Inf_R	Occipital	112	Vermis_6	Cerebellar
55	Fusiform_L	Occipital	113	Vermis_7	Cerebellar
56	Fusiform_R	Occipital	114	Vermis_8	Cerebellar
57	Postcentral_L	Parietal	115	Vermis_9	Cerebellar
58	Postcentral_R	Parietal	116	Vermis_10	Cerebellar

Appendix C: Classification results of ketamine using data cleaned with 24 motion regressors

Experimental conditions in the PLA+SAL and PLA+KET sessions were compared using data cleaned with different motion regression procedures. Data were regressed using the detrended six motion parameters, R, obtained from the realignment pre-processing and the 24 parameter model, [R R_{t-1} R^2 R_{t-1}^2], discussed in the methods section of Chapter 5. Results indicate a general similarity between group comparisons.

Table 12 - Classification results for the comparisons of conditions in PLA+KET and PLA+SAL sessions using data cleaned using R=6 and R=24 motion parameters.

Comparison	Window (sec)	Accuracy (%) R = 6	R = 24
Placebo (pre Sal) V Placebo (pre Ket)	90	**75.00**	50.00
	180	68.75	59.38
	360	68.75	59.38
	All	62.50	62.50
Placebo (pre Sal) V Saline	90	56.25	56.25
	180	56.25	56.25
	360	68.75	53.13
	All	62.50	68.75
Placebo (pre Ket) V Ketamine	90	**78.13**	68.75
	180	**75.00**	**75.00**
	360	**81.25**	**78.13**
	All	**75.00**	62.50
Saline V Ketamine	90	**90.63**	**87.50**
	180	**93.75**	**87.50**
	360	**90.63**	**87.50**
	All	**87.50**	**93.75**

Appendix D: Mean community centroids

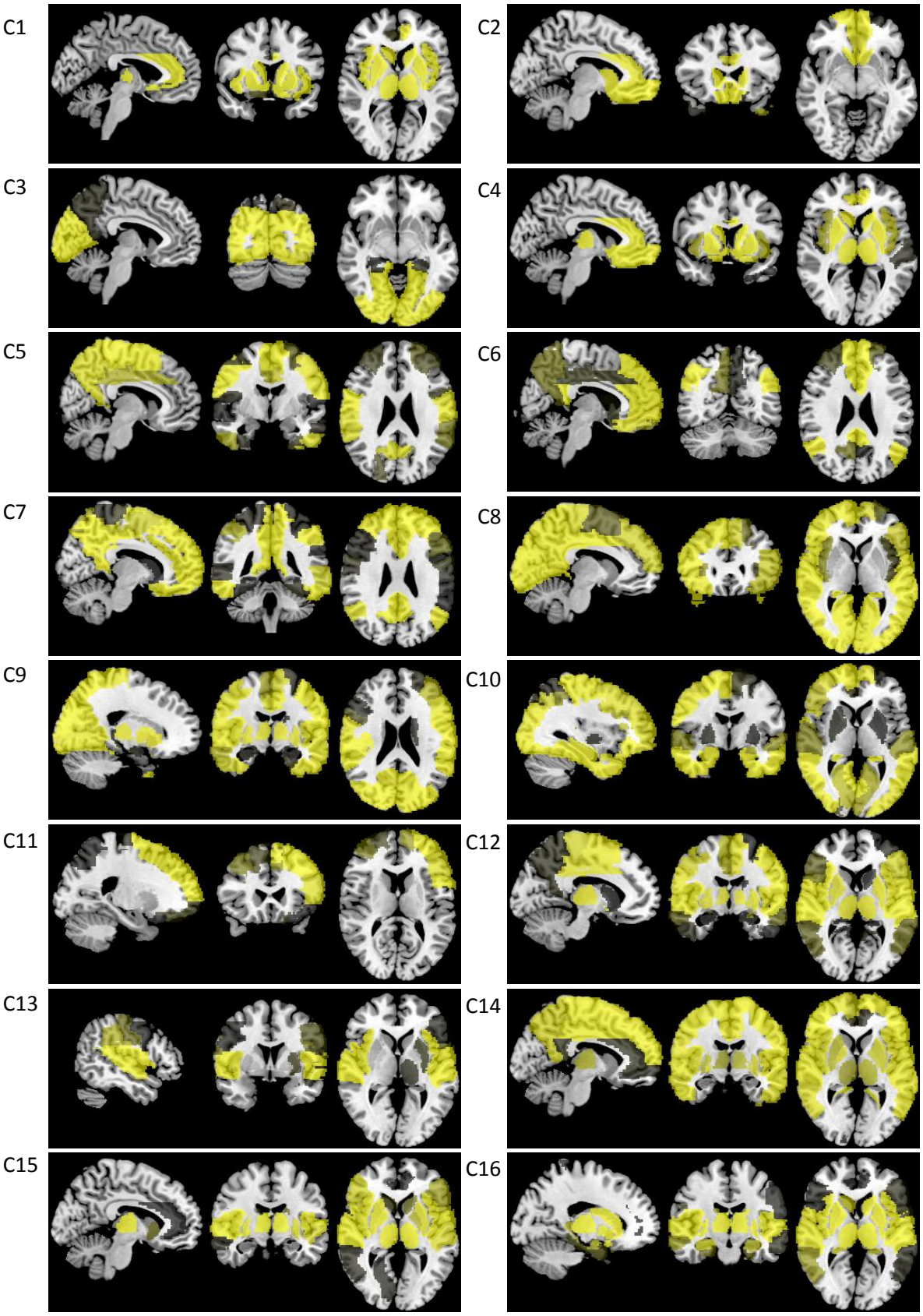

C17

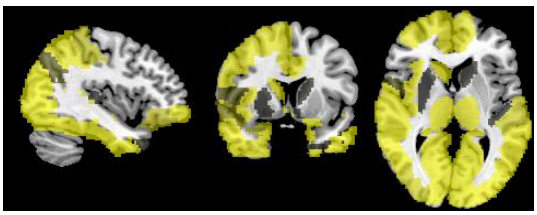

C18

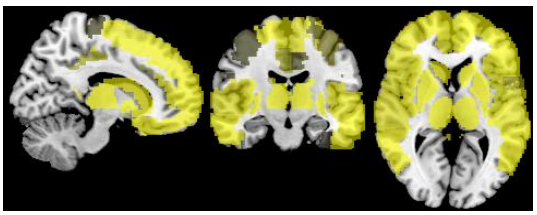

C19

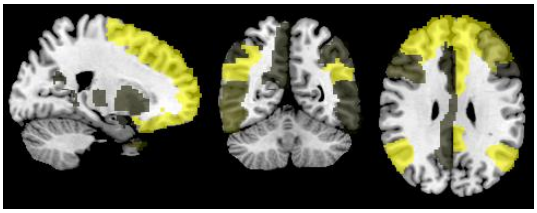

C20

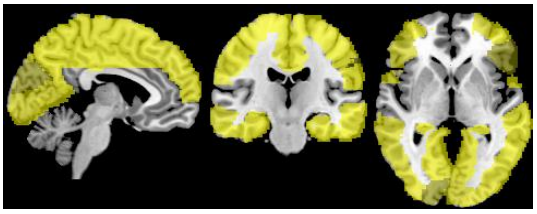

C21

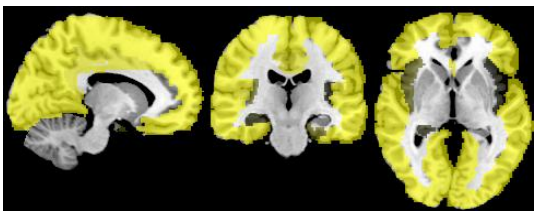

C22

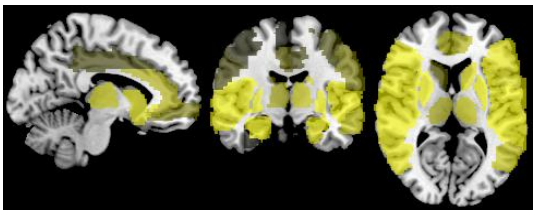

C23

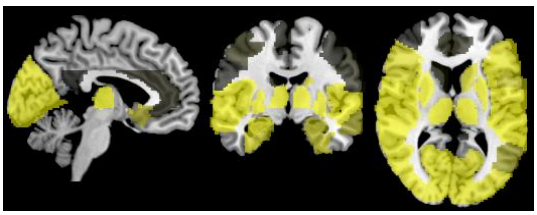

C24

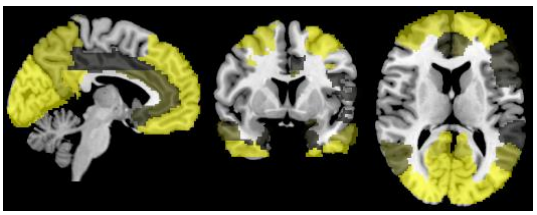

C25

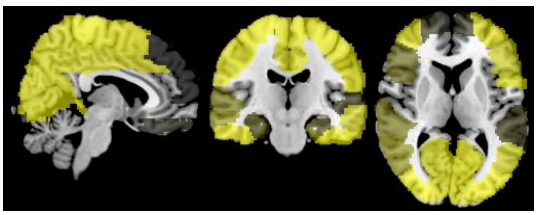

C26

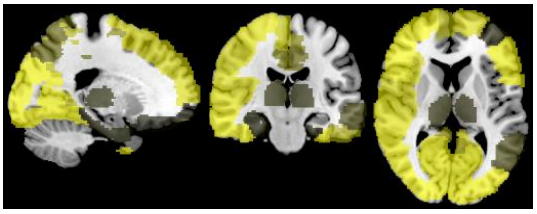

C27

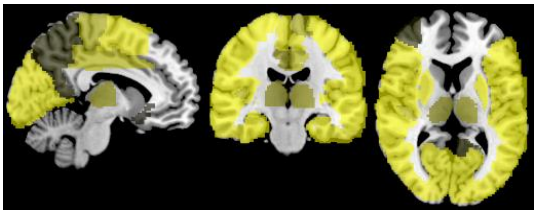

C28

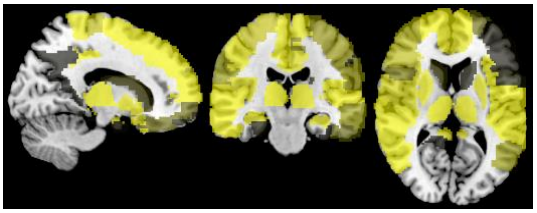

C29

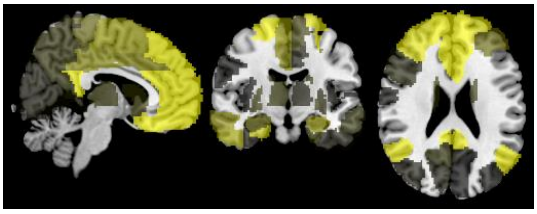

C30

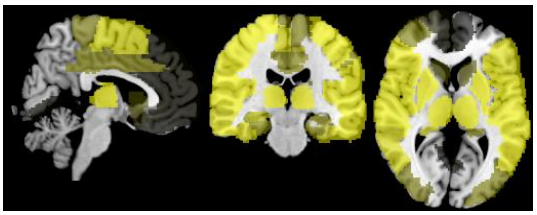

C31

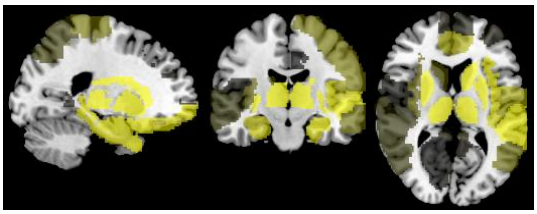

C32

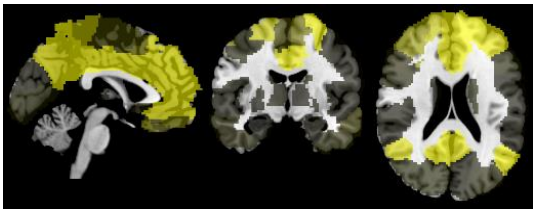

C33

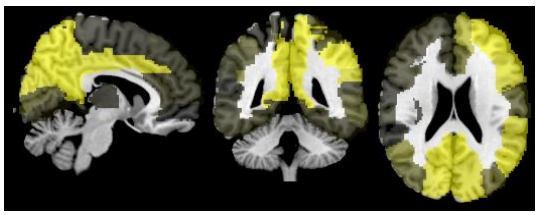

C34

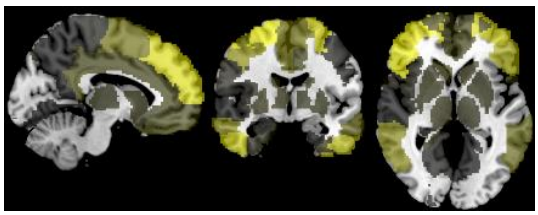

C35

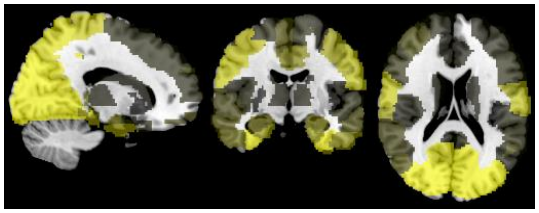

C36

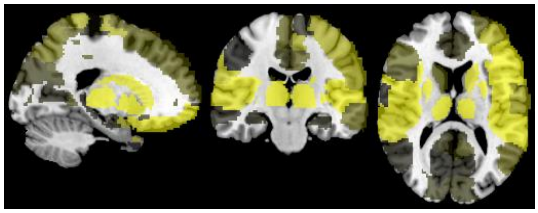

C37

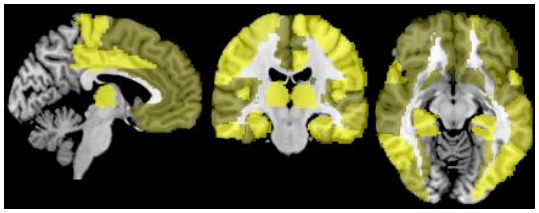

C38

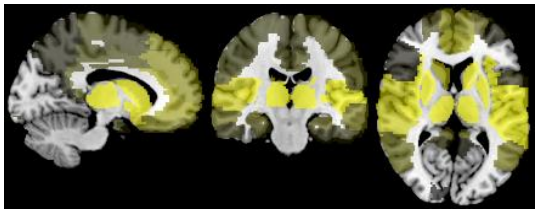

C39

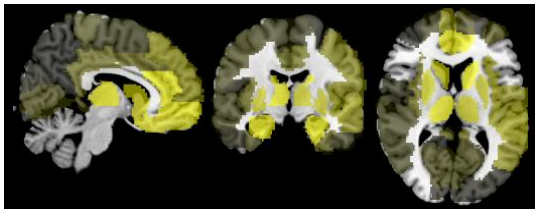

C40

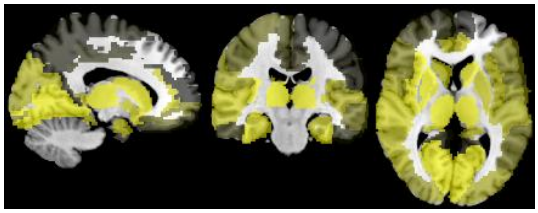

References

Abdel-aleem, S., M. K. El Awadi, et al. (1998). "Effects of phosphodiesterase inhibitors on glucose utilization in isolated cardiac myocytes." Mol Cell Biochem **180**(1-2): 129-135.

Achard, S., R. Salvador, et al. (2006). "A resilient, low-frequency, small-world human brain functional network with highly connected association cortical hubs." J Neurosci **26**(1): 63-72.

Aertsen, A., G. Gerstein, et al. (1989). "Dynamics of neuronal firing correlation: modulation of "effective connectivity"." J Neurophysiol **61**(5).

Akaike, H. (1981). "Likelihood of a model and information criteria." Journal of econometrics **16**(1): 3-14.

Allen, E. A., E. Damaraju, et al. (2014). "Tracking whole-brain connectivity dynamics in the resting state." Cereb Cortex **24**(3): 663-676.

Amodio, D. M. and C. D. Frith (2006). "Meeting of minds: the medial frontal cortex and social cognition." Nat Rev Neurosci **7**(4): 268-277.

Anderson, J. S., J. A. Nielsen, et al. (2011). "Functional connectivity magnetic resonance imaging classification of autism." Brain **134**(Pt 12): 3742-3754.

Anticevic, A., M. Gancsos, et al. (2012). "NMDA receptor function in large-scale anticorrelated neural systems with implications for cognition and schizophrenia." Proc Natl Acad Sci U S A **109**(41): 16720-16725.

Assaf, M., K. Jagannathan, et al. (2010). "Abnormal functional connectivity of default mode sub-networks in autism spectrum disorder patients." Neuroimage **53**(1): 247-256.

Bassett, D. S. and E. Bullmore (2006). "Small-world brain networks." Neuroscientist **12**(6): 512-523.

Beckmann, C. F., M. DeLuca, et al. (2005). "Investigations into resting-state connectivity using independent component analysis." Philos Trans R Soc Lond B Biol Sci **360**(1457): 1001-1013.

Beckmann, C. F. and S. M. Smith (2005). "Tensorial extensions of independent component analysis for multisubject FMRI analysis." Neuroimage **25**(1): 294-311.

Benjamini, Y. and Y. Hochberg (1995). "Controlling the false discovery rate: a practical and powerful approach to multiple testing." Journal of the Royal Statistical Society. Series B (Methodological): 289-300.

Bentley, D. and M. Konishi (1978). "Neural control of behavior." Annu Rev Neurosci **1**: 35-59.

Birn, R. M., J. B. Diamond, et al. (2006). "Separating respiratory-variation-related fluctuations from neuronal-activity-related fluctuations in fMRI." Neuroimage **31**(4): 1536-1548.

Biswal, B., A. G. Hudetz, et al. (1997). "Hypercapnia reversibly suppresses low-frequency fluctuations in the human motor cortex during rest using echo-planar MRI." J Cereb Blood Flow Metab **17**(3): 301-308.

Biswal, B., F. Z. Yetkin, et al. (1995). "Functional connectivity in the motor cortex of resting human brain using echo-planar MRI." Magn Reson Med **34**(4): 537-541.

Biswal, B. B. and J. L. Ulmer (1999). "Blind source separation of multiple signal sources of fMRI data sets using independent component analysis." J Comput Assist Tomogr **23**(2): 265-271.

Biswal, B. B., J. Van Kylen, et al. (1997). "Simultaneous assessment of flow and BOLD signals in resting-state functional connectivity maps." NMR Biomed **10**(4-5): 165-170.

Blakemore, S.-J. and A. Sirigu (2003). "Action prediction in the cerebellum and in the parietal lobe." Experimental Brain Research **153**(2): 239-245.

Blondel, V. D., J. L. Guillaume, et al. (2008). "Fast unfolding of communities in large networks." Journal of Statistical Mechanics-Theory and Experiment.

Bluhm, R. L., E. A. Osuch, et al. (2008). "Default mode network connectivity: effects of age, sex, and analytic approach." Neuroreport **19**(8): 887-891.

Bonnelle, V., T. E. Ham, et al. (2012). "Salience network integrity predicts default mode network function after traumatic brain injury." Proceedings of the National Academy of Sciences **109**(12): 4690-4695.

Braun, U., M. M. Plichta, et al. (2012). "Test-retest reliability of resting-state connectivity network characteristics using fMRI and graph theoretical measures." Neuroimage **59**(2): 1404-1412.

Bressler, S. L. and V. Menon (2010). "Large-scale brain networks in cognition: emerging methods and principles." Trends Cogn Sci **14**(6): 277-290.

Bright, M. G. and K. Murphy (2015). "Is fMRI “noise” really noise? Resting state nuisance regressors remove variance with network structure." Neuroimage **114**: 158-169.

Brodmann, K. (1909). Vergleichende Lokalisationslehre der Grosshirnrinde in ihren Prinzipien dargestellt auf Grund des Zellenbaues, Barth.

Brookes, M. J., M. W. Woolrich, et al. (2012). "Measuring functional connectivity in MEG: a multivariate approach insensitive to linear source leakage." Neuroimage **63**(2): 910-920.

Buckner, R. L., J. Sepulcre, et al. (2009). "Cortical hubs revealed by intrinsic functional connectivity: mapping, assessment of stability, and relation to Alzheimer's disease." J Neurosci **29**(6): 1860-1873.

Calhoun, V., T. Adali, et al. (2001). "A method for making group inferences from functional MRI data using independent component analysis." Hum Brain Mapp **14**(3): 140-151.

Calhoun, V. D. and T. Adali (2012). "Multisubject independent component analysis of fMRI: a decade of intrinsic networks, default mode, and neurodiagnostic discovery." IEEE Rev Biomed Eng **5**: 60-73.

Calhoun, V. D., R. Miller, et al. (2014). "The Chronnectome: Time-Varying Connectivity Networks as the Next Frontier in fMRI Data Discovery." Neuron **84**(2): 262-274.

Carchiolo, V., A. Longheu, et al. (2011). "Communities Unfolding in Multislice Networks." Complex Networks **116**: 187-195.

Carhart-Harris, R. L., R. Leech, et al. (2013). "Functional connectivity measures after psilocybin inform a novel hypothesis of early psychosis." Schizophr Bull **39**(6): 1343-1351.

Catani, M. (2006). "Diffusion tensor magnetic resonance imaging tractography in cognitive disorders." Curr Opin Neurol **19**(6): 599-606.

Chang, C., J. P. Cunningham, et al. (2009). "Influence of heart rate on the BOLD signal: the cardiac response function." Neuroimage **44**(3): 857-869.

Chang, C. and G. H. Glover (2009). "Effects of model-based physiological noise correction on default mode network anti-correlations and correlations." Neuroimage **47**(4): 1448-1459.

Chang, C. and G. H. Glover (2010). "Time-frequency dynamics of resting-state brain connectivity measured with fMRI." Neuroimage **50**(1): 81-98.

Chen, G., B. D. Ward, et al. (2011). "Classification of Alzheimer disease, mild cognitive impairment, and normal cognitive status with large-scale network analysis based on resting-state functional MR imaging." Radiology **259**(1): 213-221.

Chu, C. J., M. A. Kramer, et al. (2012). "Emergence of stable functional networks in long-term human electroencephalography." J Neurosci **32**(8): 2703-2713.

Chu, W. and Z. Ghahramani (2005). "Gaussian processes for ordinal regression." Journal of Machine Learning Research **6**: 1019-1041.

Ciccarelli, O., M. Catani, et al. (2008). "Diffusion-based tractography in neurological disorders: concepts, applications, and future developments." Lancet Neurol **7**(8): 715-727.

Concha, L., C. Beaulieu, et al. (2005). "Bilateral limbic diffusion abnormalities in unilateral temporal lobe epilepsy." Ann Neurol **57**(2): 188-196.

Cordes, D., V. M. Haughton, et al. (2001). "Frequencies contributing to functional connectivity in the cerebral cortex in "resting-state" data." AJNR Am J Neuroradiol **22**(7): 1326-1333.

Cordes, D., V. M. Haughton, et al. (2000). "Mapping functionally related regions of brain with functional connectivity MR imaging." AJNR Am J Neuroradiol **21**(9): 1636-1644.

Corlett, P. R., G. D. Honey, et al. (2011). "Glutamatergic model psychoses: prediction error, learning, and inference." Neuropsychopharmacology **36**(1): 294-315.

Cortes, C. and V. Vapnik (1995). "Support-Vector Networks." Machine Learning **20**(3): 273-297.
Craddock, R. C., G. A. James, et al. (2012). "A whole brain fMRI atlas generated via spatially constrained spectral clustering." Hum Brain Mapp **33**(8): 1914-1928.
Damoiseaux, J. S. and M. D. Greicius (2009). "Greater than the sum of its parts: a review of studies combining structural connectivity and resting-state functional connectivity." Brain Struct Funct **213**(6): 525-533.
Damoiseaux, J. S., S. A. Rombouts, et al. (2006). "Consistent resting-state networks across healthy subjects." Proc Natl Acad Sci U S A **103**(37): 13848-13853.
Danon, L., A. Diaz-Guilera, et al. (2005). "Comparing community structure identification." Journal of Statistical Mechanics-Theory and Experiment.
Dawson, N., B. J. Morris, et al. (2013). "Subanaesthetic ketamine treatment alters prefrontal cortex connectivity with thalamus and ascending subcortical systems." Schizophr Bull **39**(2): 366-377.
De Luca, M., C. F. Beckmann, et al. (2006). "fMRI resting state networks define distinct modes of long-distance interactions in the human brain." Neuroimage **29**(4): 1359-1367.
De Simoni, S., A. J. Schwarz, et al. (2013). "Test-retest reliability of the BOLD pharmacological MRI response to ketamine in healthy volunteers." Neuroimage **64**: 75-90.
Deakin, J. F., J. Lees, et al. (2008). "Glutamate and the neural basis of the subjective effects of ketamine: a pharmaco-magnetic resonance imaging study." Arch Gen Psychiatry **65**(2): 154-164.
Deco, G. and M. Corbetta (2011). "The dynamical balance of the brain at rest." Neuroscientist **17**(1): 107-123.
Deco, G., V. K. Jirsa, et al. (2011). "Emerging concepts for the dynamical organization of resting-state activity in the brain." Nat Rev Neurosci **12**(1): 43-56.
Deco, G., V. K. Jirsa, et al. (2013). "Resting brains never rest: computational insights into potential cognitive architectures." Trends Neurosci **36**(5): 268-274.
Dehaene, S., M. Kerszberg, et al. (1998). "A neuronal model of a global workspace in effortful cognitive tasks." Proc Natl Acad Sci U S A **95**(24): 14529-14534.
Deuker, L., E. T. Bullmore, et al. (2009). "Reproducibility of graph metrics of human brain functional networks." Neuroimage **47**(4): 1460-1468.
Di, X. and B. B. Biswal (2013). "Dynamic brain functional connectivity modulated by resting-state networks." Brain Struct Funct.
Dijkstra, E. W. (1959). "A note on two problems in connexion with graphs." Numerische Mathematik **1**(1): 269-271.
Dosenbach, N. U., B. Nardos, et al. (2010). "Prediction of individual brain maturity using fMRI." Science **329**(5997): 1358-1361.
Doyle, O. M., J. Ashburner, et al. (2013). "Multivariate decoding of brain images using ordinal regression." Neuroimage **81**: 347-357.
Doyle, O. M., S. De Simoni, et al. (2013). "Quantifying the attenuation of the ketamine pharmacological magnetic resonance imaging response in humans: a validation using antipsychotic and glutamatergic agents." J Pharmacol Exp Ther **345**(1): 151-160.
Driesen, N. R., G. McCarthy, et al. (2013). "Relationship of resting brain hyperconnectivity and schizophrenia-like symptoms produced by the NMDA receptor antagonist ketamine in humans." Mol Psychiatry.
Dsouza, D. C., A. Bennett, et al. (1994). "Iv Glycine D-Cycloserine to Facilitate Nmda Function in Humans." Biol Psychiatry **35**(9): 734-734.
Duncan, N. W., B. Enzi, et al. (2011). "Involvement of glutamate in rest-stimulus interaction between perigenual and supragenual anterior cingulate cortex: a combined fMRI-MRS study." Hum Brain Mapp **32**(12): 2172-2182.
Ebisch, S. J., V. Gallese, et al. (2011). "Altered intrinsic functional connectivity of anterior and posterior insula regions in high-functioning participants with autism spectrum disorder." Hum Brain Mapp **32**(7): 1013-1028.
Eccles, J. C. (1964). "The Controls of Sensory Communication to the Brain." Australas Ann Med **13**: 102-113.

Ecker, C., V. Rocha-Rego, et al. (2010). "Investigating the predictive value of whole-brain structural MR scans in autism: A pattern classification approach." Neuroimage **49**(1): 44-56.

Eckert, M. A., V. Menon, et al. (2009). "At the Heart of the Ventral Attention System: The Right Anterior Insula." Hum Brain Mapp **30**(8): 2530-2541.

Elderkin-Thompson, V., G. Hellemann, et al. (2009). "Prefrontal brain morphology and executive function in healthy and depressed elderly." Int J Geriatr Psychiatry **24**(5): 459-468.

Elliott, R., R. J. Dolan, et al. (2000). "Dissociable functions in the medial and lateral orbitofrontal cortex: evidence from human neuroimaging studies." Cereb Cortex **10**(3): 308-317.

Esposito, F., A. Bertolino, et al. (2006). "Independent component model of the default-mode brain function: Assessing the impact of active thinking." Brain Res Bull **70**(4-6): 263-269.

Fingelkurts, A. A., A. A. Fingelkurts, et al. (2007). "Impaired functional connectivity at EEG alpha and theta frequency bands in major depression." Hum Brain Mapp **28**(3): 247-261.

Fischl, B., A. van der Kouwe, et al. (2004). "Automatically parcellating the human cerebral cortex." Cereb Cortex **14**(1): 11-22.

Fortunato, S. (2010). "Community detection in graphs." Physics Reports-Review Section of Physics Letters **486**(3-5): 75-174.

Fox, M. D., D. Zhang, et al. (2009). "The global signal and observed anticorrelated resting state brain networks." J Neurophysiol **101**(6): 3270-3283.

Fransson, P. and G. Marrelec (2008). "The precuneus/posterior cingulate cortex plays a pivotal role in the default mode network: Evidence from a partial correlation network analysis." Neuroimage **42**(3): 1178-1184.

Friston, K., A. P. Holmes, et al. (1995). "Statistical Parametric Maps in Functional Imaging: A General Linear Approach." Hum Brain Mapp **2**(4): 189-210.

Friston, K. J., C. D. Frith, et al. (1993). "Functional connectivity: the principal-component analysis of large (PET) data sets." J Cereb Blood Flow Metab **13**(1): 5-14.

Friston, K. J., S. Williams, et al. (1996). "Movement-related effects in fMRI time-series." Magnetic Resonance in Medicine **35**(3): 346-355.

Fuller, W. A. (2009). Introduction to statistical time series, John Wiley & Sons.

GadElkarim, J. J., D. Schonfeld, et al. (2012). "A framework for quantifying node-level community structure group differences in brain connectivity networks." Med Image Comput Comput Assist Interv **15**(Pt 2): 196-203.

Garavan, H., T. J. Ross, et al. (1999). "Right hemispheric dominance of inhibitory control: an event-related functional MRI study." Proc Natl Acad Sci U S A **96**(14): 8301-8306.

Gass, N., A. J. Schwarz, et al. (2013). "Sub-Anesthetic Ketamine Modulates Intrinsic BOLD Connectivity Within the Hippocampal-Prefrontal Circuit in the Rat." Neuropsychopharmacology.

Glover, G. H., T. Q. Li, et al. (2000). "Image-based method for retrospective correction of physiological motion effects in fMRI: RETROICOR." Magnetic Resonance in Medicine **44**(1): 162-167.

Gochin, P. M., E. K. Miller, et al. (1991). "Functional interactions among neurons in inferior temporal cortex of the awake macaque." Exp Brain Res **84**(3): 505-516.

Goff, D. C. and J. T. Coyle (2001). "The emerging role of glutamate in the pathophysiology and treatment of schizophrenia." Am J Psychiatry **158**(9): 1367-1377.

Gomez, S., P. Jensen, et al. (2009). "Analysis of community structure in networks of correlated data." Phys Rev E Stat Nonlin Soft Matter Phys **80**(1 Pt 2): 016114.

Gong, G., Y. He, et al. (2009). "Mapping anatomical connectivity patterns of human cerebral cortex using in vivo diffusion tensor imaging tractography." Cereb Cortex **19**(3): 524-536.

Gong, Q., Q. Wu, et al. (2011). "Prognostic prediction of therapeutic response in depression using high-field MR imaging." Neuroimage **55**(4): 1497-1503.

Good, B. H., Y. A. de Montjoye, et al. (2010). "Performance of modularity maximization in practical contexts." Physical Review E **81**(4).

Greicius, M. D., B. Krasnow, et al. (2003). "Functional connectivity in the resting brain: a network analysis of the default mode hypothesis." Proc Natl Acad Sci U S A **100**(1): 253-258.
Greicius, M. D., G. Srivastava, et al. (2004). "Default-mode network activity distinguishes Alzheimer's disease from healthy aging: evidence from functional MRI." Proc Natl Acad Sci U S A **101**(13): 4637-4642.
Greicius, M. D., K. Supekar, et al. (2009). "Resting-state functional connectivity reflects structural connectivity in the default mode network." Cerebral cortex **19**(1): 72-78.
Guntupalli, J. S., A. C. Connolly, et al. "In search of functional brain atlases: Deriving common categorical representational."
Gusnard, D. A. and M. E. Raichle (2001). "Searching for a baseline: functional imaging and the resting human brain." Nat Rev Neurosci **2**(10): 685-694.
Hallquist, M. N., K. Hwang, et al. (2013). "The nuisance of nuisance regression: spectral misspecification in a common approach to resting-state fMRI preprocessing reintroduces noise and obscures functional connectivity." Neuroimage **82**: 208-225.
Hao, X., A. Lorbert, et al. (2012). Regularized hyperalignment of multi-set fMRI data. Statistical Signal Processing Workshop (SSP), 2012 IEEE.
Himberg, J., A. Hyvärinen, et al. (2004). "Validating the independent components of neuroimaging time series via clustering and visualization." Neuroimage **22**(3): 1214-1222.
Hirota, K., K. S. Sikand, et al. (1999). "Interaction of ketamine with mu2 opioid receptors in SH-SY5Y human neuroblastoma cells." J Anesth **13**(2): 107-109.
Hodgkin, A. L. and A. F. Huxley (1952). "A quantitative description of membrane current and its application to conduction and excitation in nerve." J Physiol **117**(4): 500-544.
Homayoun, H. and B. Moghaddam (2007). "NMDA receptor hypofunction produces opposite effects on prefrontal cortex interneurons and pyramidal neurons." J Neurosci **27**(43): 11496-11500.
Honey, C. J., R. Kotter, et al. (2007). "Network structure of cerebral cortex shapes functional connectivity on multiple time scales." Proc Natl Acad Sci U S A **104**(24): 10240-10245.
Honey, G. D., P. R. Corlett, et al. (2008). "Individual differences in psychotic effects of ketamine are predicted by brain function measured under placebo." J Neurosci **28**(25): 6295-6303.
Hu, H. Y., Y. van Gennip, et al. (2012). "Multislice Modularity Optimization in Community Detection and Image Segmentation." 12th Ieee International Conference on Data Mining Workshops (Icdmw 2012): 934-936.
Humphries, M. D. and K. Gurney (2008). "Network 'small-world-ness': a quantitative method for determining canonical network equivalence." PLoS One **3**(4): e0002051.
Hutchison, R. M., T. Womelsdorf, et al. (2012). "Resting-state networks show dynamic functional connectivity in awake humans and anesthetized macaques." Hum Brain Mapp.
Iacovella, V. and U. Hasson (2011). "The relationship between BOLD signal and autonomic nervous system functions: implications for processing of "physiological noise"." Magn Reson Imaging **29**(10): 1338-1345.
Jafri, M. J., G. D. Pearlson, et al. (2008). "A method for functional network connectivity among spatially independent resting-state components in schizophrenia." Neuroimage **39**(4): 1666-1681.
Jann, K., T. Dierks, et al. (2009). "BOLD correlates of EEG alpha phase-locking and the fMRI default mode network." Neuroimage **45**(3): 903-916.
Kawadia, V. and S. Sreenivasan (2012). "Sequential detection of temporal communities by estrangement confinement." Scientific Reports **2**.
Keilholz, S. D. (2014). "Review Article: The Neural Basis of Time-Varying Resting State Functional Connectivity." Brain Connect.
Khalili-Mahani, N., C. Chang, et al. (2013). "The impact of "physiological correction" on functional connectivity analysis of pharmacological resting state fMRI." Neuroimage **65**: 499-510.
Kiviniemi, V., T. Vire, et al. (2011). "A sliding time-window ICA reveals spatial variability of the default mode network in time." Brain Connect **1**(4): 339-347.

Klöppel, S., C. M. Stonnington, et al. (2008). "Automatic classification of MR scans in Alzheimer's disease." Brain **131**(3): 681-689.
Konrad, K. and S. B. Eickhoff (2010). "Is the ADHD brain wired differently? A review on structural and functional connectivity in attention deficit hyperactivity disorder." Hum Brain Mapp **31**(6): 904-916.
Konradsson, A., M. M. Marcus, et al. (2006). "Inhibition of the glycine transporter GlyT-1 potentiates the effect of risperidone, but not clozapine, on glutamatergic transmission in the rat medial prefrontal cortex." Synapse **60**(2): 102-108.
Kruskal, W. H. and W. A. Wallis (1952). "Use of Ranks in One-Criterion Variance Analysis." Journal of the American Statistical Association **47**(260): 583-621.
Krystal, J. H., L. P. Karper, et al. (1994). "Subanesthetic effects of the noncompetitive NMDA antagonist, ketamine, in humans. Psychotomimetic, perceptual, cognitive, and neuroendocrine responses." Arch Gen Psychiatry **51**(3): 199-214.
Krystal, J. H., I. L. Petrakis, et al. (2003). "NMDA receptor antagonism and the ethanol intoxication signal: from alcoholism risk to pharmacotherapy." Ann N Y Acad Sci **1003**: 176-184.
Kundu, P., S. J. Inati, et al. (2012). "Differentiating BOLD and non-BOLD signals in fMRI time series using multi-echo EPI." Neuroimage **60**(3): 1759-1770.
Lachaux, J. P., E. Rodriguez, et al. (1999). "Measuring phase synchrony in brain signals." Hum Brain Mapp **8**(4): 194-208.
LaConte, S., S. Strother, et al. (2005). "Support vector machines for temporal classification of block design fMRI data." Neuroimage **26**(2): 317-329.
Lahti, A. C., B. Koffel, et al. (1995). "Subanesthetic doses of ketamine stimulate psychosis in schizophrenia." Neuropsychopharmacology **13**(1): 9-19.
Lahti, A. C., M. A. Weiler, et al. (2001). "Effects of ketamine in normal and schizophrenic volunteers." Neuropsychopharmacology **25**(4): 455-467.
Lancichinetti, A. and S. Fortunato (2009). "Community detection algorithms: a comparative analysis." Phys Rev E Stat Nonlin Soft Matter Phys **80**(5 Pt 2): 056117.
Lanckriet, G. R. G., N. Cristianini, et al. (2004). "Learning the kernel matrix with semidefinite programming." Journal of Machine Learning Research **5**: 27-72.
Large, C. H., E. L. Webster, et al. (2005). "The potential role of lamotrigine in schizophrenia." Psychopharmacology (Berl) **181**(3): 415-436.
Leonardi, N. and D. Van De Ville (2015). "On spurious and real fluctuations of dynamic functional connectivity during rest." Neuroimage **104**: 430-436.
Liang, M., Y. Zhou, et al. (2006). "Widespread functional disconnectivity in schizophrenia with resting-state functional magnetic resonance imaging." Neuroreport **17**(2): 209-213.
Liao, W., Z. Zhang, et al. (2010). "Altered functional connectivity and small-world in mesial temporal lobe epilepsy." PLoS One **5**(1): e8525.
Lin, F., C. Yu, et al. (2007). "Diffusion tensor tractography-based group mapping of the pyramidal tract in relapsing-remitting multiple sclerosis patients." AJNR Am J Neuroradiol **28**(2): 278-282.
Liu, X. and J. H. Duyn (2013). "Time-varying functional network information extracted from brief instances of spontaneous brain activity." Proc Natl Acad Sci U S A **110**(11): 4392-4397.
Liu, Y., M. Liang, et al. (2008). "Disrupted small-world networks in schizophrenia." Brain **131**(Pt 4): 945-961.
Lloyd, S. (1982). "Least squares quantization in PCM." Information Theory, IEEE Transactions on **28**(2): 129-137.
Lohmann, G., D. S. Margulies, et al. (2010). "Eigenvector centrality mapping for analyzing connectivity patterns in fMRI data of the human brain." PLoS One **5**(4): e10232.
Lord, A., D. Horn, et al. (2012). "Changes in community structure of resting state functional connectivity in unipolar depression." PLoS One **7**(8): e41282.
Lord, L. D., P. Allen, et al. (2012). "Functional brain networks before the onset of psychosis: A prospective fMRI study with graph theoretical analysis." Neuroimage Clin **1**(1): 91-98.

Lowe, M. J., B. J. Mock, et al. (1998). "Functional connectivity in single and multislice echoplanar imaging using resting-state fluctuations." Neuroimage **7**(2): 119-132.
Lund, T. E., K. H. Madsen, et al. (2006). "Non-white noise in fMRI: does modelling have an impact?" Neuroimage **29**(1): 54-66.
Lund, T. E., M. D. Nørgaard, et al. (2005). "Motion or activity: their role in intra- and inter-subject variation in fMRI." Neuroimage **26**(3): 960-964.
Luo, C., Q. Li, et al. (2011). "Altered functional connectivity in default mode network in absence epilepsy: a resting-state fMRI study." Hum Brain Mapp **32**(3): 438-449.
Lynall, M. E., D. S. Bassett, et al. (2010). "Functional connectivity and brain networks in schizophrenia." J Neurosci **30**(28): 9477-9487.
Ma, L., B. Wang, et al. (2007). "Detecting functional connectivity in the resting brain: a comparison between ICA and CCA." Magn Reson Imaging **25**(1): 47-56.
Marquand, A., M. Howard, et al. (2010). "Quantitative prediction of subjective pain intensity from whole-brain fMRI data using Gaussian processes." Neuroimage **49**(3): 2178-2189.
Marquand, A. F., J. Mourão-Miranda, et al. (2008). "Neuroanatomy of verbal working memory as a diagnostic biomarker for depression." Neuroreport **19**(15): 1507-1511.
Marrelec, G., B. Horwitz, et al. (2007). "Using partial correlation to enhance structural equation modeling of functional MRI data." Magn Reson Imaging **25**(8): 1181-1189.
Marrelec, G., A. Krainik, et al. (2006). "Partial correlation for functional brain interactivity investigation in functional MRI." Neuroimage **32**(1): 228-237.
McGraw, K. O. and S. P. Wong (1996). "Forming inferences about some intraclass correlations coefficients (vol 1, pg 30, 1996)." Psychol Methods **1**(4): 390-390.
McKeown, M. J., S. Makeig, et al. (1998). "Analysis of fMRI data by blind separation into independent spatial components." Hum Brain Mapp **6**(3): 160-188.
Meilă, M. (2007). "Comparing clusterings—an information based distance." Journal of Multivariate Analysis **98**(5): 873-895.
Meltzer, H. Y., M. Horiguchi, et al. (2011). "The role of serotonin in the NMDA receptor antagonist models of psychosis and cognitive impairment." Psychopharmacology (Berl) **213**(2-3): 289-305.
Menon, V. (2011). "Large-scale brain networks and psychopathology: a unifying triple network model." Trends Cogn Sci **15**(10): 483-506.
Menon, V. and L. Q. Uddin (2010). "Saliency, switching, attention and control: a network model of insula function." Brain Struct Funct **214**(5-6): 655-667.
Meunier, D., S. Achard, et al. (2009). "Age-related changes in modular organization of human brain functional networks." Neuroimage **44**(3): 715-723.
Meunier, D., R. Lambiotte, et al. (2009). "Hierarchical modularity in human brain functional networks." Front Neuroinform **3**: 37.
Micheloyannis, S., E. Pachou, et al. (2006). "Small-world networks and disturbed functional connectivity in schizophrenia." Schizophr Res **87**(1-3): 60-66.
Minzenberg, M. J., J. H. Yoon, et al. (2011). "Modafinil modulation of the default mode network." Psychopharmacology (Berl) **215**(1): 23-31.
Moller, M., J. Frandsen, et al. (2007). "Dynamic changes in corticospinal tracts after stroke detected by fibretracking." J Neurol Neurosurg Psychiatry **78**(6): 587-592.
Monti, R. P., P. Hellyer, et al. (2014). "Estimating time-varying brain connectivity networks from functional MRI time series." Neuroimage **103**: 427-443.
Morgan, C. J., A. Mofeez, et al. (2004). "Ketamine impairs response inhibition and is positively reinforcing in healthy volunteers: a dose-response study." Psychopharmacology (Berl) **172**(3): 298-308.
Mourao-Miranda, J., A. L. Bokde, et al. (2005). "Classifying brain states and determining the discriminating activation patterns: Support Vector Machine on functional MRI data." Neuroimage **28**(4): 980-995.
Mucha, P. J., T. Richardson, et al. (2010). "Community Structure in Time-Dependent, Multiscale, and Multiplex Networks." Science **328**(5980): 876-878.

Murphy, K., R. M. Birn, et al. (2009). "The impact of global signal regression on resting state correlations: are anti-correlated networks introduced?" Neuroimage **44**(3): 893-905.
Nagano-Saito, A., J. Liu, et al. (2009). "Dopamine modulates default mode network deactivation in elderly individuals during the Tower of London task." Neurosci Lett **458**(1): 1-5.
Narita, M., K. Yoshizawa, et al. (2001). "A putative sigma1 receptor antagonist NE-100 attenuates the discriminative stimulus effects of ketamine in rats." Addict Biol **6**(4): 373-376.
Newman, M. E. (2006). "Modularity and community structure in networks." Proc Natl Acad Sci U S A **103**(23): 8577-8582.
Newman, M. E. and M. Girvan (2004). "Finding and evaluating community structure in networks." Phys Rev E Stat Nonlin Soft Matter Phys **69**(2 Pt 2): 026113.
Nickisch, H. and C. E. Rasmussen (2008). "Approximations for binary Gaussian process classification." Journal of Machine Learning Research **9**: 2035-2078.
Niesters, M., N. Khalili-Mahani, et al. (2012). "Effect of subanesthetic ketamine on intrinsic functional brain connectivity: a placebo-controlled functional magnetic resonance imaging study in healthy male volunteers." Anesthesiology **117**(4): 868-877.
Niogi, S. N., P. Mukherjee, et al. (2008). "Structural dissociation of attentional control and memory in adults with and without mild traumatic brain injury." Brain **131**(Pt 12): 3209-3221.
Nouretdinov, I., S. G. Costafreda, et al. (2011). "Machine learning classification with confidence: Application of transductive conformal predictors to MRI-based diagnostic and prognostic markers in depression." Neuroimage **56**(2): 809-813.
Nyberg, S., B. Eriksson, et al. (1999). "Suggested minimal effective dose of risperidone based on PET-measured D2 and 5-HT2A receptor occupancy in schizophrenic patients." Am J Psychiatry **156**(6): 869-875.
Ojemann, J. G., E. Akbudak, et al. (1997). "Anatomic localization and quantitative analysis of gradient refocused echo-planar fMRI susceptibility artifacts." Neuroimage **6**(3): 156-167.
Olson, I. R., A. Plotzker, et al. (2007). "The Enigmatic temporal pole: a review of findings on social and emotional processing." Brain **130**(Pt 7): 1718-1731.
Orrù, G., W. Pettersson-Yeo, et al. (2012). "Using Support Vector Machine to identify imaging biomarkers of neurological and psychiatric disease: A critical review." Neuroscience & Biobehavioral Reviews **36**(4): 1140-1152.
Palla, G., A. L. Barabasi, et al. (2007). "Quantifying social group evolution." Nature **446**(7136): 664-667.
Palm, G., A. Aertsen, et al. (1988). "On the significance of correlations among neuronal spike trains." Biol Cybern **59**(1): 1-11.
Pandit, S., Y. Yang, et al. (2011). Detecting communities in time-evolving proximity networks. Network Science Workshop (NSW), 2011 IEEE.
Pio Monti, R., P. Hellyer, et al. (2013). "Estimating Time-varying Brain Connectivity Networks from Functional MRI Time Series." ArXiv e-prints(1310.3863).
Platt, J. (1998). "Sequential minimal optimization: A fast algorithm for training support vector machines."
Power, J. D., A. L. Cohen, et al. (2011). "Functional network organization of the human brain." Neuron **72**(4): 665-678.
Power, J. D., A. Mitra, et al. (2014). "Methods to detect, characterize, and remove motion artifact in resting state fMRI." Neuroimage **84**: 320-341.
Pujol, J., D. Macià, et al. (2014). "Does motion-related brain functional connectivity reflect both artifacts and genuine neural activity?" Neuroimage **101**: 87-95.
Raichle, M. E., A. M. MacLeod, et al. (2001). "A default mode of brain function." Proc Natl Acad Sci U S A **98**(2): 676-682.
Rasmussen, C. E. (2006). "Gaussian processes for machine learning."
Rasmussen, C. E. W., Christopher K.I. (2006). "Gaussian Process for Machine Learning." The MIT Press.

Richiardi, J., H. Eryilmaz, et al. (2011). "Decoding brain states from fMRI connectivity graphs." Neuroimage **56**(2): 616-626.
Richiardi, J., M. Gschwind, et al. (2012). "Classifying minimally disabled multiple sclerosis patients from resting state functional connectivity." Neuroimage **62**(3): 2021-2033.
Ridderinkhof, K. R., M. Ullsperger, et al. (2004). "The role of the medial frontal cortex in cognitive control." Science **306**(5695): 443-447.
Rombouts, S. A., F. Barkhof, et al. (2005). "Altered resting state networks in mild cognitive impairment and mild Alzheimer's disease: an fMRI study." Hum Brain Mapp **26**(4): 231-239.
Rosenblum, M. G., A. S. Pikovsky, et al. (1996). "Phase synchronization of chaotic oscillators." Phys Rev Lett **76**(11): 1804-1807.
Rosvall, M. and C. T. Bergstrom (2008). "Maps of random walks on complex networks reveal community structure." Proc Natl Acad Sci U S A **105**(4): 1118-1123.
Rosvall, M. and C. T. Bergstrom (2010). "Mapping Change in Large Networks." PLoS One **5**(1).
Rubinov, M., S. A. Knock, et al. (2009). "Small-world properties of nonlinear brain activity in schizophrenia." Hum Brain Mapp **30**(2): 403-416.
Rubinov, M. and O. Sporns (2010). "Complex network measures of brain connectivity: uses and interpretations." Neuroimage **52**(3): 1059-1069.
Ryali, S., K. Supekar, et al. (2010). "Sparse logistic regression for whole-brain classification of fMRI data." Neuroimage **51**(2): 752-764.
Saad, Z. S., S. J. Gotts, et al. (2012). "Trouble at rest: how correlation patterns and group differences become distorted after global signal regression." Brain Connect **2**(1): 25-32.
Sakoglu, U., G. D. Pearlson, et al. (2010). "A method for evaluating dynamic functional network connectivity and task-modulation: application to schizophrenia." MAGMA **23**(5-6): 351-366.
Satterthwaite, T. D., M. A. Elliott, et al. (2013). "An improved framework for confound regression and filtering for control of motion artifact in the preprocessing of resting-state functional connectivity data." Neuroimage **64**: 240-256.
Schaechter, J. D., K. L. Perdue, et al. (2008). "Structural damage to the corticospinal tract correlates with bilateral sensorimotor cortex reorganization in stroke patients." Neuroimage **39**(3): 1370-1382.
Scheidegger, M., M. Walter, et al. (2012). "Ketamine decreases resting state functional network connectivity in healthy subjects: implications for antidepressant drug action." PLoS One **7**(9): e44799.
Schwarz, A. J., A. Gozzi, et al. (2008). "Community structure and modularity in networks of correlated brain activity." Magn Reson Imaging **26**(7): 914-920.
Schwarz, G. (1978). "Estimating the dimension of a model." The annals of statistics **6**(2): 461-464.
Seeley, W. W., V. Menon, et al. (2007). "Dissociable intrinsic connectivity networks for salience processing and executive control." J Neurosci **27**(9): 2349-2356.
Selverston, A. I., J. P. Miller, et al. (1983). "Cooperative mechanisms for the production of rhythmic movements." Symp Soc Exp Biol **37**: 55-87.
Shi, F., L. Wang, et al. (2013). "Altered Modular Organization of Structural Cortical Networks in Children with Autism." PLoS One **8**(5).
Shirer, W. R., S. Ryali, et al. (2012). "Decoding subject-driven cognitive states with whole-brain connectivity patterns." Cereb Cortex **22**(1): 158-165.
Shrout, P. E. and J. L. Fleiss (1979). "Intraclass Correlations - Uses in Assessing Rater Reliability." Psychol Bull **86**(2): 420-428.
Shumikhina, S. and S. Molotchnikoff (1999). "Pulvinar participates in synchronizing neural assemblies in the visual cortex, in cats." Neurosci Lett **272**(2): 135-139.
Smith, S. M., P. T. Fox, et al. (2009). "Correspondence of the brain's functional architecture during activation and rest." Proc Natl Acad Sci U S A **106**(31): 13040-13045.
Smith, S. M., K. L. Miller, et al. (2012). "Temporally-independent functional modes of spontaneous brain activity." Proc Natl Acad Sci U S A **109**(8): 3131-3136.

Smith, S. M., D. Vidaurre, et al. (2013). "Functional connectomics from resting-state fMRI." Trends Cogn Sci **17**(12): 666-682.
Sonnenburg, S., G. Ratsch, et al. (2006). "Large scale multiple kernel learning." Journal of Machine Learning Research **7**: 1531-1565.
Sorg, C., V. Riedl, et al. (2007). "Selective changes of resting-state networks in individuals at risk for Alzheimer's disease." Proceedings of the National Academy of Sciences **104**(47): 18760-18765.
Sporns, O., C. J. Honey, et al. (2007). "Identification and classification of hubs in brain networks." PLoS One **2**(10): e1049.
Stam, C. J. (2004). "Functional connectivity patterns of human magnetoencephalographic recordings: a 'small-world' network?" Neurosci Lett **355**(1–2): 25-28.
Stam, C. J., B. F. Jones, et al. (2007). "Small-world networks and functional connectivity in Alzheimer's disease." Cereb Cortex **17**(1): 92-99.
Sun, F. T., L. M. Miller, et al. (2007). "Functional connectivity of cortical networks involved in bimanual motor sequence learning." Cereb Cortex **17**(5): 1227-1234.
Supekar, K., V. Menon, et al. (2008). "Network analysis of intrinsic functional brain connectivity in Alzheimer's disease." PLoS Comput Biol **4**(6): e1000100.
Talairach, J. and P. Tournoux (1988). "Co-planar stereotaxic atlas of the human brain. 3-Dimensional proportional system: an approach to cerebral imaging."
Thomas, C. G., R. A. Harshman, et al. (2002). "Noise reduction in BOLD-based fMRI using component analysis." Neuroimage **17**(3): 1521-1537.
Tibshirani, R. (1996). "Regression shrinkage and selection via the Lasso." Journal of the Royal Statistical Society Series B-Methodological **58**(1): 267-288.
Tihonov, A. N. (1963). Solution of incorrectly formulated problems and the regularization method. Sov. Math. Dokl.
Tzourio-Mazoyer, N., B. Landeau, et al. (2002). "Automated anatomical labeling of activations in SPM using a macroscopic anatomical parcellation of the MNI MRI single-subject brain." Neuroimage **15**(1): 273-289.
Uddin, L. Q., A. M. Kelly, et al. (2009). "Functional connectivity of default mode network components: correlation, anticorrelation, and causality." Hum Brain Mapp **30**(2): 625-637.
Uddin, L. Q., A. M. Kelly, et al. (2008). "Network homogeneity reveals decreased integrity of default-mode network in ADHD." J Neurosci Methods **169**(1): 249-254.
Uddin, L. Q., K. S. Supekar, et al. (2011). "Dynamic reconfiguration of structural and functional connectivity across core neurocognitive brain networks with development." J Neurosci **31**(50): 18578-18589.
Van de Ville, D., J. Britz, et al. (2010). "EEG microstate sequences in healthy humans at rest reveal scale-free dynamics." Proceedings of the National Academy of Sciences **107**(42): 18179-18184.
van den Heuvel, M. P. and H. E. Hulshoff Pol (2010). "Exploring the brain network: a review on resting-state fMRI functional connectivity." Eur Neuropsychopharmacol **20**(8): 519-534.
van den Heuvel, M. P. and O. Sporns (2011). "Rich-club organization of the human connectome." J Neurosci **31**(44): 15775-15786.
Van Dijk, K. R., T. Hedden, et al. (2010). "Intrinsic functional connectivity as a tool for human connectomics: theory, properties, and optimization." J Neurophysiol **103**(1): 297-321.
Walsh, E., D. A. Oakley, et al. (2014). "The functional anatomy and connectivity of thought insertion and alien control of movement." Cortex.
Wang, Z., A. R. Childress, et al. (2007). "Support vector machine learning-based fMRI data group analysis." Neuroimage **36**(4): 1139-1151.
Watts, D. J. and S. H. Strogatz (1998). "Collective dynamics of 'small-world' networks." Nature **393**(6684): 440-442.
Weissenbacher, A., C. Kasess, et al. (2009). "Correlations and anticorrelations in resting-state functional connectivity MRI: a quantitative comparison of preprocessing strategies." Neuroimage **47**(4): 1408-1416.

Whitfield-Gabrieli, S., H. W. Thermenos, et al. (2009). "Hyperactivity and hyperconnectivity of the default network in schizophrenia and in first-degree relatives of persons with schizophrenia." Proceedings of the National Academy of Sciences **106**(4): 1279-1284.

Whitfield-Gabrieli, S., H. W. Thermenos, et al. (2009). "Hyperactivity and hyperconnectivity of the default network in schizophrenia and in first-degree relatives of persons with schizophrenia." Proc Natl Acad Sci U S A **106**(4): 1279-1284.

Whitlow, C. T., R. Casanova, et al. (2011). "Effect of resting-state functional MR imaging duration on stability of graph theory metrics of brain network connectivity." Radiology **259**(2): 516-524.

Williams, C. K. I. and C. E. Rasmussen (1996). "Gaussian processes for regression." Advances in Neural Information Processing Systems 8 **8**: 514-520.

Worsley, K. J., S. Marrett, et al. (1996). "A unified statistical approach for determining significant signals in images of cerebral activation." Hum Brain Mapp **4**(1): 58-73.

Yang, S. and D. Knoke (2001). "Optimal connections: strength and distance in valued graphs." Social Networks **23**(4): 285-295.

Zalesky, A., A. Fornito, et al. (2010). "Network-based statistic: identifying differences in brain networks." Neuroimage **53**(4): 1197-1207.

Zalesky, A., A. Fornito, et al. (2014). "Time-resolved resting-state brain networks." Proc Natl Acad Sci U S A **111**(28): 10341-10346.

Zalesky, A., A. Fornito, et al. (2010). "Whole-brain anatomical networks: does the choice of nodes matter?" Neuroimage **50**(3): 970-983.

Zeng, L. L., H. Shen, et al. (2012). "Identifying major depression using whole-brain functional connectivity: a multivariate pattern analysis." Brain **135**(Pt 5): 1498-1507.

Zhang, J., J. Wang, et al. (2011). "Disrupted brain connectivity networks in drug-naive, first-episode major depressive disorder." Biol Psychiatry **70**(4): 334-342.

Zou, H. and T. Hastie (2005). "Regularization and variable selection via the elastic net." Journal of the Royal Statistical Society: Series B (Statistical Methodology) **67**(2): 301-320.